



UNIVERSITY OF
BIRMINGHAM

**IMAGING GEOTECHNICAL PROPERTY
CHANGES DURING FAILURE DEVELOPMENT
OF TROPICAL RESIDUAL SOIL SLOPE**

by
Atiku Abubakar Sadiq

A thesis submitted to The University of Birmingham for the award

of degree of **DOCTOR OF PHILOSOPHY**

August 2018

Department of Civil Engineering
School of Engineering
College of Engineering and Physical
Sciences
The University of Birmingham

UNIVERSITY OF
BIRMINGHAM

University of Birmingham Research Archive

e-theses repository

This unpublished thesis/dissertation is copyright of the author and/or third parties. The intellectual property rights of the author or third parties in respect of this work are as defined by The Copyright Designs and Patents Act 1988 or as modified by any successor legislation.

Any use made of information contained in this thesis/dissertation must be in accordance with that legislation and must be properly acknowledged. Further distribution or reproduction in any format is prohibited without the permission of the copyright holder.

Abstract

Devastating cases of slope failure have been reported in many parts of the world; many of which are in tropical countries where the natural and man-made slopes are mostly made up of red tropical residual soils. Most of the failures occurred following heavy rainfall or during flooding. For this reason, the abnormal change of the soil water content is presumed to be responsible for these failures. It becomes imperative, therefore, to understand the soil-water interaction and eventual failure process in tropical residual soil, if this problem is to be effectively tackled. To achieve this aim, a research was conducted on a systematically designed and constructed slope model of a simulated tropical residual soil slope.

Preliminary studies were conducted to assess the suitability of the selected material, methodology and instrumentation to be used in the experiment. This was followed by a trial experiment on a small-sized model with a surface area of 200 mm x 370 mm and a maximum (crest) slope height of 220 mm. This small size allowed easy handling and repeatability but could not accommodate enough instrumentation, due to the limited size. To remedy this deficiency, another experimental trial was conducted on a larger-sized model constructed in a square fibreglass box with surface area of 1315 mm x 1315 mm and the maximum height of this slope was 650 mm. Before conducting the final laboratory experiment, the model was analyzed and designed with the aid of modelling software (i.e. SLOPE/W, SEEP/W and SIGMA/W). The geotechnical tests and other preliminary laboratory studies conducted at the beginning of the study provided necessary inputs during numerical modelling. This numerical modelling produced a final workable model and provided an idea about the failure mechanism of the designed model. Finally, the main experiment was conducted on the designed model which was constructed in a large acrylic glass. The surface dimension of this model was 1000 mm x 1700 mm and the maximum slope height was 750 mm.

In all the trials, a slope failure was caused by supplying water through a supply chamber, provided by the side of the crest, and allowing it to move freely to the toe. The geophysical changes and physical deformation during failure were observed using an integrated system of electromagnetic sensors (5TE and MPS6), electrical resistivity, and cameras. From the results presented and discussed, it was understood that the gradual movement of water through the slope caused a gradual reduction in matric suction, with the consequent reduction of shear strength and eventual slope movement. The physical deformation began with an initial settlement and minor surface cracks; which continually progressed to excessive settlement and larger cracks, before the final forward movement. The excessive settlement prior to the final movement appears to be associated with a soil structure collapse induced by wetting; while the forward sliding is caused by the movement of water, which tends to pull the slope downwards. The experiment provided an improved knowledge of the slope failure mechanism in tropical residual soils and has established the suitability of geophysical methods for monitoring the stability of the slopes and embankments of the tropics.

Dedication

To the loving memory of my mother who never tired of whispering into my ears and showing me in practice, the value of hard work, integrity and education.

The work is also dedicated to the two departed souls Alhaji Bala Labbo Gwandu and Alhaji Bala Shehu Azare. Both have influenced my decision to embark on a journey towards the attainment of a doctorate degree. Sadly, neither of them is alive to see the end of this journey.

It is with total submission to the will of the Almighty God that I pray for eternal rest in the gardens of paradise of all the above souls.

Acknowledgement

Thanks be to the Almighty God for keeping me alive to see the end of this stressful undertaking.

This work was conducted under the able guidance of my **main supervisor Professor Ian Jefferson**. I cannot thank him enough for his guidance and sustained confidence in my ability to conduct this research. I also wish to extend similar appreciation to my co-supervisors, **Professor Martin Culshaw** and **Dr Gurmel Ghataora**, for their criticism, support and encouragement. Martin's guidance and advice have been particularly helpful in preparing this thesis.

My deep appreciation goes to **Professor Nigel Cassidy** for his support and expert advice that led to the successful use of the electrical resistivity method in this research.

My consultations with the geophysical experts from the British Geological Survey (BGS) have contributed in no small measure in shaping my preconceived ideas on geophysics. I am very grateful to **Dr Helen Reeves**, **Dr David Gunn** and many other staff of BGS who spared time to give me useful advice during my visits to their office in Keyworth.

The invaluable support and advice received from research fellow **Dr Giulio Curioni** is highly appreciated. Similar appreciation goes to the laboratory technicians for their assistance during the period of laboratory work.

I wish to acknowledge the contribution of GeoStudio International Ltd for giving me a free licence to use their software.

My family deserves special thanks for allowing me to steal from their time and invest in this research. I begin by thanking my father **Alh. Abubakar Sadiq Dakingari** for his support, guidance and constant prayers. Next is **my wife Samira** and **daughters Zarah, Juwairiya and Maryam** for their patience and sacrifices, particularly during the trying period of their long stay in Nigeria while I was in the UK trying to prepare for my viva. I thank my brothers and sisters for being with me in prayers throughout the period of my studies.

This study wouldn't have been possible without the moral and financial support of my grand uncle **Alh. Saidu Usman Nasamu Dakingari**. My special salutation goes to him.

I wish to appreciate the support I received from Dr Bashir Gwandu and his wife Zainab, particularly when my last daughter Maryam was on her way to this planet.

I wish to acknowledge the partial funding by the Petroleum Technology Development Fund (PTDF) and financial assistance from Kebbi state government through the state scholarship board.

To my colleagues in the Department of Civil Engineering, Chris Shaw, **Jabar Rasul**, **Nesreen Al-Obaidy**, **Saif Alzabeebee**, **Raid Kraidi**, **Racheal Fisher**, **Harith Al-Ayooby** and others too numerous to mention, I say thank you all for your companionship. Similar thanks go to my friends from the Department of Mechanical Engineering, Abdulkadir Ahmed, **Rafiu Kayode** and **Hamad Aldhufairi**. I must also thank my Nigerian friends **Akilu Sada**, **Auwal Abdussalam**, **Aminu Suleiman**, **Isah Abubakar** and **Nasir Ahmed** for making my early days in the UK less stressful.

Finally, I would like to thank Mrs Janet Hingley for proofreading some chapters of my thesis.

List of Acronyms

ρ	Bulk density
ε	Dielectric constant
μ_r	Relative magnetic permittivity
τ	Shear stress
γ	Unit weight of soil
ϕ'	Effective angle of shearing resistance of soil
Θ	Volumetric water content changes
μ_s	Poisson's ratio of soil
σ	Stress, temperature slope
u_a	Pore air pressure
u_w	Pore water pressure
Θ_b	Back pressure
2D	Two dimensions
3D	Three dimensions
ALERT	Automated time-Lapse Electrical Resistivity Tomography
AE	Acoustic Emission
AEV	Air-Entry Value
BS	British Standard
BIONICS	Biological and Engineering Impact of Climate on Slopes
BGS	British Geological Survey
c (kPa)	Cohesion of the soil
C	Velocity of light in free space
CBR	California Bearing Ratio
D (m)	Depth, displacement
E (kPa)	Modulus of elasticity
EC	Electrical Conductivity
ERT	Electrical Resistivity Tomography
F	Force applied
FEM	Finite Element Method
FOS	Factor of Safety
G_{max}	Maximum shear modulus
GPR	Ground Penetrating Radar
GPS	Global Positioning System
G_s	Specific gravity
GWC	Gravimetric Water Content
H	Total hydraulic head
i	Hydraulic gradient, incident angle
K'	Stiffness, modulus number
k	Coefficient of permeability
LEM	Limit Equilibrium Method
LL	Liquid Limit
MDD	Maximum Dry Density
MS	Matric Suction
ODF	Over Design Factor
OMC	Optimum Moisture Content
PI	Plasticity Index
PL	Plastic Limit
	Particle Size Distribution

PSD

Q

r

Res2Dinv

SWCC

t

T

v

V

V_s

VWC

Flux

Refracted angle

Resistivity 2D inversion software

Soil-Water Characteristic Curve

Time

Temperature

Flow rate of water

Electromagnetic waves velocity

Shear wave velocity

Volumetric Water Content

Contents

Abstract.....	i
Dedication.....	iii
Acknowledgement.....	iv
List of Acronyms.....	v
Contents.....	vii
List of Figures.....	xv
List of Tables.....	xxi
CHAPTER ONE.....	1
1.1 Introduction.....	1
1.2 Background of the project.....	4
1.3 Statement of the problem.....	5
1.4 Aim and objectives.....	7
1.5 Brief research methodology.....	8
1.6 Contribution to knowledge.....	10
1.7 Thesis structure.....	11
1.8 Chapter summary.....	12
CHAPTER TWO.....	13
2 LITERATURE REVIEW.....	13
2.1 Introduction.....	13
2.2 Slope.....	16
2.2.1 Slope stability.....	16

2.2.2	Factors affecting slope stability.	16
2.2.3	Impact of climate change on slope stability.....	18
2.3	Slope failure mechanism	19
2.3.1	Progressive failure	21
2.3.2	Retrogressive failure Mechanism	24
2.3.3	Collapse failure Mechanism	26
2.4	Slope Failure in Residual Tropical Soils.....	28
2.5	Slope Stability Monitoring	32
2.5.1	Intrusive methods.....	33
2.5.1.1	Trial Pits and Trenches	34
2.5.1.2	Shafts and Adits.....	34
2.5.1.3	Drilling and Boring.....	35
2.5.2	Soil Sampling.....	36
2.5.3	Non-intrusive methods.....	36
2.5.3.1	Acoustic Emission	38
2.5.3.1.1	Operational Theory	39
2.5.3.1.2	Application of Acoustic Emission to the Soil Slope Stability.....	40
2.5.3.1.3	Development of Acoustic Real-time Monitoring System	46
2.5.3.2	Electrical Resistivity Tomography (ERT).....	47
2.5.3.2.1	Concept and Theory	47
2.5.3.2.2	Application to soil stability monitoring	51
2.5.3.2.3	Development of resistivity real-time monitoring system.....	53
2.5.3.3	Ground Penetrating Radar (GPR).....	53
2.5.3.3.1	Principle and Performance	55
2.5.3.4	Seismic Profiling	58

2.5.3.4.1	Types of Waves	58
2.5.3.4.2	Attenuation and Absorption	59
2.5.3.4.3	Theory and Concept	59
2.5.4	Selection of Stability Monitoring Method	62
2.6	Chapter Summary.....	64
CHAPTER 3		65
3	Production of Artificial Tropical Soil.....	65
3.1	Introduction	65
3.2	Production of artificial soils – previous studies	68
3.3	Materials.....	70
3.4	Methodology	71
3.4.1	Stage 1. Preliminary study	71
3.4.2	Stage 2. Desk study.....	71
3.4.3	Stage 3. Laboratory testing	72
3.4.4	Stage 4. Soil design and Production	72
3.5	Results	72
3.5.1	Results of Preliminary Studies.....	72
3.5.2	Grain-size Distribution.....	74
3.5.3	Laboratory confirmatory tests.....	76
3.5.4	Particle Density	78
3.5.5	Atterberg Limits.....	78
3.5.6	Compaction Characteristics	79
3.5.7	Permeability	81
3.5.8	Shear Strength.....	82
3.6	Summary and Conclusions.....	84
CHAPTER FOUR.....		86

4	NUMERICAL MODELLING.....	86
4.1	Introduction	86
4.2	Theoretical concept and selecting numerical models.....	87
4.3	Geostudio Software	91
4.3.1	SLOPE/W	91
4.3.2	SEEP/W	92
4.3.3	SIGMA/W.....	92
4.3.4	Coupled Analysis	93
4.4	Modelling failure mechanism.....	94
4.4.1	Modelling principle used	95
4.4.1.1	Seepage Analysis	95
4.4.1.2	Stability Analysis.....	97
4.4.2	Numerical Study to design a slope model.....	98
4.4.2.1	Material properties.....	98
4.4.2.2	Parameters selection	100
	Stage 1: Geometry Selection.....	100
	Stage 2: Selection of Boundary Condition.....	104
	Stage 3: Location of Boundary Condition	105
4.4.2.3	Design Output.....	106
4.4.3	Detailed analysis to predict behaviour of the model.....	106
4.4.3.1	Case definition.....	106
4.4.3.2	The material properties	107
4.4.3.3	Boundary Conditions	107
4.4.3.4	Mesh specification	108

4.4.3.5	Analysis	108
4.4.3.6	Results Presentation.....	108
4.5	Summary and concluding remarks	114
CHAPTER 5		116
5	PHYSICAL MODELLING	116
5.1	Introduction	116
5.2	Material Used	117
5.3	Instrumentation.....	118
5.3.1	5TE Volumetric Water Content Sensor	118
5.3.2	MPS-6 Matrix Suction Sensor	120
5.3.3	Time Lapse Camera	122
5.4	Feasibility Tests.....	123
5.4.1	Selecting Moulding Water content and the working density.....	123
5.4.2	Homogeneity Test.....	124
5.4.3	Infiltration and Permeability test	126
5.4.4	Assessment of Electromagnetic Sensors.....	128
5.4.5	Homogeneity Test using 5TE Sensor	133
5.4.6	Moisture Equilibrium.....	137
5.4.7	Electrical Properties	138
5.5	Small-Scale Experiment.....	142
5.5.1	Experimental Procedure	142
5.5.2	Small-Scale Trial Results.....	145
5.6	Large-scale trial experiment.....	147
5.6.1	Experimental Procedure.....	147
5.6.1.1	Design of compaction layers	148
5.6.1.2	Compaction.....	150

5.6.1.3	Control of compaction uniformity	152
5.6.1	Results of the Large Experiment.....	155
5.6.1.1	Pre-failure condition	156
5.6.1.2	Failure development process	158
5.6.1.3	Post-Failure Condition.....	162
5.7	Summary and key outcomes	162
CHAPTER SIX.....		165
6	FINAL EXPERIMENT WITH GEOPHYSICAL METHODS	165
6.1	Introduction.....	165
6.2	Experimental Set-up.....	166
6.2.1	Experimental Tank.....	166
6.2.2	Slope Construction.....	167
6.2.3	Instrumentation	168
6.2.3.1	Resistivity Apparatus.....	168
6.2.3.2	Resistivity data acquisition meter.....	169
6.2.3.3	Complete data acquisition systems.....	171
6.3	Resistivity array design	172
6.4	Experimental Programme.....	173
6.4.1	Procedure for the Trial Experiment	174
6.4.2	Procedure for the Final Experiment.....	176
6.5	Data collection.....	178
6.6	Data processing	179
6.7	Results	179
6.7.1	Results of the trial experiment	179

6.7.1.1	Initial condition before the water supply	180
6.7.1.2	Condition during the water supply	181
Figure 6-14: Sensor measurements during and after water supply		182
6.7.1.3	After the water supply	184
6.7.2	Results of the final experiment	184
6.7.2.1	Electromagnetic sensor results	184
6.7.2.1.1	Initial condition before the water supply	184
6.7.2.1.2	Experimental condition during water supply.....	185
6.7.2.1.3	After the water supply	186
6.7.2.2	Visual observations using camera	187
6.7.2.2.1	Initial condition before the water supply.....	187
6.7.2.2.2	Experimental condition during the water supply.....	187
6.7.2.2.3	Post-experimental condition - After the water supply.....	191
6.7.2.3	Resistivity Survey results	192
6.7.2.3.1	Initial condition before the water supply.....	193
6.7.2.3.2	Experimental condition during the water supply.....	195
Figure 6-29: The results showing the change of resistivity during the experiment along the side line		196
6.7.2.3.3	Post-experimental condition - After stopping the water supply	198
6.8	Summary	198
CHAPTER 7		202
7	DISCUSSION.....	202

7.1	Introduction	202
7.2	Tropical residual soil.....	202
7.3	Numerically modelling.....	203
7.4	Physical modelling	204
7.4.1	Initial (Pre-experimental) Condition.....	205
7.4.2	During the experiment	207
7.4.3	Post-experimental condition	209
7.5	Time-dependent monitoring.....	210
7.6	Summary	211
CONCLUSIONS AND RECOMMENDATIONS.....		213
8.1	Conclusions	213
8.2	Recommendations	215
References.....		217

List of Figures

Figure 2-1: Sequence of progressive failure development (After Bjerrum, 1967).....	22
Figure 2-2: Graphical representation of progressive failure development in slope Pathak et al., 2008).....	22
Figure 2-3: Failure mechanism in soft clayey slope (Wang et. al., 2016).....	26
Figure 2-4: Schematic diagram showing a set-up of AE System (adopted from US patents).	40
Figure 2-5: Diagram of AE monitoring system.....	42
Figure 2-6: Range vs frequency for AE signals (Hardy, 2005).....	43
Figure 2-7: Acoustic emission system with a waveguide (Kousteni et al., 1999).....	44
Figure 2-8: Acoustic emission system with an active wave-guide (after Dixon et. al., 2003)	45
Figure 2-9: Arrangement of array of electrodes (Hack, 2000).....	48
Figure 2-10: Different types of electrode arrays configurations.....	49
Figure 2-11: GPR antennae (Evans, 2006).....	55
Figure 2-12: Schematic of basic GPR system.....	56
Figure 2-13: Types of Seismic wave (http://www.bgs.ac.uk/discoveringGeology/hazards/earthquakes/images).....	58
Figure 2-14: Seismic refraction survey (a) ray paths, (b) graph of time versus distance of the first arrived signal (Hack, 2000).....	61
Figure 3-1: Particle size distribution of all the soils involved in this study (adopted from (Sadiq et al., 2016).....	75
Figure 3-2 Particle size distribution showing the steps of soil production (after (Sadiq et al., 2016).....	76
Figure 3-3: Compaction curve from which MDD and OMC was estimated.....	80
Figure 3-4: Mohr failure envelope.....	82
Figure 4-1: Volumetric water content (VWC) graph.....	95

Figure 4-2: Graph for material hydraulic conductivity	96
Figure 4-3: Analysis of various options of slope geometry (Continues overleaf).....	102
Figure 4-4: Analysis of various options of slope geometry (continued from the previous) ..	103
Figure 4-5: Comparing the two types of hydraulic boundary conditions	104
Figure 4-6: Comparing the flux boundary conditions.....	105
Figure 4-7: Model design.....	106
Figure 4-8 : Problem definition (a) For seepage analysis (b) For stress analysis	107
Figure 4-9: Flow vectors	109
Figure 4-10: The change of water level with time	109
Figure 4-11 Pore water distribution (a) Initial (b) Final	110
Figure 4-12 Comparison of stability analysis based on two different approaches	110
Figure 4-13: Stress changes with time (15-60mins)	111
Figure 4-14: Analysis results when constant hydraulic flux was applied.....	112
Figure 4-15: Analysis results when time step hydraulic flux was applied	112
Figure 4-16: Seepage and stability analysis with over design factor (ODF)	113
Figure 4-17: Change of FOS with time.....	114
Figure 5-1: 5TE sensor features (Decagon, 2015)	119
Figure 5-2: MPS6-6 sensor features (Deaagon 2015).....	121
Figure 5-3: Compaction curve	123
Figure 5-4: Homogeneity test with CBR mould.....	125
Figure 5-5: Infiltration test.....	126
Figure 5-6: Sensor insertion and water content measurement	129
Figure 5-7: Idealised measurement volume of 5TE sensor (Decagon, 2015).....	129
Figure 5-8: Stages in water content (VWC&GWC) measurements	130
Figure 5-9: Calibration function graph	131

Figure 5-10: Measured VWC versus GWC	133
Figure 5-11; Homogeneity test with sensor (a) Compacted sample, (b) Sealed sample with probe	134
Figure 5-12: The VWC measurements with 3 ports 5TE sensor	136
Figure 5-13: The volumetric water content measured with 5TE in the second experiment ..	137
Figure 5-14: Variation of electrical conductivity with water content.....	139
Figure 5-15: Variation of conductivity with water content	141
Figure 5-16: The prepared experimental tanks	142
Figure 5-17: Constructed slope model.....	143
Figure 5-18: Sampling for homogeneity test	143
Figure 5-19: Installed sensors	144
Figure 5-20: Experimental set-up	144
Figure 5-21: Slope dimension and instrumentation	145
Figure 5-22: Sensor measurement results	146
Figure 5-23: Stages of slope failure	147
Figure 5-24: (a) The dimension of experimental tank(b) Tank preparation	148
Figure 5-25: Depth of influence (dmax) and critical depth (dc).....	148
Figure 5-26: Critical and design depths	150
Figure 5-27: Compaction influence zones overlapping one another	151
Figure 5-28: Compaction impact diminishing with distance from the point of impact.....	151
Figure 5-29: The overlap of compaction energy waves and a less compacted peripheral flange	151
Figure 5-30: Stages involved in homogeneity test.....	152
Figure 5-31: Slope construction procedure.....	153
Figure 5-32: Burying MPS-6 sensors during slope construction.....	153

Figure 5-33: Completed slope (a) Installed 5TE sensors (b) Covered with Polythene sheet to minimise moisture loss	154
Figure 5-34: Picture showing supply and drainage chambers	154
Figure 5-35: Experimental set-up	155
Figure 5-36: Large slope dimension and instrumentation	155
Figure 5-37: Plan view and sensor locations	156
Figure 5-38: VWC and MS sensor measurements.....	157
Figure 5-39: Sensor measurements during water supply.....	158
Figure 5-40: The physical response to the flow of water.....	159
Figure 5-41: Photographs showing physical response of slope	160
Figure 5-42: Post failure shape	162
Figure 6-1: Experimental tank	166
Figure 6-2: The constructed slope in a braced transparent tank	167
Figure 6-3: The electrodes	169
Figure 6-4: Resistivity data acquisition meter (3d view). (Retrieved from http://www.allied-associates.co.uk on 2002/18)	169
Figure 6-5: Resistivity data acquisition meter (plan view). (Retrieved from http://www.allied-associates.co.uk on 20/02/18).....	170
Figure 6-6: Data acquisition connected systems.....	171
Figure 6-7: The installed electrical resistivity array	174
Figure 6-8: The installed electrical resistivity array (3D view).....	175
Figure 6-9: Flow meter Figure 6-10: Experimental set-up	176
Figure 6-11: The installed electrical resistivity array	177
Figure 6-12: Schematic sketch of slope dimension and instrumentation	177
Figure 6-13: 5TE and MPS-6 measurements.....	180

Figure 6-14: Sensor measurements during and after water supply	182
Figure 6-15: Slope physical deformation.....	183
Figure 6-16: Sensor measurements.....	185
Figure 6-17: Sensor measurement during and after water supply	186
Figure 6-18. Rise in ground water level.....	188
Figure 6-19: Visual observations with time.....	189
Figure 6-20: The initial physical response of the slope	190
Figure 6-21: The final physical response of the slope	190
Figure 6-22: Photographic picture of post-failure condition	191
Figure 6-23: Side view of post-failure condition.....	192
Figure 6-24: Sketch of slope with resistivity array arrangement.....	193
Figure 6-25: The resistivity survey results along the horizontal line before the water supply	194
Figure 6-26: The resistivity survey results along the central line before the water supply ...	195
Figure 6-27: The resistivity survey results along the side array line before the water supply	195
Figure 6-28: The change of resistivity during experiment along central line.....	196
Figure 6-29: The results showing the change of resistivity during the experiment along the side lineThe top two models are when the topography is applied whereas the bottom ones are without topography. From the comparison, bottom layer located in the middle with high resistivity values is partially displaced by the low resistivity portion that was initially at the crest location. At the toe, there isn't much change between the initial and later condition. The change is consistent with the one observed at the central survey line shown in Figure 6.29.	196
Figure 6-30: The change of resistivity result during the experiment along the horizontal survey line.....	197

Figure 6-31: Comparing the resistivity scan 2 along the side array line with camera captured photograph 200

Figure 6-32: Comparing the resistivity image of scan 3 along the central line with camera captured photograph..... 200

Figure 6-33: Comparing the resistivity image of scan 4 along the central line with camera captured photograph..... 201

List of Tables

Table 2-1: Triggers of slope failure	21
Table 2-2: Selected research works on tropical soil slope failures	31
Table 2-3: Characteristic electromagnetic properties of some materials (adopted from Hack, 2000)	57
Table 2-4: Summary of non-intrusive methods	63
Table 3-1: Tropical countries and the types of residual soil found in each country (Huat et al., 2007b)	66
Table 3-2: Soil properties previously considered in the production of artificial soil	69
Table 3-3: Geotechnical properties of three soils based on laboratory tests (adopted from (Sadiq et al., 2016)	70
Table 3-4: Oxide composition of lateritic soil from different parts of Nigeria	73
Table 3-5: Mineral composition of typical Nigerian lateritic soil (Ogunsanwo 1988, 1995)	74
Table 3-6: Mineral composition of Etruria Formation (Hutchinson et al. 1973, taken from (Sadiq et al., 2016)	74
Table 3-7: Coarse and fine fractions of the soils (Sadiq et al., 2016)	75
Table 3-8: Property comparison between the natural and artificially produced lateritic soils (after (Sadiq et al., 2016)	77
Table 3-9: Physical properties of laterite from different parts of Nigeria	77
Table 3-10: Index properties of laterite found in other parts of the world	78
Table 3-11: Permeability test result	81
Table 3-12: <i>In situ</i> and compacted permeability of some laterite soils (Nnadi, 1988)	81
Table 3-13: Shear strength parameters of some tropical soil around the world (Townsend, 1985)	83

Table 3-14: Effective strength parameters of laterite from different parent materials (Ogunsanwo, 1989).....	83
Table 4-1: Soil properties.....	99
Table 4-2: Experimental trials considered during numerical analysis.....	101
Table 5-1: Property of artificially produced residual tropical soil.....	118
Table 5-2 : 5TE sensor specification	119
Table 5-3: MPS-6 sensor specifications	121
Table 5-4: Homogeneity test result.....	125
Table 5-5: Results of permeability test	127
Table 5-6: Infiltration test results.....	127
Table 5-7: Table showing the calculated VWC and GWC values.....	130
Table 5-8: 5TE sensor measurements at different gravimetric water content	132
Table 5-9: Density and moisture distribution in the first experiment.....	135
Table 5-10: Determination of density and moisture distribution in the second experiment	136
Table 5-11. Variation of electrical conductivity with water content	139
Table 5-12: Variation of electrical conductivity with water content	140
Table 6-1: Analysis of array configurations	172
Table 6-2: Laboratory measurements and observations	178

CHAPTER ONE

1.1 Introduction

There has been a resurgence of interest in the widespread slope and embankment failures across the world due to an increase in their number and the need for remedial action to stabilise potentially unstable slopes/embankments (Donnelly et al., 2005, Shroder et al., 2005, Change et al., 2008, Dijkstra and Dixon, 2010, Winter et al., 2013).

In the UK alone, widespread failures of transport infrastructure embankments have been reported, particularly between the periods of 2000/2001 and 2007 (Dijkstra and Dixon, 2010). In England for example, the wet winter of 2000–2001, saw in excess of 30 earthworks' failures along the rail track in the southern region (Loveridge et al., 2010). During the same period, many failures have been experienced along Northern Ireland's road network (Hughes et al., 2007). Similarly, a series of landslides were experienced in August 2004 on the Scottish road network; critically, among them are the failures along the A83, A9 and A85 routes, which form a major part of the network (Winter et al., 2010a).

In the US, about 75 billion dollars was lost to this problem between 1997 and 2004, making it their most expensive natural hazard in this period (Shroder et al., 2005). Similarly, slope failures have been seen across the world, e.g. in Canada (Haug et al., 1977), Hong Kong (Pitts, 1983), Singapore (Pitts, 1983, Rahardjo et al., 2003), Kenya (Jackson et al., 2002), Spain (Quinn et al., 2007), Taiwan (Liu et al., 2012a) and Nigeria (Aghamelu and Okogbue, 2011, Tabwassah and Obiefuna, 2012).

In tropical regions slopes occur naturally or as man-made and are mostly made up of residual tropical red soils. Such soils have different physical and micro-structural properties compared to other types of soils due to the climatic, geological and geographical peculiarities (Styles et al., 2001, de Carvalho et al., 2015). Styles et al. (2001) divided the soil into two broad categories namely '*black*' and '*red*' tropical soils. In this study, we are only concerned about 'red' residual tropical soil. and is simply known as laterite in many parts of the world There are varied definitions of the term laterite but in this study, it is defined as soil material that is highly weathered, rich in secondary oxides of iron or silica or both. It is nearly void of bases and primary silicates, but it may contain a large amount of quartz and kaolinite. It is either hard or capable of hardening. Although some of these characteristics are possessed by some other soils, laterite is generally accepted as a name for a material whose composition and properties are within the limit described above (Alexander and Cady, 1962).

The term laterite was first used by to describe ferruginous, vesicular, unstratified and porous materials with yellow ochere from its iron content occurring abundantly in Malabar in India, It was locally used for building and hence the name Laterite from the Latin word 'later' meaning brick. (Awaisu, 1989). Its formation process involves chemical, physical and structural transformation. It starts with the chemical weathering of the parent rock insitu, followed by the leaching out of silica and bases (Gidigas, 1972, Gidigas, 1976).

Their peculiar mode of formation, the uniqueness of their properties, and low compliance to traditional soil mechanics' principles make tropical soils particularly challenging (Paige-Green et al., 2015). Previously, efforts to use the classical concept to describe and model tropical soils have proved unsuccessful due to the inability of classical theories to recognise some

unsaturated soil properties such as soil suction (Fredlund et al., 2012). This property is now understood to be responsible for the unusual behaviour of residual soils. The classical concept of soil mechanics is also unable to account for the weak bonding, wide varying void ratio and particle cementation existing in most residual tropical soils; thereby, making it inappropriate for residual soils (Vaughan et al., 1988). Due to its different mode of formation and the resulting unique engineering properties and performance, tropical residual soil needs to be studied separately. Assuming the two soils are the same and applying the findings on the studies on sedimentary deposits to the tropical soils could lead to significant errors (Vaughan, 1985).

Most of the failures cited are directly or indirectly caused by heavy rainfall causing water ingress into the slope leading to various degrees of instability (Pitts, 1983; Liu et al., 2012). Therefore, abnormal changes in water content within the soil are considered as one of the factors responsible for failure, although the actual failure process is still unclear. This is partially due to limited understanding of tropical soil behaviour and the associated slope failure mechanism (Fredlund and Rahardjo, 1993). Jackson et al. (2002) used electrical resistivity tomography (ERT) as a proxy for imaging moisture content changes of a road embankment made up of tropical red soil in western Kenya. The imaging capability and non-invasive nature of ERT was utilised to monitor the performance of engineered earthworks of the embankment over a period of 18 months. Due to this earlier successful experimentation employing ERT with tropical soils, the method together with electromagnetic (EM) sensors (i.e. 5TE and MPS-6) is used in this study to understand the failure mechanism of residual tropical soil. Thus, the focus of the research as presented in this thesis is to study hydrological changes within tropical slopes and how such changes are linked to the slopes' movement. The imaging capability of the

selected geophysical approaches is used to observe failure processes taking into account initial, pre-failure and ultimate failure conditions.

1.2 Background of the project

Although the increasing number of slope and embankment failures is a global problem, it has greater severity and devastation in tropical regions of developing countries, where tropical residual soil is the major construction material. In Nigeria, for example, between 2009 and 2012, several earth structures made up of red tropical soils failed (Aghamelu and Okogbue, 2011, Tabwassah and Obiefuna, 2012). In particular, the failures recorded in 2012 were attributed to heavy rainfall events, which led to flooding in many parts of the country. As a consequence, 363 lives were lost, 5,851 people were injured, 3,871,530 people were displaced, and properties were lost. According to the NEMA-Report (2012), the total loss recorded during the period was 16.9 billion US dollars, including 9.5 billion US dollars for the cost of the physical damage to the infrastructure. This infrastructure damage was mainly due to the failure of different kinds of slope-related earth structures (e.g. dams and embankments). Factors such as ground water condition, material properties and slope angle, influence slope stability. Climate change has been recently added to the list of factors (Dixon et al., 2006, Hughes et al., 2009). Climate change is predicted to increase in the next 100 years (UNISDR, 2008) and is likely to adversely affect slope stability considerably (Jackson, 2013). The implication of this, if no appropriate action is taken, more catastrophic failures are likely to be experienced in the future. The combination of high impact, low adaptive capacity, weak institutions and poverty (UNISDR, 2008), worsen the condition in Africa. In view of the above, there is a need to investigate the failure mechanism of soil slopes as it relates to their hydrological changes.

1.3 Statement of the problem

Recently, there has been increasing interest in the study of the cause, effect and possible solutions to slope failure worldwide (Tohari et al., 2000, P. Orense et al., 2004, Rouainia et al., 2009, Oh and Vanapalli, 2010, Davies, 2011, Davies et al., 2014, Hughes et al., 2015). For instance, in Nanyang Technological University (NTU), over 46 cases of slope failure of varying magnitude were recorded in November 1982, following an extreme rain event (Pitts, 1983); resulting in much research activity with many subsequent publications (Pitts, 1983, Rahardjo et al., 2001, Rahardjo et al., 2003, Rahardjo et al., 2007, Tsaparas et al., 2002, Tsaparas et al., 2003, Toll, 2001, Rahardjo et al., 2014). Similar studies have also been conducted elsewhere (Ng and Shi, 1998, Zhang et al., 2000, Muntohar and Liao, 2009, Liu et al., 2012a). However, many of these studies are purely numerical or parametric. Although useful, the numerical or parametric studies alone do not give detailed information about slope failure mechanisms. For instance, conventional calculation methods such as the limit equilibrium method used in numerical or parametric studies are not able to account for the transition from peak to residual strengths; thereby providing inaccurate information about slope stability (Gilbert et al., 1996). Some of the experimental studies used simple instruments like piezometers and tensiometers to measure groundwater and soil suction, respectively. Such instruments can only take point measurements which is possible only at discrete times. This kind of study makes it difficult to observe the process of a continuous and progressive form of failure (Fell et al., 2000).

To remedy the deficiencies of simple tools and traditional measuring techniques, non-invasive geophysical methods have been employed in similar studies in many parts of the developed world. These include, but are not limited to acoustic emission (AE) as used by Koerner et al. (1981), Jurich and Miller (1987), Kousteni et al. (1999), Shiotani et al. (2001), Dixon et al.

(2003), Dixon and Spriggs (2007) and Dixon et al. (2010); and electrical resistivity tomography (ERT) popularly used in the UK (Jackson et al., 2006, Chambers et al., 2007, Jackson et al., 2002, Chambers et al., 2008, Sellers et al., 2010, Chambers et al., 2014). Similarly, ground penetrating radar (GPR) was used in the ground investigation of all kinds of slope stability (Do, 2003, Evans et al., 2006a, Evans et al., 2006b). These methods have been found to be very efficient but were mainly applied to soils in temperate climates. To date, little or no effort has been made to apply these geophysical techniques to study the failure mechanism of residual tropical soil slopes.

Tropical soils have different properties from other types of soils due to their climate, geological and geographical factors. Therefore, findings from research conducted on soils from the temperate climates cannot be applied to tropical soils without verification as this could lead to significant errors (Vaughan, 1985). This can occur because classical theories developed through the studies of sedimentary deposits have failed to address some concepts associated with soils formed under the subtropical and tropical environment (Gidigas, 1988, Fredlund and Rahardjo, 1993, Barbour, 1998). To this end, this research seeks to answer the following questions.

- i. Can geophysical techniques used in the study and the monitoring of failures in the soils of the temperate climates be used for a similar purpose with tropical soils?
- ii. What is the failure mechanism(s) of tropical soil slopes and how can geophysical studies help in understanding the failure mechanism?
- iii. How does our understanding of the failure mechanism based on the findings of this research, help in tackling the catastrophic failures currently experienced in tropical regions?

1.4 Aim and objectives

The aim of the research is to investigate the suitability of geophysical methods to monitor slope failure in residual tropical soils; and furthermore, to determine the mechanisms leading to failure of slopes formed in tropical soils.

The research aim would be achieved through the following objectives.

1. Undertake a review of pertinent literature to establish the current understanding of slope failure mechanisms in tropical soils and methods used to assess this.
2. Produce an artificial soil to be used in the study that has physical, chemical and geotechnical similarities to the reddish-brown residual tropical soil; and so, provide a repeatable consistent proxy for naturally occurring tropical residual soils.
3. Conduct feasibility studies to determine the suitability of the material and the geophysical methods (electromagnetic sensors and electrical resistivity method) proposed to be used in the research.
4. Use numerical modelling tools to aid the analysis and design of the physical model that will be used in the experimental study.
5. Construct a laboratory scale physical slope model and use geophysical methods to study geotechnical and geophysical changes associated with failure development.
6. Analyse and interpret the results to determine the various mechanisms that lead to the ultimate failure of a tropical soil slope.

1.5 Brief research methodology

The methodology for conducting this research involves experimental study supported by numerical modelling. The study began by face-to-face consultation with experts in the field and studying the relevant literature before developing a comprehensive research plan. The preliminary studies, numerical modelling and trial experiments were conducted before the main experiment. The preliminary study on soil properties, led to the evolution of a method that was used to produce a synthetic tropical soil used in this study. Details of this, has been presented in chapter 3. During the numerical modelling, a software package comprising of SLOPE/W, SEEP/W and SIGMA/W, developed by Geo-studio Ltd was used to analyze a tropical soil slope model. The numerical modelling exercise discussed in chapter 4, served as useful aid in designing the experimental model. Before conducting the main laboratory experiment, series of feasibility studies and trial tests were conducted to determine the suitability of the chosen method, material and instrumentation for the proposed experiment. The feasibility studies and laboratory trial tests are described under physical modelling in chapter 5. Finally, the main experimental study was conducted on a physical model that is made up of compacted layers of synthetic residual tropical soil and subjected to a hydraulic boundary condition that made it fail. The failure process was monitored with combined geophysical techniques (EM sensors and ERT). The parameters monitored include soil suctions, volumetric water content, soil temperature, flow rate, embankment deformation and slope movement. Detailed description of the final experiment is given in chapter 6. Figure 1.1 is a flowchart summarizing the research methodology and how the stages of the methodology were used to achieve the research objectives.

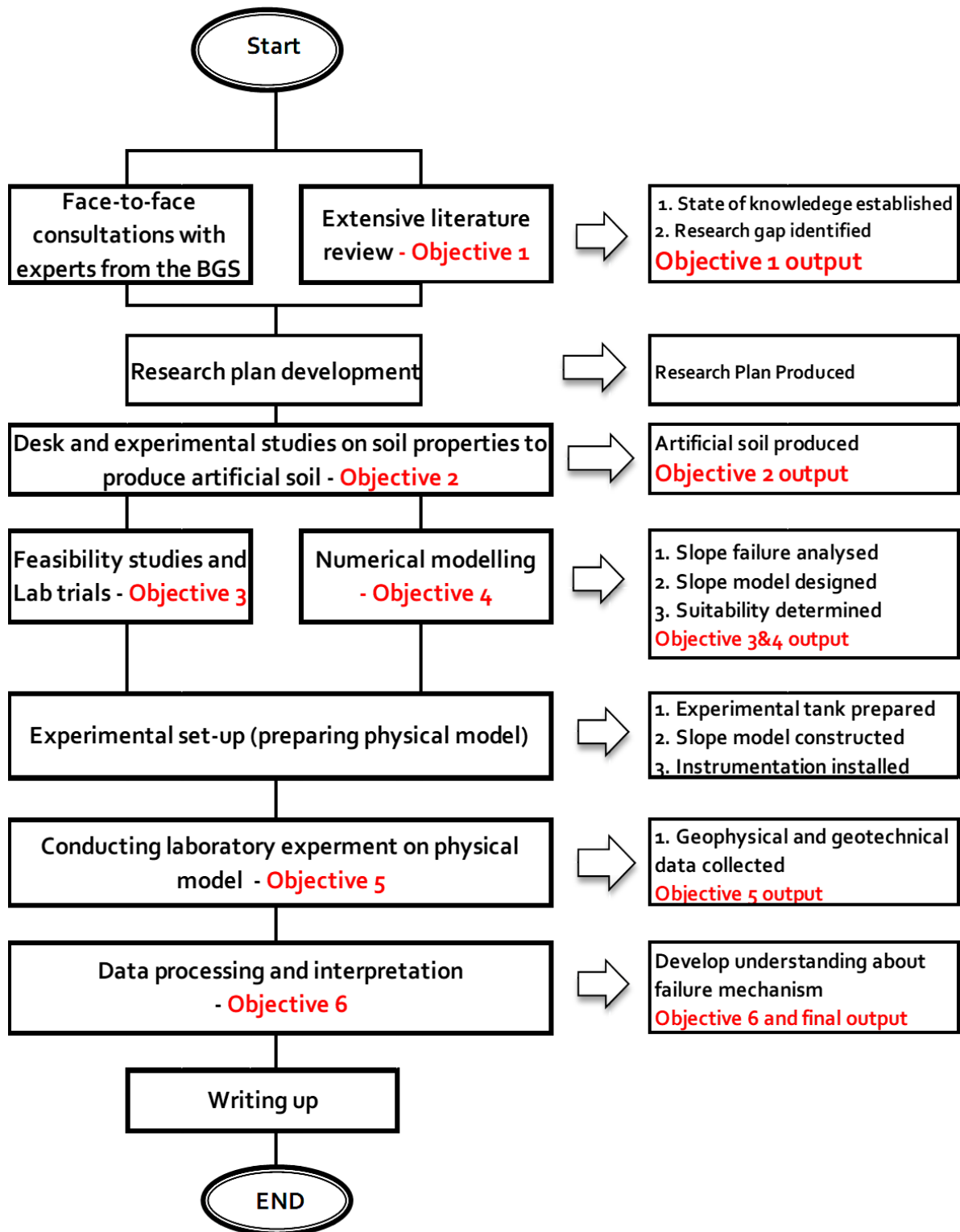


Figure 1.1. Research flow chart

1.6 Contribution to knowledge

Combined geophysical techniques including electromagnetic (EM) sensors and electrical resistivity tomography (ERT) have been used in this research to determine both pre and failure mechanisms of residual tropical soil. The study has allowed a more in-depth assessment of the processes involved in failure development, from equilibrium through pre-failure and ultimate failure conditions. The use of this kind of integrated geophysical/geotechnical method to monitor the pre and failure processes of residual tropical soil as they occur in real-time has not been conducted previous to this study. The contribution of the study includes:

1. An improved understanding of both pre and failure mechanisms for embankment slopes made from tropical soils; which is an important requirement for effective stability assessment and monitoring.
2. Utilising the capability of combining geophysical techniques to diagnose embankment stability conditions and predict failure development. For example, the use of ERT to establish weak regions within the slope at the initial stage assists in the prediction of future failure. It is interesting to note that the zones of weakness established previously were where the subsequent failures occurred.
3. The EM sensors used in the experiment have demonstrated their ability to detect time-dependent hydrological changes at the initial stage before they manifest as physical failures. This ability has confirmed their potential to provide a warning signal that can prompt some action to prevent catastrophe.

1.7 Thesis structure

The thesis presented here is divided into eight chapters. These include the introductory part as presented in this chapter and the subsequent chapters are introduced as follows.

Chapter 1 gives the general background, aim and objectives of the research. It also raised fundamental questions that the research seeks to address.

Chapter 2 reviews the existing body of literature with a view to understand the current state of knowledge and identify the existing gap therein. A general overview of slope stability, factors affecting slope stability and the slope failure mechanism are reviewed in this chapter.

Chapter 3 contains the preliminary soil studies that led to the evolution of the novel methodology for the production of artificial tropical soil used in the research. In the chapter, the relevant index and geotechnical soil properties are established.

In **Chapter 4**, the numerical simulations and modelling element of the research are presented. The simulations and models obtained are used to aid the design of the experimental set-up.

Chapter 5 describes the necessary steps taken and the detailed procedure followed to arrive at the physical model used in the experimental study and also the results obtained in that process are presented in the chapter.

Chapter 6 presents a more detailed and final experimental study, conducted using electromagnetic sensors and electrical resistivity tomography.

In **Chapter 7** the results obtained at various stages are interpreted and discussed.

General conclusions drawn from the entire research are presented in **Chapter 8**. The recommendations for future works are also contained in this chapter.

1.8 Chapter summary

In this chapter, a general overview of the problem that prompted the study of the failure mechanism of tropical residual soil using geophysical techniques was presented. This includes general and specific cases of embankment failures and their attendant consequences mostly in tropical areas. Relevant literature outlining previous works has been presented mainly in section 1.2. The works can be categorised into two groups. The first category is the group of studies on tropical soil using simple, traditional geotechnical tools. The second category presents the works carried out on the soils of temperate climates using modern geophysical techniques. Therefore, the need to study the failure mechanism of residual soil slope has been established. . The distinction between tropical soil and the soils of temperate climates as postulated by many scholars, the shortcomings of the traditional geotechnical tools as pointed out in the copious literature, and the need to tackle the widespread and catastrophic failure in tropical regions, are the combined factors that justify the conduct of this research. The aim and objectives, as well as the summarised methodology, have been outlined in this chapter.

CHAPTER TWO

LITERATURE REVIEW

2.1 Introduction

An increase in the world's population has resulted in a greater demand for slope-related engineering facilities (e.g. road and railway embankments) and a corresponding growth in their construction (Abramson, 2002, Ashour and Ardalán, 2010). However, the methods used by the relevant authorities to provide these facilities have met with the challenges of recent widespread embankment failures. Over the last few years, a number of embankment failures have been recorded in the UK, the US and across Africa (Donnelly et al., 2005, Shroder et al., 2005, Change et al., 2008, Dijkstra and Dixon, 2010, Winter et al., 2010b).

The increase in embankment failures is disturbing, considering the catastrophic nature of some of these failures and their associated negative consequences to the socio-economic life of the people. To give a picture of the problem, Shroder et al. (2005) reported as follows. *“Ground failure is the most expensive natural hazard in the United States”. “Between 1925 and 1975, U.S. national losses as a result of ground failure amounted to \$75 billion (not adjusted for inflation or depreciation) and were >\$2 billion annually (Schuster, 1996). In dollar equivalents, ground failure costs Japan ~\$1.5 billion annually, and Italy \$1.1 billion per year (Alexander, 1989). In the United States alone, some 25 to 50 people die each year as a result of slope failure (Schuster, 1996) Page 217-.”.*

While most of the recorded failed slopes in the humid climates are made up of sedimentary deposits, in tropical regions, natural and man-made slopes are mostly made up of residual tropical red soil. The soil is often referred to as 'laterites' or 'lateritic soils' and has good and unique engineering properties, such as an open structure, cementation of soil particles and high shear strength, but low compliance to the traditional soil mechanics' principles (Paige-Green et al., 2015).

Due to the increasing number of these failures and the associated high socio-economic cost, the international interest in slope failures has increase (Schuster, 1996) globally. The topic has been receiving attention among researchers within and from outside the geotechnical community, particularly in the 20th century (Shroder et al., 2005; Egeli and Pulat, 2011).

As a result, the traditional causes of instability, such as pore water pressures, have been fairly well understood; while emerging causes such as climate change effects are continuously under experimental study. Similarly, several corrective measures to be taken on the failed or failing slope, such as soil nailing and other types of reinforcements, have been identified.

Glendinning et al. (2009a), divided slope failures into serviceable (within the serviceability limit state) and ultimate (reaching an ultimate limit state) failures. In the limit state failure, appropriate stabilisation measures can be taken to control it before it reaches an ultimate or catastrophic failure. The measure taken may be to restore the failed or failing structure to its original or near original condition, so as it is able to function as desired. On the other hand, with ultimate failure or a collapsed infrastructure, it cannot be restored by remedial works but requires reconstruction with huge financial implications.

Although knowledge of the causes of the problem and the corrective measures to be taken as identified above are important, preventive action is the most effective way of tackling this problem. This agrees with the wise saying ‘prevention is better than cure’. The identified ways of preventing slope failure are through periodic assessment and constant monitoring using modern geophysical and remote sensing techniques (e.g. ERT, GPR and LIDAR).

Stability assessment involves continuous planned cycles of inspection, monitoring and analysis aimed at identifying any serviceable failure or sign of failure. This information enables appropriate remedial action to be taken to avoid catastrophe. It also enables the programme for maintenance and improvement to be designed and implemented to ensure a sustainable stability of the assets, despite increasing traffic, environmental impacts and an increasing threat from climate change (Glendenning et al., 2009a).

In this chapter, various methods and techniques used for slope assessment and monitoring are discussed. The methods include both the traditional geotechnical investigations and the modern geophysical survey based on sensing technologies.

In monitoring slope failure or stability, there is a need for a proper understanding of the failure process. For this reason, a number of research efforts have been carried out in many parts of the world (Tohari et al., 2000, P. Orense et al., 2004, Rouainia et al., 2009, Oh and Vanapalli, 2010, Davies, 2011, Davies et al., 2014, Hughes et al., 2015). In section 2.2 of this chapter, an attempt is made to review the existing literature relevant to slope stability and factors affecting it. This is followed by a review of slope failure and the failure mechanism in section 2.3. Section 2.4 deals with various ways of monitoring slope stability or failure processes, with

emphasis on non-intrusive geophysical methods. The last part of the chapter presents valid reasons why there is need to use geophysical methods to study failure mechanisms of tropical residual soils, as presented in section 2.5. The previous efforts in that direction have been reported and the areas that need further development have been identified.

2.2 Slope

The ground surface is formed of hills, rivers and drainage systems, occurring either naturally or man-made. Such features existing on the earth surface rising above or lowered below the horizontal plane of the earth to form an angle are referred to as slopes. It could be fill such as embankment or cut such as excavation for foundation.

2.2.1 Slope stability.

Slope stability analysis is an important topic in geotechnical engineering and is essential in the design and construction of slope-related civil infrastructure such as embankments. Slopes need to be stable for safety and functionality. Stability analysis is necessary to determine whether a slope is safe and if not, decide the suitable stabilization measure (Liu et al., 2012b). A slope is considered stable if it satisfies its intended need and has a suitable factor of safety (Cernica, 1995). The factor of safety is the ratio of forces resisting movement to those disturbing it. Water pressures and gravitational forces are the main disturbing forces. While the slope material strength and geometry determined its ability to resist movement.

2.2.2 Factors affecting slope stability.

The stability of a slope whether natural or engineered is dependent on a variety of factors. These factors include geometry, geology, material properties and groundwater conditions. In this section, effort is made to explain how slope stability is affected by these factors.

Soil consists of particles and voids, with the voids being filled with water and air. The study of soil slopes particularly concerns negative pore water pressure that occurs when air pressure is zero, resulting in an increase in soil shear strength and stability (Zhu et al., 2012). An increase in the water in the soil raises pore water pressure (i.e. the negative pore water pressure becomes positive) causing a decrease of shear strength and consequent slope failure. Failures caused by water conditions have been divided into two categories by Winter et al. (2007). These include rainfall or overland flow that infiltrates into a potentially mobile soil, and the water that remains within the soil causing pore water pressure to build. Both can lead to a sufficient decrease in shear strength and possible slope movement.

The presence of old slips' surfaces that resulted from tectonic activities or previous landslides can develop zones where the shearing strength is at a residual state due to the prior movement, leading to the slide resistance reaching its peak value (Abramson, 2002).

Slope geometry is another factor that influences its stability. As the angle of a slope increases, its stability decreases. The steepness of a slope has a negative effect on its stability (Liu and Deng, 2011, Winter et al., 2007). The steeper the slope, the less stable it is. In a high steep slope, slope movement can easily be triggered by ground water change or human activities such as excavation at the toe.

Stability analysis in a natural slope is most difficult and uncertain since these slips are not easily identifiable. However, in an engineered slope, the material used in the construction is well known and therefore more predictable than in a natural slope.

2.2.3 Impact of climate change on slope stability

‘Global warming’ and ‘climate change’ are some of the terms used to describe changes or anomalies in the atmosphere. Their occurrence and attendant consequences on human life have recently been the subject of discussion by stakeholders (mentioned in the next paragraph) globally. The literature has confirmed that there has always been change in the world’s climate but the rate at which it has rapidly altered in recent years is creating a serious cause for concern (Change et al., 2008, Reduction, 2008). This unusual anomaly and its potential impact on the quality of life has been predicted to increase in the next 100 years (Dixon et al., 2006) and will affect various sectors of human life, slope stability inclusive (Dijkstra and Dixon, 2010).

In the UK, the potential impact of climate change on slopes has been debated in a series of workshops by individuals and corporate bodies, or in projects such as CLIFFS (Climate Impact Forecasting For Slopes) and the UKCIP (United Kingdom Climate Impact Panel) (Dijkstra and Dixon, 2010). The general consensus is that the parameters that determine slope stability would surely be affected by the climate change; and failure to take action is risky (Winter et al., 2010b).

Having reached this consensus, the question remains, how does it affect them? An attempt is made to answer this question in the following paragraph.

It can be understood that changes in world temperature and rainfall will surely affect the stability of slopes, either positively or negatively. For example, an increase in rainfall can promote the growth of vegetation which prevents erosion and stabilises soil by reinforcement with its growing root (Glendinning et al., 2009b). On the other hand, excess rainfall is capable

of mobilizing a weak deposit through infiltration or causing an increase in pore water pressure that may lead to failure (Winter et al., 2013).

The groundwater regime is another factor influencing slope stability and its magnitude and distribution is highly dependent upon climate. The UK has experienced many failures in transport embankments recently, particularly during the large amount of rainfall received in 2000/2001 and August 2004 (Dijkstra and Dixon, 2010). The rainfall received in August 2004 in some areas of Scotland is more than 300% of the usual average August rainfall and has affected part of the Scottish road network causing significant impact on the socio-economic life of the people (Winter et al., 2013). These failures are attributed to the repeated shrink-swell process in response to cyclic pore pressure changes, driven by moisture variations which cause strain-softening and the development of weak zones leading to shear failure (Dijkstra and Dixon (2010). Many parts of the world have their share of the problem including the US (Change et al., 2008).

Considering the predicted scenario of an increase in this global anomaly and the consensus opinion on its potential impact on slope stability, climate change should not be underestimated in slope stability assessment.

2.3 Slope failure mechanism

Natural and human activities have been responsible for disrupting the balance of natural and man-made slopes. In this section, various forms of slope failure will be discussed. Due to the hazards to life and property, as well as the economic consequences associated with slope failure, there is a need for a precise description of its failure mechanism.

Generally speaking, slope failures occur gradually, due to the agents and processes discussed previously; or suddenly, when caused by some triggers. A good understanding of the means by which slope failure occurs (failure mechanism) has important implications in determining the trigger (Owen et al., 2011). Changes in stress, groundwater flows and strength due to either cyclic increase in pore fluid pressure or high-intensity rainfall can trigger a slope failure (Egeli and Pulat, 2011).

Natural phenomena such as earthquakes, flooding and rapid drawdown due to a change in climate or any other causes can trigger slope failure. In fact, earthquakes and rainstorms individually are identified as major triggers (Wieczorek and Jäger, 1996).

There is a varied understanding of the triggering mechanisms of slope instability, but it is commonly known that an external stimulus initiates or accelerates the failure process (Sultan et al., 2004). The triggers most commonly identified have been summarised in Table 2-1. Effective assessment and monitoring of slope failure depends on the proper understanding of the development of the failure. The wrong assumption of the failure process may lead to incorrect or wrong conclusions with attendant consequences. For example, impending failure signs may be ignorantly allowed to degenerate into catastrophe as they are thought not to be associated with the developing failure (Quinn et al., 2007). Slope failure takes different modes some of which are identified and discussed in this section.

Table 2-1: Triggers of slope failure

S/No	Trigger	Failure Mechanism
1	Earthquake	Exposing loose, saturated granular slope material to strong earthquake ground shaking caused the grains to compact, squeeze together and occupy less space. Since the process occurs rapidly, the time is too short to drain water; there is a decrease in the effective, confining stress and the consequent increase of pore water pressure.
2	Water condition	Infiltration of high-intensity rainfall or rapid melting of snow pack increases the level of groundwater, which causes the pore water pressure to build up.
3	Freeze-Thaw conditions	Freezing of water in the soil can block the pores or voids and results in the build-up of cleft pressure and triggering of slope movement.
4	Human activities	Excavation at the slope, its toe or along the orientation parallel to the bed of the rock slope can cause downward movement by sliding. Other human triggering activities include loading of a slope, mining, drawdown in a reservoir and artificial vibrations due to machines working at, or near the site; or other works involving blasting.

2.3.1 Progressive failure

Like many engineering infrastructures, slopes undergo gradual loss of strength in consequence of ageing, adverse weather conditions or due to creep and fatigue. Depending on the slope material, the gradual loss of strength could progress continuously in the sequence shown in Figure 2-1, until final ultimate failure occurs. The gradual building of high stress and loss of strength in slopes is known as a progressive failure, as discovered by Bjerrum (1967). Bjerrum observed that some cohesive materials undergo deformation through a gradual strength transition from the peak to residual state (Petley et al., 2005). The failure mechanism has been summarised as follows, based on the work of Gilbert et al. (1996) and Fell et al. (2000).

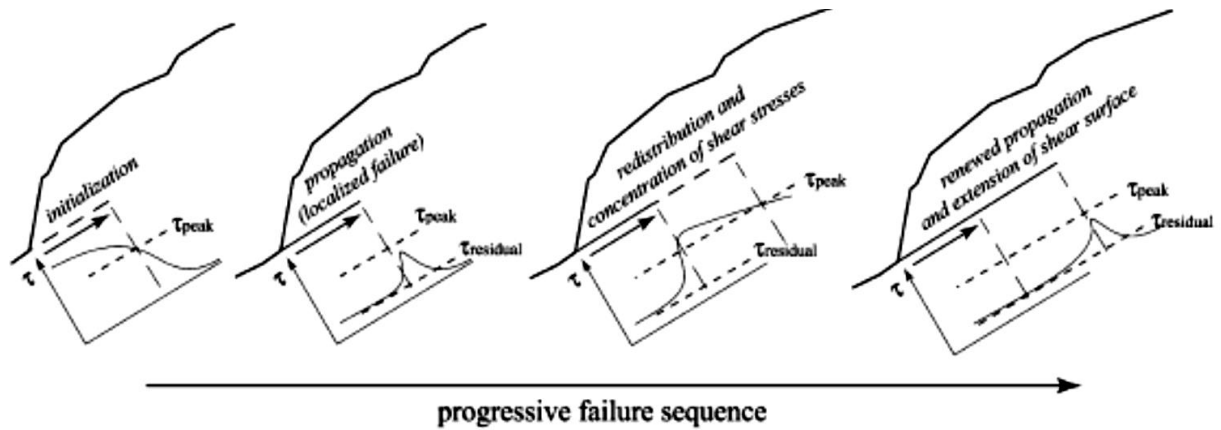


Figure 2-1: Sequence of progressive failure development (After Bjerrum, 1967)

In strain-weakening soil, the failed elements of soil support decrease the shear stress as the strain increases. When there is part of the stress that may not be supported by the failed element, this is then transferred to the neighbouring stable soil element, making it fail in turn. This process is shown in Figure 2-2, and it continues until equilibrium is reached between shear stress and the strain in the soil. Otherwise, the process continues until the failure condition is extended to the entire failure surface. The final shear failure occurs after the shear surface is fully formed.

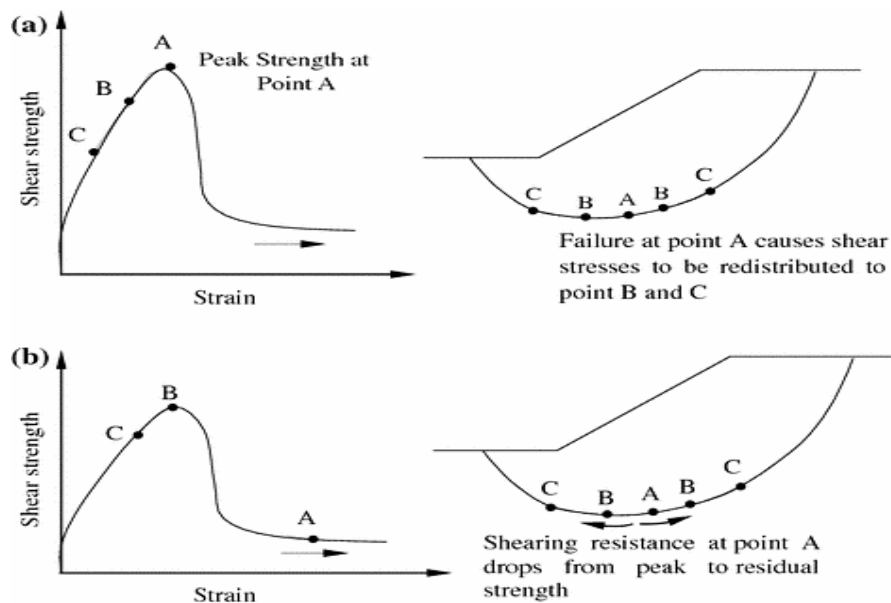


Figure 2-2: Graphical representation of progressive failure development in slope (Pathak et al., 2008)

Progressive slope failure occurs in many strain-softening materials (e.g. clay), but the failure process is dependent on the nature of the material (Fell et al., 2000). Human activities mentioned in Table 2.1 can initiate a failure making it to continue in a progressive manner. This failure process has been studied using analytical modelling and the study confirmed that this progressive strain-softening behaviour is capable of causing shear failure in slope (Gilbert et al., 1996).

Law and Lumb (1978), tried to analyse progressive failure using the limit equilibrium method. Although the study recorded considerable success towards an understanding of the process, there were oversimplifying assumptions. This includes assuming the presence of post-peak strength anytime a local failure occurs. This is not always the case. The use of the limit equilibrium method has been criticized for its inability to account for the transition from peak to residual strengths, thereby providing misleading information about slope stability. According to Gilbert et al. (1996), the key principle of the method is establishing an interface where the limiting shear resistance and the required shear resistance maintain equilibrium; this is difficult to achieve in strain-weakening soil. Gilbert et al. (1996) further stated that assuming the availability of peak strength along the entire failure surface could be unsafe and it is excessively conservative to assume only residual strength is at the surface.

Although some attempts have been made to understand progressive slope failure, its effect on slope stability needs to be fully understood. A proper understanding of its concept, recognising its contribution to slope failure, and devising an alternative to the current traditional means of monitoring will go a long way in tackling the problem of slope failures.

2.3.2 Retrogressive failure Mechanism

Retrogressive failure as described by Wang et al. (2016), is a kind of dynamic process in slope failure development, where the initial slide and the material in the failure flow away in a block. Usually, due to the high degree of strength loss, the support of the remaining soil body is removed, resulting in another failure similar to the previous one. This process repeats itself in a multiple-retrogressive manner and can result in a bigger failure. Retrogressive failures are mostly experienced in sensitive clay and tend to occur very rapidly; but the theories regarding their mechanics are not well developed (Quinn et al., 2007)

Bjerrum (1955) used the retrogressive failure mechanism to describe the series of slumps observed in a failed slope of Norwegian quick clays. He described the failure as been “characterised by their retrogressive course, an initial slide followed by a series of slides in the rear areas”.

Haug et al. (1977) studied landslides that occurred near the east bank of the South Saskatchewan River in Saskatoon, Canada. In this study, the University of Saskatchewan's slope software was used to analyse the failure slides with the simplified Bishop method. At the end of the analysis, it was concluded that the hypothesis of a retrogressive mechanism is valid and can best describe the failure at the site under study.

In the most recent study, Wang et al. (2016) used a numerical framework to study and demonstrate the retrogressive slope failure mechanism and this is described using Figure 4. In the figure, the material points location indicates the displaced soil while the coloured contours represent the accumulated plastic shear strain. The factor of safety of the slope is 0.96. This

has been determined separately using the strength reduction method. The analysis of the slope was done by applying gravity to enable the soil's *in situ* stresses (due to self-weight) to be generated. The self-weight triggers the slope failure as the initially unstable slope is considered.

Fig. 2-3(a) shows the initial band of plastic shear strains indicating the initiation of the failure from the slope toe. Then, the band propagates backwards and upwards, soon forming a complete slip surface; this is shown in Fig. 2-3(b), which occurred 2.5 seconds from the commencement. Thereafter, the sliding of the soil body above the critical slip surface starts along the surface, and the second slip plane, also originating from the slope base, starts to form a second failure block. The remaining slope body remains largely intact (elastic). Fig. 2-3(c) shows that the sliding soil moves in blocks in a discrete form. The formation of soil wedges with shapes of graben and horst is shown in Fig. 2-3(d); it is the conceptual model explaining the mechanism of retrogressive failure. The movement continues backwards and upwards in retrogression. After about 41 s the exposed back scarp at the rear of the second slide becomes large enough so that as a result of the removal of the down-slope support, it causes destabilisation and triggers the third slide, as shown in Fig. 2-3(e). Unlike the previous slide, the current block of almost intact clay moves laterally on the horizontal plane. Fig. 2-3(f) shows the displacement of the final stable section indicating the final stage of failure which occurred at the time of 73.5s. From this study, it can be observed that there is an increase in the time interval between successive slides as the failure propagates backwards.

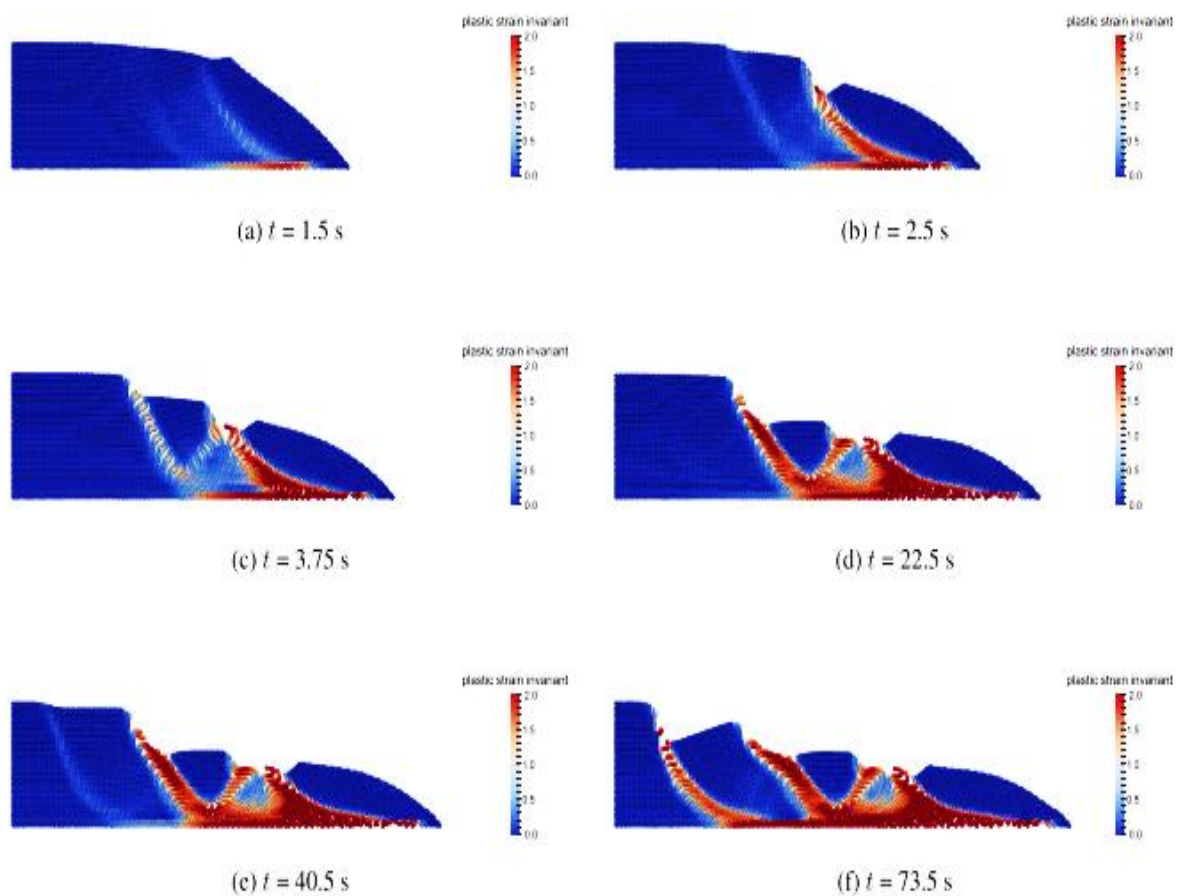


Figure 2-3: Failure mechanism in soft clayey slope (Wang et. al., 2016)

2.3.3 Collapse failure Mechanism

Collapse mechanism is another type of failure process experienced by some types of soils. Many scholars have tried to define or describe collapsible soils or the collapse failure phenomenon, but the following is the description given by Schwartz (1985).

“...a soil which can withstand relatively large imposed stresses with small settlements at a low in situ moisture content but will exhibit a decrease in volume and associated settlement (which could be in large magnitude) with no increase in the applied stress if wetting up occurs.”

From separate studies conducted by (Barden et al., 1973) and (Rogers, 1995), the factors responsible for a collapse failure can be itemised as follows:

1. An open soil structures.
2. A high void ratio
3. A low dry density
4. A high porosity
5. High enough value of applied stress to develop a metastable condition
6. High enough value of soil suction to stabilize intergranular contacts and whose reduction on wetting will lead to collapse.
7. Geologically young or recently altered deposit
8. High sensitivity
9. Low inter-particle bond strength.

The first four factors describe the material that has the ability to permit the flow of fluid through it and can rearrange itself structurally with a consequent reduction in volume.

From the foregoing discussion, it can be deduced that when a partially saturated soil with collapsible fabric experiences an increase in moisture content and is subjected to an applied stress greater than the overburden pressure, the collapse will take place. The main trigger in this type of failure is water condition and has been explained in Table 2.1.

There is very limited information about the collapsible nature of residual tropical soils but considering the fact that most of the properties listed above, are exhibited by some residual tropical soils, makes collapse behaviour a likely property of these types of soils.

Brink (2012) listed South African tropical soils among the collapsible soils. The soil is derived from the granite of the basement complex by weathering. His description of the mode of formation and its chemical composition shows that it is similar to the lateritic soil found in many parts of the tropics.

2.4 Slope Failure in Residual Tropical Soils

Just like slopes of other soil types, there are several reported cases of soil slope failures in tropical soils. The following are few examples.

Liu et al. (2012a) reported a serious slope failure of the Ali Mountain Highway (route T18) in southern Taiwan. The failure occurred following the strike of Typhoon Morakot on August 8, 2009. The route had to be closed to traffic over a period of three months to allow temporary rehabilitation to be carried out. A post event site investigation conducted through extensive field surveys and aerial photo analysis, revealed that, the exposed parts of the rocks are made up of various sizes of yellow brownish sandstone occasionally interbedded with mudstone and have weak cementation of stone particles. Although, geological terms were predominantly used to describe to characterise site, it can be deduced from the description that the failed slopes were made up of either yellowish brown particles mixed with boulders (colluvium) or highly weathered sedimentary rocks resulting in the superficial sliding of the residual soils.

In Hong Kong, the problem of slope failures is very serious and the severity is far more than that of Singapore, although more failures have been recorded in Singapore (Pitts, 1983). Ng and Shi (1998) adopted a typical unsaturated cut slope in Hong Kong in a study to investigate

the effect of various rainfall events and initial ground conditions on slope stability. In this study the geology of Hong Kong has been described as consisting of granitic, volcanic and sedimentary rocks which undergo chemical and physical weathering processes resulting in the formation of saprolitic and residual soils.

In Nan yang Technological University (NTU) alone, The large number recorded is probably due to the topography and geology of the area, which consists of a series of hills and valleys located on the decomposed sedimentary rocks of the Jurong formation (Pitts, 1983, Rahardjo et al., 2003).

In Africa, vertical and lateral deformations were observed on a tropical soil embankment of a Kenyan road. Failure occurred at the edge of the carriageway, close to the shoulder and manifested on the pavement surface in the form of large longitudinal cracks (Jackson et al., 2002)

In Nigeria, there are many recent cases of dam and highway embankment failures reported from many parts of the country (Aghamelu and Okogbue, 2011, Tabwassah and Obiefuna, 2012). Personal experience and eye-witness accounts confirmed that the failure of the road embankment along Kaduna-Birnin Gwari Road in north-western Nigeria in 2009, is the most serious failure recorded in the region in recent years. Since then, more embankment failures have been experienced in the area. Although the number of tropical soil embankment failures is increasing the effort to tackle it through effective monitoring and in-depth study of the failure process is minimal.

The large number of failures experienced at NTU in Singapore has opened a window for research and many attempts have been made to study the failures (Pitts, 1983, Rahardjo et al., 2001, Rahardjo et al., 2003, Rahardjo et al., 2007, Tsaparas et al., 2002, Tsaparas et al., 2003, Toll, 2001, Rahardjo et al., 2014). There are also some similar studies conducted elsewhere (Ng and Shi, 1998, Zhang et al., 2000, Muntohar and Liao, 2009, Liu et al., 2012a). However, some of these studies are numerical or parametric studies as shown in Table 2-2. Even the experimental studies, used simple instruments like piezometers and tensiometers to measure groundwater and soil suction, respectively. These instruments take point measurements at certain intervals by intruding into or probing the parent material. Apart from the disturbance or distortion brought about by the intrusion, the point measurements do not give detailed information about the ground conditions.

Non-invasive geophysical methods are the most appropriate and have been tried in the monitoring and studying of embankment failures of the temperate climates, with great success. Little effort has been made to apply these techniques to monitor and aid understanding of the failure process of tropical soil embankments. For example, Jackson et al. (2002) have illustrated the use of ERT on a road embankment constructed of tropical red soil in western Kenya. The survey, which was conducted at KM19+300 along Molo-Oleuguru Road in Kenya, took 18 months to complete and 40 electrodes, spaced equally at 1 m intervals, were used. The moisture variation within the embankment was studied and a meaningful result was obtained. Based on the results, it was concluded that the technique could be used to monitor the stability of tropical soil embankments. Although this singular trial on the tropical soil embankment was successful in assessing the moisture variation, it was not able to study the failure mechanism as this was not the objective of the experiment. Therefore, a geophysical survey on a real-time

Table 2-2: Selected research works on tropical soil slope failures

S/No	Reference	Study Area	Research Summary	Methodology	Instrumentation
1	Pitts (1983)	NTU, Singapore	In this work, an inventory of series of slope failures occurred at Nanyang Technological Institute (NTU) in Singapore was presented. Based on the presented failures and analysis of site features, possible causes of failures were discussed.	Desk study	
2	Ng and Shi (1998)	Hong Kong	This is parametric study conducted to investigate the influence of various rainfall events and initial ground conditions on slope stability.	Parametric study	
3	Zhang et al. (2000)	China	A field infiltration tests, conducted at a hillside near the ship lock of the Three Gorges Dam in Hubei Province, China. The test site consists of residual soil and decomposed granite.	Field study	Tensiometers
4	Toll (2001)	NTU, Singapore	In this study, numerical modelling was used to investigate the influence of several hydrological parameters on the seepage conditions in a typical residual soil slope in Singapore.	Analysis based on the secondary data derived from the literature	
5	Rahardjo et al., (2001)	NTU, Singapore	In this work, numerical modelling to understand the effect of antecedent rainfall was conducted . Different rainfall patterns were simulated and their effect on slope stability has been evaluated.	Parametric studies	
6	Tsparas et al., (2002)	NTU, Singapore	This is a numerical modelling conducted to investigate the effect of some hydrological parameters on the stability of typical residual soil slope in Singapore. The parameters examined are rainfall intensity, antecedent rainfall, different initial conditions and saturated coefficients of permeability.	Parametric study	
7	Tsparas et al., (2003)	NTU Singapore	In this paper, analysis of a 12-month long field study of the infiltration characteristics of two residual soil slopes in Singapore, is presented. Data collected consisted of rainfall data and pore-water pressure changes at several depths and at several locations on the slopes.	Field study	Tensiometers, rain gauge, and piezometer.
8	Rahardjo et al., (2003)	NTU Singapore	In this study, the effectiveness of horizontal drains in stabilising tropical residual soil slopes against rainfall-induced slope failures, has been examined. The study was conducted through field investigation on two residual soil slopes complemented with a parametric study relating to drain position.	Field and parametric studies	Tensiometers, Piezometers and rainfall gauges
9	Rahardjo et al., (2005)	NTU Singapore	A field study aimed to understand the response of tropical residual slope to different rainfall patterns and the resulting changes in pore-water pressures and water contents.	Field study	Jet-fill tensiometers and Time-domain reflectometry
10	Rahardjo et al., (2007)	NTU Singapore	This is a parametric study aimed to highlight the relative importance of soil properties, initial ground water level, rainfall intensity and slope geometry in inducing soil slope failure.	Parametric study	
11	Muntohar and Liao (2009)	Mountain area, Taiwan	This is numerical modelling conducted to study a slope response to rain infiltration during heavy rainfall in a mountain area of Taiwan. During the study a method was proposed to predict the potential and timing of a landslide.	Parametric study	
12	Liu et al., (2012a)	Ali mountain Highway, Taiwan	This paper studied series of slope failures and their attendant loses at five different locations along the Ali Mountain Highway in Taiwan. The study is a post event site investigation conducted through extensive field surveys and aerial photo analysis.	On site visual observations and aerial photography	
13	Rahardjo et al., (2014)	NTU Singapore	In this paper, different types of instruments for real time monitoring of flux boundary conditions are illustrated to study the effect of rainfall and evaporation on pore-water pressure and water content in slope. The data captured automatically using a data acquisition system were transported to a secured website in real time.	Field and parametric studies	Piezometer, tensiometer, time-domain reflectometry, rainfall gauge and weather station

residual tropical soil embankment is crucial in understanding slope failure mechanisms in this kind of soil.

More than any other, tropical soil slope embankment problems need more research effort and the use of modern technologies to understand the failure mechanism. This is because there is a lack of sufficient knowledge and theories that explain their behaviour, as stated earlier. Furthermore, most of the regions where this kind of soil exists are developing countries with a low capacity to bear the cost of emerging cases of embankment failures. Africa is particularly vulnerable, due to low adaptive capacity, weak institutions and poverty (Change et al., 2008).

There is a need to use non-invasive methods to monitor residual tropical soil embankments. This study will achieve a dual purpose of understanding the failure process in a residual tropical soil slope and establishing the efficiency of geophysical methods in monitoring the stability of a residual tropical soil embankment.

2.5 Slope Stability Monitoring

Soil slopes can be prone to instability and therefore need to be monitored rigorously and continually to ensure sustainable stability. From an engineering point of view, the system does not have to collapse before it is said to have failed. A slope or embankment is said to have failed once some signs of instability are observed, visually or with equipment (Glendinning et al., 2009a). Some slopes may appear stable when inspected visually, but careful assessment using specialised equipment and methods may reveal otherwise. This is more so when they are under adverse environmental and weather conditions. Continuous monitoring assessment is

particularly important considering recent predictions of climate change. The assessment of slope stability under future climate conditions revealed indications of the likelihood of increased slope failure due to the potential impact of climate change (Mantovani et al., 1996). The challenge, therefore, is not only monitoring slopes with visible signs of failures or known historical movements but all slopes or embankments need to be monitored to guarantee stability and prevent unexpected, catastrophic failure.

Observation and monitoring methods have been practiced by engineers and geologists for many decades and in the process many tools and techniques have evolved. Traditionally, trial pitting, drilling, boring, trench excavation and other geotechnical methods have been used to assess and monitor ground stability for both natural and engineered slopes. While acknowledging the fact that these methods for this purpose have achieved great success, it is also worth noting that they have their shortcomings. Often, the use of these methods requires intrusion into the ground under investigation; thereby damaging a portion or the whole area of the ground. Apart from this, observations using traditional geotechnical methods are done at discrete times and locations. This kind of observation may not provide information about the actual process of progressive failure. This makes the methods costly and less efficient. Therefore, better alternative tools and techniques with high precision that allow the collection of a large volume of data at faster rate, have been developed. In the subsequent sections, various monitoring techniques (intrusive and non-intrusive) are discussed.

2.5.1 Intrusive methods

Intrusive methods are used to obtain information about soil structure by intruding into or probing the parent material. These include such operations as borehole drilling, sampling and

in situ testing, test pit excavation, trench excavation, wash boring, auger boring, and percussion drilling. The choice of a particular method depends on the objective of the survey, the site condition, and the material type, among others. Brief descriptions of some of these intrusive methods are given as follows.

2.5.1.1 Trial Pits and Trenches

Pitting and trenching are important parts of slope stability investigation and monitoring, particularly on sites with easy access. These involve excavation to a required depth to assess the ground's near-surface condition. The depth of excavation is normally limited to the depth of the hard layer reached during excavation, which is either an obstruction or bedrock. Depending on the mode of the excavation, the width is generally between 1 m and 2 m depending on whether it is a trench or a pit. The information obtained from these methods includes an assessment of the fault activity, determination of the soil profile, and extraction of samples for laboratory testing. This method allows extraction of high quality soil samples with limited disturbance; thus, its advantage over drilling and some other sampling methods (Fell et al., 2000). In small-scale projects, trenches and pits have been found to be cost-effective in determining site stratification, exposure of fabric of a deposit, mapping and sampling (Fell et al., 2000).

2.5.1.2 Shafts and Adits

Shaft and adits are another useful means of slope stability monitoring, but are not frequently used due to the high construction cost, even though they are proven to be cost-effective in very large slope failure projects (Fell et al., 2000). They allow assessment of the ground condition by direct inspection, through the provision of access or entrance into the ground. When properly constructed, shaft and adits provide a good working site for *in situ* testing and

sampling, in addition to water drainage; thus serving the dual purpose of monitoring and stabilisation (Fell et al., 2000).

2.5.1.3 Drilling and Boring

Drilling and boring are among the oldest methods used to obtain information about the subsurface conditions of a site. Boreholes, in particular, have been found very useful in soil stability assessment and have been used in many slope stability monitoring projects. These generally involve driving circular tubes of variable diameters into the ground by hammering or by the action of rotary metal screw of a specified diameter (Jackson, 2013). Some operations under this category include wash boring, auger boring, percussion drilling and rotary drilling.

Information derived from this method includes the soil profile and groundwater conditions. In groundwater investigation, it is recommended for boreholes water levels to be recorded at short and regular intervals during sinking to avoid missing occasional perched groundwater, which is only displayed in a mixed potential at the completion of the borehole drilling (Fell et al., 2000). Failure to record readings at frequent intervals may not give the exact groundwater condition of the soil.

Harris et al. (2001), recommended the use of rotary drilling in undertaking a geotechnical investigation into European mountain permafrost. Similarly, percussion boreholes were used in an attempt to investigate the causes of failure of historic Edinburgh Castle, in which 27 boreholes were sunk within the Castle area and at the top of the slope of Johnston Terrace (Winter et al., 2013). Limitations of borehole drilling in slope stability monitoring include the inability of the borehole to stay open when a slope is badly disturbed, and the likelihood of

introducing error to piezometric pressure reading when excess drilling fluid is used (Fell et al., 2000).

2.5.2 Soil Sampling

Sampling is done to obtain information about the site's condition by studying a representative sample. The sample could be disturbed, undisturbed or of high quality. The degree of disturbance introduced to the sample depends on the sampling procedure. The disturbed sample could be obtained by percussion drilling, trial pits or trenching. Samples taken at the topsoil and subsequent layers are done at a depth interval that represents the soil profile and lithology (Jackson, 2013).

The consistency of a soil and its relative density are two important properties and are usually assessed using standard penetration testing (SPT) in most percussion borehole drilling (Donnelly et al., 2005).

2.5.3 Non-intrusive methods

Non-intrusive methods otherwise known as non-invasive methods are increasingly becoming popular in slope stability monitoring and failure studies. This is due to their many advantages over traditional geotechnical methods. Chief among them is the ability to sample the soil mass as a whole with good coverage contrary to point sampling used by the conventional boring and drilling (Fell et al., 2000, Glendinning et al., 2009a).

These modern techniques facilitate easier and faster collection of data at a lower cost. Some of these non-intrusive techniques employ the use of a remote sensing principle in their operation. In some of these techniques, observations are made and data are acquired without even physical

contact with the ground under investigation, let alone damaging it. However, there are non-intrusive geophysical methods that are not quite remote but utilise the sensing technology to obtain information from a soil body without damaging or disturbing it.

Earth observations using remote sensing provide data in a spatial format with a synoptic view; the area coverage could be large, depending on the technique and weather conditions. The measurements are made from a spacecraft, aircraft or ground station.

Conte Robles (2012), reported several slope stability projects where one or more of the following methods were effectively used: optical fibre sensors, GPS, airborne remote sensing, satellite remote sensing, or ground-based remote sensing. Similarly, Mantovani et al. (1996) cited examples where various kinds of remote sensing techniques were used in Spain, Italy and Great Britain.

Many geophysical tools are used for slope stability studies; which include but are not limited to, establishing pre-failure conditions, material in-homogeneities and boundaries, and post-failure investigations. Most methods are well known and their potential has since been appreciated (Mantovani et al., 1996). However, in the last few decades, most methods have become easier to use, data interpretations have become more reliable, more accurate and cheaper, due to the advance of cheap computer power Hack (2000).

There are many methods, but the four most popular and frequently used in slope stability studies are discussed in this section. These include acoustic emission (AE) in 2.5.3.1, electrical resistivity tomography (ERT) in 2.5.3.2, electromagnetic (EM) otherwise known as ground penetrating radar (GPR) in 2.5.3.3, and seismic profiling in 2.5.3.4.

2.5.3.1 Acoustic Emission

Acoustic emission (AE) is a term used to describe an activity characterised by the low-level seismic signal emitted by solids, when they are undergoing deformation or are under a stress condition (Hardy Jr, 2005).

Terms like microseismic activity, seismic-acoustic activity, rock talk or rock noise, elastic shocks, elastic radiation and sub-audible noise are used to refer to acoustic emission (Lord Jr, 2012, Hardy Jr, 2005, Dixon and Spriggs, 2007). The concept has long been established in metallic objects and rocks, but its application in soil stability monitoring is somewhat recent. The technique has been applied widely, including for surface structures such as dams, bridge piers and abutments, foundations, and underground structures such as tunnels and mines (Hardy Jr, 2005).

In soil, laboratory experimental studies of AE have been conducted on a small and a large scale before it was later applied in the field. It is now generally accepted to be among the methods of stability monitoring in natural and engineered slopes.

Although AE is a non-intrusive technique, it does not utilise a full remote sensing principle as the monitoring equipment is placed in contact with the soil body to be investigated. This technique has the ability to provide an early warning of failure, thereby allowing appropriate stabilisation measures to be taken. Some advantages over other geotechnical methods are shown in its ability to delineate an area of instability, and it does not require long processes and measurements to establish failure (Dixon et al., 2003).

2.5.3.1.1 Operational Theory

The principle of acoustic emission has been explained by many authors, including Hardy Jr (1981), Choi and Kang (2003) Dixon et al. (2003) and Lord Jr (2012) as described here using Figure 2-4. In the figure, the receiving transducer (labelled 2), which could be geophones, an accelerometer, hydrophones or a simple AE sensor, monitors changes in velocity from the source (labelled 1) caused by the presence of AE activity. A pre-amplifier (labelled 3) is employed to amplify the output of the AE sensor resulting in AE activity, which is very small, normally in the order of microvolts. This small output signal is often amplified 100 to 1000 times or even greater to enable it to be recorded. The filtering system is generally used to eliminate some of the AE signals on the basis of their frequencies. A low or high pass filter can be used for this purpose, but a band filter (labelled 4) with combining features is used in this system to eliminate extraneous low and high-frequency signals. The acoustic waves are transmitted down a cable over long distances, depending on the specimen material property. A comparator transforms the AE of proper frequency into square-wave signals and then transmits it to the microprocessor. A microprocessor (labelled 6) is a data capture and processing unit that records and counts times for partial discharge per second; and the output of this is displayed on a screen or display (as labelled 7), which is shown in analogue or digital format.

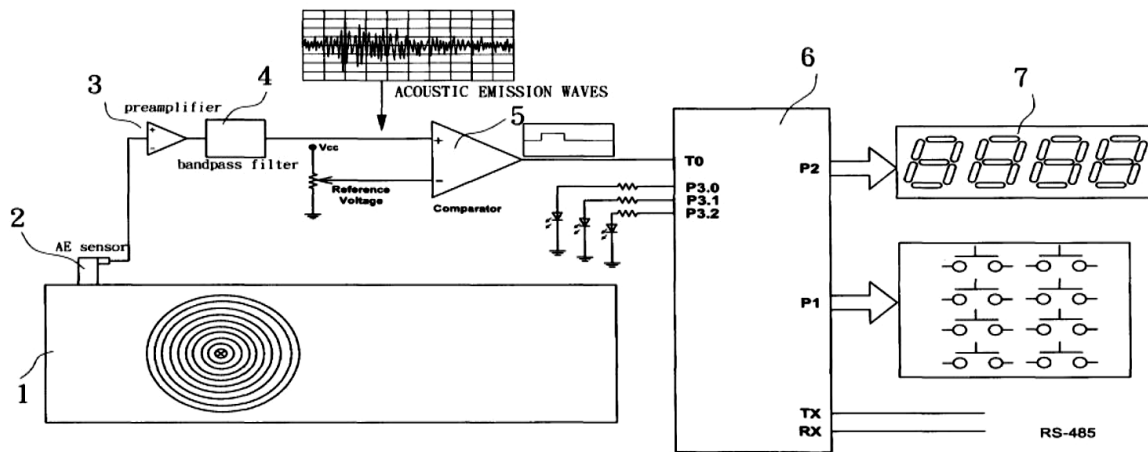


Figure 2-4: Schematic diagram showing a set-up of AE System (adopted from US patents)

In summary, the AE monitoring system consists of a transducer that monitors AE activity, and amplifiers and a recording system which captures, processes and displays the final output in an analogue or digital form, as shown in the above diagram.

2.5.3.1.2 Application of Acoustic Emission to the Soil Slope Stability

The application of acoustic emission in soil monitoring is now well known. It is a technique used in detecting the instability or deformation of a soil's structure by generating a sub-audible noise (Dixon et al., 2003).

Soils like many other solid materials generate acoustic stress waves when undergoing deformation. The acoustic waves or sub-audible noise is generated when there is friction among the soil particles while in rock it is due to the fracture development and propagation (Shiotani et al., 2001, Dixon et al., 2003). This AE or noise is detectable using an appropriate transducer or set of transducers.

In the field, a single transducer or an array of transducers is used to observe AE events, depending on whether the objective is source location or general survey. In the field, a single

transducer or array of transducers are used to observe AE events, depending on whether the objective is source location or general survey. Drnevich and Gray (1981), reported two stages in soil slope stability monitoring: namely, general and source monitoring. They described general monitoring as a process of establishing the occurrence of AE activity and the determination of the AE associated parameters. It is carried out with a limited number of transducers, normally only one. While location monitoring involves the use of an array of transducers installed at various locations on the site under study, to locate the actual source of AE as accurately as possible. This later stage is important in estimating the true magnitude of an observed AE activity.

The principle and procedure of AE in soil monitoring simply requires a suitable transducer to be attached to the soil structure or specimen under study, and the acoustic signals arising from stress or deformation of the specimen are monitored by this or a different transducer; the signals are subsequently processed and recorded as a final output.

In early studies, the sonic technique which utilised two transducers (i.e. transmitter and receiver) was used, but in the late 20th century when the method was maturing, it was discovered that AE signals can be detected at the receiver even without the transmitter. Hence the discovery of a new technique in the 1970s (Hardy Jr, 2005).

Following the discovery of this new method, many researchers have successfully employed the technique for the monitoring of ground stability. Among them are Jurich and Miller (1987), Kousteni et al. (1999), Shiotani et al. (2001), Dixon et al. (2003), Dixon and Spriggs (2007) and Dixon et al. (2010) The overall simple AE monitoring experimental set-up as described by

Hardy (2005), include a transducer (e.g geophone), amplifiers, a filter and a recorder as shown in Figure 2-5.

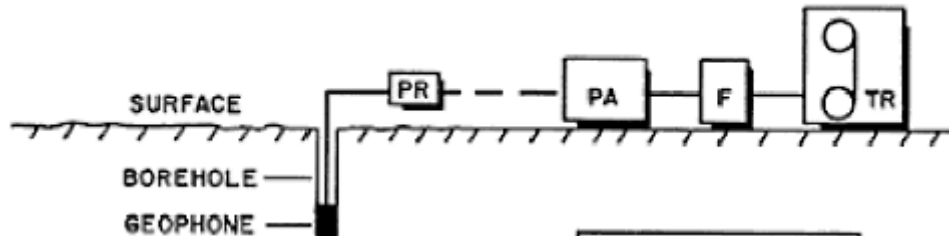


Figure 2-5: Diagram of AE monitoring system

To monitor AE activity at a depth below the surface, a transducer is placed in a suitable borehole of 8-30 m depth. The activity which is normally in a microscopic signal, is amplified by the pre-amplifier (PR) and post-amplifier (PA) respectively, so it can be read by the tape recorder (TR). A filter (F) is normally included in the system to eliminate undesirable extraneous signals before it is read by the recorder.

Despite the success recorded in the use of AE in slope stability, some shortcomings were observed. One of these is presented when the sensor cannot detect an acoustic signal in a body with a very large distance, due to attenuation caused by energy loss during AE transmission (Koerner et al., 1981, Dixon et al., 2010). Depending on the type of wave propagation used, the attenuation can increase in both horizontal and vertical directions. Bulk waves (longitudinal and shear) for example, propagate away from a source in three dimensions, so the attenuation also increases with distance from the source along the three directions (Hardy Jr, 2005).

Generally, the attenuation or the range to be covered by an acoustic signal depends on the frequency used. A higher frequency is less affected by the background noise but is associated with high attenuation and the consequent loss of energy. Conversely, a low-frequency signal is more likely to be contaminated by the background noise (e.g. machines' vibration) but has low attenuation. This means when monitoring equipment is placed at a far distance from the source spectrum, only a fraction of the AE event will be observed; and if the depth is too large and the source spectrum of the event does not contain a significant low-frequency component, the event cannot be detected (Hardy Jr, 2005). Figure 2.6 shows the relationship between range and frequency.

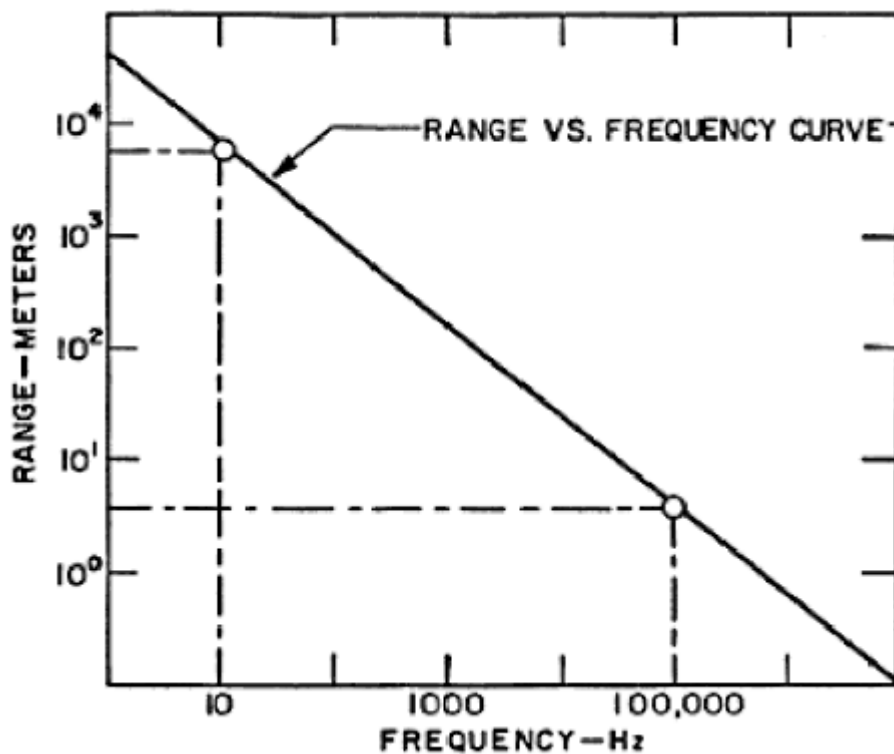


Figure 2-6: Range vs frequency for AE signals (Hardy, 2005)

From Figure 2-6, it can be seen that at 10 Hz the signal can be detected up to a distance of 7000 m. While at a higher frequency of 100 kHz, the range to be covered is less than 10 m.

Due to the attenuation, the depth at which an AE device can detect AE signals is usually in the order of units of metres, depending on the type of geologic material. If the depths from the source is in the order of tens of metres, a waveguide is required to relay the signal to the measuring transducer. A waveguide was developed to provide a low-attenuation acoustic path (Dixon et al., 2003, Dixon and Spriggs, 2007, Kousteni et al., 1999). The waveguide could be passive or active, depending on the material type. The passive systems are used in a material with low AE activity like clay, so that no additional AE event is introduced into the waveguide in the process of installation. Although active waveguide systems can be installed in a cohesive material, it has to be in a borehole which is filled with granular material, as shown in Figure 2-7, for it to produce high AE (Kousteni et al., 1999). This is confirmed by the laboratory experiment conducted by (Dixon and Spriggs, 2007).

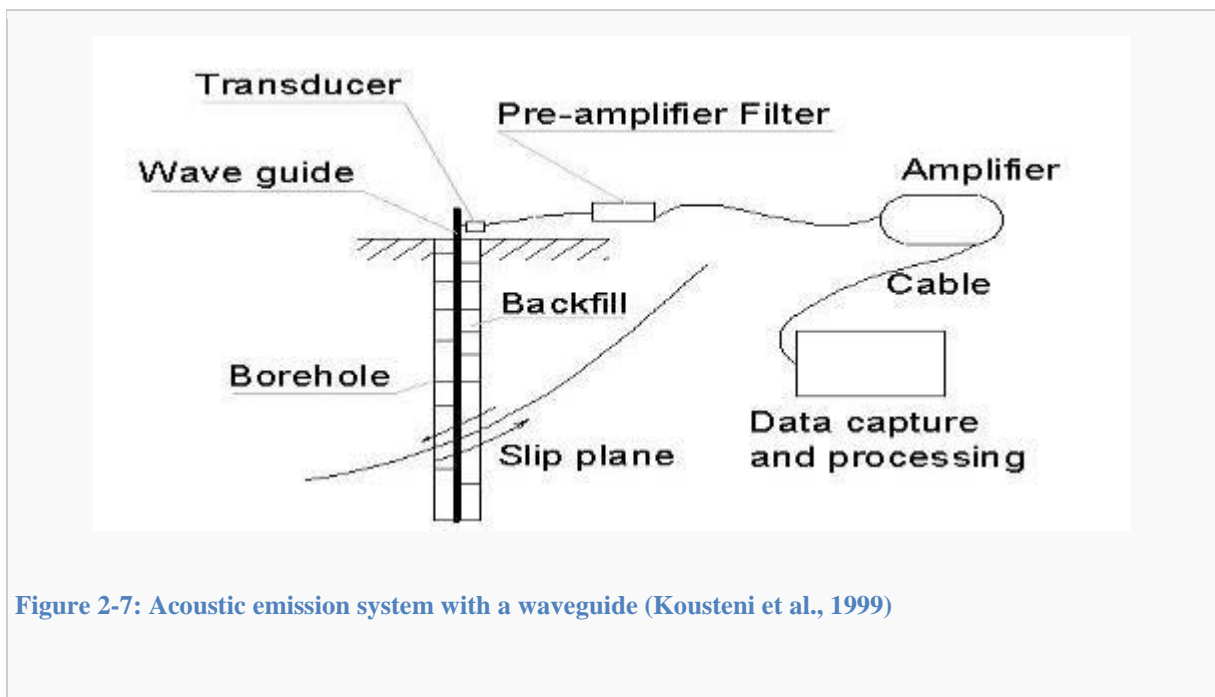


Figure 2-7: Acoustic emission system with a waveguide (Kousteni et al., 1999)

In the experiment, Dixon and Spriggs used steel waveguides with a 55 mm diameter and 3 mm wall thickness. The waveguide was backfilled with sub-angular crushed river gravel with a nominal size of 5 mm. A sensor with resonant frequency of 50 kHz was connected to the

waveguide using a magnetic device with a layer of silicon gel to aid acoustic transfer. Other components of the set-up include amplifiers and a filtering system as shown in Figure 2-8.

Although attenuation of the AE in soil is significant at the high frequencies used in this experiment, the acoustic path length between the deforming backfill and the steel tube allows the AE signal to be detected by the sensor. The signal was recorded after it had been converted from an analogue voltage input to a digital value.

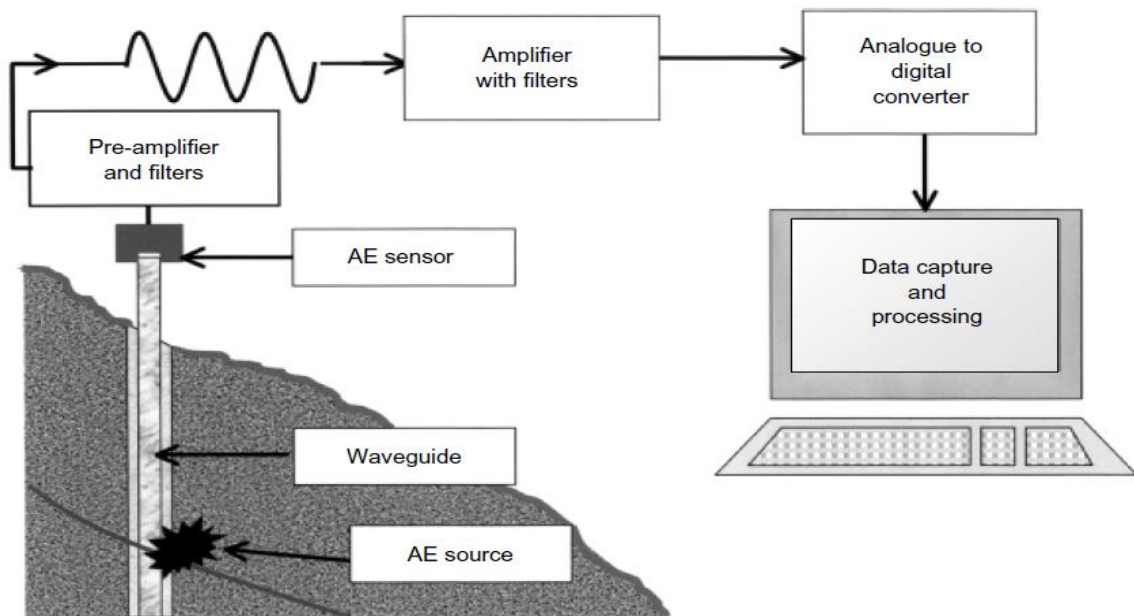


Figure 2-8: Acoustic emission system with an active wave-guide (after Dixon et al., 2003)

The waveguide could be anything, provided it can successfully transfer the AE activity from the source to the transducer. It could be a steel reinforcement rod, construction units, or a steel pipe (Kousteni et al., 1999). Dixon et al. (2003) used a steel pipe in a study to validate the active waveguide concept. The results of the laboratory tests and that of the field study have confirmed the suitability of the AE equipment with an active waveguide for detecting AE

signals in a deeper soil position. Figure 2-8 shows components of the equipment used with an active waveguide.

2.5.3.1.3 Development of Acoustic Real-time Monitoring System

Recent increases in processing the power and portability of instrumentation provide the possibility of developing specialist equipment for field monitoring that can operate continuously (Dixon et al., 2003).

The ongoing research aimed at exploring the potential of the acoustic wave in slope stability monitoring has led to a number of breakthroughs in recent times. Building on the successes achieved, Dixon et.al. (2012) tried to improve the capability of his earlier developed AE device, to enable it to provide early warning information of slope failure by capturing the failure process as it occurs in real-time. The project conducted at Newcastle University by utilising the EPSRC funded BIONICS test facility, succeeded in developing a real-time AE monitoring system in 2009. (*www.slopealarms.com. Accessed 21/09/2014*).

To augment this progressive effort, the British Geological Survey (BGS), through EPSRC funding, used its state-of-the-art facilities and highly skilled human resources to add value to the previously invented low-cost device by Dixon of Loughborough University (*www.bgs.ac.uk accessed 04/04/2015*). This formal collaboration led to the upgrading of this concept for field application and the results have demonstrated the ability of AE sensors to detect rapid changes in the displacement rate of a slope, which is the basic requirement of a monitoring system to give timely warnings. (*www.slopealarms.com accessed 21/09/2014*).

The output of this joint effort is the development of a new technology called Assessment of Landslides using Acoustic Real-time Monitoring Systems (ALARMS), and field trial testing of this technology has been successfully conducted on the UK sites and overseas (Dixon et al., 2012). These include a trial on an active landslide at Hollin Hill, North Yorkshire, and a large rock slope in the eastern Italian Alps. In each trial, the performance of this method compared favourably with the traditional methods such as inclinometer measurements.

2.5.3.2 Electrical Resistivity Tomography (ERT)

The ERT method has been in use in slope stability assessment for many years. This method is an old concept in the oil industry as it has been used to assess the water content in rock reservoir for more than half a century (Jackson et al., 2006). Its application in the investigation of earth embankments to assess their stability has received much attention in recent years (Chambers et al., 2007, Jackson et al., 2002, Chambers et al., 2008). The method tries to find the difference in resistivity between different materials of the earth's subsurface layers. The method was initially conceived as tedious due to its associated highly complicated mathematical computations (Hack, 2000). This problem has now been overcome due to the continuous upgrade of knowledge, availability of equipment and the development of many computer programmes (Hack, 2000). For example, inversion of resistivity values can now be done easily with Res2DInv (Sudha et al., 2009, Chambers et al., 2007). In fact, the empirical relationship between the moisture content of a soil and electrical resistivity has been since understood (Jackson et al., 2006). This relationship will be explained in section 2.5.3.2.2

2.5.3.2.1 Concept and Theory

The equipment for a site electrical survey comprises of arrays of metal electrodes which pass electric current to the ground and the resulting potential difference is measured. The obtained values of electrical resistance are inverted to obtain an electrical resistivity of the subsurface

material (Chambers et al., 2007, Jackson et al., 2006, Gunn et al., 2005, Gunn et al., 2008, Jackson et al., 2002). This can be achieved in many ways, but the common method utilises an array of four electrodes, out of which two pass current into the ground and the remaining two measure the potential difference caused by the current flowing through the ground between any two electrodes (Hack, 2000) as shown in Figure 2-9.

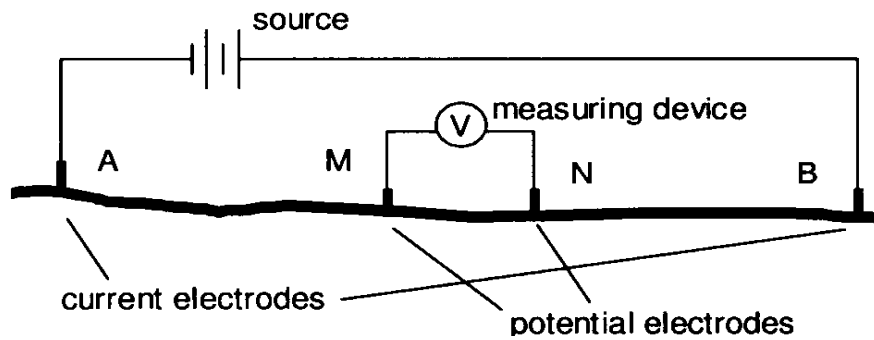


Figure 2-9: Arrangement of array of electrodes (Hack, 2000)

With reference to Figure 2-10, the five common configurations of electrode arrays are described by (Hack, 2000) as follows.

(a)

(b)

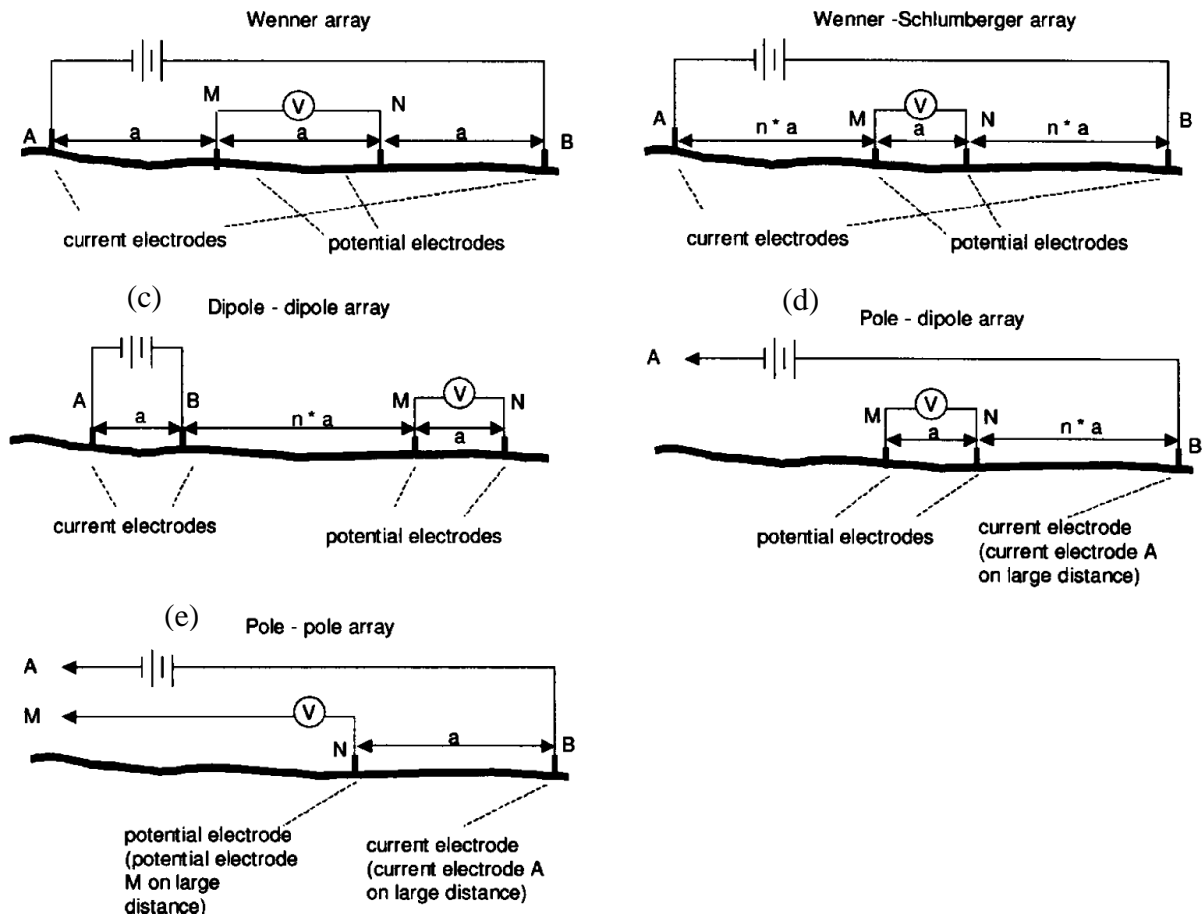


Figure 2-10: Different types of electrode array configurations

a) Wenner array

In the Wenner array configuration, the electrodes are equally spaced, 'a' as shown in Figure 2.10(a). This type of array configuration is relatively sensitive to changes in the subsurface resistivity and therefore suitable for surveying horizontal structures. The Wenner array has good signal strength.

b) Wenner-Schlumberger array

In this type of configuration, the spacing of potential electrodes at the middle of the electrodes is kept constant; while the spacing of current electrodes away from the potential electrodes is varied in the multiples 'n' of the middle spacing 'a', as shown

in Figure 2.10(b). When $n = 1$, the array is effectively the Wenner type of configuration. As 'n' increases, the depth of investigation increases, but the signal strength decreases. The array is moderately sensitive to both horizontal and vertical changes and can be used for surveying both horizontal and vertical structures.

c) Dipole-dipole array

In the dipole-dipole array configuration, the spacing between the current and potential electrodes are respectively constant; while the distance in between them is varied in multiples 'n' of spacing 'a', as shown in Figure 2.10(c). Just like in the Wenner-Schlumberger, in dipole-dipole array, the signal strength becomes smaller when the values of the 'n' become larger. The array is more suitable for vertical structures, and less for identifying horizontal structures. The depth of investigation is small compared to that of the Wenner array.

d) Pole-dipole array

The pole-dipole array shown in Figure 2.10(d) is similar to the Wenner-Schlumberger array, but the difference is that one of the current electrodes is placed at a sufficiently far distance from the survey line. The array has a higher signal strength than the dipole-dipole array and is less sensitive to noise than the pole-pole array. This is because the distance between the potential electrodes is not very large. The depth of investigation is relatively large.

e) Pole-pole array

This is the type of array where only one current and one potential electrode are placed at a fixed distance of 'a' between them, as shown in Figure 2.10(e). The second of each of the electrodes is placed at a far distance usually more than 20 times the distance 'a'. This array could be associated with a practical problem, particularly where there is a limited space to place the electrodes. The array is sensitive to noise due to the large distance between the potential electrodes. The depth of investigation and horizontal coverage is quite large.

The choice of the array depends on the type of features at a particular site to be surveyed. The comparative analysis of the various array configurations will be made in section 6.3.

Apart from the above-explained surface surveys, borehole methods also exist. In this method, all electrodes are placed in either the same or different boreholes. If one borehole system is used, the measurement is the same as that of the usual surface resistivity surveys, but two borehole systems result in tomography (Hack, 2000). Daily et al. (1992), outlined a procedure for the resistivity measurement between two dipoles. In the experiment, he used 8 electrodes spaced equally to study infiltration events.

2.5.3.2.2 Application to soil stability monitoring

The moisture content of a soil influences its strength and density, the two most important factors in determining the stability of soil slope or embankment (Jackson et al., 2002). The theory of electrical resistivity assumes that there is a correlation between moisture content and its electrical conductivity. The theory has for a long time been applied with success in slope stability studies. In soil, high resistivity values are indicative of a low conductive zone; while

low resistivity values are a signature of a high conductive zone, indicating that it is a weak zone (Abidin et al., 2012).

In slope stability studies, it is important to know that; electrical resistivity is dependent on material type. Different geological units with different material composition may give varied resistivity values even if they are under the same moisture condition. This is because electrical resistivity of a soil is also dependent on density, pore-fluid resistivity, matrix resistivity and pore space morphology (Jackson et al., 2006, Jackson et al., 2002). Therefore, clays generally have low resistivity values while loose dry sand and gravel have high resistivity.

The need to optimise the electrical resistivity technique, resulted in the introduction of new equipment and the development of many computer programmes to collect and process data. This allowed the resistivity data to be processed and presented in 2- and 3-dimensional resistivity tomography – ERT (Hack, 2000).

Zhou et al. (2001), used ERT to monitor 3-D spatial and temporal variations of moisture content in the field. In their work, 88 electrodes were used to pass current and the potential of the electrodes was obtained by pole-pole and Wenner array methods and the inverted resistivity data collected during the experiment compared favourably with traditional, conventional method of water content measurement.

Sudha et al. (2009), also used the ERT technique in soil characterisation and 72 electrodes were used; the potential difference was measured using the Schlumberger-Wenner method..

Similarly, Chambers et al. (2007) used the technique by installing imaging arrays to monitor seasonal moisture content changes of an earth embankment.

2.5.3.2.3 Development of resistivity real-time monitoring system

Subsequent to the successful use of the electrical resistivity technique in soil stability projects, another innovation was introduced to make it more responsive to stability monitoring needs. This is time-lapse electrical resistivity tomography (Chambers et al., 2008). It has the capability to provide imaging variation in moisture content and consequent changes in geotechnical properties, as they occur in real time in full space.

In view of the above, the British Geological Survey (BGS) made a fruitful effort by upgrading the emerging technology by combining the time-lapse electrical resistivity tomography with data telemetry and intelligence systems (Chambers et al., 2008). This newly enhanced technology has the capability of monitoring and diagnosing an embankment's internal structure, giving a warning of an impending failure in the form of an alert seen on the data telemetry e.g. Global System for Mobile communication, GSM (Chambers et al., 2008). The technology is called ALERT (Automated time-Lapse Electrical Resistivity Tomography) or ALERT-ME (Automated time-Lapse Electrical Resistivity Tomography for Monitoring Embankments) and was developed in 2010 (www.bgs.ac.uk accessed 04/04/2015).

2.5.3.3 Ground Penetrating Radar (GPR)

Ground-penetrating radar (GPR) is a non-intrusive geophysical method that is used in investigating the ground subsurface conditions and features. Although its concept has been in existence for a very long period, its development as a technique for ground investigation was

not until the second half of the 20th century (the 1960's) and its application to the road, in particular, was in the 1970's (Evans et al., 2006a).

GPR is used in diverse applications; including the mapping of geological conditions and the thickness and depth of soil and sediment strata, determination of the depth of the groundwater table, and the detection of subsurface cavities and fractures in rocks (Do, 2003). Others include deriving information from layers of road pavement structure and mapping of rail track substructure conditions (Olhoeft and Selig, 2002). In general, the technique is used in the ground investigation of all kinds including bedrock condition assessment as well as bound material layers and foundation materials (Evans et al., 2006a, Evans et al., 2006b). Its increasing acceptance in the geophysical investigation is due to its greater processing power, relatively easy operation, easy and fast interpretation of data with the aid of user-friendly software and its relative portability (Evans et al., 2006a). It may be deployed from the surface, in a borehole or between boreholes, from aircrafts or satellites (Slob et al., 2010). Its antenna can be pulled either by hand or towed by a vehicle. A typical GPR antenna is shown in Figure 2-11. As one of the established non-intrusive techniques, GPR has the highest resolution of all the geophysical methods in subsurface imaging and can penetrate to the depths of 5,400 mm depending on the properties of the material (Slob et al., 2010, Do, 2003)

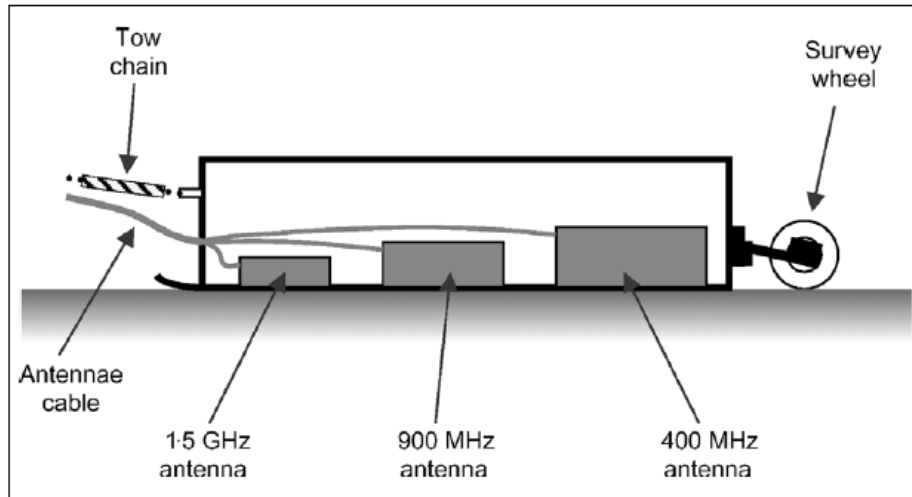


Figure 2-11: GPR antennae (Evans, 2006)

However, a major limitation of GPR is its sensitivity to unwanted noise from various sources such as vehicles and nearby machines and unwanted signals (Do, 2003, Slob et al., 2010).

These if not adequately handled can interfere with GPR signals thereby affecting the quality of the data obtained.

2.5.3.3.1 Principle and Performance

The principle of GPR like most geophysical methods is gradually becoming popular amongst geotechnical engineers. The basic principle of GPR as outlined in many publications including Evans et al. (2006b) and Slob et al. (2010), is described in this section.

The ultra-high frequency radio waves are transmitted into the ground through a transducer or antenna. The transmitted waves are then reflected from the material and returned to the same antenna or separate antenna which receives and stores the data in the digital control unit, as shown in Figure 2-12. The time taken for the reflection to return to the antenna is recorded.

The time it takes for the signal to get to the transmitter and return to the receiver depends on the property of the radar and the medium.

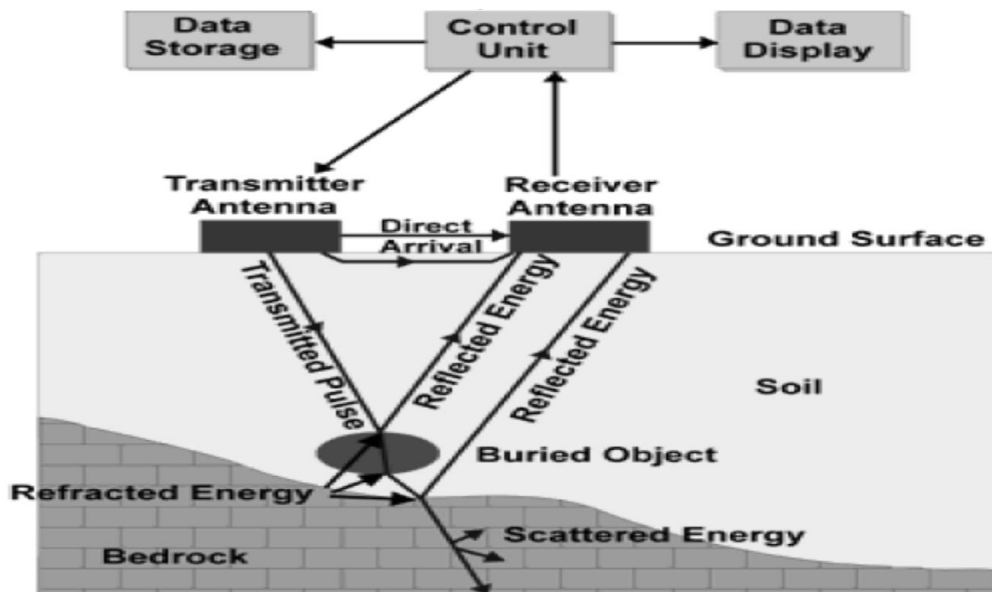


Figure 2-12: Schematic of basic GPR system

The amount of radar energy reflected through the process of electromagnetic wave propagation and scattering is dependent on the reflection coefficient, which in turn is dependent on the difference in the dielectric properties of materials, as demonstrated in equation 2-1:

$$\rho = \frac{[(\sqrt{\epsilon_1}) - (\sqrt{\epsilon_2})]}{[(\sqrt{\epsilon_1}) + (\sqrt{\epsilon_2})]} \dots\dots\dots 2-1$$

where ρ = bulk density

ϵ = dielectric constant

The dielectric constant can be obtained from GPR velocity using equation 2-2 as follows:

$$V = \frac{c}{[\sqrt{\mu_r \epsilon_r}]} \dots\dots\dots 2-2$$

V = velocity of the electromagnetic wave (cm/s)

C = velocity of light in free space (cm/s)

μ_r = relative magnetic permittivity (unitless)

ϵ_r = dielectric constant i.e. relative permittivity (unitless)

The dielectric constants are affected by the material type, temperature, water content and pore fluid properties. Therefore, the passage of radar waves through a material is dependent on these factors. Most ground materials have different and contrasting dielectric constants and this is an important requirement of this technique. Table 2-2 shows dielectric constants of different types of commonly used materials.

Table 2-3: Characteristic electromagnetic properties of some materials (adopted from Hack, 2000)

Material	Dielectric Constant	Electric Velocity (for frequency 100 MHz) (m/ns)	Attenuation (for frequency 100 MHz) (dB /m)
Air	1	0.3	0
Metal			Infinite
Fresh water	80	0.33	2 x 10 ⁻¹
Sea water	80	0.01	1 x 10 ⁻¹
Dry sand	3 - 5	0.15	1 x 10 ⁻²
Wet sand	20 - 30	0.06	0.03 – 3
Lime stone	4 - 8	0.12	0.4 – 1
Clay	5 - 40	0.06	1.0 – 300
Granite	4 - 6	0.13	0.01 - 1.0
Rock salt	5 - 6	0.13	0.01 - 1.0
Shale	5 - 15	0.09	1.0 – 100

A range of GPR frequencies have been in use, but 10 MHz and 2 GHz are typically used for engineering investigations (Evans et al., 2006b, Evans et al., 2008). Generally, a higher signal frequency gives better resolution (i.e. a more precise indication of depth) but lower frequencies penetrate deeper into the soil subsurface (Evans et al., 2006a).

2.5.3.4 Seismic Profiling

Seismic profiling is one of the geophysical methods used in slope stability assessment. If not the best, it is one of the most suitable methods in determining slope stability, because it can be used to determine the internal structure of a soil or rock body which is an important requirement of slope stability assessment (Hack, 2000). It is a reliable and cost-effective way of assessing a site's condition through the determination of ground stiffness by studying its elastic parameters (Madun, 2012).

2.5.3.4.1 Types of Waves

Common types of seismic waves include compressional waves (also called P-waves), shear waves (also known as S-waves) and surface wave (e.g. Rayleigh and ground waves) (Hack, 2000, Madun, 2012). In terms of their oscillation, P-waves can be described as longitudinal, S-waves as transverse, while Rayleigh waves are circular. The waves can also be described in terms of speed of travel. In that case, P-waves are fastest and arrive early, then S-waves, then surface waves, as shown in Figure 2-13.

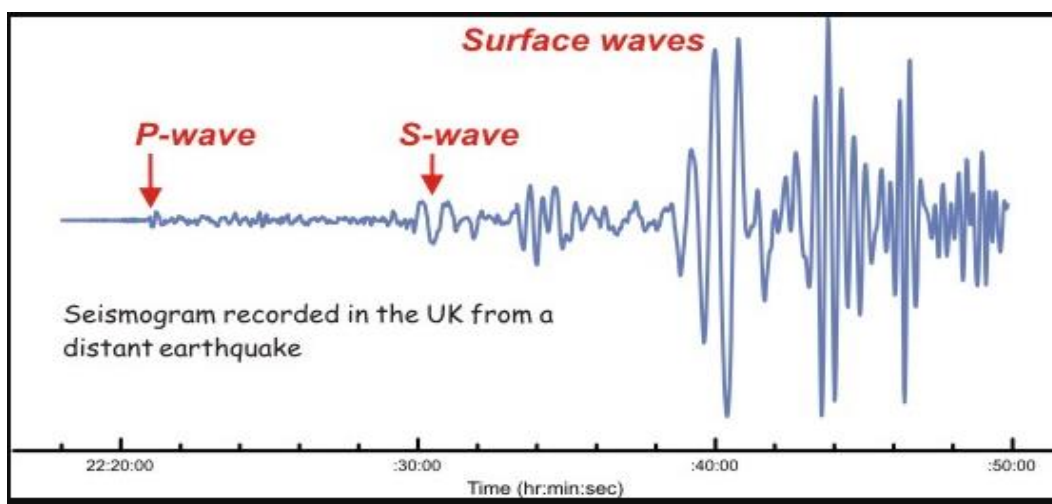


Figure 2-13: Types of Seismic wave (<http://www.bgs.ac.uk/discoveringGeology/hazards/earthquakes/images>)

The behaviour of a wave is influenced by the type of material it passes through and this varies with the type of wave. Compressional waves are commonly used because they are easy to generate, and they are sensitive to normal stiffness change. While shear and surface waves are more affected by shear stiffness, which is related to the shear strength properties of the geological material. Therefore they are more applicable to slope stability studies (Hack, 2000).

2.5.3.4.2 Attenuation and Absorption

The energy of the seismic wave attenuates as the distance from the source increases because of absorption due to non-ideal elastic properties of the soil and rocks; and it is dependent on the frequency of the wave, as there is more absorption in higher frequencies than lower frequencies. Some other causes of attenuation are wave travelling behaviour (reflection, refraction and diffraction) and the loss at the interfaces as the wave changes from a P-wave to an S-wave for example.

2.5.3.4.3 Theory and Concept

In many slope stability assessments, a high-frequency seismic signal is required to carry out measurements with high resolution. To achieve this, many sources are considered with each having its merits and demerits. The sources include the traditional use of hammer blows on a metal plate, use of explosives and the emitted signal from a controlled source known as ‘vibro-seis’ (Hack, 2000). With this latter source, although it releases lower energy per unit time than the explosive sources, the correlation of the controlled signal with the received signals is far better; its energy is concentrated in the desired high frequency, and the noise/signal ratios of the received signal can easily be increased (Hack, 2000). For a surface wave, a mass is dropped to induce an impulsive signal into the ground to generate vibration and about 2/3 of the vibration is transformed into surface waves. (Madun, 2012). The P- and S-waves interfere on

the ground surface to form Rayleigh waves (Xia et al., 2002) and the wave velocity is measured and recorded.

The seismic wave velocity method can be applied to the determination of ground stiffness for both homogeneous stratum and layered ground. In a homogeneous soil, there is no variation of surface wave with frequency; but in layered soil with different material properties, the wave velocity varies with frequency (Madun, 2012) by the following relation:

$$G_{\max} = \rho V_s^2 \dots\dots\dots 2-3$$

Where ρ is mass soil bulk density and is calculated as follows:

$$\rho = \frac{2\pi DE}{I} \dots\dots\dots 2-4$$

Where

G_{\max} = maximum shear modulus

V_s = shear wave velocity

D = depth of penetration

E = modulus of elasticity

Once the wave velocity is measured the stiffness profile of the soil can easily be estimated.

This is illustrated by Hack (2000) in the following paragraph and with reference to Figure 2-

14

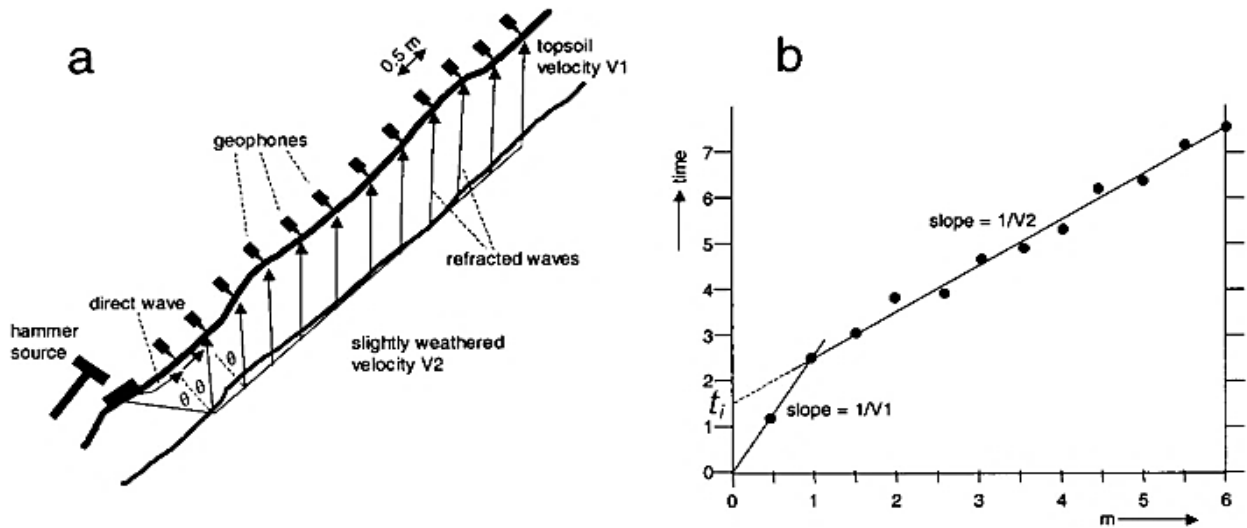


Figure 2-14: Seismic refraction survey (a) ray paths, (b) graph of time versus distance of the first arrived signal (Hack, 2000)

Assuming an array of geophones are used for a seismic refraction survey on a two-layered soil (of differing soil properties) as shown in Figure 2-14(a), the first arriving signal at the geophones is for the first two geophones, the direct signal travelling through the topsoil layer; while for remaining geophones there is the refracted wave travelling through the underlying layer. In this case, the law of refracted waves applies: that is, the angle of incidence and that of refraction equal θ . The top layer has velocity V_1 and the overlaid soil mass velocity V_2 . The angle θ is given by:

$$\frac{\sin i}{\sin r} = \Theta, \dots\dots\dots 2-5$$

While,

$$\sin (\Theta) = \frac{V_1}{V_2} \dots\dots\dots 2-6$$

The refracted elastic waves travelling through sediment of different material properties can be measured by plotting a graph in Figure 2-14(b). The depth or thickness can be conveniently calculated with the following relation:

$$d = \frac{1}{2} \frac{V_1.t_1}{\cos(\arcsin(\frac{V_1}{V_2}))} \dots\dots\dots 2-7$$

Where

t_1 = time intercept of the two velocities obtained from the graph

d = depth

2.5.4 Selection of Stability Monitoring Method

Various methods used in the investigation and monitoring of slope stability have been highlighted in the preceding sections. These include both intrusive and non-intrusive methods.

The non-intrusive methods are now the popular and most preferred in slope stability monitoring due to their numerous advantages over the intrusive methods, as discussed earlier. Different kinds of non-intrusive, geophysical methods do exist, but those that have been frequently used in stability monitoring in recent times are summarised in Table 2-4. Among them, two methods are selected for use in the experimental element of this research. They are electromagnetic also known as ground-penetrating-radar (GPR) and electrical resistivity tomography (ERT) methods. The comparative advantages of these methods are shown in Table 2-4. Unlike acoustic emission and seismic profiling methods, the GPR and ERT methods are not affected by attenuation and therefore have high resolution. In the past, these methods were not commonly used due to their associated complex mathematical computations. With the advent of computer processing power and their relatively cheap and easy access, these drawbacks have been overcome. The data can now be computed and interpreted very easily and with greater accuracy using the friendly software.

Table 2-4: Summary of non-intrusive methods

Method	Operational Theory	Recent Advancement	Advantages
Acoustic Emission (AE)	The acoustic emission (AE) is a term used to describe an activity characterised by the low-level seismic signal emitted by solids when they are undergoing deformation. The AE device is installed on site to monitor ground movement by listening to the noise generated during deformation.	Development of new technology called Assessment of Landslides using Acoustic Real-time Monitoring Systems (ALARMS) which provides early warning information of slope failure by capturing the failure process as it occurs in real time.	<ul style="list-style-type: none"> i) Allows detection of deformation or micro-movement ii) Captures the failure as it occurs in real time iii) Ability to delineate of instability iv) Does not require many computations to establish
Electrical Resistivity	The method tries to find the difference in resistivity between different materials of the earth's subsurface layers. The equipment for a site electrical survey comprises of arrays of metals used as electrodes which pass electric current to the ground and the resulting potential difference is measured. The acquired values are inverted to obtain electrical resistivity tomography of the subsurface material.	Development of a device that has the capability of monitoring and diagnosing an embankment's internal structure; giving a warning of an impending failure in the form of an alert. It is called ALERT (Automated time-Lapse Electrical Resistivity Tomography).	Early warning information of slope failure.
Ground - Penetrating Radar (GPR)	GPR operates based on the principle that ground materials have different and contrasting dielectric constants. The ultra-high frequency radio waves are transmitted into the ground and then reflected back to the antenna. The time taken and the amount of radar energy reflected is dependent on the dielectric properties of materials.		<ul style="list-style-type: none"> i) High resolution ii) Greater processing iii) Relatively easy to use iv) Relatively portable
Seismic Profiling	The method can be used to determine the internal structural set-up of a soil or rock body, which is an important requirement of slope stability assessment. It assesses the site condition through determination of ground stiffness by studying its elastic parameters.		<ul style="list-style-type: none"> i) It is reliable and cost-effective ii) Accuracy in estimating depths of structural layers

2.6 Chapter Summary

In this chapter, the problem of embankment failure was highlighted with practical examples. Although there are corrective measures to restore the failed or failing embankment, the most effective way of tackling the problem is by preventive action. This can be done through periodic assessment and constant monitoring, using non-intrusive methods. The degree of effectiveness of this is largely dependent on the level of understanding of the failure process, and the appropriate monitoring strategy used. For this reason, the concepts of slope stability and failure mechanism were presented based on a review of the existing literature. Different methods of monitoring embankments were also presented.

During the literature survey, various methods of monitoring were studied, and geophysical methods have been found to be the most effective means of monitoring slope stability and its failure mechanism. This is due to their numerous advantages over the conventional geotechnical methods. The methods have been successfully used in the study of many cases of the failure of embankments made up of sedimentary soils in temperate climates. There has previously been, however, little or no attempt to apply the technique to the study of the slope failure mechanism of tropical residual soil. This is against the backdrop that more slope failures in residual tropical soils have been recorded in the last few years. Moreover, it has been confirmed that it could be erroneous to apply the findings from other types of soils to residual tropical soil. This is because the established classical theories have failed to address some concepts associated with soils formed under the subtropical and tropical environment (Gidigas, 1988).

CHAPTER 3

Production of Artificial Tropical Soil

3.1 Introduction

Residual tropical soils are extensively used in the construction of embankments in tropical and subtropical countries, where they exist in abundance. The definition of the soils and their peculiar properties that make them different from other types of soils is given in chapter 1. Although there is varied definitions of the soil, there appears to be a consensus view about it been formed by intense weathering (involving decomposition and leaching) of underlying igneous, sedimentary or metamorphic rock, resulting in the material rich in iron and aluminium oxides (Styles et al., 2001, Huat et al., 2007a). The variability in the definition of the soil reflects the variability of its nature and properties (Gogo-Abite, 2005). Although, the locations where residual soils are found may be distant apart on the geographic space, they have the same basic tropical and subtropical climates that favour the above described intense weathering. Some of these countries with their typical soils are given in Table 3.1.

Due to the variability in climatic conditions (i.e. rainfall and temperature) and geographical location the two controlling factors of geology and the degree of weathering of the parent material, the physical properties of tropical residual soil vary from region to region. Therefore, residual tropical soil is a name used to describe a wide variety of soil rather than distinct, clearly defined soil material. In this study, the wider meaning is adopted by considering the varied physical properties of the soil from different parts of the world. Intensive research undertaken on tropical soils in many parts of the globe make the properties readily accessible, Therefore, a wide range of literature was consulted to establish these properties.

Table 3-1: Tropical countries and the types of residual soil found in each country (Huat et al., 2007b)

Parent rock		Degree of working			Transported soils	
Country	All types	Completely: Original structure destroyed?	Completely: Original structure intact?	Highly: Structure intact, Soil >50%?	Colluvium included?	Other included?
Australia	Yes	?	Yes	Yes	Yes	Yes
Brazil	No	Yes?	No	No	No	No
China	Yes	?	Yes	Yes	?	No?
Germany	Yes	?	Yes	?	No	No
Ghana	Yes	?	Yes	Yes	?	?
Hong Kong	Yes	Yes	Yes	Yes	Yes	No
India	Yes	?	Yes	Yes	No	No
Japan	Yes	?	No	Yes?	Yes	?
Malaysia	Yes	Yes	Yes?	Yes?	No?	No
New Zealand	Yes	Yes	Yes	Yes	Yes?	?
Nigeria	Yes	Yes	Yes	Yes	Yes?	Yes
Pakistan	Yes	No	Yes	Yes?	No	No
Philippines	Yes	No	Yes	Yes	Yes	No
Singapore	Yes	Yes	Yes?	Yes	?	No?
South Africa	Yes	Yes?	Yes	Yes	?	Yes
Sri Lanka	Yes	Yes	Yes	Yes	Yes	No
U.K.	Yes	Yes	Yes	Yes	No	No
U.S.A.	Yes	Yes?	Yes	Yes	No	No

Not minding the variability in the physical properties of tropical residual soils at global scale, some researchers hold the view that the properties and behaviour of tropical soils established in one location could be assumed to be similar at another locations of similar climatic condition, especially where the soils are from the same parent rock or of similar geological formation (Gogo-Abite, 2005). However, studying tropical soils at regional or local scale will be more precise than considering it globally. For this reason, the study focussed more on tropical residual tropical soil typically found in Nigeria with

special emphasis to the northern Nigeria. This is in line with the study background and problem statement, both outlined in chapter 1.

The idea of narrowing down the study to a locality of Nigeria is to allow for an in-depth investigation to establish with precision the properties of the material under study. To achieve this objective, the abundant information about Nigerian lateritic soil available in the literature was studied. Additionally, laboratory tests on a soil material sourced from Zaria in northern Nigeria, were conducted to establish index and geotechnical properties. Previously, similar tests were conducted on the same material from the same source by Madu, 1977, Ola, 1978, Ogunsanwo, 1989, Osinubi, 1998a, Osinubi, 1998b, Osinubi and Nwaiwu, 2006, Osinubi et al., 2009. The results of all these tests will be presented and discussed in this chapter.

The primary aim of the whole research project is to study a failure mechanism in tropical residual soil. It was a great challenge to conduct this research on tropical soils in a geographical location like the UK where such soils do not exist. This is because sourcing the required quantity (i.e. 10 tons) of soil from sites in tropical countries for detailed laboratory studies in the UK is very tasking due to the travel distances involved. Even if there is enough budgetary provision to cover cost of haulage, transfer of such quantity across the borders of the countries is often prohibited (<https://www.gov.uk/guidance/moving-prohibited-plants-plant-pests-pathogens-and-soil>). To find a solution, utilizing the materials available in the UK to produce pseudo-tropical soil. emerged as the most practical solution. For this reason, a novel methodology was developed to modify locally available materials to obtain an artificial soil of desired properties. This ensured that sample produced where of the quality required and could be produced in a consistent and repeatable fashion. Similar approaches have been successfully used in the previous studies e.g. Vaughan et al. (1988), Dibben (1998), Zourmpakis et al. (2005) and (Jiang et al., 2012). This chapter presents how the artificial tropical soil material was produced and validated as a suitable proxy for natural tropical soil samples.

It should be noted that substantial part of the work presented in this chapter, has been earlier presented as conference paper by Sadiq et al. (2016). which was undertaken as part of the research programme presented in this thesis. The points, figures and tables taken from this paper have been duly acknowledged.

3.2 Production of artificial soils – previous studies

One of the past attempts to develop methods of producing artificial soil for practical purposes included mixing two or more naturally occurring soils in a standard laboratory at a very high temperature over a certain period. This method was used by Vaughan et al. (1988) and Malandraki and Toll (2000). The main aim here was to replicate the bond strength and density of the natural tropical soils.

In an alternative to firing, Haeri et al. (2005) produced artificial residual soils by the addition of cement to alluvium to reproduce the strength properties of a natural Iranian soil. Similarly, Jefferson and Ahmad (2007) produced in the laboratory an artificial collapsible soils that was used to assess collapse properties of soil in a repeatable controllable fashion, overcoming difficulties obtaining field samples. In this method silt sized material with varying amount of processed kaolinite, English China Clay was used applying three different approaches, adopted from the previous work of (Lawton et al., 1989, Trofimov, 1990, Basma and Tuncer, 1992, Assallay et al., 1997, Dibben, 1998, Zourmpakis et al., 2005). The three approaches include the air fall, the wet, and the bonding methods.

The air fall method involves mixing silt sized particles with clay at dry condition and sieving the mixture through a 63 μ m sieve falling from a height of 250mm directly into an oedometer ring placed on a porous stone/filter paper. After filling the oedometer, the surface is levelled off before adding a small static weight to reduce the void ratio to a value closer to typical metastable loess soils. In the wet method, a paste is form by mixing clay and silt particles with water. This paste is then placed in the

specimen ring before loading it with static load varying between 5 and 100Kpa to create a void ratio like that of the natural deposit. In the third technique i.e. the bonding method, the paste formed in the wet method is left to dry before crushing and placing it into the ring in layers via sieving as in air fall method. A fine mist is then applied on each of the layers to achieve a predetermined water content before loading it as described in wet method. Finally, the specimen is dried in the oven to create bonding between the particles.

After creating artificial soils with similar magnetic properties to the Cambodian soil, Styles et al. (2001) concluded that, though it is difficult, it is possible to produce an artificial soil that can reach a large extent in replicating the properties of the natural soil.

From the above cited works, it is clear that soil can be created artificially. However, many of the existing methods attempt to replicate one or two key geotechnical properties and no attempt was made to reproduce basic index properties such as particle size distribution, Atterberg limits and density, which are important in engineering applications such as stability of slopes and embankments. The properties looked by the authors cited above are given in Table 3-2. Whilst these materials do not fully replicate natural materials, they do overcome many challenges commonly encountered when working with challenging soils from overseas such as a tropical residual soil.

Table 3-2: Soil properties previously considered in the production of artificial soil

Author(s)	Method used	Replicated Properties
Vaughn (1988)	Firing of soil mixture	Strength and density
Malandraki and Toll (2000)	Firing of soil mixture	Strength and density
Styles et al. (2001)		Magnetic properties
Haeri et al. (2005)	Added cement to alluvium	Strength
Jefferson and Ahmad (2007)	Air fall, wet and bonding methods	Void ratio, density and collapsibility

In this research, a better approach to soil modification has been formulated. This chapter presents the methodology for producing pseudo-tropical soil and the result obtained using the new approach, which draws from the methods presented in the literature (see section 3.4.1.).

3.3 Materials

As stated earlier in section 3.1, in this study, tropical residual soil is considered in general, but laterite typically used for the construction of engineering infrastructure in Nigeria, is selected as a case study. A sample material sourced from Zaria in Northern Nigeria was tested in Nigeria to establish its geotechnical properties given in Table 3.3. The properties of the soil from this source previously established by (Madu, 1977, Ola, 1978, Ogunsanwo, 1989, Osinubi, 1998a, Osinubi, 1998b, Osinubi and Nwaiwu, 2006, Osinubi et al., 2009, Bello, 2011) will be presented and discussed in the later section 3.4.. Table 3.3 also contains properties of other natural materials (i.e. Etruria formation and Builders sand), sourced and tested in the UK and were used to produce artificial tropical soil to be discussed in this chapter.

Table 3-3: Geotechnical properties of three soils based on laboratory tests (adopted from (Sadiq et al., 2016))

Soil Type	Etruria Formation Mudrock Material	Natural Tropical Soil	Builders' Sand
Properties			
Liquid limit, (%)	38	41	-
Plastic limit, (%)	19	23	-
Plasticity Index, (%)	19	18	-
% Gravel	0.4	1.1	-
% Sand	8.6	37.7	99.9
% Fines	92	61.2	-
Specific Gravity	2.82	2.7	2.53
Maximum Dry Density, Mg/m ³	1.99	1.92	1.335
Optimum Moisture Content, (%)	13.5	16.2	14

3.4 Methodology

3.4.1 Stage 1. Preliminary study

The first stage was a preliminary review of tropical residual properties, from the literature. Tropical residual soil in different parts of the world was considered first, before specifically studying Nigerian residual soil known as laterite. This is in recognition of the possible variation in properties of the soil, due to the differences in climatic conditions and geographical locations as discussed in section 3.1. Among the published works consulted in the literature are that of (Madu, 1977, Ola, 1978, Ogunsanwo, 1989, Osinubi, 1998a, Osinubi, 1998b, Osinubi and Nwaiwu, 2006, Osinubi et al., 2009, Bello, 2011). The aim here was to identify key properties of tropical residual that will serve as a basis for identifying a British soil that will match those properties. After this, a broad range of British soils were reviewed, again with reference to available literature. Of all the soils reviewed, Etruria formation mudrock (from the UK stratigraphic unit) was found to possess similar index properties to the targeted tropical soil and, thus was selected for further study.

3.4.2 Stage 2. Desk study

Following stage 1, a visual inspection was undertaken on the selected British soil i.e Etruria formation, to examine key aspects of physical appearance, including color and texture of the soil selected in stage 1. Next, More in-depth study on the Etruria Marl including its chemical and physical properties was undertaken at this stage., This was done by consulting a wide range of literature again including (Gidigasu, 1972, Hutchinson et al., 1973, Madu, 1977, Ola, 1978, Cripps and Taylor, 1981, Ogunsanwo, 1988, Reeves et al., 2006, Robertson, 1931). Again, comparison of this more in-depth studied British soil was made with the tropical soil under study.to assess similarities and differences between the two. From this the suitability of the soil selected in the previous stage was confirmed. It was then decided to modify the selected British soil to arrive at artificial tropical soil.

3.4.3 Stage 3. Laboratory testing

Laboratory tests were then undertaken to check the desk study findings. It was felt that particle size distribution should be determined first as this gives a useful indication of other physical properties of the soil, e.g. the permeability and the rate of deformation of saturated soils. From the particle-size distribution curve, sand and fines fraction of each of the two soils was estimated and it gave an idea of the proportions needed to be added to modify the chosen British soil to reach the target final product. From this, mix ratios for the modification were established. Grading tests were carried out in accordance with BS 1377:1990.

3.4.4 Stage 4. Soil design and Production

The mix formula designed on the basis of the sand-Etruria Marl ratio, decided in the previous stage, was used to produce the artificial soil. This was followed by more laboratory test to determine index and geotechnical properties of the produced soil. The index tests were conducted in accordance with BS1377:1990 part 2, while particle density and compaction characteristics were conducted in accordance with BS1377:1990 part 2 and 4, respectively. The results of these tests on artificial tropical soil, were compared with the properties of the soil to be replicated. From the comparison, the similarity of the values with that of the target natural tropical residual soil was established. Thus, the final ratio to be used to produce the artificial tropical residual soil was confirmed.

3.5 Results

3.5.1 Results of Preliminary Studies

Etruria Formation mudrock was observed to have most resemblance with the natural tropical residual soil based on the comparison of their properties found in the preliminary studies. This, despite the fact that the Carboniferous Etruria Formation used was some 300 million years older than the target Quaternary tropical residual soil and was partially lithified by burial (Robertson, 1931). This is

because, reddish to dark brown colour and texture of the Etruria Formation mudrock and the natural tropical residual soil, were suitably close.

Colour is particularly important as it indicates the environmental processes that a given soil has experienced as well as its minerals make up. For example for both the selected base soils and the target soil the reddish brown colour indicates iron oxide is present.

Table 3.4 summarizes examples of published chemical properties of the tropical residual soils giving typical ranges seen in different parts of Nigeria. From Table 3.4 it can be seen that Ferric oxide (Fe_2O_3) contents are variable, ranging from a low of 2% to a high of just over 40%. Similarly, Table 3.4. shows that the percentage of bases are very low while a large amount (>c.35%) of silica are contained in all soils included.

Table 3-4: Oxide composition of lateritic soil from different parts of Nigeria

Reference	Madu (1977)	Nnadi (1988)			Ogusanwo (1989)	Ogusanwo (1995)					Osinubi (1998b)
Region and Location	Various parts of eastern Nigeria	Eastern Nigeria			Western Nigeria						Northern Nigeria
		Onisha	Imo Airport	Okigwe	Uni-Ife	Ife-Ondo Rd	Ife-Akure Rd	Maryland	Uni-Ife	Ife-Ifewara Rd	Zaria
SiO ₂	34.80 - 58.33	56.8	49.5	54.7	51.41 - 62.37	62.59	68.83	67.11	62.37	51.41	35.6
Al ₂ O ₃	7.63 - 16.03	17.6	12.3	11.5	23.93 - 25.82	25.4	19.3	21.21	23.93	25.82	27.4
Fe ₂ O ₃	19.45 - 42.16	6.45	5.98	4.75	5.30 - 12.52	3.87	2.36	5.87	5.3	12.52	2.4
TiO ₂	1.15 - 1.55	1.27	0.801	0.754	0.64 - 0.81	0.47	0.64	0.9	0.64	0.81	
MgO	0.33 - 2.10	0.106	0.059	0.054		-	-	-	-	0.19	0.22
CaO	1.39 - 2.58	0.01	0.01	0.01	1.91 - 4.99	0.49	0.62	0.32	0.17	0.57	0.28
Na ₂ O	0.14 - 0.18	0.12	0.16	0.075	4.23 - 5.73	-	-	-	0.11	0.13	
K ₂ O	0.01 - 0.12	0.148	0.069	0.07		0.43	2.62	0.22	1.63	4.1	
P ₂ O ₅		0.13	0.2	0.1							
MnO		0.017	0.015	0.01							
Loss of ignition	8.52 - 11.05	4.44	5.29	5.14							1.46

Tables 3.5 and 3.6 show typical mineralogy of British Etruria mud rock and natural tropical residual soils occurring in Nigeria, respectively. Both types of soil consist mainly of quartz, kaolinite and goethite. However, only the natural residual tropical soil, which contains significant feldspar.

Table 3-5: Mineral composition of typical Nigerian lateritic soil (Ogunsanwo 1988, 1995)

Sample Location	Feldspar	Quartz	Kaolinite	Muscovite	Goethite	Reference
Uni-Ife	50	30	10	-	10	Ogunsanwo 1988
Ife-Ifewara rd	30	Traces	55	5	10	Ogunsanwo, 1988
Ife-Ondo Rd.	-	40	25	30	Traces	Ogunsanwo, 1995
Ife-Akure Rd.	Traces	60	35	-	15	Ogunsanwo, 1995
Unife	50	30	10	-	10	Ogunsanwo, 1995
Ife-Ifewara rd	30	Traces	55	-	15	Ogunsanwo, 1995
Maryland	-	50	35	-	15	Ogunsanwo, 1995

Table 3-6: Mineral composition of Etruria Formation (Hutchinson et al. 1973, taken from (Sadiq et al., 2016)

Mineral	Quarry samples (in situ and largely unweathered) (Holdridge, 1959)	
	Maximum (%)	Extreme range (%)
Quartz	30.5 to 41	20 to 56
Kaolinite (disordered)	33 to 42	26 to 56
Mica/illite (disordered)	14.5	6 to 22
Expandable mixed-layer clay		
Goethite/limonite	10	3 to 22
Rutile	1.3	1 to 1.5
Carbonates	0.6	0 to 5

From the above analysis, it can be concluded that, the similar physical appearance of Etruria Marl and lateritic soils is due their common chemical and mineralogical composition. The minor difference in percentage composition of some chemical and mineralogical constituents might be due to the difference in mode of formation.

3.5.2 Grain-size Distribution

Figure 3.1 shows the results of grading tests on the three soils involved in this study. They are Etruria Formation mudrock, the natural residual tropical soil and the sand. In addition, two references are shown on the graph. They are for the range of typical Etruria mudrock presented by Hutchinson et al., (1973) is provided for reference and the grading curve for naturally occurring residual tropical soil based on the previous test conducted by Bello (2011).

From the graph it can be seen that, the grading curve of Etruria mudrock is within the envelope established by Hutchinson et al., while that of tropical soil tallies with the one provided by Bello.

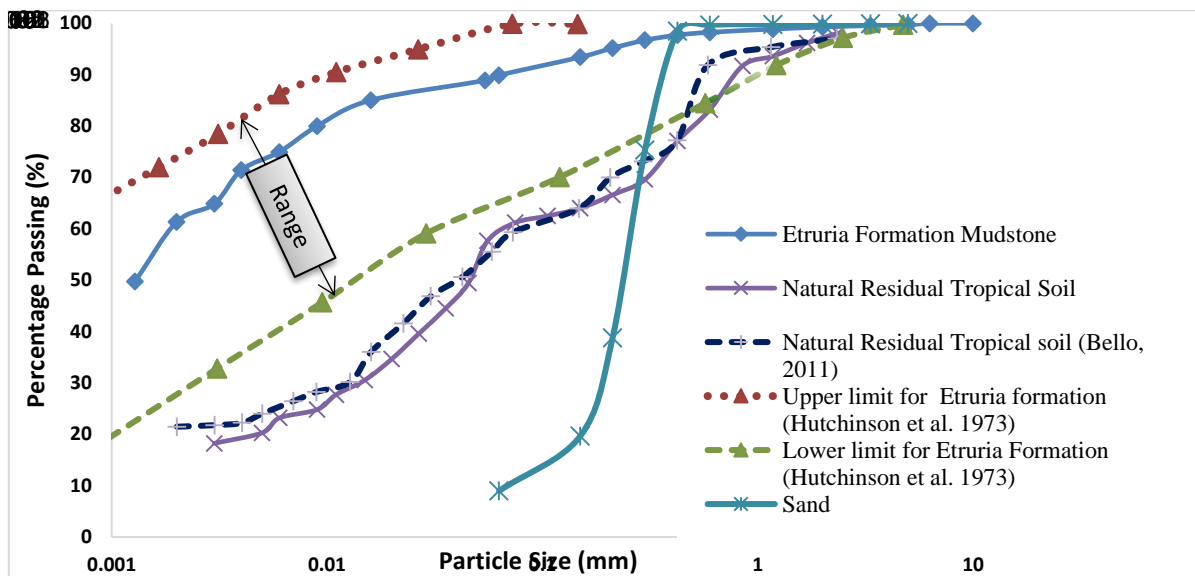


Figure 3-1: Particle size distribution of all the soils involved in this study (adopted from (Sadiq et al., 2016))

Using the soil grading curve presented in Figure 3.1, the constituents of each of the three soil has been determined as shown in Table 3.7. It can be seen from the table, that silty sand needs to be added to Etruria Formation mudrock to increase the percentage of sand and lower the clay content to bring it closer to that of the tropical soil

Table 3-7: Coarse and fine fractions of the soils (Sadiq et al., 2016)

Soil Type	Clay (%)	Silt (%)	Sand (%)	Gravel (%)
Natural residual tropical soil	17	44.2	37.7	0.8
Etruria Formation mudrock	61.8	29.2	8.5	0.3
Sand	0	0	99.9	0

Based on the constituents of the three soils presented in Table 3.7 it was decided that 10 to 50 percent of sand needed to be added to Etruria Formation mudrock to replicate the natural residual tropical soil. By undertaking a series of trial mixes as indicated in Figure 3.2, the desired mix ratios of sand to Etruria Formation mudrock that yielded a grading curve close to that of the targeted soil was

determined. It was found that a ratio of 60% sand-40% Etruria Formation mudrock material provide the best fit to the target soil. This ratio was adopted to create the artificial tropical soil.

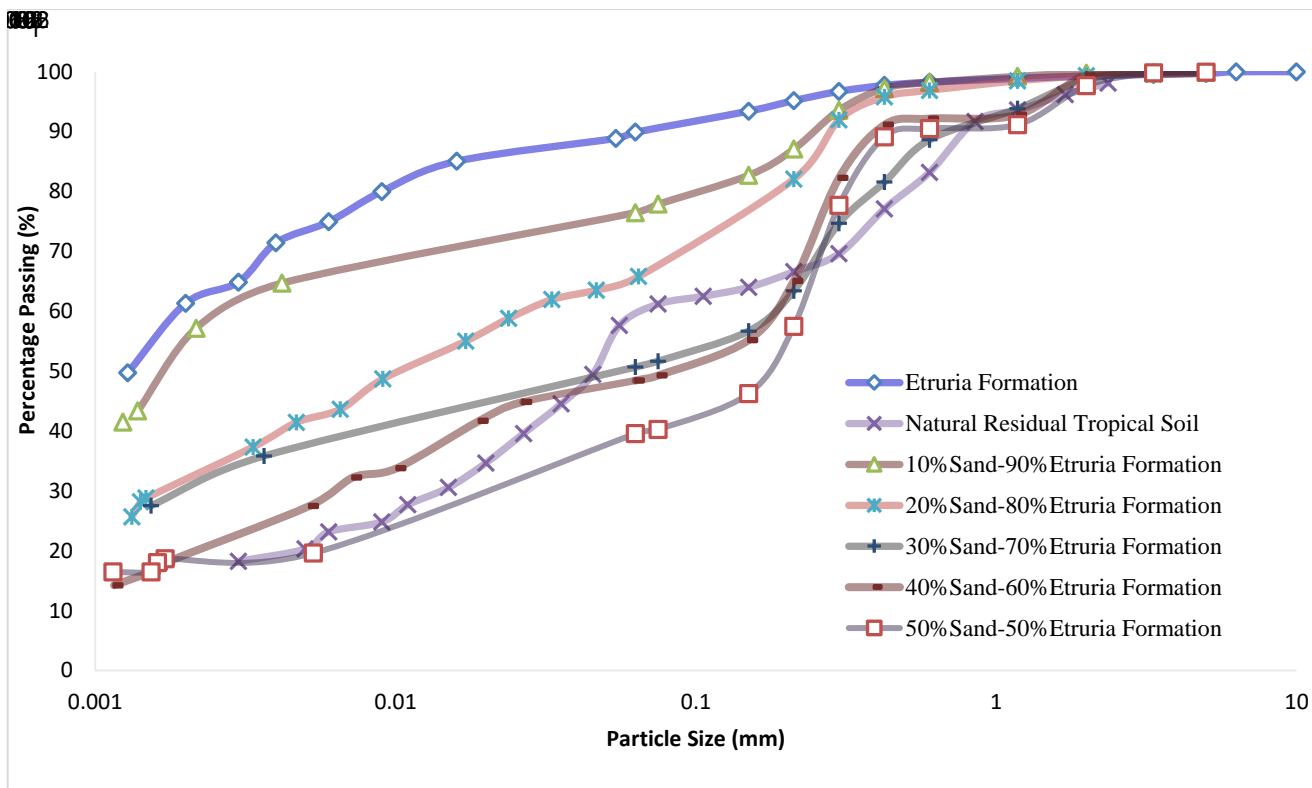


Figure 3-2 Particle size distribution showing the steps of soil production (after (Sadiq et al., 2016))

3.5.3 Laboratory confirmatory tests

After producing the artificial soil, further laboratory tests to confirm whether the geotechnical properties of the produced soil, is the same as that of the natural soil yielded the results shown in Table 3.8. In the table, the results were compared with the properties of the natural residual tropical soil earlier established through laboratory testing. The result is also comparable with those obtained during the previous studies in different parts of Nigeria and in other parts of the world. The results of these previous works are presented in Tables 3.9 and 3.10 respectively. Discussion on the individual properties are presented in the following sub-sections.

Table 3-8: Property comparison between the natural and artificially produced lateritic soils (after (Sadiq et al., 2016))

Index Properties	Produced Artificial Tropical Soil	Natural Tropical Soil
Liquid limit, (%)	31	41
Plastic limit, (%)	12	23
Plasticity Index, (%)	19	18
Specific Gravity	2.68	2.7
Maximum Dry Density, Mg/m³		
BS Standard Proctor	1.94	1.92
Optimum Moisture Content, (%)		
BS Standard Proctor	11.5	16.2
Strength Parameters	1.83x10 ⁻⁸	
Cohesion (kPa)	26	
Angle of frictional resistance (o)	21.4	
Permeability		
BS Standard Proctor	1.83x10 ⁻⁸	
Less than BS Standard Proctor	10 ⁻⁵ -10 ⁻⁶	

Table 3-9: Physical properties of laterite from different parts of Nigeria

Reference	Madu (1977)	Nnadi (1988)			Ola (1978)	Osinubi (1998b)	Osinubi et. al. (2009)	Bello (2011)
Region and Location	Eastern Nigeria				Northern Nigeria			Western Nigeria
	Various locations	Onisha	Imo Airport	Okigwe	Zaria			Ibadan
Liquid limit, (%)	42.0-57.8	33.7	44.2	32.8	42	44	41	43-48
Plastic limit, (%)	21.3 - 40.9	16.4	23.2	17.6	25	24	24	28-32
Plasticity Index, (%)	15.5-24.0	17.3	21	15.2	17	20	17	14-16
Specific Gravity		2.65	2.64	2.74	2.7	2.62	2.62	2.62-2.66
Maximum Dry Density, Mg/m³								
BS Standard Proctor	1.71-1.97					1.84		1.74-1.78
Optimum Moisture Content, (%)								
BS Standard Proctor	15.5-19.9					19.1		15.1-17.8
Strength Parameters								
Cohesion (kPa)					26.5			
Angle of frictional resistance (o)					24.1			
Permeability								
BS Standard Proctor								
Less than BS Standard Proctor						2.50x10 ⁻⁵		

Table 3-10: Index properties of laterite found in other parts of the world

Property	Townsend (1970)	Townsend and Manke (1971)	Tsaparas (2003)		Rahardjo (2005)	
			Type 1 (Surface layer)	Type 2 (10m below the surface)	Type 1 (Surface layer)	Type 2 (1.5m below the surface)
Liquid Limit %	60	57.8	45	46	47	34
Plastic Limit %		39.5	26	29		
Plastic Index %	21	18.3	19	17	21	13
Specific Gravity	2.8	2.8			2.67	2.72
Proctor Density (Kg/m ³)		84.5*			1.86	2.27
Saturated gravimetric moisture Content %		35			35	13.5

3.5.4 Particle Density

The particle density of the artificial soil is found to be 2.68, which is sufficiently close to the values for natural laterite presented in Table 3.3. It compared favorably with the value 2.7 of the natural soil in Table 3.8 and is consistent with the typical values for laterite from different parts of Nigeria and around the world as presented in Table 3-9 and 3-10, respectively.

3.5.5 Atterberg Limits

Atterberg limits are very important as they indicate water content of a soil, with its upper plastic limit (or simply known as plastic limit) and that of the lower plastic limit (simply known as liquid limit). The difference between the two limits gives the plasticity index and it is the main measure of plasticity of a soil and is often used to determine other characteristics/properties of soils (Mitchell and Soga, 2005), as these index properties are controlled by the same factors that control all other geotechnical properties. During the Atterberg limit test, the liquid limit of the soil was found to be 31 while its plasticity index is 19. Although the values found with the artificial soil are lower than of the natural deposits (see Table 3.8), their plasticity are almost identical to those of the natural soil, being the same as the plasticity indices found in many tests previously conducted on Nigerian soil. These include the

works done by Madu (1977), Ola (1978), Nnadi (1988) and Osinubi (1998b) as shown in Table 3.9. Similar values were also obtained by Townsend et al. (1971) and Tsaparas et al. (2003) for laterites in Hawaii and Singapore, respectively as shown Table 3.10.

The lower values of the plastic and liquid limits recorded could be due to the mineralogy and nature of the soil colloids of the added soil, and whilst slightly deviates from replicating the natural soil fully, is deemed suitable for the purposes of this research, where relative changes in water contents are key. The liquid and plastic limits of soil are dependent on its mineralogy and can be used to relate the water content to its consistency (Vaughan et al., 1988).

3.5.6 Compaction Characteristics

For the compaction test, the optimum moisture content (OMC) is 11.5% and the maximum dry density (MDD) was found to be 1.94 Mg/m³. When compared with the value of 1.92 Mg/m³ of the natural soil shown in Table 3.6, it was found that artificial soil has a slightly higher MDD. However, this is within the range established by Madu (1977). The lower value of 11.5 for the OMC seen with the artificial soil (see Table 3.6) is probably due to the mineral content or particle shapes of the added sand. Mineral content and microstructure of the soil particle of the fractions of the soils will influence the behaviour of the resulting mixture of the soil and this is well established (Mitchell and Soga, 2005).

Due to the unique microstructure of natural tropical soil, microaggregate stability (such as laterite concretions) and microporosity control the compaction behaviour of the soil. During compaction, the initial increase in density with the increase in moisture content is due to the lubrication between the soil particles which causes rearrangement of soil particles and consequent reduction of voids, though the particle might remain loosely bound by natural concretion (de Carvalho et al., 2015). This process continues with increase in moisture allowing more compaction energy to extend to the contact between

the micro aggregates preserved until now. As the process continues, the soil molecules becomes closely packed resulting to the continuous density increase, until maximum dry density (MDD) is reached.

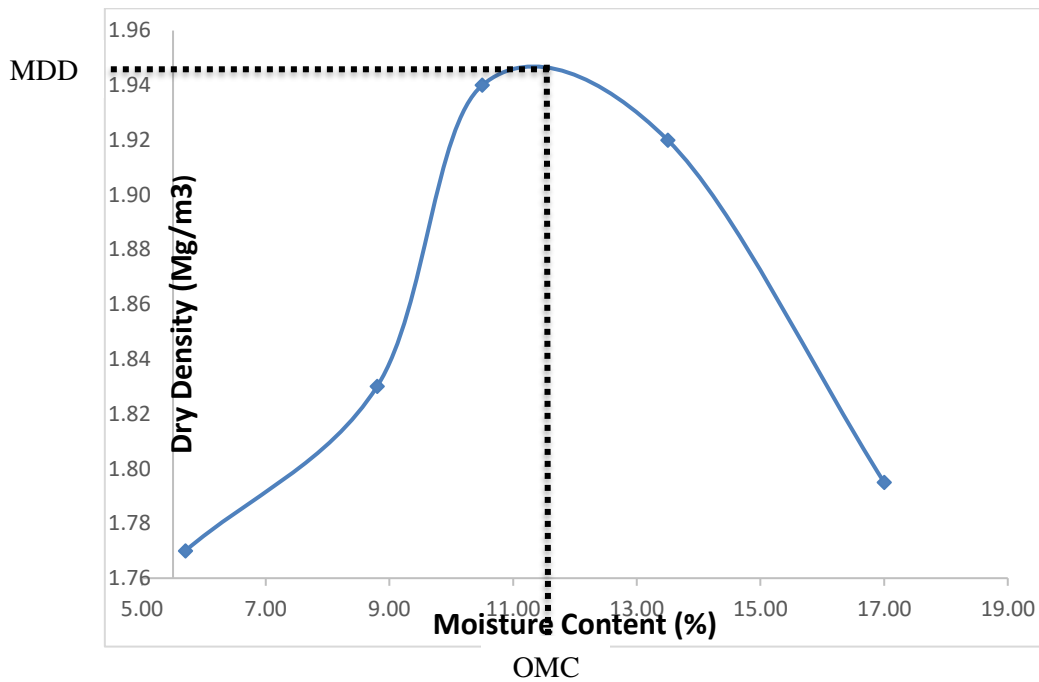


Figure 3-3: Compaction curve from which MDD and OMC was estimated

It is possible to reach the MDD without destroying the micro structure of the soil. This behaviour is responsible for the high OMC values in natural tropical soil. However, if micro pore are destroyed, the compaction process renders the soil more fined-grained and more sensitive to moisture variation (de Carvalho et al., 2015). In that case, a low value of OMC, comparable to that of artificial soil will be recorded. In this study, replicating the microstructural property is not the priority. What is important is to produce a soil that is similar to the natural one in terms of physical or engineering properties. In this case the maximum dry density of the soil is the most important, as it is the main parameter that determines the strength of a soil. Since the Maximum dry density value of the two soils are close, the soil is said to be similar

3.5.7 Permeability

The permeability of soil was tested using a falling head method in accordance with the traditional geotechnical practice. The average value of hydraulic conductivity obtained using standard proctor compaction (25 blows) is 1.83×10^{-8} cm/s as shown in Table 3.11. Higher values were however, recorded at less compactive efforts as will be seen later in chapter 5. This values are within the range of values for Nigerian soil found in the literature (Ogunsanwo, 1989, Osinubi, 1998b). The range is also the same as the one established by (Ola, 1980, Nnadi, 1987) as shown in Table 3.12 taken from (Nnadi, 1988). Also in the table are the values of permeability coefficient of tropical residual soils from Kenya, Venezuela and Brazil reported by (Foss, 1973, Prusza et al., 1983, Dias, 1985, Vilar et al., 1985) and, respectively.

Table 3-11: Permeability test result

Measured/Calc. Parameter	TEST 1	TEST 2	TEST 3
Dia. of a stading tube (cm)	0.21	0.21	0.21
Area of the tube, a (cm ²)	0.03	0.03	0.03
Dia. of sample (cm)	10	10	10
Area of sample, A (cm ²)	78.5	78.5	78.5
Length of sample, l (cm)	14.1	14.1	14.1
Initial height ho (cm)	53	45	42
Final height h ₁ (cm)	45	42	34
Time, t (s)	61488	25524	61056
Perm. Coefficient, k (cm/s)	1.65E-08	1.68E-08	2.15E-08
Average k, (cm/s)	1.83E-08		

Table 3-12: *In situ* and compacted permeability of some laterite soils (Nnadi, 1988)

Soil Type	Location	Clay Content (%)	Permeability (cm/sec)		Reference
			Compacted	In situ	
Red Residual soil	Kenya	78 - 90	10^{-1}	10^{-4}	Foss, 1973
Laterite Soil	Nigeria	N.A	10^{-0} to 10^{-10}	N.A	Ola, 1980
Granite Laterite	Venezuela	N.A	10-0	10^{-4}	Prusza, 1983
Cenozoic	Brazil	10 - 40	N.A	10^{-3} - 10^{-4}	Villar, 1985
Latosol	Brazil	68	$6.2 - 1.3 \times 10^{-8}$	1.5×10^{-5}	Dias & Gonzales 1985
Laterite Soil	Nigeria	15 - 20	10^{-1} - 10^{-8}	N.A	Nnadi, 1987

3.5.8 Shear Strength

The shear strength parameters were obtained by direct shear test. Figure 3-4 shows the maximum shear stress at each applied normal stress. The relationship is not perfectly linear as shown by the curvilinear form of the original Mohr failure envelope. This unusual behaviour is exhibited by some tropical soils due to the weak bonding existing among the coarse particulate materials (de Carvalho et al., 2015).

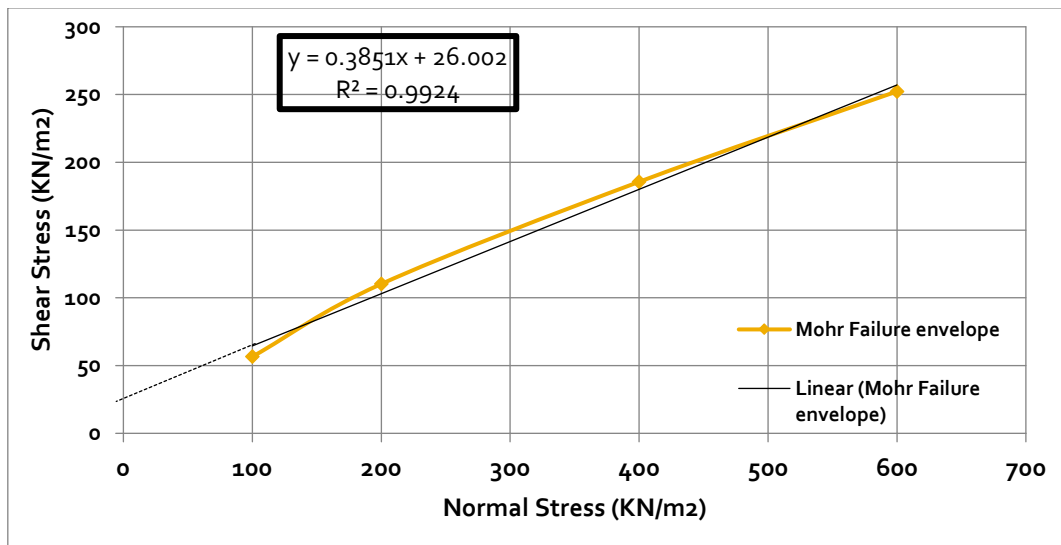


Figure 3-4: Mohr failure envelope

To obtain the strength parameters, a linear trend line was plotted, and from the straight line effective cohesion intercept was obtained. The values obtained are 26 kPa and 24° for cohesion and angle of internal resistance respectively. The result is consistent with Ola (1978) who conducted a research on a soil from the same source as the soil tested in this research. He obtained 26.5kPa and 21.4° for cohesion and angle of shear resistance, respectively, as shown in Table 3.9. The values of shear strength parameters obtained in other parts of the world, are tabulated by Townsend (1985) as shown in Table 3.13. The table contains similar values of strength parameters of lateritic clays from Africa and Venezuelan granitic lateritic soils, respectively reported by (Horn, 1982) and Prusza et al., 1983. In particular, the c' value for andasol reported by Wesley (1974) is identical to the value of artificial soil obtained in this study.

Table 3-13: Shear strength parameters of some tropical soil around the world (Townsend, 1985)

Soil type and location	Φ' in degrees	C' in kPa	Reference
Lateritic gravels, Africa	37.5	0-40	Horn (1982)
Lateritic clays, Africa	22.5	0-100	Horn (1982)
Lateritic soil, Panama	38	0	Townsend (1970)
Granitic lateritic soil, Venezuela	21.5	20	Pursza (1983)
Granitic laterite, Brazil	31	0	Vargas (1953)
Andasol, Java	36	24	Wesley (1974)

Based on the comparison made between the shear strength parameters of the produced artificial soil and that of the natural soil, it can be concluded that, the two have similar strength property. Like other properties of residual tropical soils, the strength property can vary considerably depending on the controlling factors of formation and soil makeup. The strength parameters are influenced by the mineralogy and chemical composition which in turn depend on the parent material, degree of weathering and climatic factors. Cohesion increases with the increase in kaolinite content, while the angle of friction increases with increasing sesquioxides content (Gogo-Abite, 2005). Ogunsanwo (1989), illustrated how the strength parameters vary with the variation of parent material by testing laterite from different geological origin as shown in Table.3.14.

Table 3-14: Effective strength parameters of laterite from different parent materials (Ogunsanwo, 1989)

Parent Material	ϕ' (deg)	c' (kPa)
Quartz schist	31	15
Mica schist	31	35
Granite gneiss	30	15
Amphibolites	27	45
Benin sand	26	26

From Table 3.14 it can be observed that, laterite from Benin Sand is the closest to the one sourced from Zaria, which is replicated in this study.

3.6 Summary and Conclusions

Tropical soil required for the research intended to be conducted in UK, is not readily available at this geographical location. Due to impossibility of sourcing the material from tropical countries where they exist, it was decided to modify locally available materials to arrive at the artificial soil with desired engineering properties. Although there are existing methods of soil modification, none of them could give a satisfactory procedure to achieve the desired objective. For this reason, a new method is hereby developed based on the intensive study of properties of tropical residual soil typically found in Nigeria and around the world. With the established method, the available British mudrock material and sand were used, to produce an artificial tropical residual soil.

In the chapter, the methodology developed was presented and discussed. It involved extensive literature research through which chemical and physical properties of all the soils involved were studied. Laboratory tests to assess the properties of the British soil and sand involved in this study were also conducted. A mix formula was then designed by varying the soil composition and conducting the particle size distribution (PSD). At the end, sand-Etruria ratio of 2:3 gave a PSD that is the nearest to that of the targeted tropical soil. To confirm the product of the experiment tallies with the prediction of analysis and design, the properties of the resulting soil were determined by laboratory testing. The results obtained, were compared with the properties of natural tropical soils.

The physical properties such as particle size distribution, specific gravity, plasticity index and maximum dry density of the artificial soil are found to be similar to that of the natural tropical, though the liquid limit and OMC are little lower than required. The little difference in moisture sensitivities between the natural and artificial soils is due to the possible differences in mineralogy and microstructure between the two soils. These were not considered in this study, as the main objective is to replicate the physical or engineering properties of the natural soil.

Based on the similarity in colour, chemical constituents, and physical properties, it can be concluded that when 40% of a commercial sand used for building is added to 60% of Etruria formation mudrock material an artificial soil is produced that is comparable with the natural residual tropical soil from Nigeria.

CHAPTER FOUR

NUMERICAL MODELLING

4.1 Introduction

Numerical modelling and simulations have now been generally accepted as a research tool in geotechnical engineering. The modelling is conducted for many reasons. Some of them mentioned by Barbour and Krahn (2004) include making a prediction about the behaviour and performance of a part or whole of engineering infrastructure, comparing options to make decisions, verifying some established governing scientific principles or validating a physical or full-scale model (Krahn, 2012). All these reasons are relevant to this research as explained as follows.

In slope stability studies, the flow of water through the soil, the positive and negative pore pressures generated due to the flow of water and instability or deformation in response to the hydrological processes, are the major processes involved. The process can be quite complex and requires the application of mathematical relationships and other scientific principles to describe (Barbour and Krahn, 2004). Fortunately, many numerical tools have been developed to handle these complexities, in recent years. Such tools are used in this research, to complement the physical modelling employed in the experimental element of the research. Specifically, the numerical modelling was used to achieve the following twofold objective.

First, is to aid the design of the physical model to be used later in the experimental study. This was done by comparing alternatives, varying boundary conditions and studying different scenarios before selecting the best option that meets the requirement of the research objective. Second, is to study the designed slope model in a more detail manner, to get an idea about the failure behaviour of the designed model.

The process began by selecting the appropriate numerical software that can model the above processes before using it to achieve the above objective. The steps taken to achieve the above objectives and the outcome of the exercise are presented in this chapter.

4.2 Theoretical concept and selecting numerical models

Many numerical models have been developed and applied in slope stability studies. Davies (2011), after reviewing many of them, grouped the models into two broad categories. Those that model the flow of water in the soil are called the hydrological models while those that are concerned about physical deformation are termed, mechanical models. Before selecting the right numerical model, it is essential to have a good understanding of the theory and concepts involved in the study.

Naturally, tropical soils exist as unsaturated soil due to their deep water table (Fredlund and Rahardjo, 1993). The region above phreatic surfaces experiences negative pore water pressures (suction) which contributes significantly to the stability of a slope (Rahardjo et al., 2005), As unsaturated soils, they differ in many ways from the saturated soils due to the differences in their basic composition. Saturated soil is two-phase made up of solid and water, while the unsaturated soil is multi-phase composed of soil particles, water, air and air-water interphase (Fredlund and Rahardjo, 1993, Egeli and Pulat, 2011, Barbour, 1998).

In this study, the properties of interest are the flow of fluids, the resulting change of soil strength and volume (deformation). There are state variables that control these behaviours. For instance, the variable that controls flow behaviour is flux or hydraulic head.

Although most of the laws governing the flow of water in soil are fundamentally meant to apply on saturated soil condition, the same laws can be used to describe the flow behaviour in an unsaturated

soil. For example Darcy (1856) applies to both saturated and unsaturated flow. The law relates the rate of flow of water through a soil with the hydraulic head gradient as equation 4-1.

$$V = ki \dots\dots\dots 4-1$$

Where,

V = flow rate of water (m^3/s)

k = coefficient of permeability with respect to the water phase (cm/s)

$i = \frac{\partial h}{\partial y}$ = hydraulic head gradient in the y-direction

However, while in saturated soil, coefficient of permeability, k is constant, in unsaturated soil, k varies with water content or the matric suction (Fredlund and Rahardjo, 1993, Rahardjo et al., 2005, Egeli and Pulat, 2011). The constitutive relation that shows how the function k varies with water content or suction is known as soil water characteristic curve (SWCC).

The partial differential equation describing the flow of water is given by equation 4-2.

$$\frac{\partial}{\partial x} \left(Kx \frac{\partial H}{\partial x} \right) + \frac{\partial}{\partial y} \left(Ky \frac{\partial H}{\partial y} \right) + Q = 0 \dots\dots\dots 4-2$$

Where,

K = Hydraulic conductivity

H = Total hydraulic head

Q = Flux

x and y are the coordinates on the Cartesian plane

The equation applies to the saturated flow which can be likened to the steady flow where there is no change in water storage with time. The equation can be interpreted as the rate of change of volumetric water content in the x and y directions plus the applied flux in the domain equals to zero. For

saturated isotropic flow, the material permeability in both directions is the same. Therefore, the flow is only dependent on the hydraulic head as stated by Darcy's law.

In contrast to the saturated condition, the rate of change of water content per unit time in an unsaturated flow, is dependent on the water flux, hydraulic gradient and the hydraulic conductivity as given in equation 4-3. Details about the derivations can be found in (Fredlund et al., 2012).

$$\frac{\partial}{\partial x} \left(K_x \frac{\partial H}{\partial x} \right) + \frac{\partial}{\partial y} \left(K_y \frac{\partial H}{\partial y} \right) + Q = \frac{\partial \theta}{\partial t} \dots\dots\dots 4-3$$

Where,

θ = volumetric water content changes

t = time

x and y are the coordinates on the Cartesian plane

State variables describing the flow behaviour as presented above, is somehow clear and easy to comprehend. In contrast, the state variables that describe the mechanical behaviour (i.e., the volume change, deformation, and shear strength) of a 4-phase unsaturated soil is complex. Due to its complexity, the limited space provided here is not adequate to fully describe it. It is, however, important to note that changes in volume and shear strength are fundamentally controlled by changes in effective stress. In an unsaturated flow, stress state changes in the air-water inter phase otherwise known as contractile skin contributes to these changes. It can cause soil to change water content, shear strength and volume (Fredlund and Rahardjo, 1993). Recognising this fact, Fredlund et al. (1978) extended the Mohr-coulomb equation to include the effect of soil suction as shown equation 4-4.

$$T = c + (\sigma - U_a) \tan \theta + (U_a - U_w) \tan \theta_b \dots\dots\dots 4-4$$

Where,

T = Shear stress (kPa)

σ = Normal stress (kPa)

C = Cohesion (kPa)

U_a = Air pressure (KN/mm²)

U_w = Air pressure (KN/mm²)

θ = Angle of shear resistance (degrees)

θ_b = Angle of shear resistance due to back pressure (degrees)

To this end, it is shown that, all the saturated flow theories apply to the unsaturated flow but in a different way. It is also understood that, the unsaturated soil behaviour is non-linear. It is best formulated as a partial differential equation and solved using numerical techniques (Fredlund et al., 2012). The numerical software required for that purpose must have the capability to model the following hydrological and mechanical processes.

- i) Saturated-unsaturated flow of water in a soil body.
- ii) Generated pore pressure (including soil suction) and the associated stresses due to the flow described above.
- iii) The effect of hydrological changes on the strength and stability of the slope.
- iv) Volume change or slope deformation due to the above changes.

Geo-studio has satisfied all the above requirements. The software can analyze and give result in pictorial and graphical forms. The graphical form enables the relation between any two variables to be easily established. A brief description of the software is given in the next section.

4.3 Geostudio Software

Geo-studio is a suite of geotechnical numerical analysis software developed by Geo-slope Int. Ltd. It is made up of many components but those that are relevant to this study are SLOPE/W, SIGMA/W and SEEP/W. All these modelling tools are meant for 2-Dimensional numerical simulations and are sufficient for this study. Each of these modules is briefly explained in this section.

4.3.1 SLOPE/W

SLOPE/W was initially developed by Fredlund at the University of Saskatchewan and has been commercially available since 1977 (Krahn, 2012). It is arguably the first commercially available geotechnical software for analyzing slope stability. The analysis is based on the oldest technique of analysing slope stability, the limit equilibrium method (LEM). In the analysis, possible slip surface is created, and the associated factor of safety is computed. This is repeated for many possible slip surfaces and, at the end, the trial slip surface with the lowest factor of safety is deemed the governing or critical slip surface.

One of the limitations of limit equilibrium stability analysis is that it considers only static equilibrium equations. This results in not allowing the variation of the value of safety factor and unrealistic stress distributions is obtained (Krahn, 2003). To overcome these limitations, some finite elements (FE) based software such as SEEP/W and SIGMA/W have been developed by Geo-studio and made to work in an integrated form with SLOPE/W. The integrated approach increased analysis possibilities and remedied the deficiency of the purely limit equilibrium formulations.

Although SLOPE/W can be used as a stand-alone product, the incorporation of finite element computed pore-water pressures and stresses in the stability analysis has in no small measure increased the capability of the program and improved our understanding of the slope failure process.

4.3.2 SEEP/W

SEEP/W is mainly a hydrological model that simulates seepage and other hydrological processes through a porous medium. Its ability to handle both saturated and unsaturated flows made it ideal for this research. The Saturated/Unsaturated material enables it to model both saturated and unsaturated flow. The basic material property required for the analysis is hydraulic conductivity. It has been shown in section 4.2 that the property is not constant but changes with the change in volumetric water content (VWC) and soil suction. SEEP/W has a special function to establish this relationship.

In seepage analysis, the boundary conditions are the driving force that causes the flow. It is either the hydraulic head (H) difference between two points or flow quantity (Q) into or out of the system as shown the previous equations. Q is sometimes expressed as a rate per unit area or time across the edge of an element (q). SEEP/W provides a function to input any of the known alternative boundary conditions and the resulting solution gives the other alternative. The basic constitution equation is given as in 4-5.

$$[K](H) = [Q] \dots\dots\dots 4-5$$

Where, K = Material property known as hydraulic conductivity in m/s

A review boundary condition is a potential seepage face in SEEP/W where water is expected to exit the slope and is flagged under boundary conditions of SEEP/W.

4.3.3 SIGMA/W

SIGMA/W is used to perform stress and deformation analyses and it is a tool for a more accurate assessment of slope stability under both working and ultimate loading.

Change in volumetric water content is dependent on the material properties and the stress condition in the soil. There are many constitutive relationships that describes the process. One of them is the linear

(perfectly) elastic model. It is based on Hooks law of elasticity which states that as the force is applied, there is a corresponding elastic deformation. For this reason, the soil stiffness (K) is required to compute the displacement (D), for every force (F) applied. The basic constitutive relation is represented by equation 4-6. Basically, all the boundary conditions are categorized into two, namely force or displacement.

$$[K](D)=[F].....4-6$$

SIGMA/W, though FE based software, its analysis is fundamentally based on the principle of static equilibrium in which at least one part of the geometry is specified as zero displacements (i.e. fixed) boundary condition to enable the unknown condition at the rest of the part of the boundary be determined. It is common to specify left and right sides along with the bottom edge of a problem as fixed ‘bound’ condition. The specified boundary conditions on a geometry are applied to the underlying nodes or elements.

4.3.4 Coupled Analysis

As stated earlier, to overcome the limitation of LEM used in SLOPE/W, the FE based components (SEEP/W and SIGMA/W) of GEOSTUDIO are used. The analysis involving the use of all these software at the same time is called a coupled analysis. Mathematically, analyzing both seepage dissipation and stress-deformation in a single case requires the relevant equations be solved simultaneously. Therefore, a simultaneous equation is formed by putting together, the two respective equations in SEEP/W and SIGMA/W.

With the coupled analysis, it is no longer necessary to have SEEP/W as well as SIGMA/W. In a single analysis, all the properties and boundary conditions are developed, applied and the problem resolved.

4.4 Modelling failure mechanism

The study of failure mechanism is the central aim of the entire research. The research is mainly experimental, but a numerical modelling back-up was added to make it more robust.

Prior to the numerical study, some laboratory tests were conducted to determine the index and geotechnical properties of the soil to be used in this experiment. Additionally, some trial tests to determine the homogeneity and infiltrability or water percolation of the proposed model. A full account of the index tests has been given in chapter 3 while the trial tests can be found in chapter 5. These initial tests provided crucial information about the behaviour of the proposed model and the results obtained during those tests served as inputs during the numerical modelling.

The modelling of the slope failure was done by considering how the groundwater changes and accompanied changes in pore water pressure, affect the strength and stability of soil slope. The physical properties of interest are the water flow, shear strength and volume change. There are many state variables that describe the unsaturated soil behaviour but those that are related to three mentioned properties are the ones considered during this study. The soil index and geotechnical properties were obtained by direct laboratory measurements while properties like residual moisture content, that could not be measured were estimated using soil-water characteristic curves (SWCC) in accordance with the recommendation of the established protocols by Fredlund et al. (2012). SWCC was also used to relate the variables that describe the unsaturated flow. It is generally accepted as a vital tool and constitutive model in describing unsaturated soil behaviour (Barbour, 1998).

The first stage of modelling exercise was aimed at designing the physical model while the second stage was a more detailed study aimed at predicting the behaviour of the designed model. Geo-studio package comprising of SLOPE/W, SEEP/W and SIGMA/W software described above, was used to

achieve this twofold objective. The initial process of designing the model was done by coupling SLOPE/W with SEEP/W, while SIGMA/W was included in a fully coupled analysis, to capture stress and deformation in the final detailed study as will be seen later in section 4.4.3.

4.4.1 Modelling principle used

The main steps involved in each of the two modelling stages include identifying the state variables, establishing the constitutive relations, formulating the problem and using numerical solver to solve the problem. This sequence is in line with the established procedure by Fredlund (2012). The sequence was maintained at each modelling stage. The main modelling process involved seepage and stability analysis.

4.4.1.1 Seepage Analysis

In seepage analysis, the required properties are the hydraulic conductivity and volumetric water content. It has been stated earlier that both properties are not constant in an unsaturated flow. They vary with soil suction. A built-in soil sample in SEEP/W was used to define the volumetric water content function in terms soil suction as shown in Figure 4-1. Based on this established relation, the unsaturated hydraulic conductivity was defined as shown in Figure 4-2.

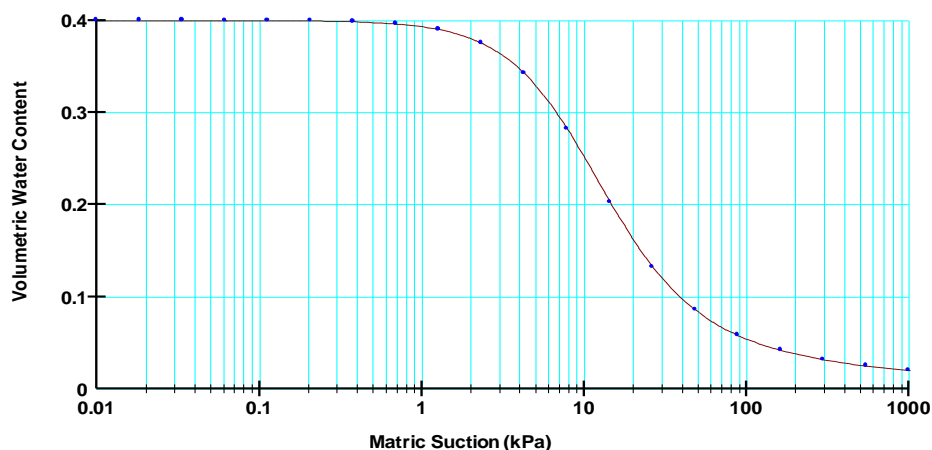


Figure 4-1: Volumetric water content (VWC) graph

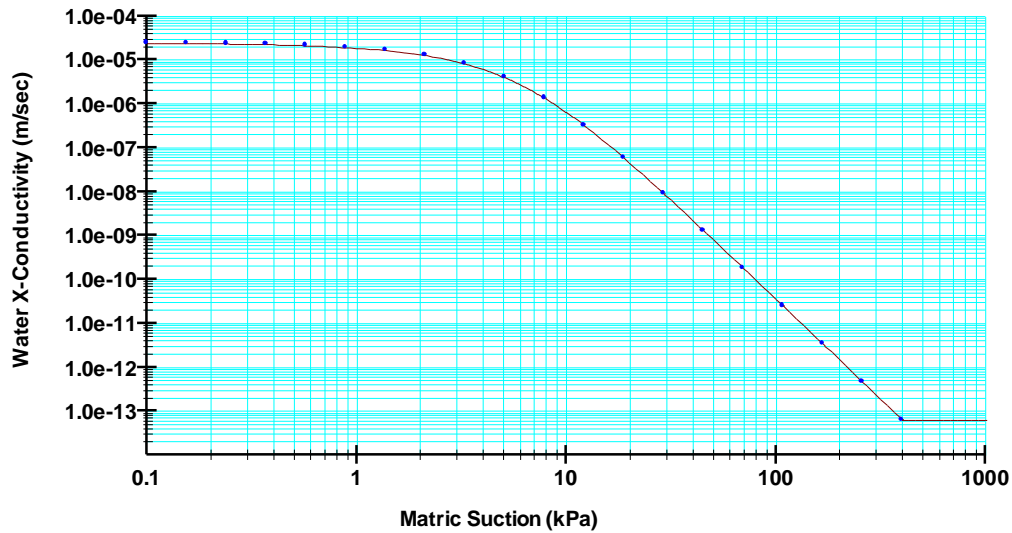


Figure 4-2: Graph for material hydraulic conductivity

The hydraulic conductivity was defined as a function of the soil suction using Van Genuchten (1980) method. It is one of the many method proposed to best fit laboratory data on the SWCCs based on closed-form, empirical equations as listed by Fredlund et al. (2012). It was mentioned in this publication that the method best fit to define the central portion between air-entry value (AEV) and residual condition of the SWCC. This portion, known as transitional zone is dominated by the continuous change in water content and is crucial to this study since it is the range where the failure is expected.

Since finite element was used in seepage analysis, mesh specification was required. Meshing is an important feature of FE analysis. In this study, precision and processing time were the two factors considered in selecting the mesh size. Coarser mesh gives less precision in the computed factor of safety than the finer mesh though the difference in most cases does not exceed 2% (Griffiths and Marquez, 2007). On the other hand, the finer size takes longer time to do the required computations (Suryo, 2013). Striking the balance between the two extremes, a medium size unstructured mesh with the dimension 0.05m was used. The mesh has unstructured pattern made up of quadrilateral and

triangular elements and is recommended by the software developer (Krahn, 2012). More details about the mesh is given in 4.4.3.4.

The slope stability analysis started first by conducting a steady state analysis to establish the initial condition. Thereafter, a transient seepage analysis was conducted. To simulate the saturated and unsaturated condition anticipated, a saturated/unsaturated model was used during the analysis. More details can be found in section 4.4.2.

4.4.1.2 Stability Analysis

The pore-water condition computed using SEEP/W was used as inputs to simulate hydrological conditions during stability analysis. Other inputs required for stability analysis include the mechanical properties of soils. There are many material properties model used for stability analysis but in this study, Mohr-coulomb model was used. The model was used because it satisfies the requirement of providing information about soil mechanical strength that can be compared with the forces acting on the slope to obtain a factor of safety.

Stress and deformation analysis require the young's modulus to be specified. This was described by the stress-strain relation using linear elastic model.

After specifying the material properties and the potential slip surface, the problem was solved using limit equilibrium (LE) method. There are many methods of analysis using LE but, in this research,, Morgenstern-Price was used. The method was used because it satisfies both force and moment equilibrium static equations unlike some other methods like Bishop and Janbu. Additionally, it applies both inter-slice normal and shear forces, while other methods use only normal force, or none.

Above, is the general procedure used in the numerical study presented in this chapter. Specific details are provided under relevant sections of the two modelling stages.

4.4.2 Numerical Study to design a slope model

Factors affecting the stability of slope have been reviewed in a considerable detail in chapter 2. These factors include soil properties, slope geometry and groundwater condition. At this stage, available options for each of these three factors were analyzed and the best options were considered in designing an experimental slope model. The objective was to arrive at the best combination of factors that can cause failure. The reason is that, unless the slope is made to fail, the central objective of studying its failure mechanism cannot be achieved.

At every stage of the numerical analysis, a single parameter was varied to conduct seepage and stability analysis using limit equilibrium while the rest of the parameters are kept constant. The option that gave the least factor of safety was considered the best and therefore selected for further study. During this exercise, accuracy or the magnitude of the computed values is of less significance. The only thing that matters is the comparison between alternatives and change between simulations (Krahn, 2012). For this reason, this stage, the slope stability analysis was conducted using SLOPE/W based on only SEEP/W computed pore-pressures. The resulting factor of safety (FOS) was used as an evaluation criterion. To get the pore pressure, both steady and transient states seepage analysis was conducted, while the factor of safety was obtained using the limit equilibrium method.

4.4.2.1 Material properties

The soil material properties obtained by laboratory test at optimum compaction (i.e. optimum moisture content) have been presented in chapter 3. To favour slope failure, a trial slope was constructed and

tested to failure with a compaction density and moisture less than the optimum values (i.e. on the dry side of the compaction curve). They are therefore less than the optimum values. This is done to make the material factor contribute to the slope failure so that the requirement for studying failure mechanism can be met. The properties are shown in Table 4-1 and the procedure for obtaining the properties has been presented under feasibility tests in chapter 5.

Generally, shear strength parameters i.e. cohesion ‘c’ and angle of frictional resistance ‘ θ ’ obtained at a compaction level dry of optimum, are lower than their optimum counterparts. There is a great difference in terms of ‘c’ but for ‘ θ ’ the difference is very small. This observation is corroborated with the findings of (Vanapalli et al., 1997). The hydraulic conductivity value of a soil compacted at a moisture content dry of optimum as shown in Table 4-1, is higher than those obtained at optimum condition due to the higher void ratio at that compaction level.

Table 4-1: Soil properties

Properties	Value
Liquid limit, (%)	12
Plastic limit, (%)	31
Plasticity index, (%)	19
Specific Gravity	2.68
Density, Mg/m ³	1.87
Gravimetric Moisture Content, (%)	10
Sat. volumetric Moisture Content, (cm ³ /cm ³)	0.4
Residual Moisture Content, (cm ³ /cm ³)	0.05
Cohesion (KPa)	5.2
Angle of internal resistance (°)	19.2
Permeability (m/s)	2.41x10 ⁻⁵

The soil material properties were kept constant during this stage sensitivity studies of this stage while geometry and the hydraulic boundary condition were varied.

4.4.2.2 Parameters selection

Stage 1: Geometry Selection

It is important to keep in mind that, the main objective of employing numerical modelling in this study is to aid the design of physical model to be used for laboratory experiments. Therefore, after the soil properties as in 4.4.2.1, the first stage in the design is to know the geometry and dimension of the model. The geometry of slope consists of slope angle, height, width and the dimensions of toe and crest. These features were designed with the following considerations.

- i) The dimensions must be accommodated by the experimental tank prepared for the experimental study. The tank is an acrylic tank with dimension 2000mmx1000mmx1000mm. When the water supply and discharge chambers are subtracted from the lengths of the tank, the effective lengths for the slope model is 1700mm.
- ii) Slope features such as height, slope angle, crest and toe are to be designed to favour slope failure.

In view of the above, the length (1700mm) and width (1000mm) as in (i) are kept constant, while the features in (ii) were varied in the analysis to determine an option with the highest tendency to fail. Ten trials were run, with each conducting seepage and stability analysis. The pore pressure developed during the steady seepage analysis was imported to conduct stability analysis. The option that gave the lowest FOS was considered the best and selected for further study. Table 4-2 and Figure 4.3 – 4.4 show the options considered with the variable slope height, crest and toe dimensions, and slope angle.

Table 4-2: Experimental trials considered during numerical analysis

TRIAL No.	OVERALL DIMENSIONS			TOE DIMENSION		CREST WIDTH	F.O.S
	Length (mm)	Width (mm)	Height (mm)	Length (mm)	Depth (mm)	(mm)	
1	1700	1000	650	900	150	300	4.93
2	1700	1000	650	600	150	300	4.26
3	1700	1000	650	500	100	300	4.00
4	1700	1000	650	500	200	300	3.98
5	1700	1000	650	1000	200	300	3.85
6	1700	1000	700	600	200	600	3.80
7	1700	1000	700	700	200	500	3.73
8	1700	1000	700	200	200	600	3.69
9	1700	1000	700	600	100	500	3.10
10	1700	1000	750	600	100	500	2.91

From the results shown in Figure 4-3 – 4-4, option 10 gave the lowest FOS and therefore considered for further studies. The factors responsible for the low factor of safety in option 10, includes the higher slope height (0.75m) and larger angle of slope (45^0) compared to the other options. As the angle of inclination increases, the ratio of sliding forces to that of stabilising forces increases. Steep slope has a negative effect on the stability of a slope(Liu and Deng, 2011, Winter et al., 2007).

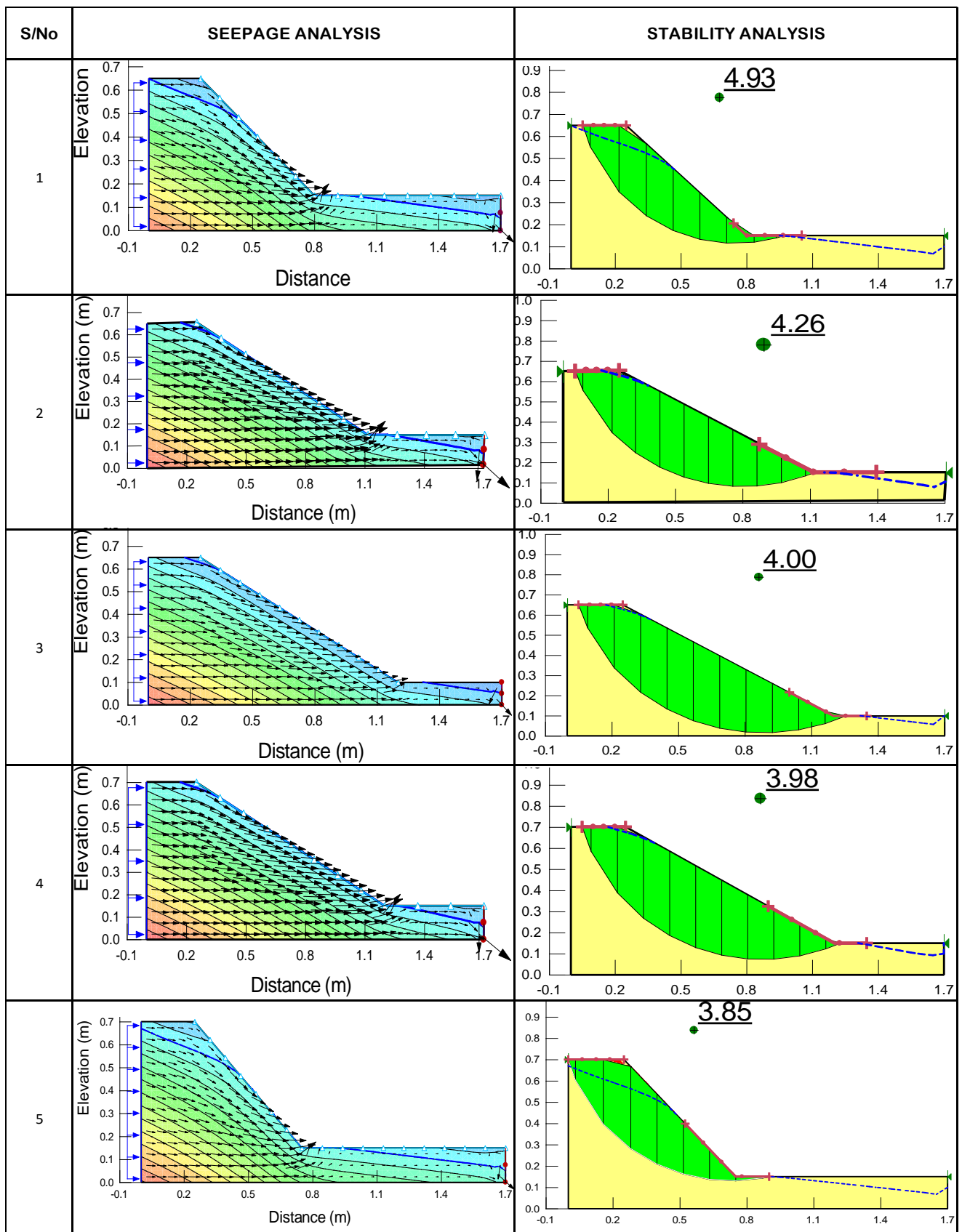


Figure 4-3: Analysis of various options of slope geometry (Continues overleaf)

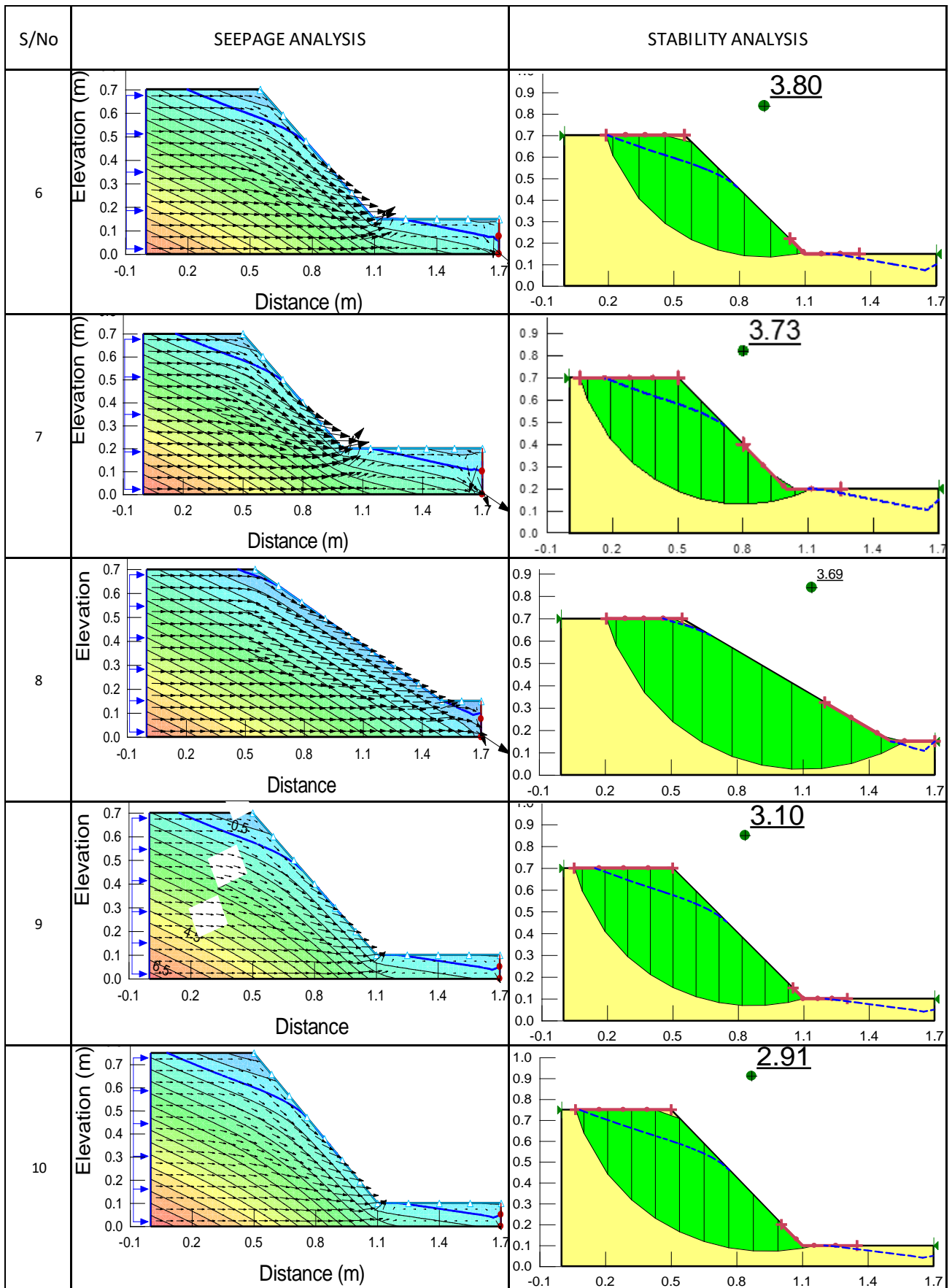


Figure 4-4: Analysis of various options of slope geometry (continued from the previous)

Stage 2: Selection of Boundary Condition

In seepage analysis, there are two possible hydraulic boundary conditions namely head (H) and flux (Q or q). In the previous stage, only flux condition was used for geometry selection. At this stage, the two conditions were compared as in Figure 4-5. The applied boundary conditions include the 0.75m and $9.67 \times 10^{-6} \text{cm/s}$ for total head and constant flow rate, respectively. The flux boundary condition was selected based on the results obtained during the initial laboratory studies.

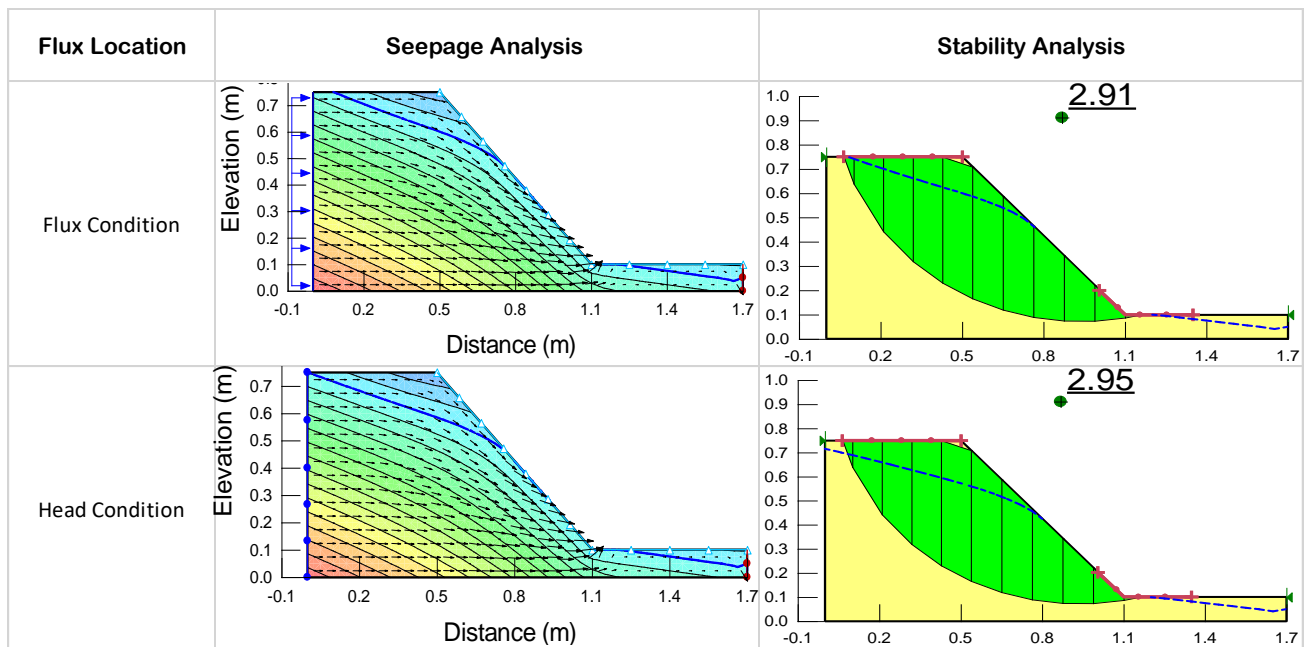


Figure 4-5: Comparing the two types of hydraulic boundary conditions

From Figure 4-5, it was observed that the flux condition gives the lower FOS, though with a negligible difference. It was therefore selected for the next stage. Another reason that justifies the selection of flux condition is for practical convenience. The water flow rate can easily be controlled in the laboratory experiment using a flow meter. Additionally, head boundary condition is difficult to use in a practical laboratory set-up involving a slope physical model with compaction parameters lower than the optimum, it is difficult to measure the changes at zero time.

Stage 3: Location of Boundary Condition

Having decided to apply the flux boundary condition, the right location that can easily cause failure needed to be determined. To achieve this, three possible options were considered. These include applying the flux at the top end, bottom end or full height of the slope as shown in Figure 4-6. From the comparison, it can be observed that the full height application produced the least factor of safety and therefore selected.

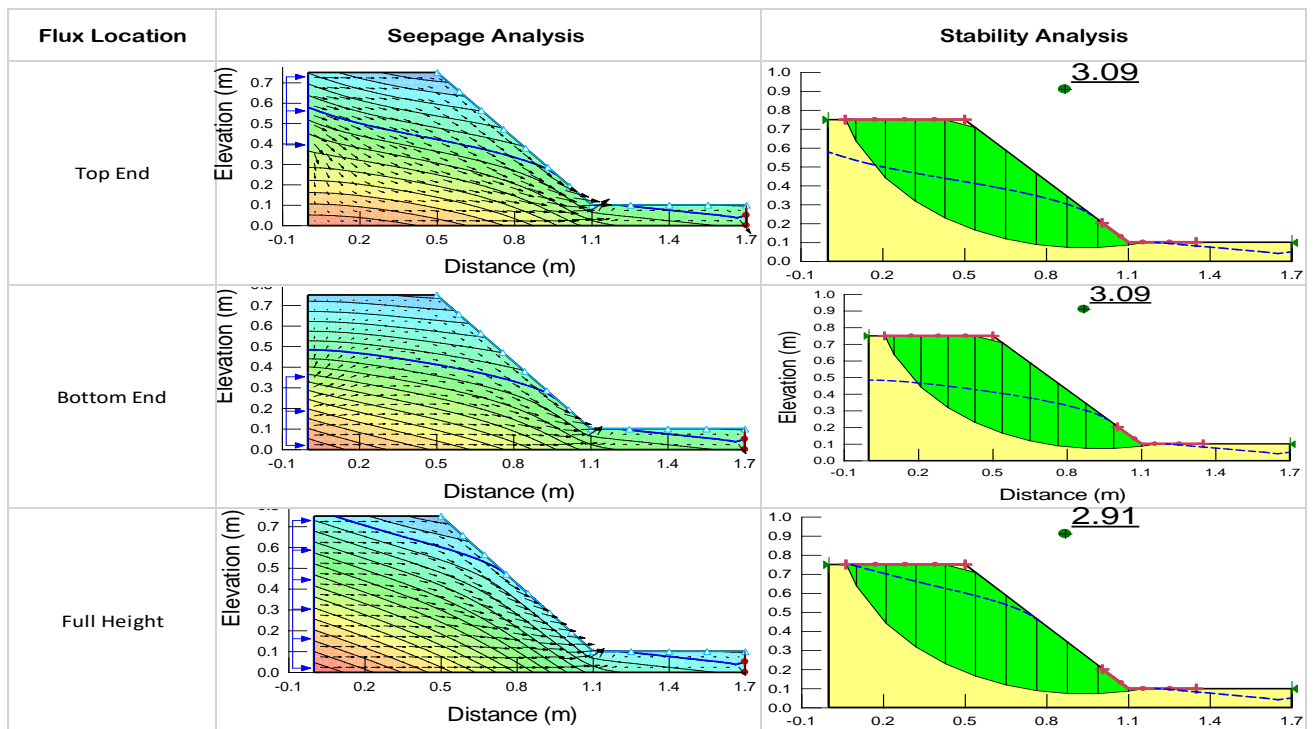


Figure 4-6: Comparing the flux boundary conditions

4.4.2.3 Design Output

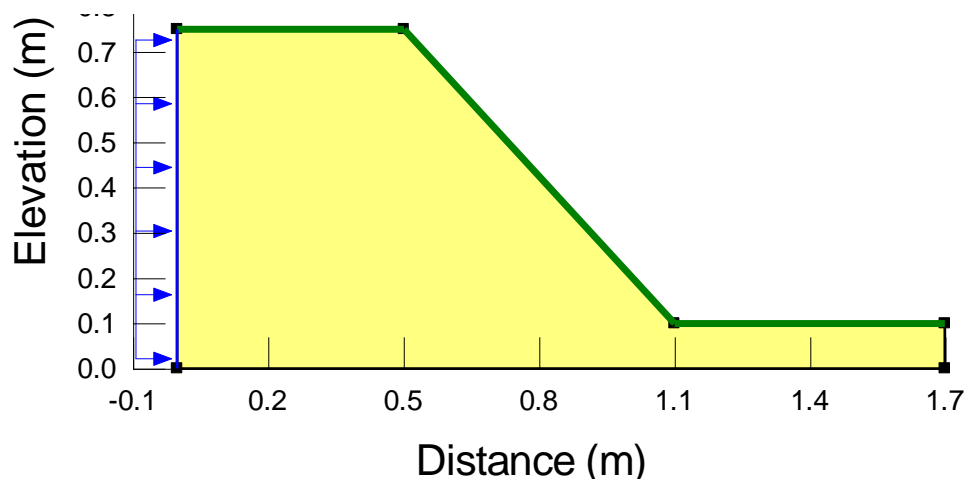


Figure 4-7: Model design

At the end of step by step analysis, the final produced slope model is the one shown in Figure 4-7. It has an angle of 45° , the total length of 1.7m, the height of 0.75m, a crest width of 0.5m and the dimension of the toe is 0.6m \times 0.1m. A hydraulic flux rate is to be applied by the left end height of the slope. The material properties remain the same as shown in Table 4.1.

4.4.3 Detailed analysis to predict behaviour of the model

In the previous section, although the pore-water pressure was used in the slope stability analysis, the only evaluation criterion was the factor of safety. In this section, the modelled pre-failure failure processes such as unsaturated water flow, development of pore-water pressure, stress and deformation mechanism are analyzed and presented. The objective is to study the designed model in a greater detail to get an idea of the failure behaviour of the model. The analysis conducted includes seepage, stress and stability analysis.

4.4.3.1 Case definition

To conduct a detailed seepage analysis, the model designed at the previous design stage was used and is shown in Figure 4-8 in two forms. Figure 4-8(a) shows the case definition for seepage analysis while Figure 4-8(b) shows the case definition for stress analysis.

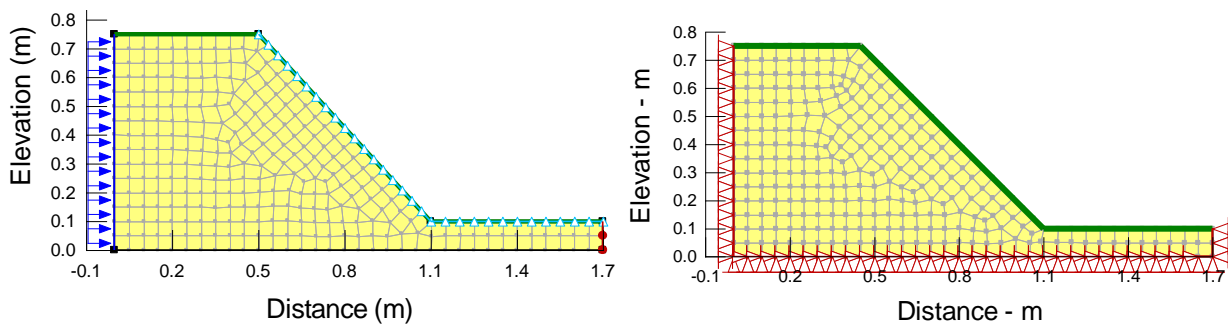


Figure 4-8 : Problem definition (a) For seepage analysis (b) For stress analysis

4.4.3.2 The material properties

The soil material used in both types of analysis is the same but the properties of interest in each analysis are different. In seepage analysis, the required properties are the hydraulic conductivity and volumetric water content while in slope stability analysis, Mohr-coulomb material model requires strength parameters (c' and θ') and the self-weight (unit weight) as inputs. Stress and deformation analysis require the young's modulus and poisson ratio to be specified. These was described by the stress-strain relation using linear elastic model. Each of the soil parameters was specified using the appropriate material function of the modelling software.

4.4.3.3 Boundary Conditions

Both hydraulic and stress boundary conditions were used in the analysis as shown in Figure 4.8. To simulate increase in water volume experienced during flooding, flux boundary was applied in steps between the orders of 10^{-07} cm/s to 10^{-05} cm/s as a function of time over a total period of 4000 seconds.

The stepped application of flux was possible through the hydraulic functions of SEEP/W.

The flux was assigned to the left vertical boundary and the bottom boundary was considered as “no flow”. On the right-hand side, the review boundary also known as seepage face was specified while zero pressure has been indicated on the vertical side of the toe.

For the stress analysis, the movement was constrained along x-direction at the left and right-hand sides while the bottom end was specified as fixed in both x and y directions.

4.4.3.4 Mesh specification

Mesh properties were kept the same as the one used in the previous stage. The properties is described in section 4.4.

4.4.3.5 Analysis

Seepage, stress and stability analysis were conducted to obtain the required details. The analysis was done using a coupled approach of geo-studio. In the same package, SEEP/W, SIGMA/W and SLOPE/W were used. The approach is explained in section 4.3.3.

A steady-state analysis was first conducted to establish the initial condition. Thereafter, the transient analysis was conducted over a period of one hour. Various available models in SEEP/W, relating the VWC and K_{sat} were applied. The one-hour period was selected based on the experience with the preliminary laboratory studies.

To analyse stresses, the stress- strain relationship was described by a linear elastic constitutive model while linear-plastic theory (Mohr-coulomb) was used in the stability analysis.

4.4.3.6 Results Presentation

From the analysis, the rate of change of water content with time, the pore-water distribution and the change in hydraulic gradient were studied. The graphical representations of each of the conditions above are shown in Figure 4-9..

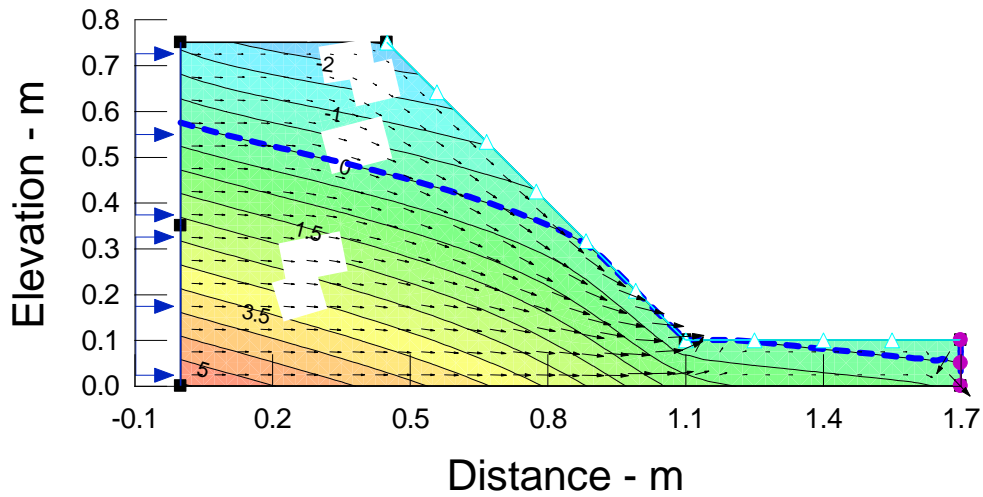


Figure 4-9: Flow vectors

Figure 4-9 shows the flow vectors showing the direction of water flow and the level of water at the end of the simulation period. The change of groundwater level with time obtained during a transient seepage analysis is illustrated by isolines as indicated in figure 4-10.

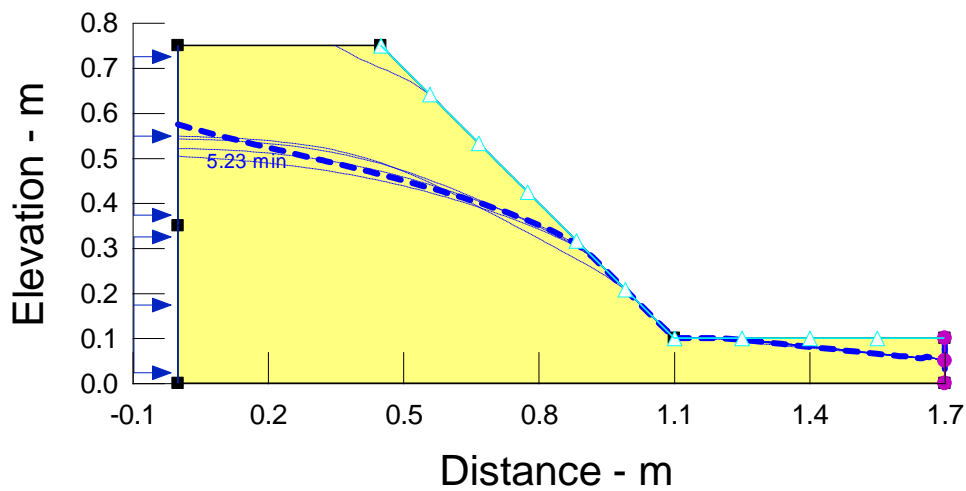


Figure 4-10: The change of water level with time

The change in water content within the soil at each time step is accompanied by the change of pore-water pressure and ground stresses. The pore-water distributions at the initial and final stages of the analysis period are shown in Figure 4-11.

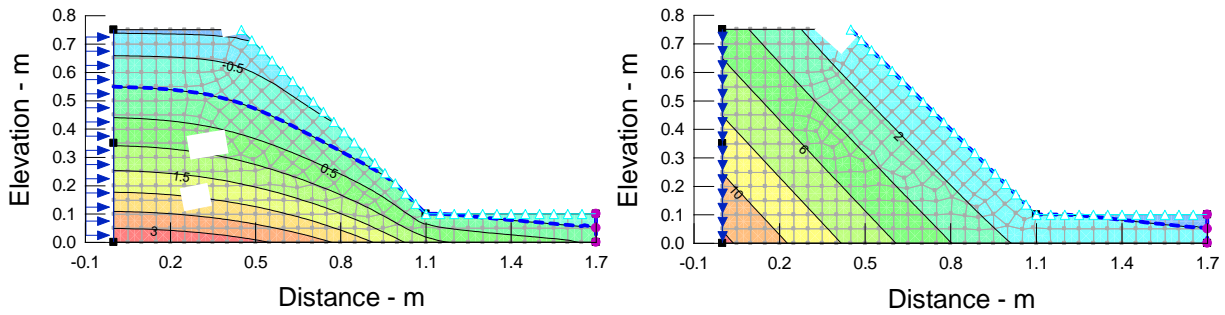


Figure 4-11 Pore water distribution (a) Initial (b) Final

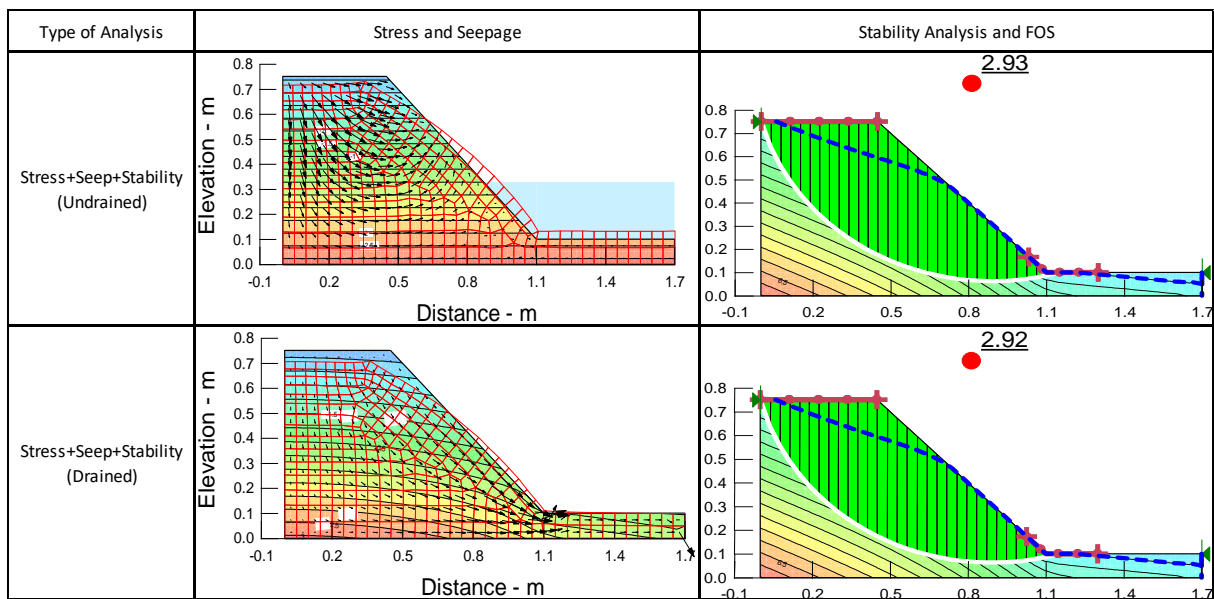


Figure 4-12 Comparison of stability analysis based on two different approaches

In a stress analysis, in addition to the above parameters, the change in ground stress condition with time was also studied.

The results presented in Figures 4-11-4-13 represent the outcome of two types of analysis. These include purely seepage analysis, and the stress analysis based on the pore-water pressure obtained during seepage analysis.

The effect of water content change and the corresponding changes in stress and pore-water pressure on slope stability were studied by incorporating the computed parameters in the stability analysis. Figure 4-12 shows a comparison of results of slope stability analysis based on the two categories of analysis. In one of the analysis water seeping out of the slope is not allowed to drain out of the system. Instead, it was made to pond on the surface of the toe. In the second analysis, a free drainage is allowed. The deformation pattern of the two as shown by their deformed meshes is different but their effect on slope stability is of negligible difference. The negligible difference between their factor of safety, attest to this fact.

Figure 4-13 shows the water content and pore-water pressure conditions at different times when the water is not allowed to drain out of the system.

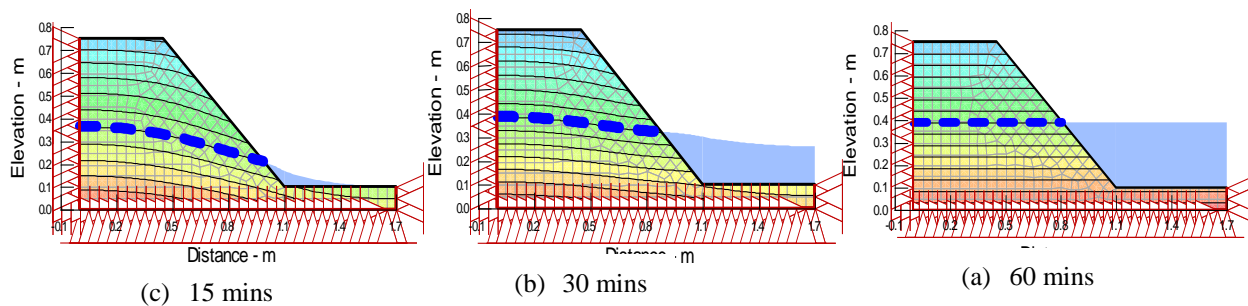


Figure 4-13: Stress changes with time (15-60mins)

Comparing the results of stress analysis in Figure 4-12 with that of the selected option during seepage analysis, shown in Figure 4-14, indicates that the two types of analysis arrived at almost the same FOS. This shows that the stability results are virtually the same; though the accuracy and the amount of information obtained in stress coupled analysis is more than that of seepage analysis. For example, stress and seepage coupled analysis result provides stress-deformation behaviour as shown in Figure 4-12. This is not possible to obtain in seepage alone analysis. Since the stability results are virtually the same, seepage alone analysis is considered in the further analysis.

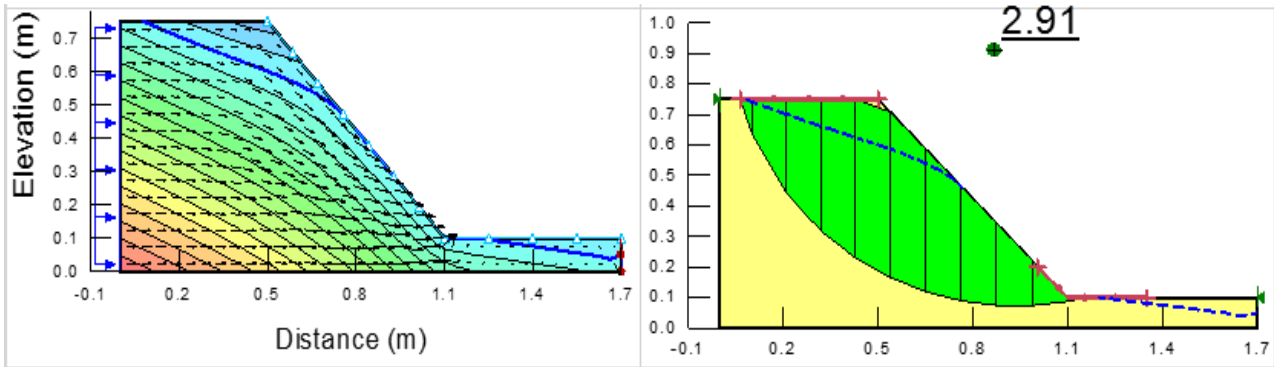


Figure 4-14: Analysis results when constant hydraulic flux was applied

Until this point, the factors of safety obtained during stability analyses are based on the applied constant uniform flux boundary condition. The next figure i.e. Figure 4-15 shows the factor of safety obtained when a stepped uniform flux described in section 4.4.2.3 was applied. The stepping is to simulate sudden increase in water content experienced during flooding.

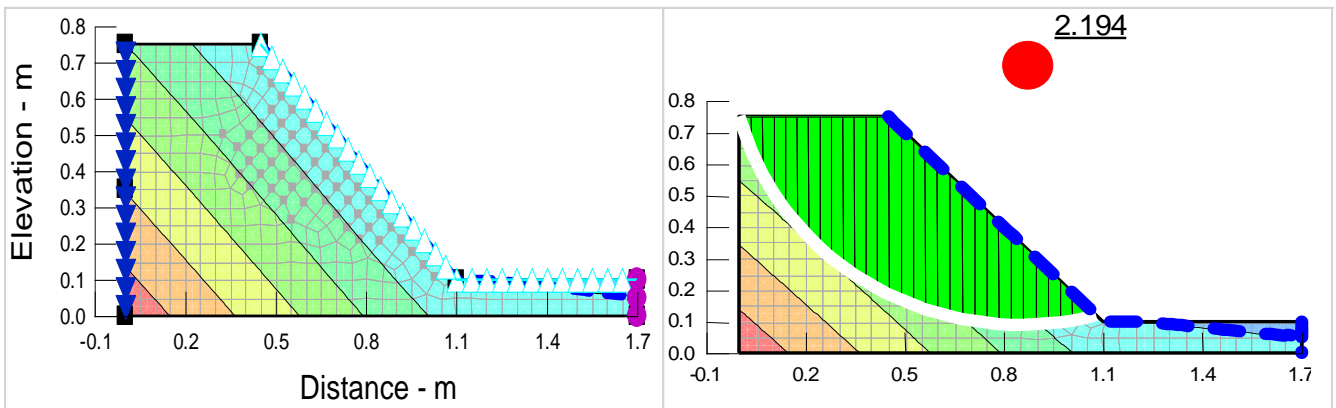


Figure 4-15: Analysis results when time step hydraulic flux was applied

The factors of safety obtained up to this point are unfactored safety factors which are not safe enough due to some risks associated with the design of steep and reinforced slopes. To make it safer, partial factor of safety is applied in accordance with BS8006: 1995 Section 7. The relevance of reviewing the factors has been discussed by Corbet and C (2010). The factored safety factors also known as over

design factors (ODF) is used to account for some uncertainties related to the material strength and loading. In accordance with BS8006: 1995 Section 7, the values for soil unit weight, earth resistance and effective cohesion are multiplied by 1.5, 1.25 and 1.6, respectively. The obtained ODF during the analysis are given in Figure 4-16, while the variations of factors with time are plotted on a graph in Figure 4-17

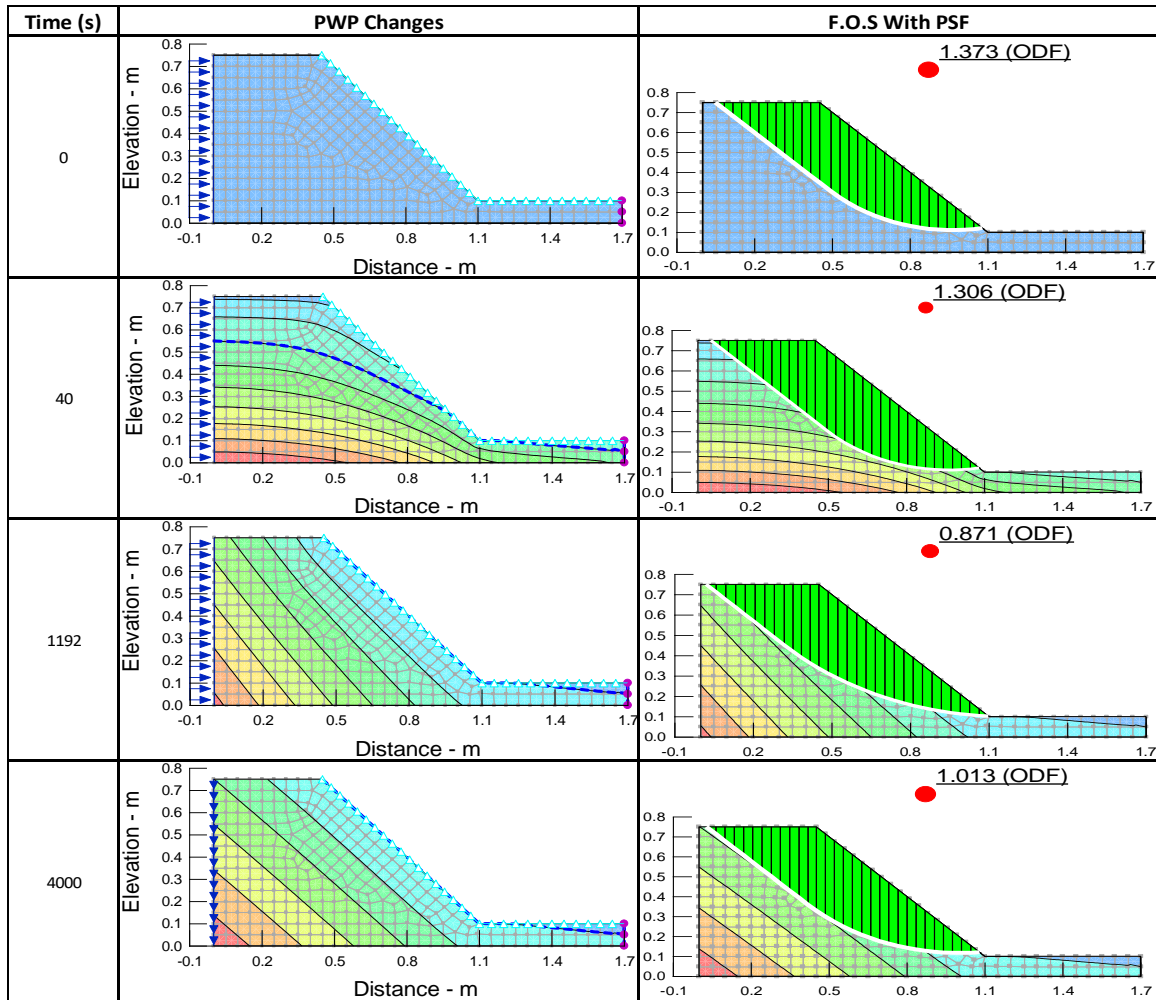


Figure 4-16: Seepage and stability analysis with over design factor (ODF)

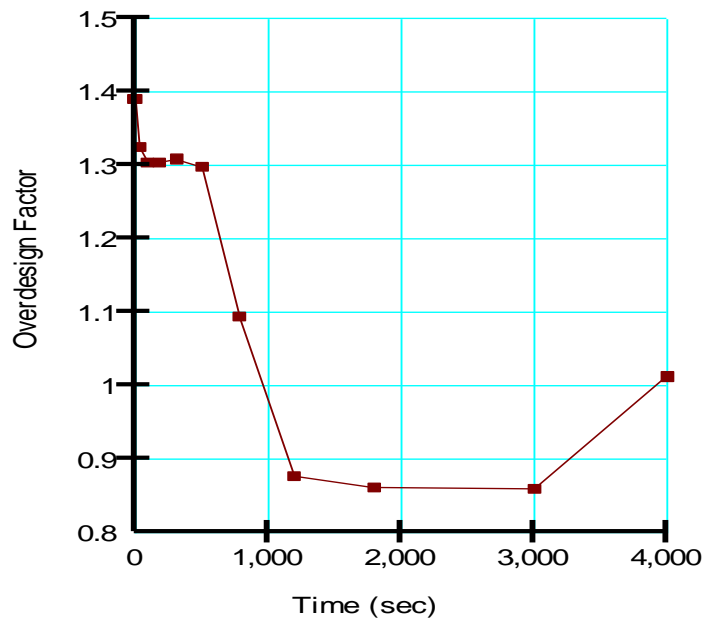


Figure 4-17: Change of FOS with time

4.5 Summary and concluding remarks

Before selecting the right numerical software to use, the fundamental theories were reviewed to understand how flow of water causes changes in pore-water pressure and strength of the soil. This allowed the parameters to be captured in the numerical modelling, to be highlighted.

The numerical modelling was conducted in two stages. In the first stage, the model was designed by comparing alternatives in geometry and boundary conditions. In the second stage, the detailed analysis of the designed model gave a good understanding of the hydrological processes taking places within the slope and their impact on slope stability. It also provided ideas about the failure mechanism of the slope.

In section 4.4.2, a step-by-step analysis made to arrive at the designed model has been shown. It involved comparing possible alternatives of the three factors affecting slope stability. Comparing the ten alternatives of geometry as shown in Figure 4-4 shows option ten is the one that produced the least

factor of safety. During this exercise, the flux boundary condition was kept constant while varying the geometry. After selecting the right geometry, the two alternative hydraulic boundary conditions were compared in Figure 4-5 before maintaining the flux boundary condition in the design. The result of comparison of three possible options as shown in Figure 4-6 indicates that the best option is to apply a flux at the full height instead of top or bottom end. At the end of this stage, the model produced is the one shown in Figure 4-7.

In section 4.4.3, results of the detailed analysis of the designed model were presented. The results shown in Figures 4-9-4.13 analyzed the various changes in hydrological and stress conditions while Figure 4.14 shows the impact of these changes on the slope stability. The factors were further reduced by applying partial safety factors in accordance with the BS8006 section 7, to obtain more realistic values. The variation of the final factors of safety with time, in response to the changes in water and pore-water pressure, is shown in Figure 4-16 – 4 -17.

The results are only presented in this chapter, discussion will be made in chapter 7. Here, the point of interest is to gather necessary information that can aid the setting-up of the laboratory experiment. The numerical modelling procedure and results presented in this chapter has satisfied this requirement.

CHAPTER 5

PHYSICAL MODELLING

5.1 Introduction

Physical modelling and its use in studying slope stability problems, is gaining popularity due to its numerous advantages over the full-scale field tests. With physical modelling, it is possible to obtain a reliable information and straightforward visual perception of progressive slope failure under controlled laboratory conditions (Ni et al., 2016).

The hallmark of this research is building a physical model and subjecting it to the condition that will make it fail thereby allowing its failure process to be studied using geophysical methods. To achieve this, the designed model and planned experiment were broken into simple components. Each component was assessed separately before building up to the complex model. The initial assessment of the individual component is what is referred in this section as feasibility tests. The feasibility study was aimed at ascertaining the possibility of using the selected material, methodology and instrumentation for the designed physical modelling of this research.

During the feasibility study, the initial water content and density to be maintained during compaction were decided, the method of ensuring the homogeneity (i.e uniformity of moisture and density) of a sample was devised, and the permeability of the soil material to be used was determined. Additionally, the electromagnetic sensors to be used in the modelling were assessed. Since the electrical resistivity method is intended to be used in the final experiment, the electrical properties of the soil were assessed at this stage. The ability of the 5TE volumetric water content (VWC) sensor to measure electrical conductivity made this assessment possible.

After being satisfied with the results of the feasibility tests, the physical model was constructed and the experiment was conducted to test the model. The experiment was first conducted on a small model (Length = 370mm, Width =200mm, Maximum height = 220mm) before the large-scale (Length =1050mm, Width =1000mm, Maximum height =650mm) experiment. Detailed schematic diagrams with dimension can be found in the later sections i.e. 5.5.2 and 5.6.2, respectively. The small-size trials were aimed at getting an initial idea about the failure mechanism associated with the slope. Due to its size, it was easy to conduct many repeatable tests with relative ease. However, its small size limited the number of instrumentations in the study. This limitation was overcome with large-scale testing. Moreover, in large-scale physical modelling, boundary and scale effects are minimised (Jia et al., 2009). This buttressed the reason why a large-scale model is used in the main experiment.

In this chapter, the steps followed to develop a physical model and subsequently conduct an experiment on the developed model has been described. The result obtained at each step has been presented. The chapter began with the introduction of the materials and instrumentation used in the research.

5.2 Material Used

A reddish-brown tropical soil, extensively used in the construction of embankments of civil engineering related infrastructure in tropical and subtropical countries (like Asia, Africa and Southern America), was used in this research. Due to non-availability of the material in the UK where the research was conducted, the material was produced by systematically modifying the available British mud rock material called 'Etruria Marl' with commercially available British sand known as 'builders sand' to obtain a pseudo-tropical soil with similar engineering properties to the original type found in Nigeria. The detailed procedure for the production of this soil is given in chapter 3. The properties of pseudo-tropical soil as contained in that chapter are given Table 5-1.

Table 5-1: Property of artificially produced residual tropical soil

Property	Value
Liquid limit, (%)	12
Plastic limit, (%)	31
Plasticity index, (%)	19
Specific Gravity	2.68
Maximum Dry Density, Mg/m ³ (BS Standard Proctor)	1.945
Optimum Moisture Content, % (BS Standard Proctor)	11.5
Cohesion, C' (KN/m ²)	26
Angle of internal resistance Θ (°)	21
Permeability (cm/s)	2.41x10 ⁻⁶

5.3 Instrumentation

The instrumentation includes 5TE and MPS-6 sensors which were used to monitor soil volumetric water content (VWC) and matric suction (MS) respectively. The 5TE sensor also measures soil temperature and electrical conductivity of the soil. To measure the physical deformation, cameras were used to capture digital images through the transparent experimental box. Each of these parameters and their measuring instruments will be briefly described in this section. Detailed experimental set-up will be provided under final experiment in Chapter 6. More detailed sensor description can be found in the Decagon devices manuals (Decagon, 2015, Decagon, 2017).

5.3.1 5TE Volumetric Water Content Sensor

5TE is one of the new electromagnetic sensors developed by Decagon Inc. to measure soil water content, electrical conductivity and temperature. Unlike other types of sensors that use gold traces to

measure electrical conductivity, 5TE uses two stainless steel screws as an array for electrical conductivity measurement. The use of stainless steel array makes it more robust than the other types of sensors. This is because it is less affected by polarisation. The two-point array is located on the two of the three sensor prongs shown in figure 5-1. The sensor specifications are given in Table 5-2.

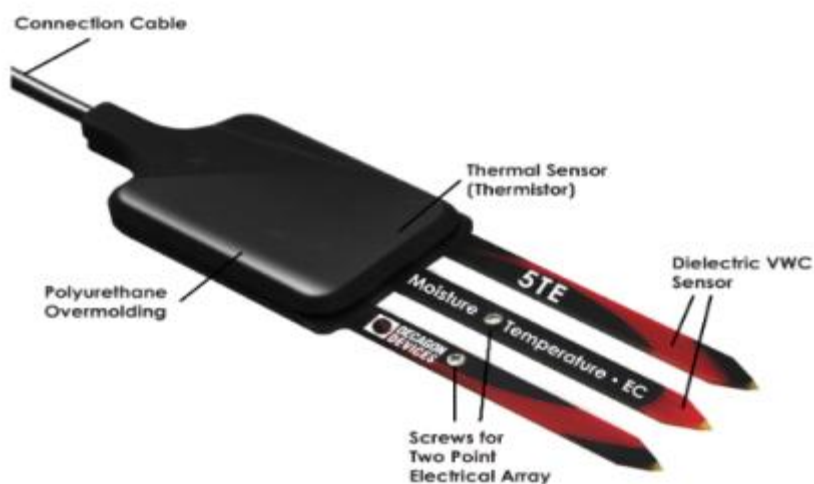


Figure 5-1: 5TE sensor features (Decagon, 2015)

Table 5-2 : 5TE sensor specification

Measured Parameter	Range	Resolution	Accuracy
Apparent dielectric permittivity (Unitless)	1 (air) to 80 (water)	1-20: 0.1 ϵ_a (unitless) 20-80: <0.75 ϵ_a (unitless)	1-40 (soil range): $\pm 1 \epsilon_a$ 40-80(VWC): $\pm 15\%$
Volumetric water content (%VWC)	0-50	0.08	$\pm 1-2$
Bulk Electrical Conductivity (dS/m)	0-23	0 - 7 : 0.01 dS/m, 7 - 23 : 0.05 dS/m	0 -7dS/m: $\pm 10\%$, user calibration required above 7 dS/m
Temperature ($^{\circ}\text{C}$)	-40 to 50	0.1 $^{\circ}\text{C}$	$\pm 1 \text{ }^{\circ}\text{C}$

To measure the water content, a 70MHz oscillatory wave is supplied to the sensor prongs that charges according to the dielectric property of the surrounding material. The microprocessor measures the stored charge and brings an output value dielectric permittivity from the sensor. The stored charge is proportional to the soil dielectric and volumetric water content. Decagon devices convert raw dielectric permittivity values using the mathematical relationship between dielectric permittivity and volumetric water content in soil developed by Topp et al. (1980) popularly known as Topp equation.

To measure the electric conductivity (EC), an alternating current is applied to the two stainless steel screws that serve as electrodes and the resistance between them is measured. To obtain electrical conductivity, the inverse of the measured resistance ie the conductance is multiplied by the cell constant. The measured electrical conductivity is normalised to 25°C.

Temperature measurement is a more straight-forward than the previous measurements. The 5te uses a thermistor to measure the temperature. The thermistor is located underneath the sensor overmold

5.3.2 MPS-6 Matrix Suction Sensor

MPS-6 is another electromagnetic sensor developed by Decagon Inc. to measure soil hydraulic properties. The sensor shown in Figure 5-2, measures soil water potential otherwise known as matrix suction. The sensor has a low power requirement and can continuously measure suction with the help of data logger. The sensor also measures temperature, making it possible to compare suction readings at various temperatures. The feature used for the temperature measurement is the same as the one used in the 5TE sensor. The sensor specifications are given in Table 5-3.

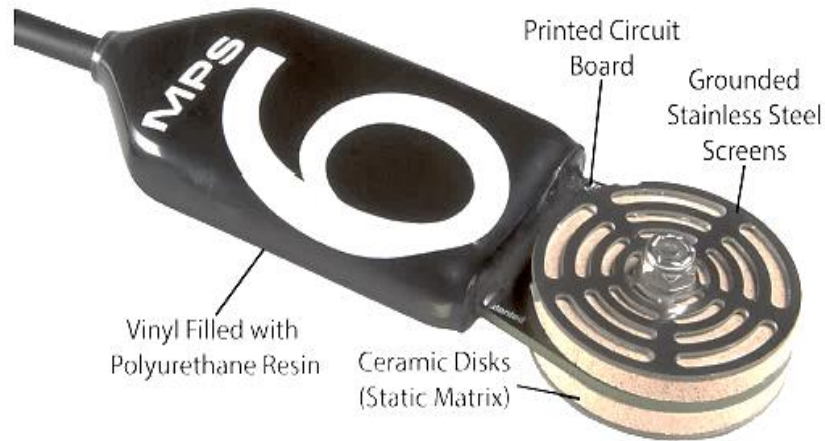


Figure 5-2: MPS6-6 sensor features (Deaagon 2015)

Table 5-3: MPS-6 sensor specifications

Measured Parameter	Range	Resolution	Accuracy
Matric Suction (kPa)	-9 to -100,000	0.1	10% of reading + 2 kPa
Temperature (°C)	-40 to 60	0.1 °C	±1 °C

There are two basic parameters that describe the state of water in soil: one is soil water content or the amount of water per unit of soil, and the other is soil suction or the energy state of water in the soil.

All soil suction measurement techniques measure the potential energy of water in a state of equilibrium with water within the soil. According to the Second Law of Thermodynamics systems with differing energy levels if connected together tends to move toward attaining equilibrium energy level. When an object comes into hydraulic contact with the soil, the water potential of the object comes into equilibrium with the soil water potential.

Pore pressure measuring instruments such as tensiometers, psychrometers and hygrometers make use of this equilibration principle to measure soil suction. For the sensors that use a solid matrix equilibration technique, a known material with a known static matrix of pores is introduced into the soil and allowed to come into hydraulic equilibrium according to the Second Law of Thermodynamics. Once the two are in a state of equilibrium, measuring the suction ability of the solid matrix gives the

matrix suction of the soil. The same principle is used by MPS-6, but the sensor measures the dielectric permittivity of a solid matrix (porous ceramic discs) instead, to determine its matrix suction. The dielectric permittivity of air, the solid ceramic, and water are 1, 5, and 80 respectively. So, the dielectric permittivity of the porous ceramic discs depends on the amount of water present in the ceramic disc pore spaces.

Water content and water potential are related by a relationship, called the moisture characteristic curve. Thus, the matrix suction of a soil is inferred with the moisture characteristic curve after measuring the water content of the ceramic.

5.3.3 Time Lapse Camera

Brinno Time-lapse camera 64x46x106mm in size. It is a very portable and durable camera that captures images continuously at a specified time interval and then converts the captured images to video for easy viewing. This ability of continuous capturing and conversion of the image to video makes ideal for monitoring slope movement. The camera is easy to operate, and its lens can be rotated up to 120° making it possible to adjust the view to the desired position. It has a focal length of 26mm, minimum focus distance of 75mm and angle of view of 59°. It has the capacity capture up to four frames, but the custom time interval is 1 second to 24 hours. The output image resolution is 1280x720. The camera is powered by 4AA battery and can last for 78 days if the image capturing interval is set at 24 hours.

5.4 Feasibility Tests

5.4.1 Selecting Moulding Water content and the working density

Among the index and geotechnical tests conducted, the compaction test is considered to be very important as the two parameters i.e Maximum dry density (MDD) and Optimum moisture content (OMC) are crucial in determining the initial moulding water content. The compaction test was conducted in accordance with the British Standard (BS1377-5, 1990). The standard Proctor mould was used for the test and the variation of moisture contents with density recorded during the test is shown in Figure 5-3.

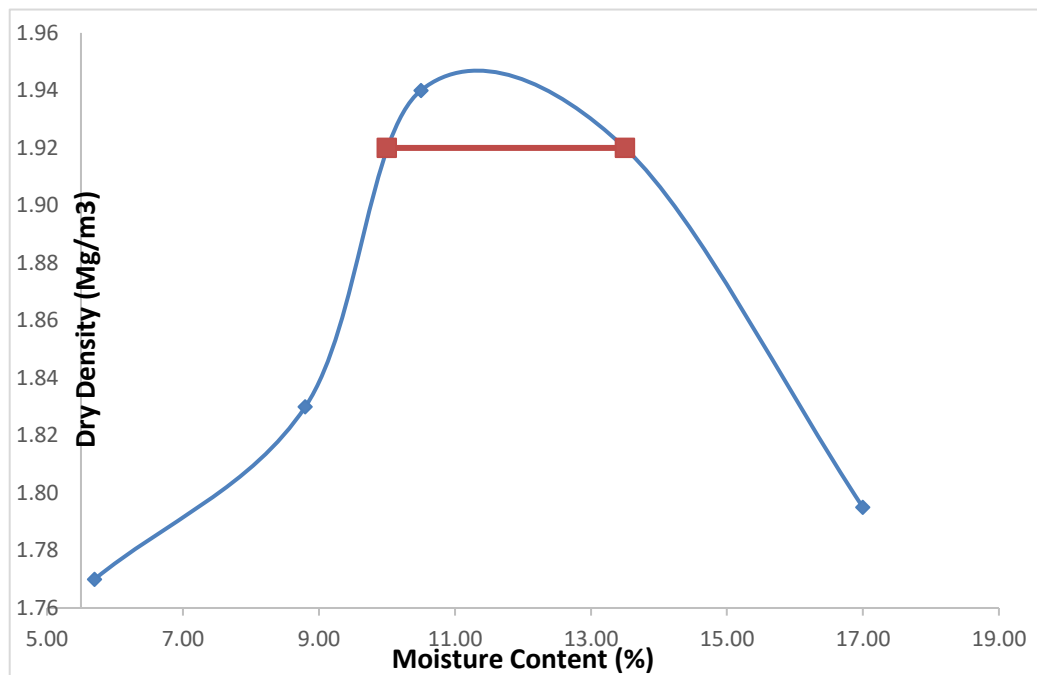


Figure 5-3: Compaction curve

From Figure 5-3, the MDD and OMC were found to be 1.942Mg/m³ and 11.3% respectively. These were considered as reference parameters. The right side of the peak point of the curve is called the ‘wet side’ which covers moisture content higher than the OMC with softer sample consistency, while the ‘left side’ has lower water content than the ‘OMC’ with stiffer consistency (Egeli and Pulat, 2011).

It was also observed during the test, that the moisture content of the soil influenced the ease at which soil can be manipulated (spreading and compaction). When the soil moisture was greater than 10% but less than 13% as indicated by a red line on figure 5-3 above, the soil was hard to manipulate. Mixing, spreading and compaction became more difficult.

Based on results obtained and the observation made during the test, the density and initial water content of the soil to be used in the subsequent tests were decided to be lower than those optimum values to achieve the objective of making slope to fail thereby allowing the failure mechanism to be studied. Particularly the moulding water content of 10% was decided and used in the subsequent experiment to arrive at the density less than the MDD.

5.4.2 Homogeneity Test

Having decided the moulding water content and the working density, it was then considered necessary to control these parameters for repeatability and test result comparison. For this reason, a homogeneity test was conducted. The objective was to determine how best these parameters can be kept as uniform as possible. To achieve this objective, soil types were mixed in the right proportion and compacted at moisture content (10%) less than the optimum moisture content. A standard CBR mould was used and each sample was compacted in three layers as specified by BS 1377. During compaction, a light metal plate was placed on the soil surface and 2.5kg hammer was used to apply the number of blows required to the plate surface area. Samples were taken by coring to determine the homogeneity in moisture and density as shown in Figure 5-4.

Table 5-4 shows the results obtained during the test. From the result, it can be seen that the values of density and moisture content of three sub-samples are almost the same. Similarly, the values of the

5.4.3 Infiltration and Permeability test

The ease at which water infiltrates or permeates into the soil was studied in two ways. First, the standard falling head permeability test was conducted in accordance with the generally accepted traditional procedure as reported by Head and Epps (1994). Secondly, a test procedure for infiltration test used by Johnson (1963) was employed and is briefly described as follows.

Two soil samples of 1000mm³ volume each, were compacted in two different moulds at a specified moisture content, one of which is shown in Figure 5-5(a). The samples were compacted at different densities. A known quantity of water was poured on the surface of the samples as in 5-5(b), and the time taken for water to infiltrate (draw down) into each sample, as in 5-5(c&d) was recorded.



Figure 5-5: Infiltration test

The result for standard permeability test is shown in Table 5-5 while that of filtration test is shown in Table 5-6.

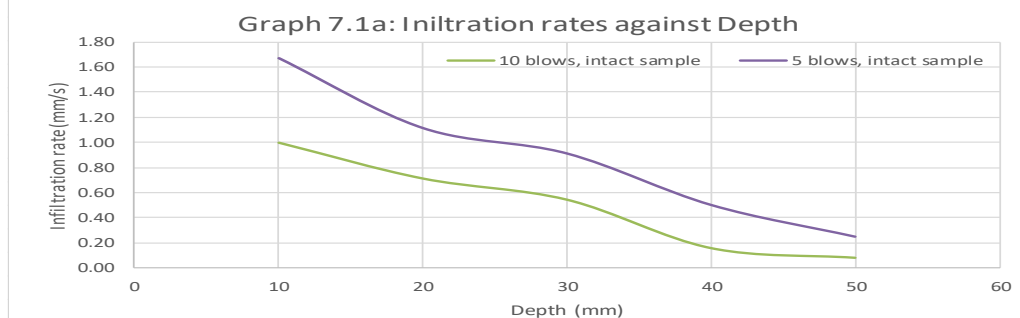
Table 5-5: Results of permeability test

a). Permeability				
Measured Parameter	10 Blows		5 Blows	
Dia. of a pipe (cm)	0.21		0.21	
Area of pipe, a (cm ²)	0.03		0.03	
Dia. of sample (cm)	10.00		10.00	
Area of sample, A (cm ²)	78.50		78.50	
Length of sample, l (cm)	14.10		14.10	
Initial height h ₀ (cm)	77.00		77.00	
Final height h ₁ (cm)	47.00		47.00	
Time, t (s)	126.00		16.00	
Permeability, $k = a/At * \ln(h_0/h_1)$, (cm/s)	0.000024		0.000192	
b). Compaction				
Compaction Effort	10 Blows		5 Blows	
Sample	Sub sample 1		Sub sample 1	
Wt of mould and wet soil (W ₂)	5400.90		5288.60	
Wt of mould (W ₁)	3334.80		3335.80	
Wt of wet soil (W ₂ -W ₁) g	2066.10		1952.80	
Vol. of wet soil m ³	1106.85		1106.85	
Bulk density = m/v,	1.87		1.76	
Cont No,	T11	B32	NC	SI
Wt of wet soil and cont. g	16.56	14.98	13.29	13.05
Wt of dry soil and cont. g	15.55	14.05	12.51	12.25
Wt of cont. g	5.49	4.95	5.58	5.52
Wt of dry soil. g	10.06	9.10	6.93	6.73
Wt of moisture g	1.01	0.93	0.78	0.80
Moisture content %	10.04	10.22	11.26	11.89
Average Moisture content %	10.13		11.57	
Dry Density	1.69		1.58	

Note: 2.5kg hammer was used for this test

Table 5-6: Infiltration test results

Compaction	Length (mm)	Diam. (mm)	Volume (mm ³)	
	127	152	2303.35	
Compaction Effort	5 blows		10 blows	
Wt of mould and wet soil (W ₂)	9983.00		10660.00	
Wt of mould (W ₁)	6590.00		7097.00	
Wt of wet soil (W ₂ -W ₁) g	3393.00		3563.00	
Vol. of wet soil m ³	2303.35		2303.35	
Bulk density = m/v,	1.47		1.55	
Infiltration				
Depth (mm)	5 blows		10 blows	
	Time (s)	Inf. Rate	Time (s)	Inf. Rate
10	6	1.67	10	1.00
20	18	1.11	28	0.71
30	33	0.91	55	0.55
40	80	0.50	251	0.16
50	202	0.25	609	0.08



Note: 1.8kg hammer was used for this test

In the standard permeability test, 2.4×10^{-5} cm/s was obtained when 10 blows of 2.5kg was applied resulting in a dry density of 1.69Mg/m^3 . When 5 blows of the hammer were applied 1.58Mg/m^3 dry density was obtained and the resulting permeability is 1.92×10^{-4} cm/s.

The infiltration test result shows that the time taken for 1L of water to infiltrate a soil sample compacted in CBR mould with 10 blows of the small hammer is 88s while the value of 55s was obtained under the same condition but with 5 blows. This shows that the amount of effort applied influences the resulting density and the infiltration rate. The time taken for the water level to fall to various depths was recorded and the results of 5 and 10 blow compaction are shown in the figure attached to Table 5-6. The test shows that if the soil is compacted to a density less than MDD, appreciable permeability values can be obtained. It also shows that the infiltration rate decreases as the water level increases.

5.4.4 Assessment of Electromagnetic Sensors

The performance of the electromagnetic sensors for possible use in the main experiment was assessed by first calibrating the sensors before using it later for soil homogeneity test.

The procedure involves compaction to the desired density of a representative soil sample into a 2 litre plastic container and then inserting the 5TE sensor that measures volumetric water content, bulk electrical conductivity and the temperature of the sample. Figure 5-6 shows the compacted soil sample with an inserted 5TE sensor while Figure 5-7 shows the exact position of the sensor in the sample as specified in the sensor application note prepared by Cobos and Chambers (2010). The procedure as contained in this technical note is based on the procedure developed by Starr et al. (2002). It involves comparing direct indirect measurement of water content and will be described in the later part of this section. The procedure above was repeated to ensure repeatable insertion quality and average readings were taken



Figure 5-6: Sensor insertion and water content measurement

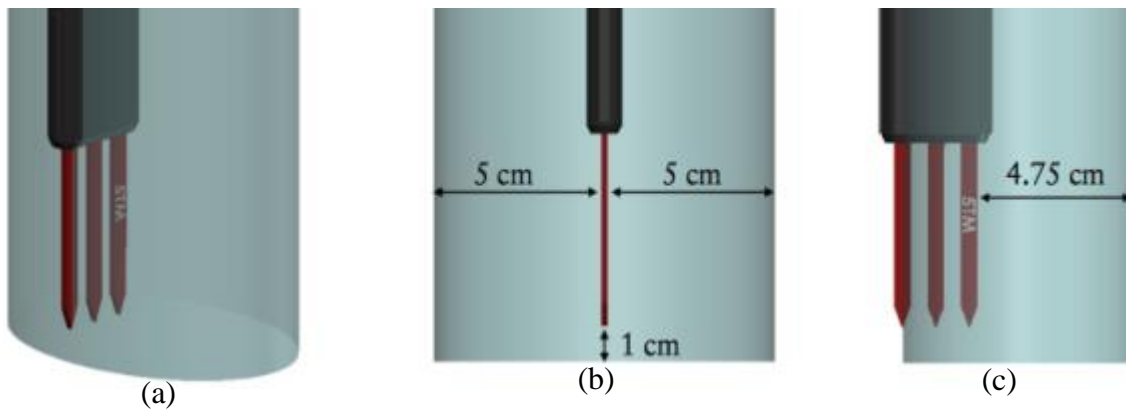


Figure 5-7: Idealised measurement volume of 5TE sensor (Decagon, 2015)

The volumetric soil sample was obtained by inserting the volumetric soil sampler into the undisturbed soil near the sensor and taking the intact soil core inside it as shown in Figure 5-8(a). The entire soil core was placed into a drying container and weighed before oven drying the sample for water content determination.

The above procedure was repeated with an increase in water until the soil nears saturation. This was evident by softening of the soil and glistening after compaction as shown in Figures 5-8 (b and c)

The volumetric water content is the volume of water per volume of bulk soil and was calculated for each sample and result is shown in Table 5-7. Sensor measurements are shown in Table 5-8.



Figure 5-8: Stages in water content (VWC&GWC) measurements

Table 5-7: Table showing the calculated VWC and GWC values

Sample Label	Sensor Output (Counts)	Container Mass (g)	Sample volume (cm ³)	Wet soil + Container (g)	Dry soil + container (g)	Mass & vol. of water (cm ³)	Dry soil mass (g)	Soil Bulk Density (g/cm ³)	Calculated VWC (cm ³ /cm ³)	Measured VWC (cm ³ /cm ³)	Gravimetric Water Content (%)	
A	B	C	D	E	F	G = E-F	H = F-C	I = H/D	J = G/D	K	L = (G/F)*100	M=Avg(L)
1a	238	9.75	45.34	81.56	80.68	0.88	70.93	1.56	0.02	0.07	1.09	
1b	237	9.98	45.34	81.94	81.07	0.87	71.09	1.57	0.02	0.07	1.07	1.08
2a	299	37.89	45.34	109.83	106.64	3.19	68.75	1.52	0.07	0.10	2.99	
2b	300	20.96	45.34	94.00	90.79	3.21	69.83	1.54	0.07	0.10	3.54	3.26
3a	451	17.62	45.34	95.04	88.02	7.02	70.40	1.55	0.15	0.17	7.98	
3b	449	27.42	45.34	107.90	100.48	7.42	73.06	1.61	0.16	0.17	7.38	7.68
4a	898	23.79	45.34	111.51	96.33	15.18	72.54	1.60	0.33	0.34	15.76	
4b	898	37.93	45.34	126.85	111.07	15.78	73.14	1.61	0.35	0.34	14.21	14.98

In accordance with the calibration procedure, the calculated values were plotted against the average of raw sensor counts as shown in Figure 5-9. From the graph, the relationship between VWC and sensor raw counts, in form of mathematical model was established. This relationship is referred to as

calibration function. It is a linear equation obtained by trendline function of Microsoft excel and is shown on the graph.

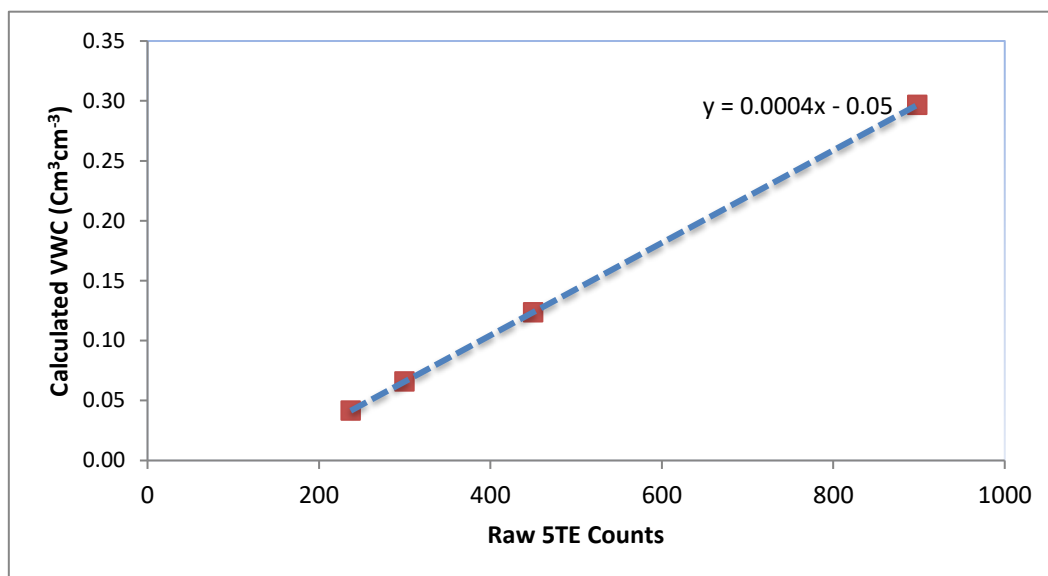


Figure 5-9: Calibration function graph

The obtained calibration function was applied to the sensor data collected subsequently. When logging data this equation is applied to the raw data downloaded from the logger. It is stated in Decagon (2015) note, that “*the resolution, precision, repeatability, and sensor to sensor agreement of the sensors are excellent, so the soil specific calibration of one sensor can be applied to all other sensors of that type in that particular soil*”.

It is noteworthy that feasibility tests were concluded with the test on the 5TE sensor. No any trial test was conducted on the MPS6 sensor, as it was not considered necessary. This is because the two sensors work based on the same principle.

Table 5-8: 5TE sensor measurements at different gravimetric water content

Gravimetric Water Content (%)	Measurement Time	VWC m ³ /m ³	Temp °C	Bulk EC mS/cm	Corrected Bulk EC mS/cm
1.1	12:18 PM	0.074	24.3	0.00	0.00
	12:19 PM	0.074	24.2	0.00	0.00
	12:20 PM	0.072	23.8	0.00	0.00
	12:21 PM	0.076	23.3	0.00	0.00
	12:22 PM	0.074	24.0	0.00	0.00
	12:23 PM	0.072	24.2	0.00	0.00
	Average		0.07	23.97	0.00
3.3	02:02	0.10	23.0	0.02	0.02
	02:04	0.09	23.1	0.03	0.03
	02:06	0.09	23.9	0.02	0.02
	02:12	0.09	24.0	0.02	0.02
	02:14	0.09	23.5	0.02	0.02
	02:16	0.09	23.1	0.02	0.02
	Average		0.09	23.65	0.02
7.7	5:28	0.169	24.5	0.28	0.28
	5:29	0.169	24.4	0.29	0.29
	5:30	0.168	24.2	0.29	0.29
	5:31	0.168	24.1	0.29	0.30
	5:32	0.168	24.0	0.30	0.31
	5:33	0.177	23.7	0.31	0.32
	Average		0.17	24.15	0.29
15	6:42	0.318	21.7	0.60	0.64
	6:44	0.319	21.6	0.60	0.64
	6:50	0.319	21.3	0.61	0.66
	6:54	0.326	21.2	0.60	0.65
	6:56	0.319	21.2	0.60	0.65
	Average		0.32	21.39	0.60

Water content is the quantity of water contained and is expressed as a ratio of volume or mass. For simplicity and accuracy, it was considered necessary to establish a mathematical relationship between the two. Therefore, the calculated GWC values in table 5.5 were plotted against measured VWC values. The relationship is shown in Figure 5-10. The relationship in form of linear equation is applied to the sensor data collected subsequently. So that, when a volumetric water content is known, the gravimetric water content can be estimated, and vice versa.

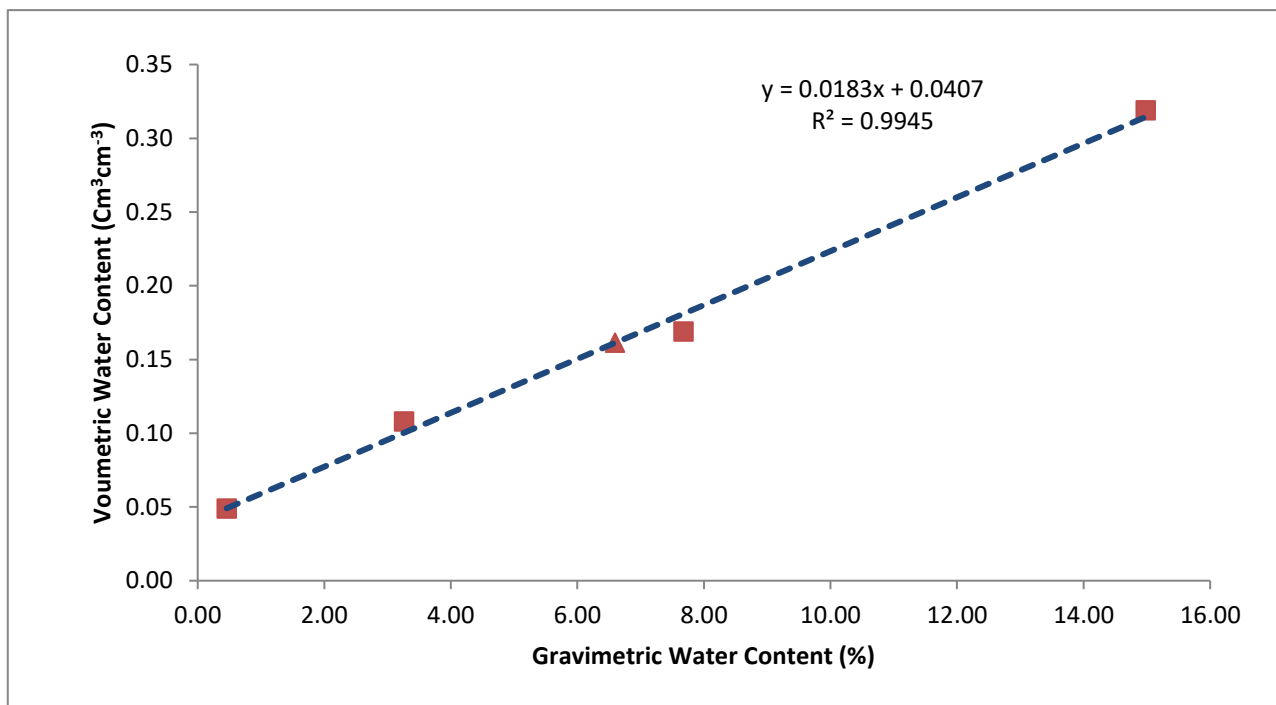


Figure 5-10: Measured VWC versus GWC

5.4.5 Homogeneity Test using 5TE Sensor

To control the amount of compaction on the sample and hence the density, a sample was compacted in a plastic box in layers. The box and the soil are shown in Figure 5-11. A rigid wooden plate of 25mm thickness was placed on the soil surface and a hammer was used to compact the soil as described in 5.4.2. The compacted sample is shown in Figure 5-11(a)

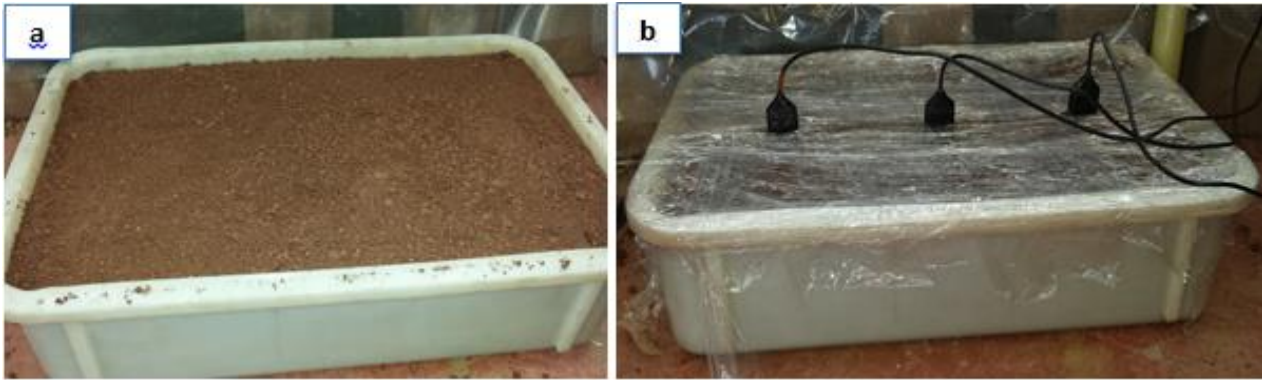


Figure 5-11; Homogeneity test with sensor (a) Compacted sample, (b) Sealed sample with probe

Three 5TE sensors equally spaced were inserted vertically into the soil and measurement of VWC with the sensor commenced immediately. Then, the core was taken from the sample while sensor measurements were being made. This was done by inserting the coring tube into the undisturbed soil by the two sides of each sensor to take the cores. From these samples, the average density and moisture content surrounding each sensor were determined. The entire box was then sealed with a non-conductive cling film to avoid moisture loss for the period when sensor measurement was being taken as shown in Figure 5-11(b)

Since the sensors can measure soil temperature and bulk electrical conductivity while measuring the soil moisture, these parameters were recorded during the above-mentioned tests. With the results, the electrical properties with respect to moisture and density variations were assessed. Table 5-9 shows the moisture and density around each of the sensor probe used in the study.

The traditional assessment shows that the parameters are almost uniform at all the three probes locations. In terms of moisture, the percentage difference between point 1 and 2 is 5.25% while the percentage difference between point 2 and 3 is only 2.5%. In terms of density, the percentage difference between the average density of point 1 (1.19Mg/m³) and that of point 2 (1.22Mg/m³) is 1.1%. While the percentage difference between point 2 and 3 (1.17) is 4%. Since the moisture difference between

the 3 points is 5.25% or less and that of the density is 4% or less, it can be concluded that the sample is relatively homogeneous. It is, important to note that the moisture difference is higher between points 1 and 2 than that between 2 and 3 while in terms of density the reverse is the case.

Table 5-9: Density and moisture distribution in the first experiment

Compaction Test							
Weight of mould and wet soil (W2)	404.990	514.970	409.990	519.770	403.390	512.670	
Weight of mould (W1)	206.300	309.520	206.300	309.520	206.300	309.520	
Weight of wet soil (W2-W1) g	198.690	205.450	203.690	210.250	197.090	203.150	
Vol. of wet soil. m ³	1.519E-04	1.519E-04	1.519E-04	1.519E-04	1.519E-04	1.519E-04	
Bulk density in Mg/m ³ = m/v,	1.31	1.35	1.34	1.38	1.30	1.34	
Cont No,	5A	5B	6A	6B	7A	7B1	
Weight of wet soil and cont. g	37.35	46.46	46.29	50.82	46.05	46.67	
Weight of dry soil and cont. g	36.87	45.34	45.05	49.20	44.72	45.50	
Weight of cont. g	32.05	33.09	32.88	32.96	32.05	33.09	
Weight of dry soil. g	4.82	12.25	12.17	16.24	12.67	12.41	
Weight of moisture g	0.48	1.12	1.24	1.62	1.33	1.17	
Moisture content %	9.96	9.14	10.19	9.98	10.50	9.43	
Average Moisture content %	9.55		10.08		9.96		
Dry Density	1.19		1.22		1.17		

The volumetric water content data collected with the sensor measurements are compiled in Appendix A and the results are graphically shown in Figure 5.12. Unlike the traditional geotechnical method, the geophysical measurement using sensor shows less degree of homogeneity. As shown in the Appendix, the percentage difference between point 1 and 2 is initially on the average of 12% and later stabilised to the average of 11%. Similarly, the percentage difference between 2 and 3 was initially on the average of 7% before stabilising to the average value of 6%. Despite this disparity, one thing is common to both traditional geotechnical and sensor geophysical methods of homogeneity assessment. That is, the difference in moisture between point 1 and 2 is higher than that of between 2 and 3 in both methods. This validates the use of the sensors for homogeneity test.

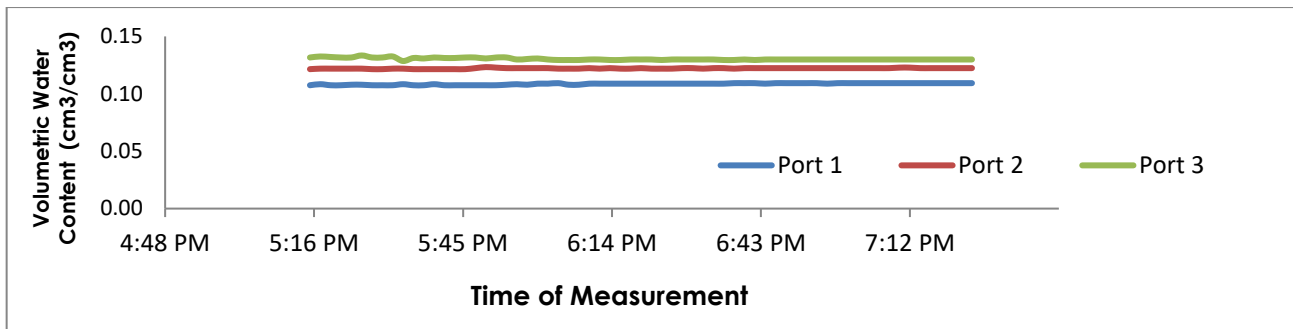


Figure 5-12: The VWC measurements with 3 ports 5TE sensor

There are many reasons why the percentage difference is higher in sensor measurements than in traditional compaction method. One of the reasons is the high sensitivity of the sensors to disturbance or attenuation (Decagon, 2015). Taking the sample with an iron pipe, for density test and moisture content determination may affect the sensor measurement. For this reason, another sample was prepared for the repeat of the test. In the second experiment, same method and compaction effort were used as the previous but samples for moisture content determination were taken from the compacted sample the next day, to avoid error due to sample disturbance. This was done after the successful completion of the sensor measurements. A better result was obtained in the second experiment as shown in Table 5-10 and Figure 5-13. Appendix B gives more details of the sensor measurements.

Table 5-10: Determination of density and moisture distribution in the second experiment

Compaction Test	1		2		3		4	
Weight of mould and wet soil (W2)	454.500		466.930		465.790		463.090	
Weight of mould (W1)	309.520		309.520		309.520		309.520	
Weight of wet soil (W2-W1) g	144.980		157.410		156.270		153.570	
Vol. of wet soil. m ³	1.134E-04		1.190E-04		1.190E-04		1.156E-04	
Bulk density in Mg/m ³ = m/v,	1.28		1.32		1.31		1.33	
Cont No,	A5	C10	C8	E-5	C12	C3	GG1D	1600-1
Weight of wet soil and cont. g	27.68	28.58	36.60	27.27	21.99	33.89	46.28	23.89
Weight of dry soil and cont. g	26.63	27.99	35.61	26.34	21.39	32.95	45.30	22.41
Weight of cont. g	14.07	20.48	22.88	15.16	14.13	21.10	32.90	4.84
Weight of dry soil. g	12.56	7.51	12.73	11.18	7.26	11.85	12.40	17.57
Weight of moisture g	1.05	0.59	0.99	0.93	0.60	0.94	0.98	1.48
Moisture content %	8.36	7.86	7.78	8.32	8.26	7.93	7.90	8.42
Average Moisture content %	8.11		8.05		8.10		8.16	
Dry Density	1.18		1.23		1.21		1.23	

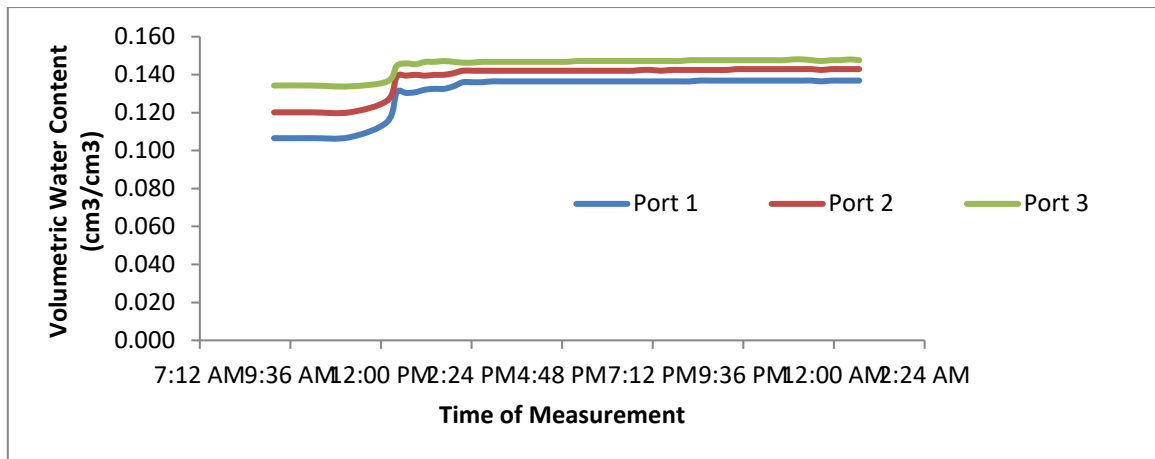


Figure 5-13: The volumetric water content measured with 5TE in the second experiment

From the results, it can be seen that the percentage difference between the measurements made with port 1 and 2 was initially 11% then 5% before stabilising to 4%. Similarly, the difference between ports 2 and 3 was initially 11% then 5% before it stabilised to 3%. This second experiment confirms that the moisture distribution between one point of the sample to another, is at least 96% uniform and the difference between the measured three points is negligible. More discussion on Figure 5.13 can be found in the following section 5.4.6.

5.4.6 Moisture Equilibrium

From the experiments in 5.4.5, a knowledge about the moisture equilibrium of the soil sample can be derived. The graph in Figure 5.13 shows that the moisture content changes were non-uniform at the beginning but the uniformity was achieved after 4-5 hours, giving steady values thereafter. At this time the sample can be said to reach its equilibrium stage. It is a time when no further moisture movement occurs. The result from the two experiments shows that the moisture equilibrium can be achieved within some hours from the completion of compaction and sealing of the sample, but it is preferable to allow the period of 24 hours before running the test. This is done to eliminate any doubt and avoid uncertainty on the test.

5.4.7 Electrical Properties

To measure the material electrical property, a current of known density has to pass through the material and the potential difference across the flow path distance be recorded (Sellers et al., 2010). From Ohm's law, we know that the potential difference between any two given electrodes is directly proportional to the supplied current and inversely proportional to the resistance of the material i.e. $V=IR$. From that relation, if the conductivity of the material is known, the resistivity can easily be estimated.

5TE uses a two-sensor array located on the screws of two of the 5TE prongs shown in Figure 5.1, to measure the electrical conductivity (EC). The array measures the EC by applying an alternating electrical current to the two electrodes and measuring the resistance between them. To get the conductivity, the inverse of the resistance (conductance) is multiplied by the cell constant (Decagon, 2015).

The temperature effect on electrical properties of the soil has been stressed by many researchers (Sellers et al., 2010). To account for the temperature variations effect on the measured electrical conductivity, the measured values are normalized to 25°C. A reference temperature T of 25°C is normally used as a standard and bulk electrical conductivity measured at a particular temperature EC_T is adjusted to a reference EC_{25} , using equation 5.1 developed by Keller and Frischknecht (1977).

$$EC_{25} = \frac{EC_T}{1+\sigma(T-25)} \dots\dots\dots 5.1$$

Where σ denotes temperature slope compensation which is commonly considered as 0.0191_C-1. This value for σ was experimentally proven to be approximately 1.9% increase in EC per each 1_C increase anywhere on the temperature scale (Ma et al., 2011).

The procedure used in assessing the electrical properties of the soil is the same as the calibration procedure explained in 5.4.4. As the volumetric water content is measured the corresponding value of electrical conductivity and the temperature are also recorded. The electrical conductivities are then normalised using Keller and Frischknecht equation shown and explained above. Based on this procedure Table 5-11 is formed from the data collected earlier.

Table 5-11. Variation of electrical conductivity with water content

VWC (cm ³ /cm ³)	Temp. (°C)	EC (mS/cm)	Corrected EC (mS/cm)	GWC (%)
0.074	30.3	0.00	0.00	1.82
0.165	30.7	0.05	0.05	6.79
0.242	30.6	0.38	0.34	11.00
0.310	29.1	0.47	0.44	14.72

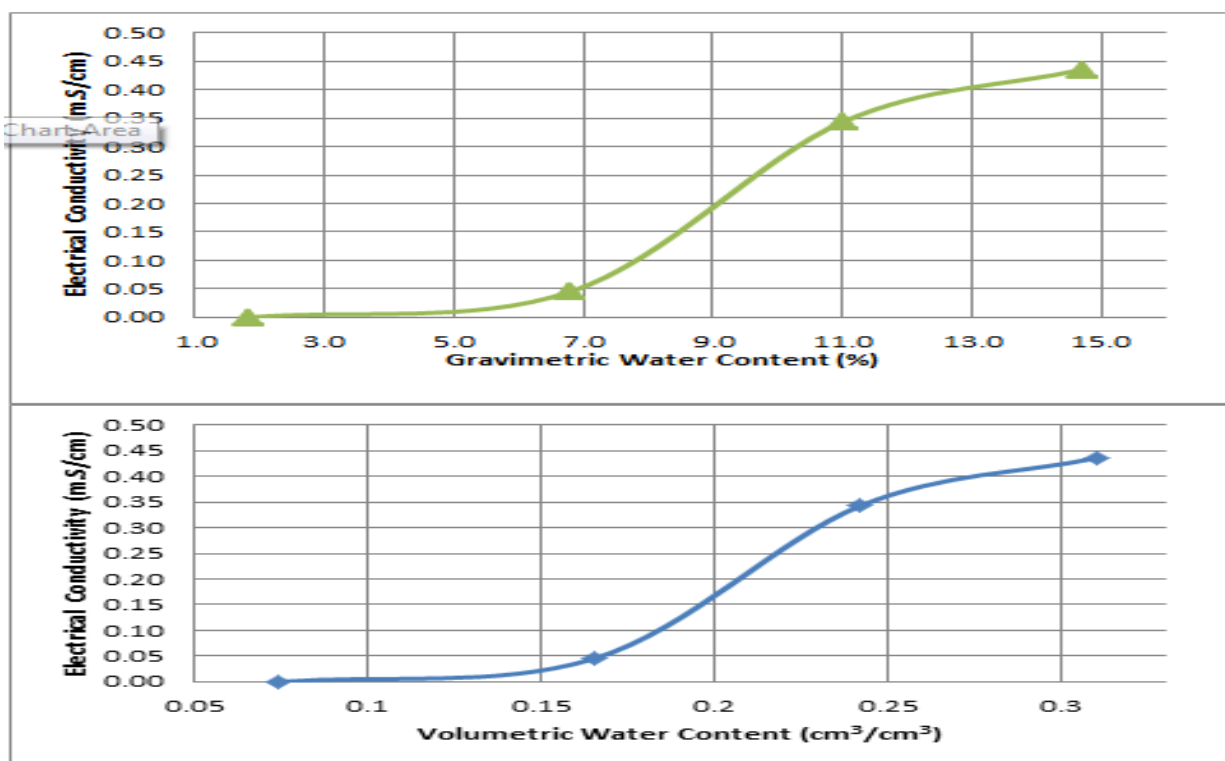


Figure 5-14: Variation of electrical conductivity with water content

The conductivity values were plotted against both gravimetric and volumetric water content respectively as shown in Figure 5-13. From the graph it can be seen when the gravimetric water content was 0%, there was no conductivity. When the value is between 3-4% a negligible value of conductivity was recorded. A reasonable value was recorded when the gravimetric water content was around 5%. The conductivity increases rapidly with the gravimetric water content at the value between 5% and 11%. Beyond this value, the rate of increase of conductivity with water decreases. The graph shows that the trend of variation of electrical conductivity with water content is the same for the volumetric and gravimetric water contents.

In a separate experiment, the change of conductivity with the water content was studied. In this experiment, the effect of density variation was also studied. Table 5-12 gives the data obtained from this experiment. It shows a similar trend to the previous test as both shows that no conductivity recorded at zero water content and the values increase with an increase in water content up to a certain optimum value. Two tables with detailed data measurements taken by traditional geotechnical and sensor geophysical methods, respectively, are given in Appendix C.

Table 5-12: Variation of electrical conductivity with water content

VWC	Temp	Bulk EC	Correct. EC	GWC
m³/m³	°C	mS/cm	mS/cm	%
0.14	22.50	0.04	0.04	5.30
0.22	22.50	0.40	0.42	9.70
0.29	22.00	0.60	0.63	15.80
0.31	21.50	0.60	0.63	24.65

In this experiment, the conductivity value of 0.63m.S/cm remains constant after reaching optimum value 15% water content as shown in Figure 5.14. From the graph, it can be seen that the density increases with the increase in moisture content up to the optimum moisture content of 15% yielding a maximum dry density of 1.5Mg/m³.

From the two tests conducted and the results obtained and analysed, it can be shown that there is no conductivity in a dry or nearly dried soil sample. The electrical conductivity is very sensitive to change in water content at a value higher than 5% but less than optimum water content, whereas when wet of optimum, electrical conductivity is less sensitive to the changing water content. This is corroborated by the finding of Abu-Hassanein et al. (1996). The experiment gave an idea of the electrical properties of the soil as well as density and water content to be used when conducting electrical resistivity tomography (ERT) experiment. It also shows that ERT is suitable for use in the main experiment.

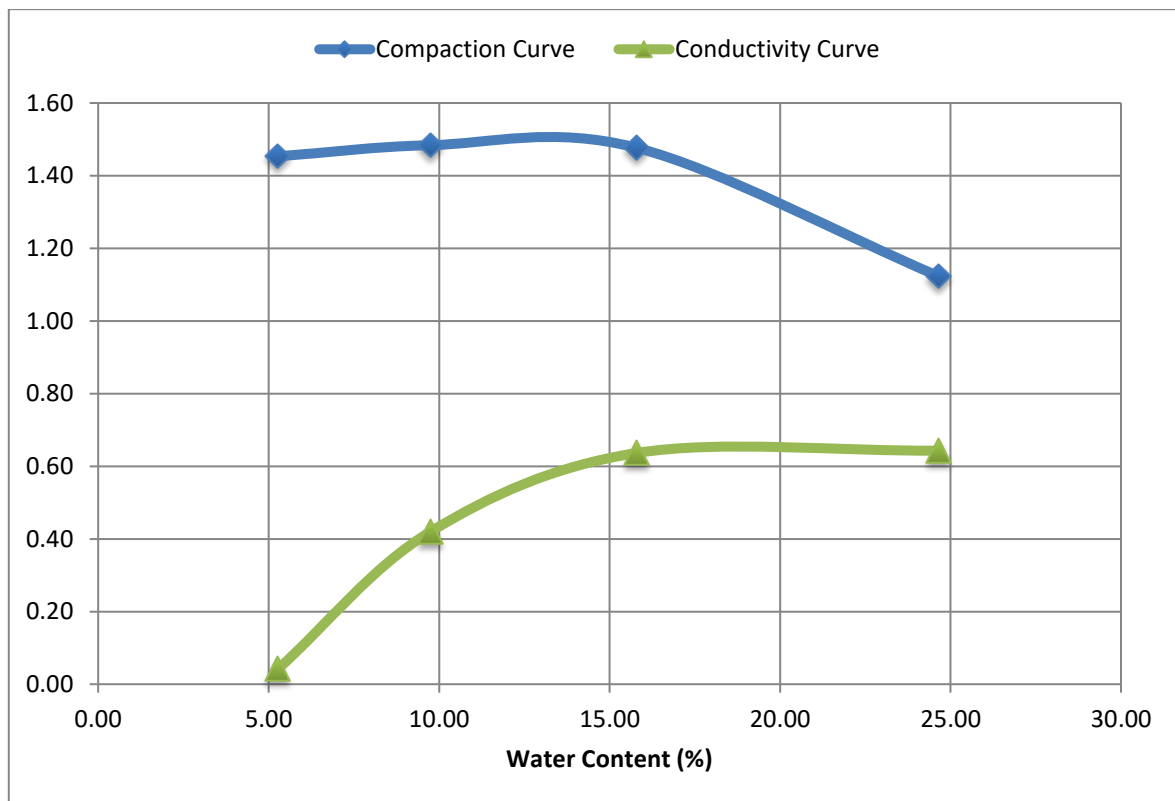


Figure 5-15: Variation of conductivity with water content

5.5 Small-Scale Experiment

5.5.1 Experimental Procedure

Two small tanks were used for this experiment as shown in Figure 5-16. Each tank was made up translucent acrylic sheet with a dimension of 370x200x500mm. The tank has a supply and discharge chambers provided at the two ends of the tank. Before construction, the designed shape of the slope was first drawn against the wall of each tank. The bottom surface was roughened by laying and sticking a sandpaper to it. This technique was used to avoid the sliding of soil body along the slope-base interface (Tohari et al., 2007). To minimize friction along the surface of the side walls, a Teflon lubricant was sprayed. The fluid was previously used by Jia et al. (2009) for this purpose.

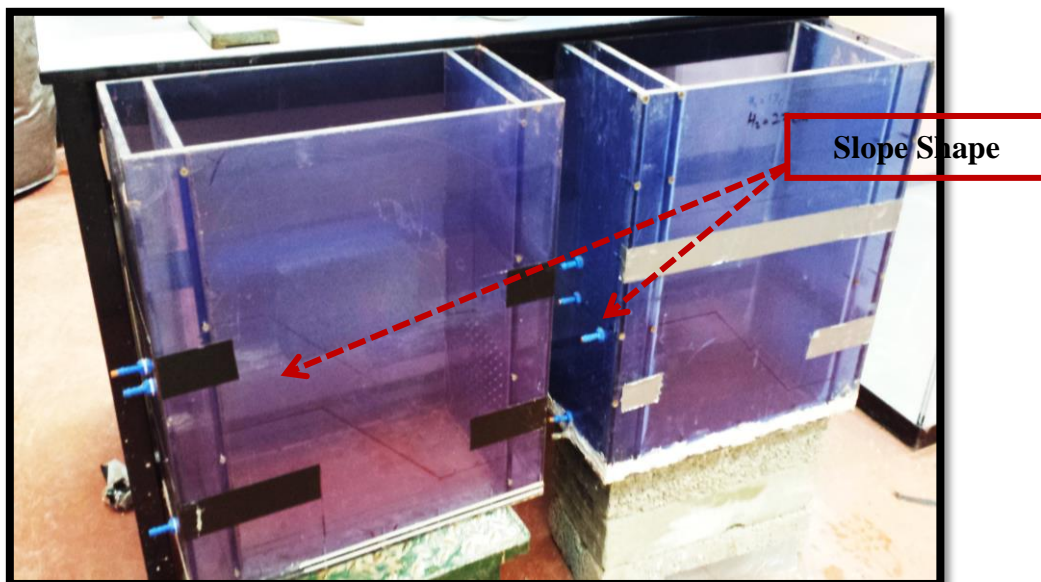


Figure 5-16: The prepared experimental tanks

The soil described in section 5.2 was used for the construction of homogeneous slope. About 35kg of the soil was oven dried at a temperature of 105°C for 24 hours. The soil was divided into two and each portion was mixed with 10% water. The chosen moisture content is little drier than OMC (11.5%) and was previously determined during feasibility tests. Etruria mudrock and sand was first mixed at dried stage, before adding water to mix again. At both stages, the soil was thoroughly mixed using mechanical mixer to achieve homogeneity. Two identical slope models were built. Each slope was

constructed by placing a prepared sample of soil in three horizontal layers, in the experimental tank. On the surface of each layer, a purpose-made plastic plate of 220x190x10mm was placed to cover compaction area, and 2.5kg hammer was used to compact the soil by applying a number of blows on the surface of the plate. After compaction, the soil slope was trimmed to form the desired geometry following the shape previously drawn against the walls of the tank as shown in Figure 5-17. One of the two models was used to test the homogeneity of the sample and the second one was preserved for the experiment. More details about slope construction procedure will be provided in section 5.6.1. Homogeneity test was conducted by taking samples at different locations of the slope and determining the moisture and density. Figure 5.18 shows points where samples were taken for homogeneity test.



Figure 5-17: Constructed slope model



Figure 5-18: Sampling for homogeneity test

For the experimental slope, instrumentation was made after the construction as shown in Figure 5.19 and initial condition was measured. The box was then covered with polyethene sheets to reduce the moisture loss. The model slope was allowed for more than 24 hours to cure and achieve moisture equilibrium. The experimental set-up is shown in Figure 5-20

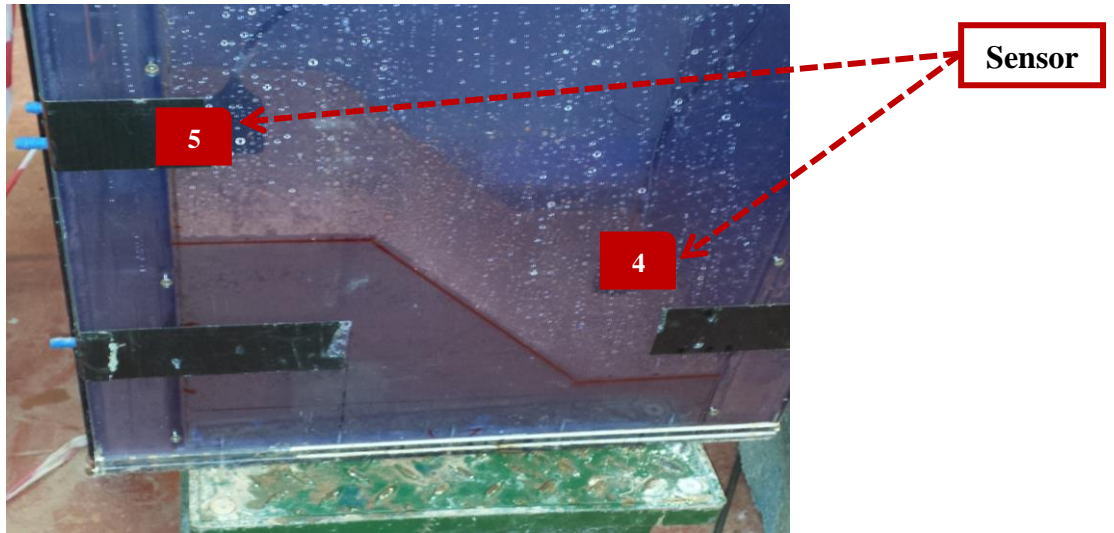


Figure 5-19: Installed sensors

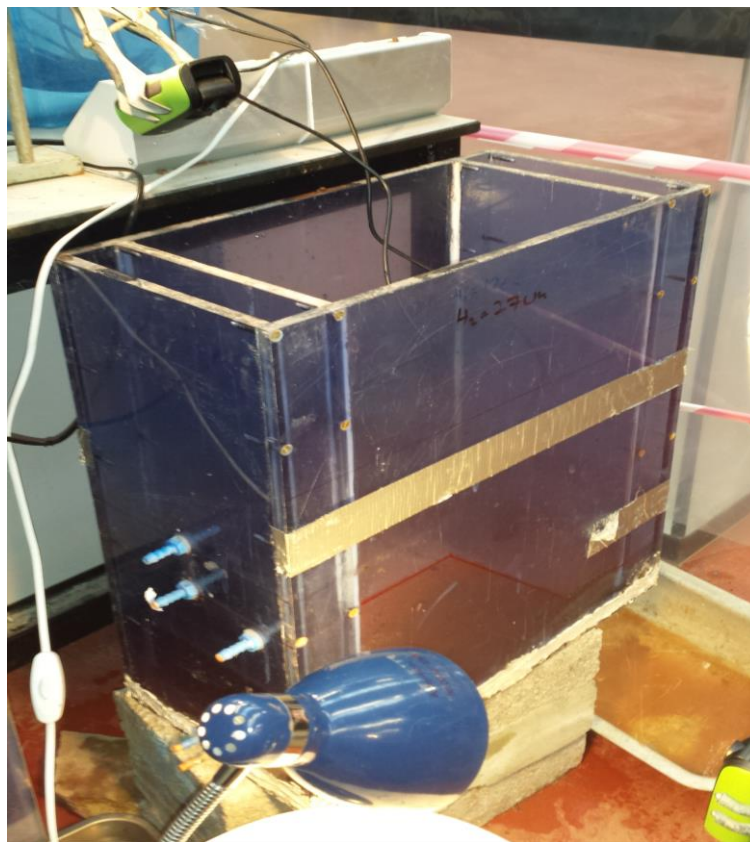


Figure 5-20: Experimental set-up

The test started by watering the surface to simulate rainfall. When no failure was observed in response to the applied rainfall, the rainfall was suspended, and water was later supplied into the slope model through the supply chamber at the side of the upper end of the slope. The geophysical processes taking place and geotechnical changes caused by the water supplied was monitored using electromagnetic sensors, while the physical changes in response to the geophysical processes were observed using cameras.

5.5.2 Small-Scale Trial Results

Two sensors each for 5TE and MPS-6, labelled Ports 4 and 5 respectively, were used in this experiment. The locations of these sensors on the slope are shown in Figure 5-21.

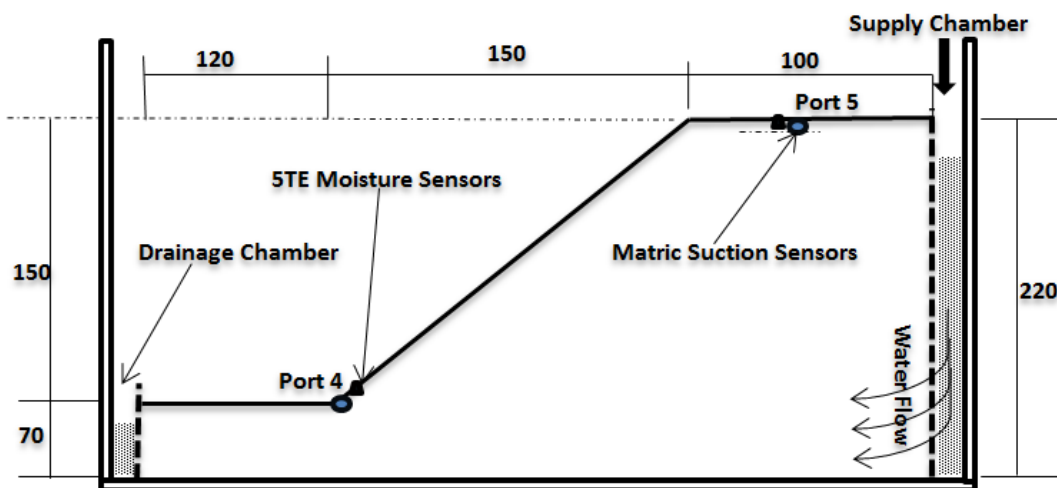


Figure 5-21: Slope dimension and instrumentation

The results shown on Figure 5-22 indicate initial irregular readings for both water content and matric suction. This can be seen on section AB of the graph. Moving further along the graph, fairly regular values can be observed for both soil matric suction (MS) and volumetric water content (VWC) as shown by section BC. Section CD of both graphs shows gradual changes in MS and VWC respectively. This can be observed to have started shortly after 4.30pm, the time when water was supplied through the supply chamber. A rapid increase in VWC at 4.46pm followed by a rapid decrease in MS by

4.52pm can be seen on section DE. Beyond this point, all the readings remain fairly constant after reaching their optimum values as shown by section EF of the same Figure 5-22.

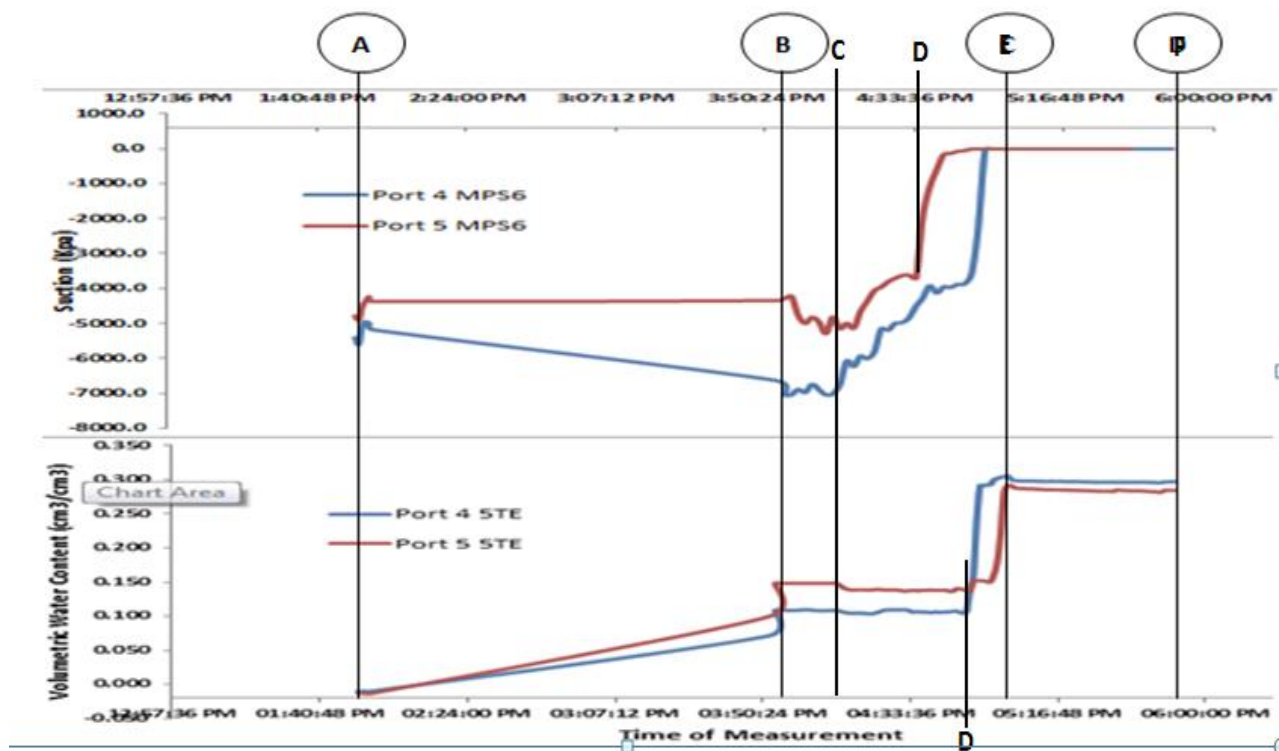


Figure 5-22: Sensor measurement results

The physical response to geophysical processes happening within the soil began by 4.39pm with a minor initial settlement shown on Figure 5.23A. Thereafter, an increase in water content and a decrease in matric suction led to the excessive settlement (collapse) and potential forward sliding as shown in figure 5.23B. A collapse movement and forward movement as shown on figure 5.23C were observed around 5.00pm. At every stage of slope movement, the difference between the original and new shape of the slope is shown by the solid and dotted lines respectively.

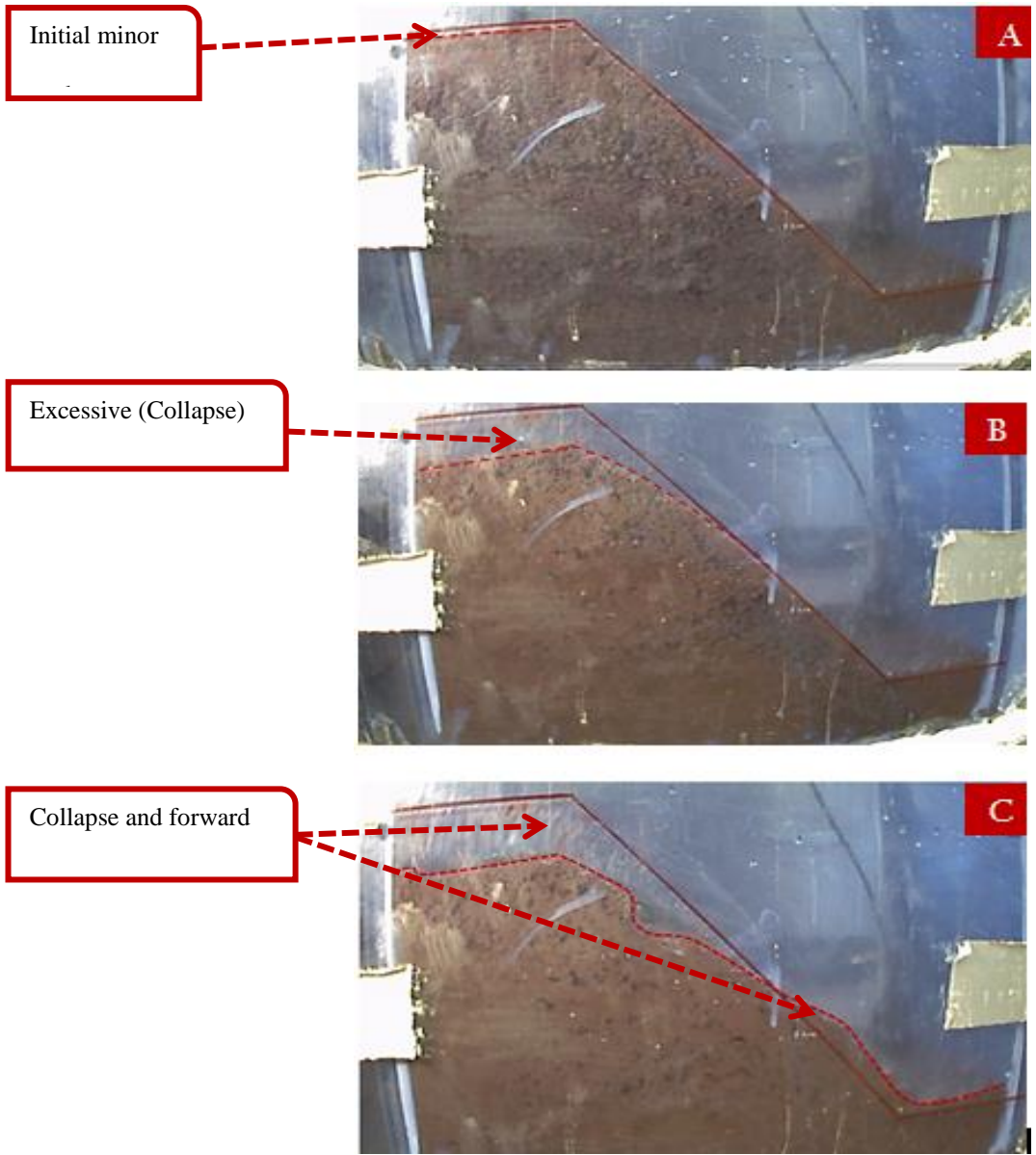


Figure 5-23: Stages of slope failure

5.6 Large-scale trial experiment

5.6.1 Experimental Procedure

A Large fibreglass tank with the shape and dimension in mm shown in Figure 5-24(a) was used for this experiment. Inlet and outlet chambers were created at the two ends of the box. They are for the supply and discharge of the water into and out of the model respectively. The preparation of tank and soil used for the slope construction is the same as in the small-scale experiment described in 5.5.1.

However, the procedure for slope construction is given in more detail in this section. The tank prepared for the experiment is shown with dimension in Figure 5-24(a&b). The slope construction was preceded by the design of the compaction layers and each is described in the following subsections.

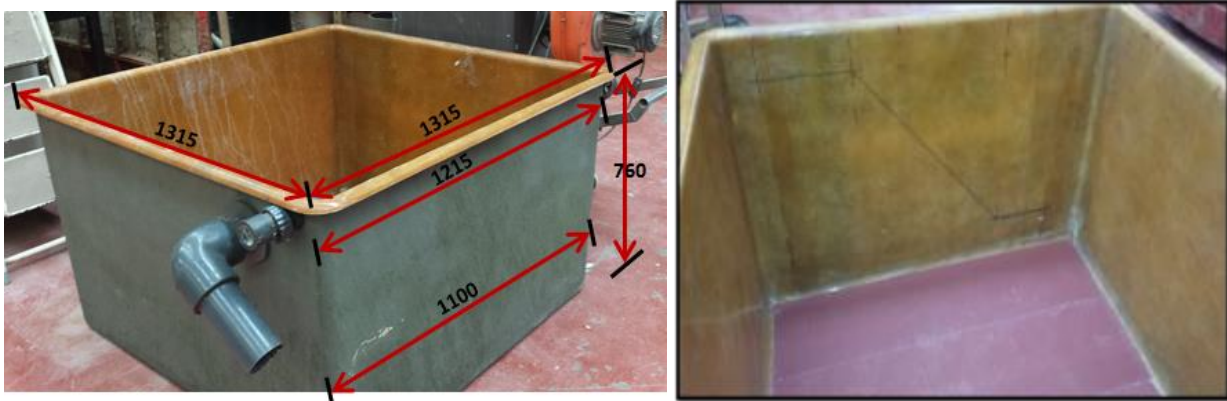


Figure 5-24: (a) The dimension of experimental tank(b) Tank preparation

5.6.1.1 Design of compaction layers

The experimental slope was constructed by placing and compacting a prepared sample of soil in horizontal layers of soil, in the experimental tank. The layer thicknesses were designed before the commencement of slope construction. The designed is based on the principle developed and advanced by Menard 1975. Menard compaction first developed in 1969 (Mayne et al., 1984), is based on the energy waves transmitted into the layer compacting soil due to the weight of the dropping hammer and the height from which the hammer drops on the soil. The energy is transmitted from the point of impact to a certain maximum depth d_{max} called a depth of influence. Beyond this point, the compaction has no effect as illustrated in Figure 5.25. Menard estimates this depth using equation 5-2.

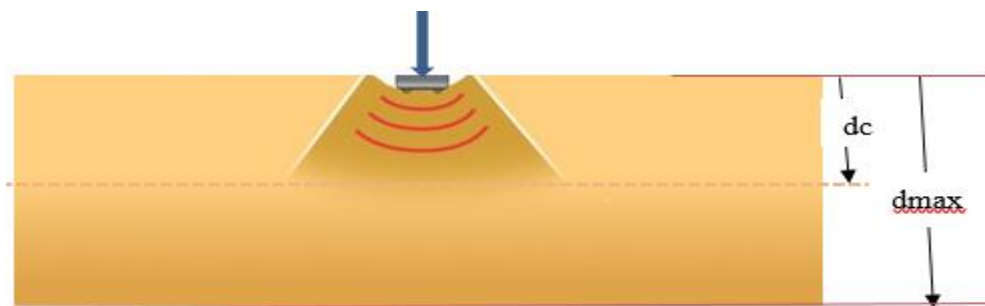


Figure 5-25: Depth of influence (d_{max}) and critical depth (d_c)

$$d_{\max} = \sqrt{WH} \dots\dots\dots 5-2$$

Where W is weight in tons, and H is the height of the free fall.

According to Mayne et al., (1984), equation 5-2 has gone through series of modification resulting to equation 5-3. Mayne et al., (1984) also opined that, a glance through the literature confirmed that about half of the depth of influence effectively feels the intensity of the impact, beyond which it diminishes with depth until reaching d_{\max} . That effective depth is called critical depth d_c , and is shown in Figure 5-25.

$$d_{\max} = \frac{1}{2}\sqrt{(WH/n)} \dots\dots\dots 5-3$$

Where n is the unit factor which is tones per unit length

The two depths, d_{\max} and d_c are related by equation 5-4

$$d_c = \frac{1}{2} d_{\max} \dots\dots\dots 5-4$$

In this study, a hammer of 4.5kg weight, falling from a height of 460mm on a square wooden plate of 300mm length, placed on the surface of a soil layer. To calculate the maximum depth (d_{\max}) that will feel the impact of the compaction, equation 5-3 applies.

Therefore, since $W=4.5\text{Kg}$ (0.0045tons), $H=460\text{mm}$ (0.46m) and 0.3m square length is considered, then $n = 0.015\text{ton/m}$ and $d_{\max} = 0.186\text{m} = 186\text{mm}$

From the above calculation, it can be concluded that the depth of influence using 4.5kg hammer falling from 460mm is 186mm and a layer of this thickness can be compacted with that hammer. However, only about half of this layer thickness (i.e 93mm) will be effectively compacted as the further depth i.e beyond critical depth d_c , the impact diminishes with depth. For his reason, it was decided that the

soil be compacted in layers of 100mm thickness. 8mm deeper than the critical depth but less than the depth of influence. In a successive layers of a slope as shown in Figure 5-26, this trade-off is aimed to avoid over compaction of the underlying layer or under compacting the bottom of the current layer.

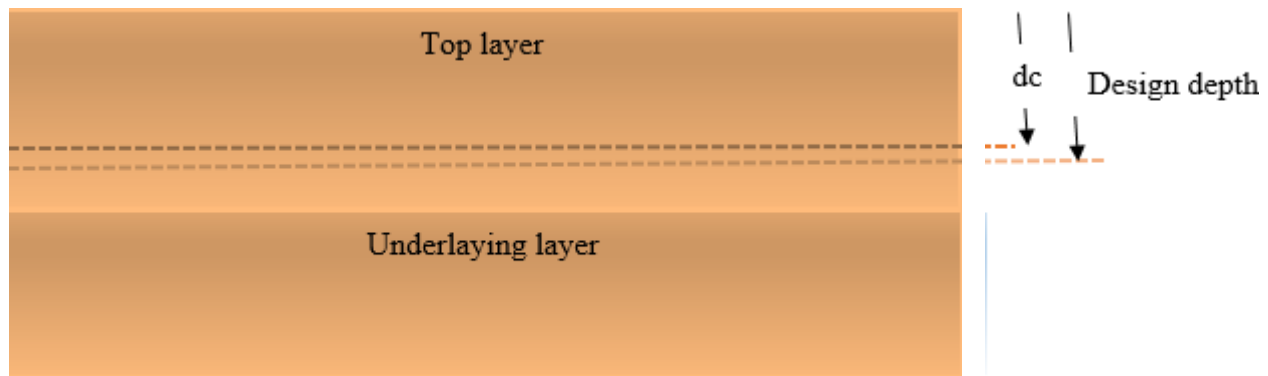


Figure 5-26: Critical and design depths

5.6.1.2 Compaction

On the surface of each layer, a purpose-made wooden plate of 300x300x25mm was placed and 4.5kg hammer was used to compact the soil by applying 3 blows on the surface of the plate. On each layer of 100mm, the hammer falling freely from a height of 460mm delivered 2416J/m^3 per blow yielded a dry density of 1.6Mg/m^3 .

During compaction, the wooden board was moved around the soil compaction surface with the unit areas covered by compaction plate (known as influence zones), overlapping one another as shown in Figure 5-27. This was done in consideration of the fact that the impact of the blow attenuates (Mayne et al., 1984), thereby making the perimeter of the influence area feeling less impact than the inner zones closer to the point of impact as illustrated in Figure 5-28. The overlapping enables the less compacted peripheral areas (marked 2) to achieve compaction near equal to the inner zone (marked 1) as can be seen in Figure 5.29

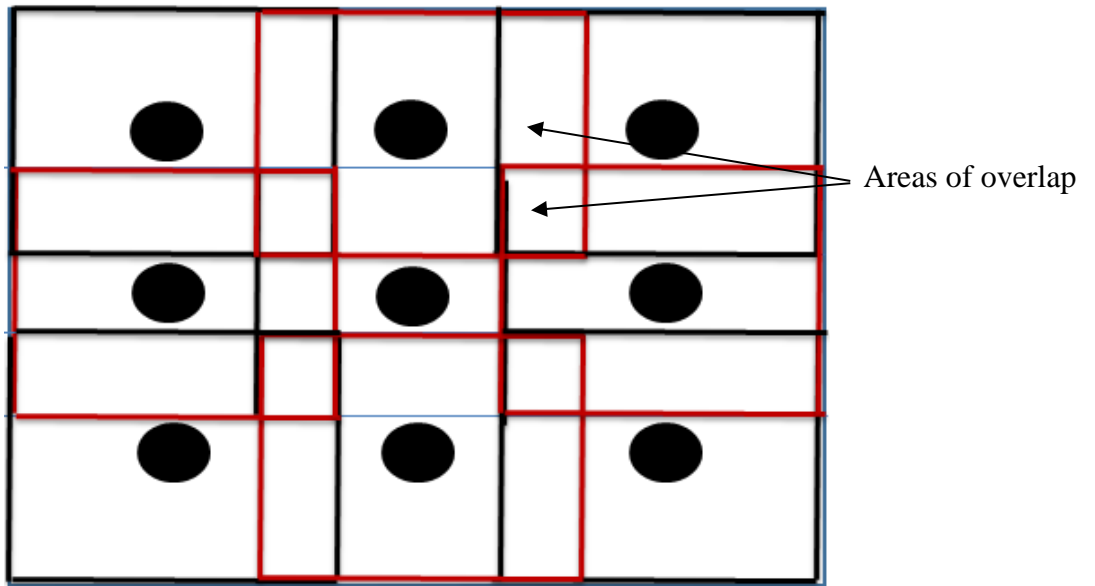


Figure 5-27: Compaction influence zones overlapping one another

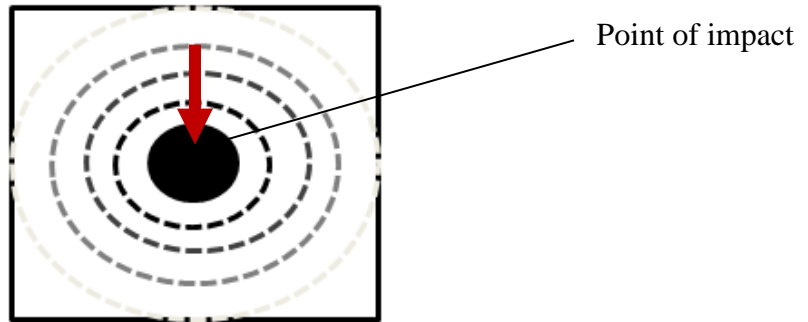


Figure 5-28: Compaction impact diminishing with distance from the point of impact

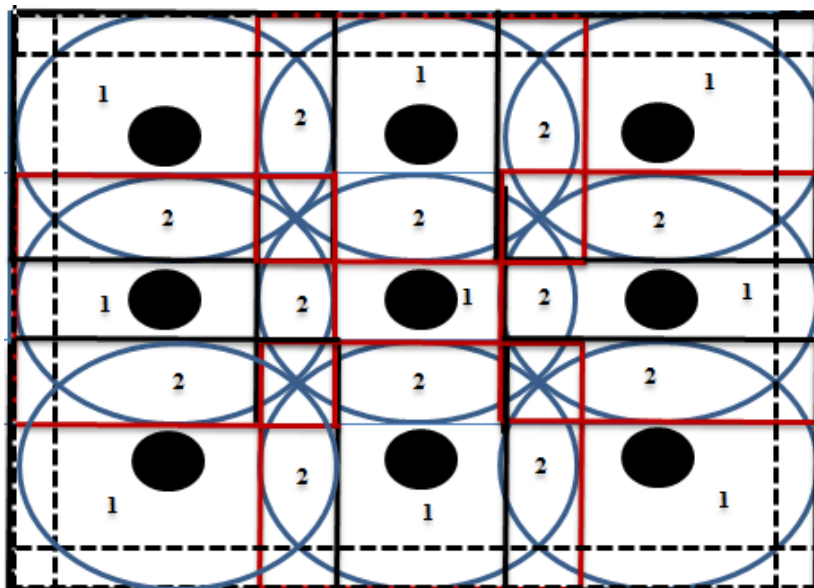


Figure 5-29: The overlap of compaction energy waves and a less compacted peripheral flange

However, there is still a peripheral flange formed along the perimeter of the surface that is less compacted than the interior zones (Maynard) as indicated by dotted lines in Figure 5.29. To prevent the potential problem that might be caused by peripheral flange during the subsequent experiment, the area at the perimeter was further compacted manually, until it was seen to have reached the compaction level of the remaining interior zone.

5.6.1.3 Control of compaction uniformity

In spite of the design and the necessary measures put in place to ensure uniformity during compaction as described above, quality control was still considered necessary to ensure the compacted layers meet the specification of the design (Menard and Broise, 1975, Mayne et al., 1984).

Part of the soil prepared for the experiment was used to conduct a trial test prior to experimental slope construction. The same compaction procedure used in the trial experiment was used in the main test. The procedure involved compacting soil and coring sample at different parts of the slope to determine the moisture and density. Figure 5.30 shows the stages involved in the homogeneity test.



Figure 5-30: Stages involved in homogeneity test

As stated earlier, the soil was laid and compacted in layers, each of 100mm thickness. Upon completion the soil slope was trimmed to form the desired geometry as in Figure 5-31. MPS6 pressure sensors

were buried as shown Figure 5.5-32 while 5TE sensors were installed immediately after completing the compaction as shown in Figure 5.33(a). The box was then covered with polyethene sheets to reduce moisture loss from the soil due to evaporation as shown on Figure 5.33(b). The model slope was allowed for 24 hours to achieve moisture equilibrium.

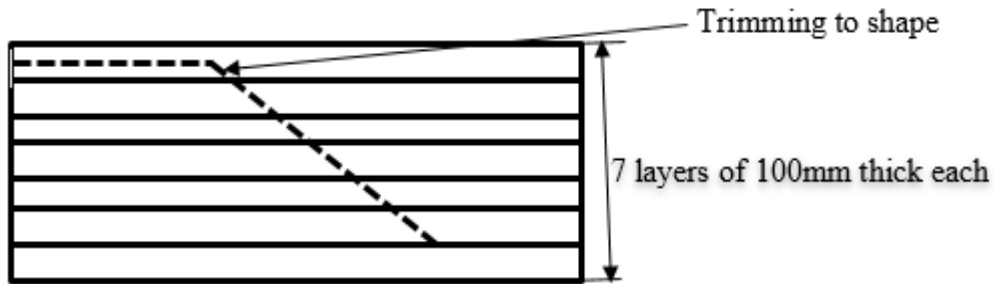


Figure 5-31: Slope construction procedure



Figure 5-32: Burying MPS-6 sensors during slope construction

Before building the slope, the experimental tank was adequately braced with two lengths of 45mm x 45mm x 5mm mild steel angle sections crossed against the two parallel sides of the tank walls and connected to the two high tensile steel rods of 21mm diameter crossed at the other two sides of the tank, as shown in Figure 5.33(b). Gravel and sharp sand were used to serve as filter material in the

supply and drainage chambers as shown in Figure 5.34. The materials also protect the non-woven fabric of polypropylene geotextile material placed between the chambers and main soil body. The use of the filter materials and the geotextile wall is to prevent internal erosion and scouring during the increase in water level(Tohari et al., 2007).



Figure 5-33: Completed slope (a) Installed 5TE sensors (b) Covered with Polythene sheet to minimise moisture loss

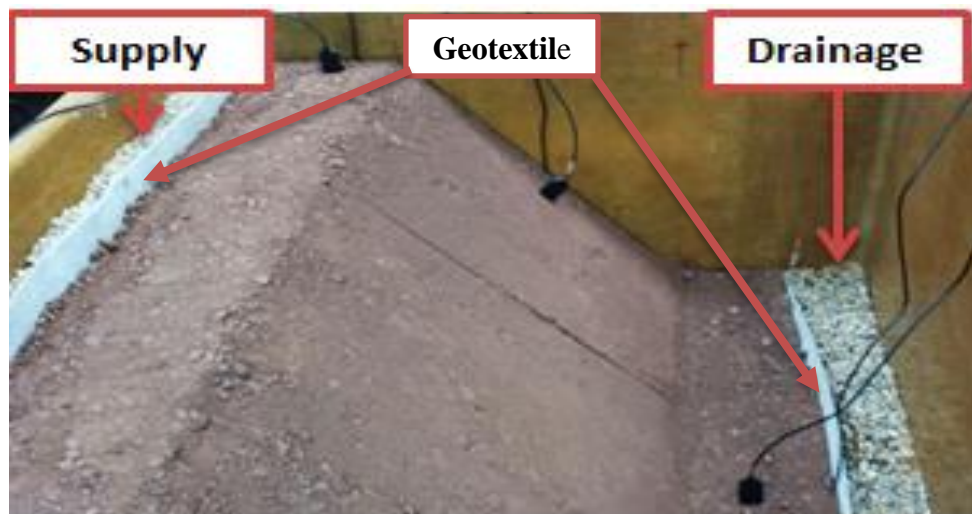


Figure 5-34: Picture showing supply and drainage chambers

Experimental set-up and other details with dimensions are shown in Figure 5.35 and 5.36, respectively. The test started by supplying water into the slope model through the supply chamber at the side of the upper end of the slope. The geotechnical changes and geophysical processes due to the water flow were monitored using sensors, while the physical response was observed using cameras mounted at the adjacent sides as shown in Figure 5.35

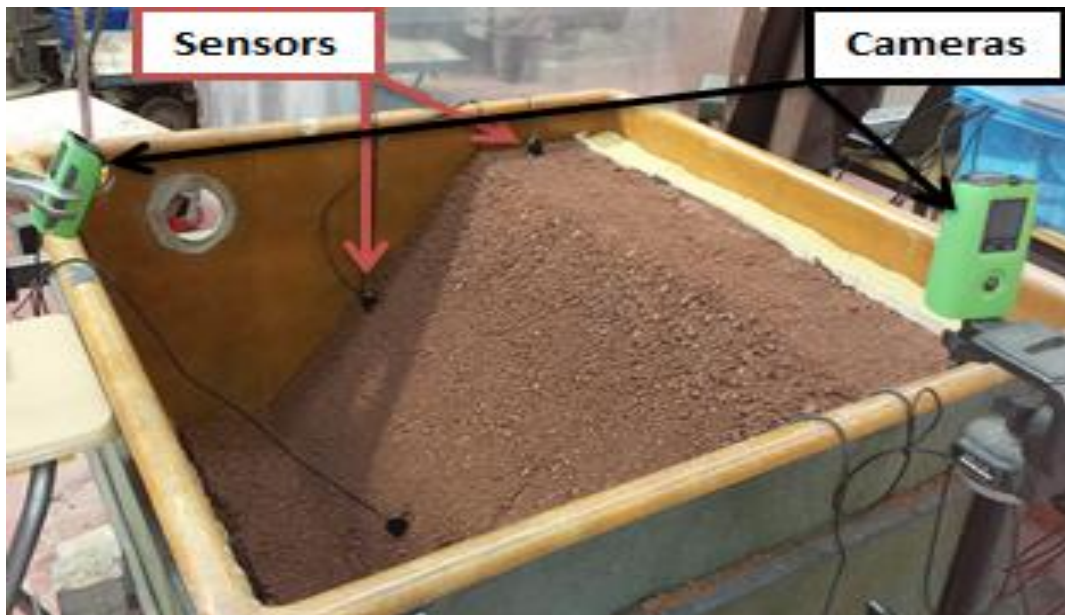


Figure 5-35: Experimental set-up

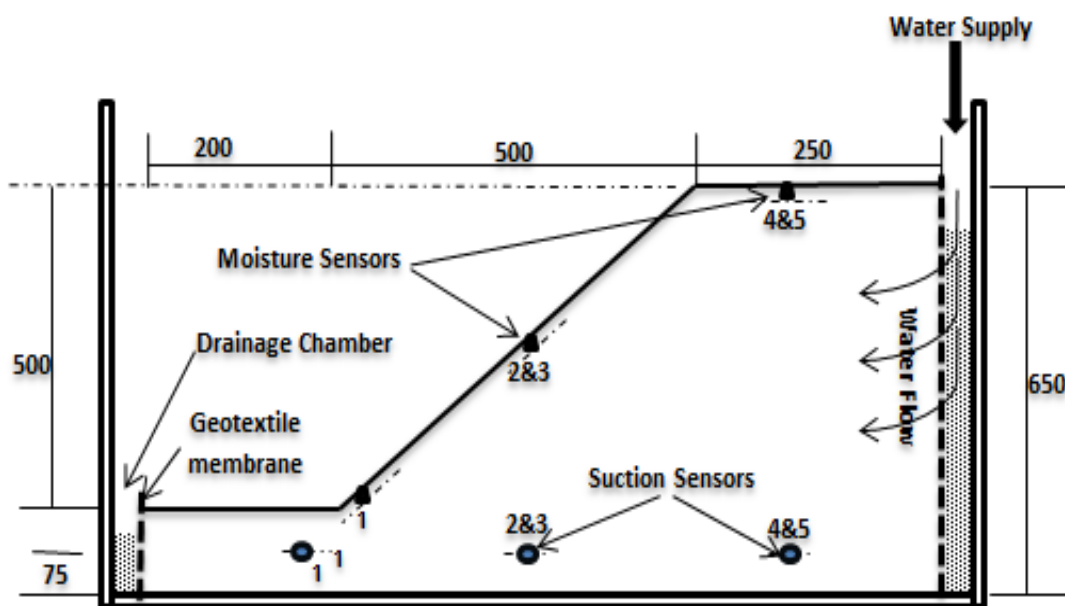


Figure 5-36: Large slope dimension and instrumentation

5.6.1 Results of the Large Experiment

Before presenting the results, it is useful to understand the positions of the various sensor ports (5TE and MPS6) used to take measurements. The plan view in Figure 5.37 provides these details.

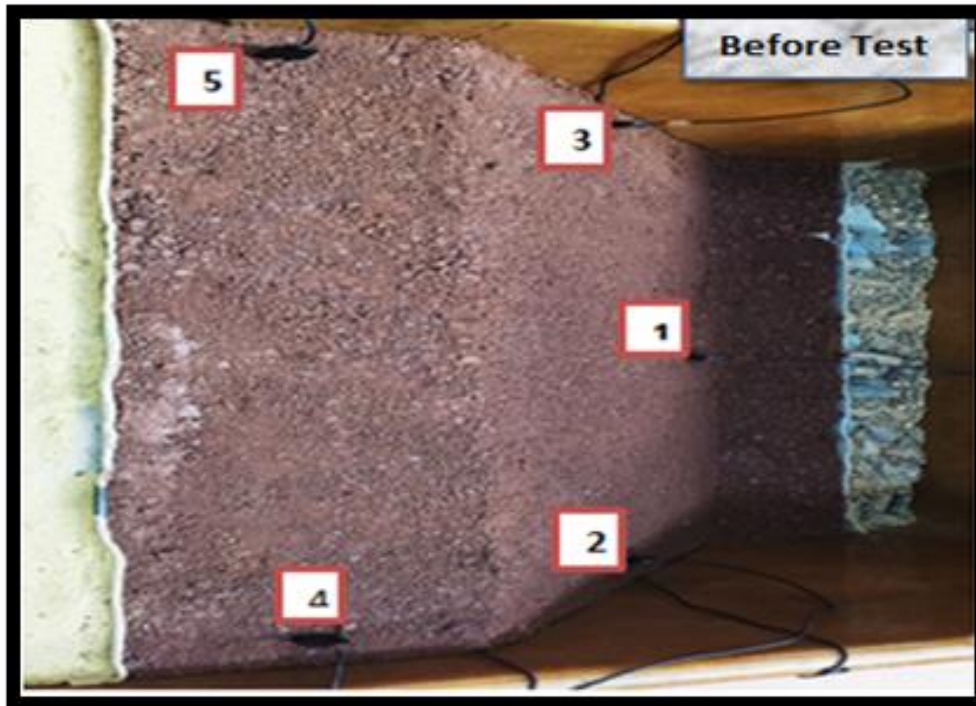


Figure 5-37: Plan view and sensor locations

Figure 5.38 shows the changes in matric suction and volumetric water contents measured with ports 1-5 each of 5TE and MPS6 respectively. The results are presented in three parts namely, pre-failure condition, failure development process and post-failure results.

5.6.1.1 Pre-failure condition

With reference to Figure 5-38, the section between A and D represents the period when water was not supplied and the measurement made during this period captured the pre-failure condition. Volumetric water content (VWC) graph shows initial irregular readings before reaching constant values as shown by sections AB and BC of the graph respectively. On the MS graph, this initial period was characterized by the decrease in matric suction before recording fairly constant values. This is shown on sections AB' and B'C of the graph, respectively. Section CD shows some changes on both VWC and MS graphs. These began around 1.45pm on 16/08/2016, the time when polyethene cover was removed to prepare the sample for testing. The section indicates by a rough or nearly zig-zag section on VWC

graph, and continuous increase of values on MS graph. Ports 1 and 5 of the matric suction graph show some anomaly. Port 5 shows a continuous increase in suction, while Port 1 shows a similar trend but has a short relatively flat section. The anomaly could be due to sensors malfunction.

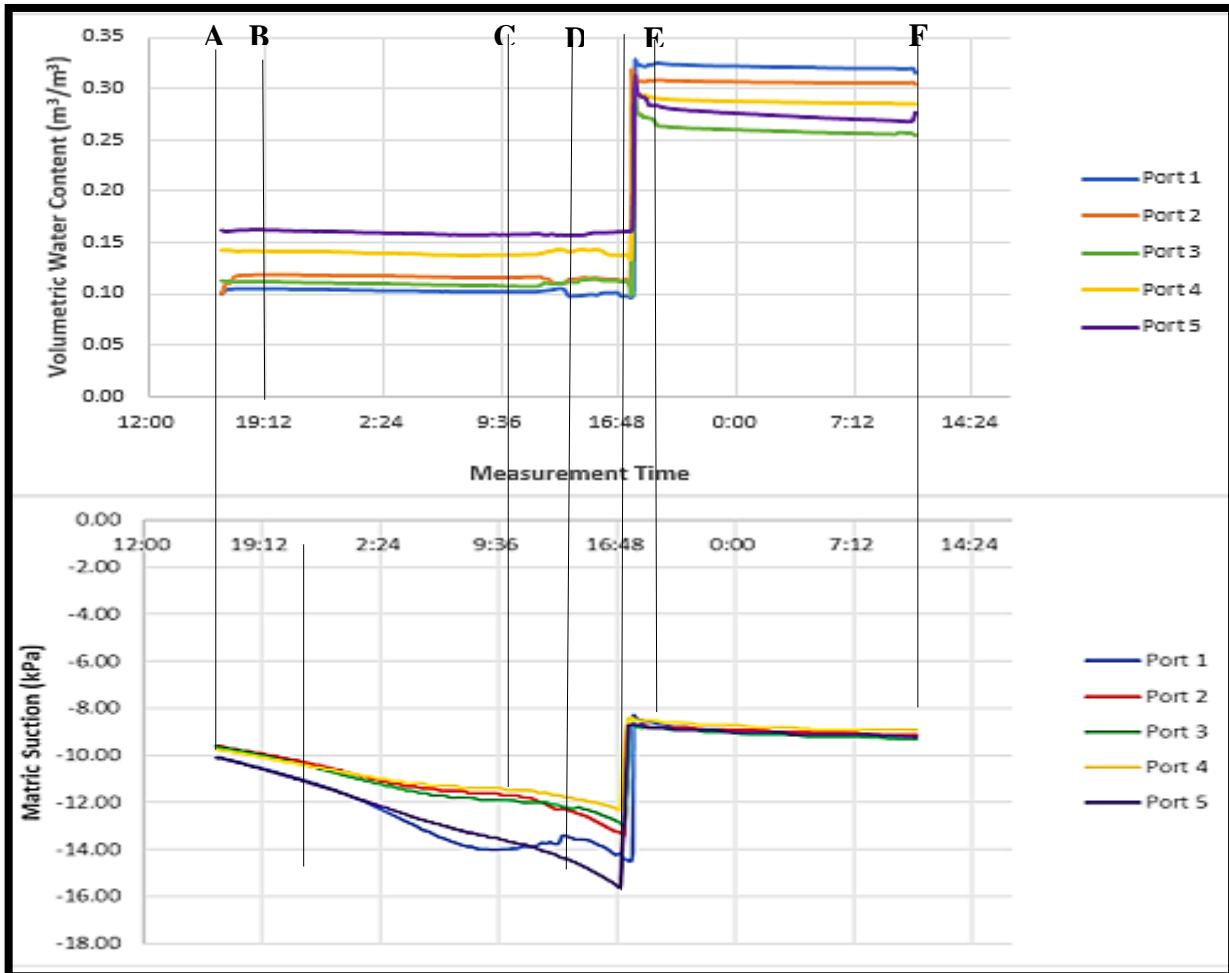


Figure 5-38: VWC and MS sensor measurements

Before the water supply, the initial volumetric water content values of 0.11cm³/cm³, 0.11 cm³/cm³, 0.10 cm³/cm³, 0.14 cm³/cm³, and 0.15 cm³/cm³ was respectively recorded at point 1,2,3,4 and 5 by 5TE sensor ports. Similarly, initial values of soil suction before the test as recorded by MPS6 ports were 14.1, 13.2, 12.7, 12.2 and 15.4kpa for ports 1,2,3,4 and 5 respectively.

5.6.1.2 Failure development process

Failure development process began after the water has been supplied into the slope. This commenced by 3.41pm on 16/08/16. Geophysical processes captured by the sensors are shown on section DEFG of Figure 5.38. To get a clear picture of what happened at this stage, the section has been carved out and enlarged as Figure 5.39.

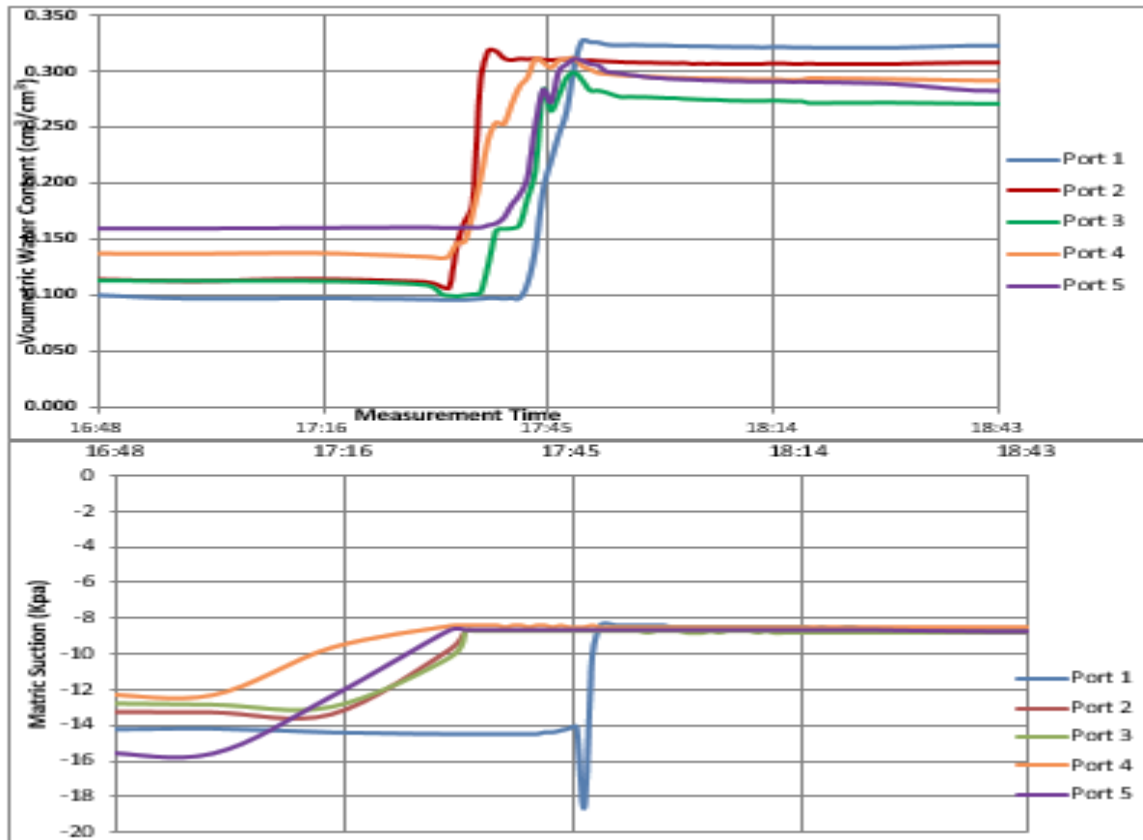


Figure 5-39: Sensor measurements during water supply

A gradual change was first recorded by the sensors until around 5.00pm when a rapid decrease of sensors was observed, followed by a rapid increase in water content. By 5.39, all the VWC and MS sensors have respectively responded rapidly except at port 1. The trend shows that for both VWC and MS sensors located at the crest, near the supply chamber (ports 4 and 5) are the first to respond to changes, followed by those located at the sloping section (ports 2 and 3) before port 1 located at the toe. The first rapid change in MS and VWC was experienced at port 1 (the toe) by 5.44pm.

All VWC sensors except port 1, recorded their maximum value of $0.310\text{cm}^3/\text{cm}^3$ around 5.50pm before dropping down, following the suspension of water supply, with only a minute interval between the first and second sets of readings. Port 1 recorded its maximum value of $0.328\text{cm}^3/\text{cm}^3$ at 6.06pm. The matric suction readings took a similar trend, but the readings were decreasing as opposed to the increase in moisture content. The rapid changes continued until it reached the peak after which there was a slow and gradual change after the initial drop down from the peak values as shown in Figure 5-39.

While these hydrogeological processes were taking place, within the soil, the physical responses were being observed. The observed physical processes can be reported with reference to the sketch of Figure 5-40. The observed responses to the flow of water were in two ways. First, there was a minor settlement shown by the difference in level (D), drawn against the wall of the experimental tank in Figure 5-33. A similar difference (D') in the height of the geotextile wall has also been observed. This was observed to have occurred around 4.15pm. The second response of the slope was in form of a minor failure sign (F) near the middle of the slope. It happened 5 minutes after the earlier sign. The two responses are captured in the photograph of Figure 5-41A.

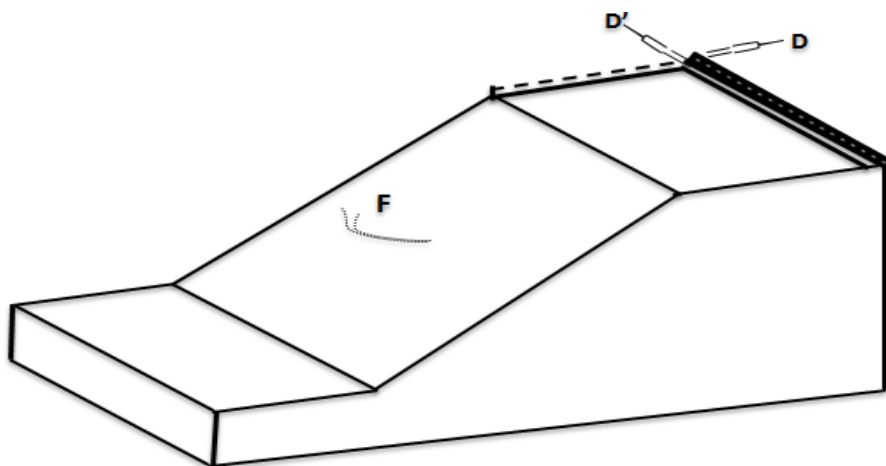


Figure 5-40: The physical response to the flow of water

Figure 5.41B and 5.41C show the progression of the earlier observed responses. Figure 5.41D and 5.41E show that earlier observed D and D' have increased beyond normal settlement. Similarly, the

failure sign F has progressed and formed more or less a transverse crack across the width of the slope surface. Water was first observed to appear at the surface of the toe below Port 2 at 4.31pm. Water continued to surface, and it was all over the slope face by 4.48pm and the water supply was stopped at this point. The above-observed failure continued to progress gradually and steadily. Forward movement was observed to occur partially and later changed to total slope movement at 5.36pm.

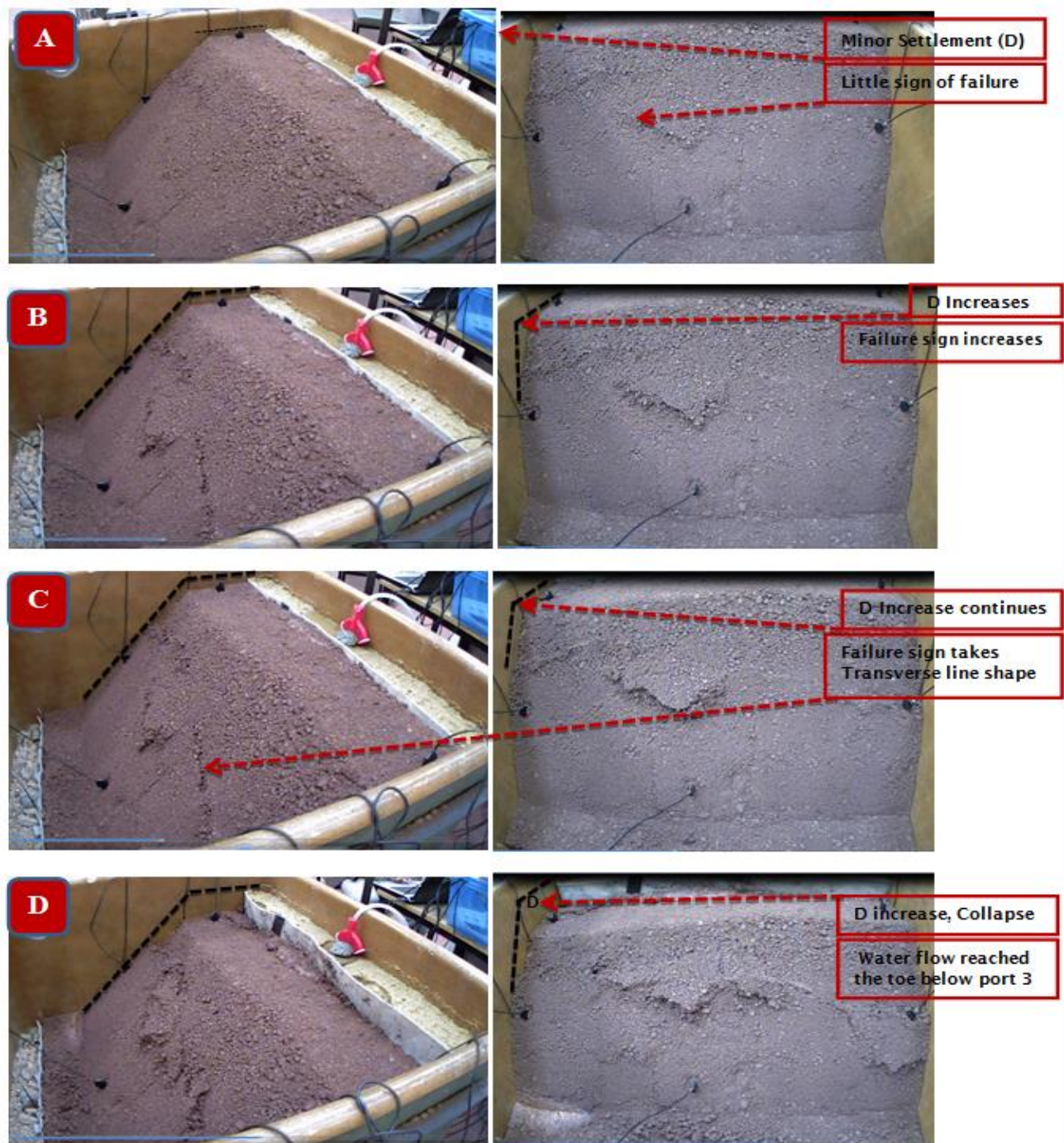


Figure 5-41: Photographs showing physical response of slope

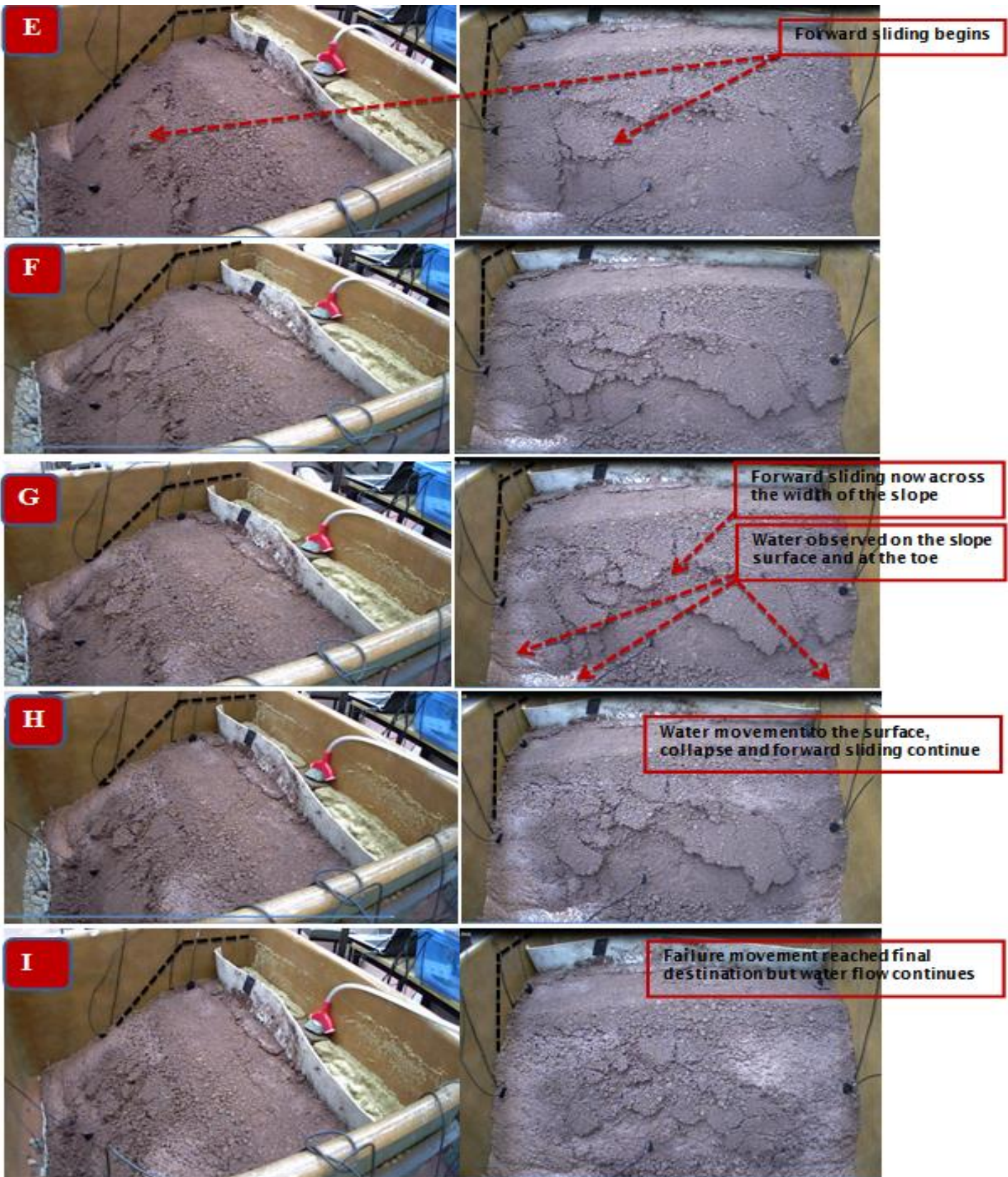


Figure-5.41 (Continued): Photographs showing physical response of slope to the flow of water

5.6.1.3 Post-Failure Condition

After suspending the water supply, port 1 increased to 0.328 while the rest dropped to 0.30 and less. During this time, the gradual movement of slope still continued and the final destination was reached around 5.49pm. The failure was in form of collapse and forward motion as shown on Figure 15. This was observed with a camera and visually by observing how the slope deviates from its original shape drawn against the walls of the tank and is shown in Figure 5-41(F to I).

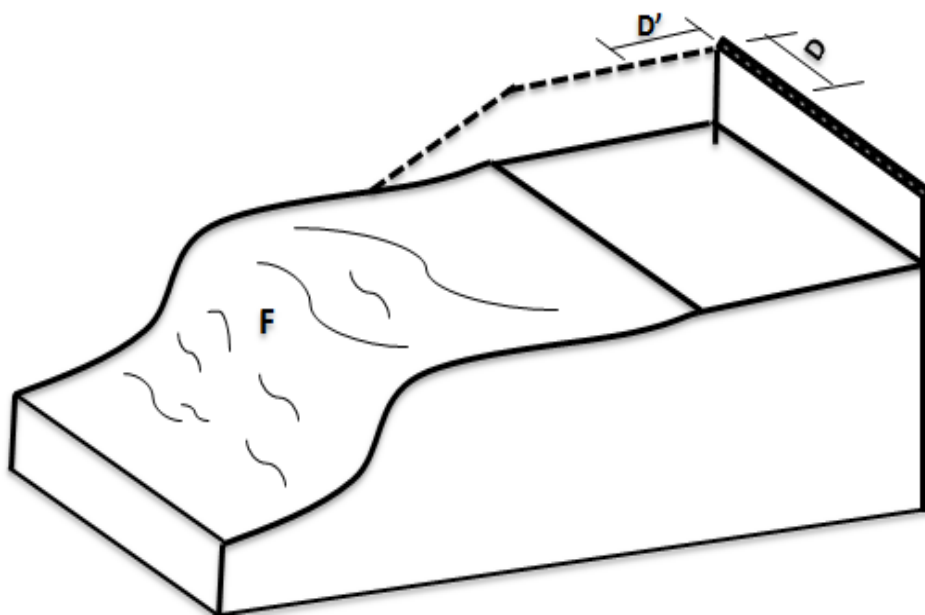


Figure 5-42: Post failure shape

At the end of the movement, the observations made as shown in Figure 5-42 were as follows.

1. The earlier observed failure sign progressed to multiple cracks across the surface of the slope
2. The D has increased excessively, indicating collapse settlement
3. The water flows out of all over the slope surface to the drainage chamber
4. There was a forward sliding movement towards the toe.

5.7 Summary and key outcomes

In this chapter, the steps followed to develop a physical model has been presented. These included the feasibility tests and trial experiment on the developed experimental physical models. During the

feasibility studies, the suitability of the selected methods, material and instrumentation were assessed. The results obtained during both the initial trial test on the small physical model and the final large-scale experiment were presented. The geophysical changes that occurred before, during and after slope as recorded by the sensors are one part of the results presented. The second part is the camera captured images of the physical deformation during failure development. The results are presented in this chapter only to give the initial idea about failure mechanism of the slope. A detailed discussion can be found in chapter 7. The following are the key outcomes of the physical modelling exercise as presented in this chapter.

- i. During this test, the maximum dry density at the optimum moisture content was determined. With reference to this optimum values the moulding water content and the working density to be maintained in the subsequent experiments were decided. The decision was supported by the experience acquired during the compaction test.
- ii. For repeatability and test result comparison, the compaction parameters (moisture and density) have to be kept as uniform as possible. To achieve this, homogeneity test was conducted using both traditional geotechnical method and modern geophysical approach (using 5TE sensor). The results presented have shown that sample homogeneity is achievable.
- iii. Permeability is another important soil property that needs to be considered in assessing the suitability of a soil for the main experiment. Both standard falling head permeability test and unconventional infiltration test have confirmed that the soil is suitable for the main experiment.
- iv. The performance of electromagnetic sensors to be used in the main experiment were assessed and were found suitable for both parameters measurement and their control. This was demonstrated through homogeneity test.
- v. The suitability of electrical resistivity tomography (ERT) method in the final experiment was confirmed by assessing the electrical properties of the soil using electromagnetic sensor (5TE).

- vi. The trial test on a small-scale physical model gave an initial idea about the geophysical processes occurring in the soil body and their consequences on slope stability. Many repeatable tests were conducted with consistent results.
- vii. A large-scale experiment conducted produced a similar result with an improved understanding of hydrological changes and the corresponding slope movements. This is because its size allowed enough instrumentation to be installed and made it possible to collect more data that is necessary for detailed study.

From the above, it can be summarized that the steps followed led the successful development of a physical model, and the results obtained from the trial experiments on the physical model provided a useful information about failure mechanism of tropical residual soil slope. With that information coupled with knowledge gained from numerical modelling (see chapter 4), a final experiment on a well-designed physical model was confidently conducted (see chapter 6).

CHAPTER SIX

FINAL EXPERIMENT WITH GEOPHYSICAL METHODS

6.1 Introduction

Geophysical methods are becoming popular in slope stability monitoring and other ground studies over traditional geotechnical methods due to their many advantages (Shiotani et al. (2001), (Hardy Jr, 2005),(Evans et al., 2006b),Dixon and Spriggs (2007), Chambers et al., (2008)). One of such advantages is the ability to sample soil mass as a whole against the point sampling used by the conventional methods (Fell et al., 2000, Glendinning et al., 2009a). The most widely used geophysical methods in slope stability studies i.e. acoustic emission (AE) method, Electrical Resistivity Tomography (ERT), Ground Penetrating Radar (GPR) and seismic profiling have been discussed in chapter 2. The GPR method otherwise known as electromagnetic (EM) method has been tried and the results of this trial has been presented in chapter 5. The last trial experiment conducted in a fibre glass tank as presented in chapter 5 has been repeated and is presented in this chapter, before presenting the final experiment. In other words, this chapter presents the final stage of this research, comprising of the repeat trial experiment conducted in a large fibre glass tank described and presented in chapter 5 and a final test performed in a large transparent acrylic glass. Unlike the trial experiments presented in the previous chapter, in both experiments presented in this chapter, ERT was used in addition to EM method used previously. The aspects of the experimental methodology that have been discussed in the preceding chapters are not repeated in this chapter. More discussion of the results presented here can be found in chapter 7.

6.2 Experimental Set-up

The experimental set-up consists of the physical model constructed in a large transparent experimental tank and instrumented with measuring devices to monitor the changes during the test. The physical model was constructed in accordance with the specification of design made during numerical modelling where the optimal dimension of the physical model and the appropriate boundary conditions were obtained. The following is the brief description of each part of the experimental set-up.

6.2.1 Experimental Tank

The tank shown in Figure 6.1 was used for the final experiment. The overall dimension of the tank is 1000mm x 2000mm x 1000mm and is made-up of transparent acrylic sheets of 25-mm thickness. The entire structure is designed to be watertight to prevent leakages. The side walls of the box were made smooth enough to simulate plain strain condition. They are thick and rigid enough to avoid deflection. At the interface along the side walls, a transparent lubricant (Teflon) was applied to reduce friction to a minimum. The bottom surface was glued with sandpaper, to simulate rough and hard impermeable foundation.

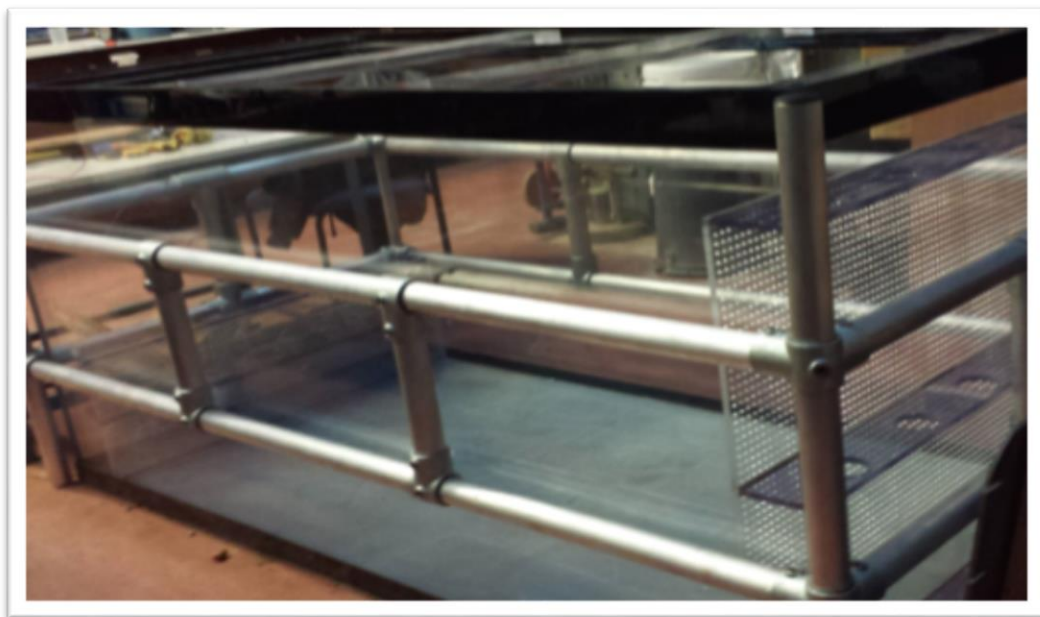


Figure 6-1: Experimental tank

Chambers were provided at the two ends of the box to allow for inlet and outlet of water, in and out of the slope. When the water supply and discharge chambers are subtracted from the lengths of the tank, the effective length is 1700mm. The box was adequately braced to avoid deflection during soil compaction and during subsequent stages of the experiment. The bracings are made up of aluminium pipes of 50mm diameter. Further details of the tank can be found in the appendix D, while the positions of the instruments will be provided in section 6.4.1 and 6.4.2.

6.2.2 Slope Construction

Before the slope construction, the shape of the slope was drawn against the side transparent walls. This served as a setting-out for the model construction and meant to guide the measurement of slope deformation during the future experiment. The completed slope is shown in Figure 6.2

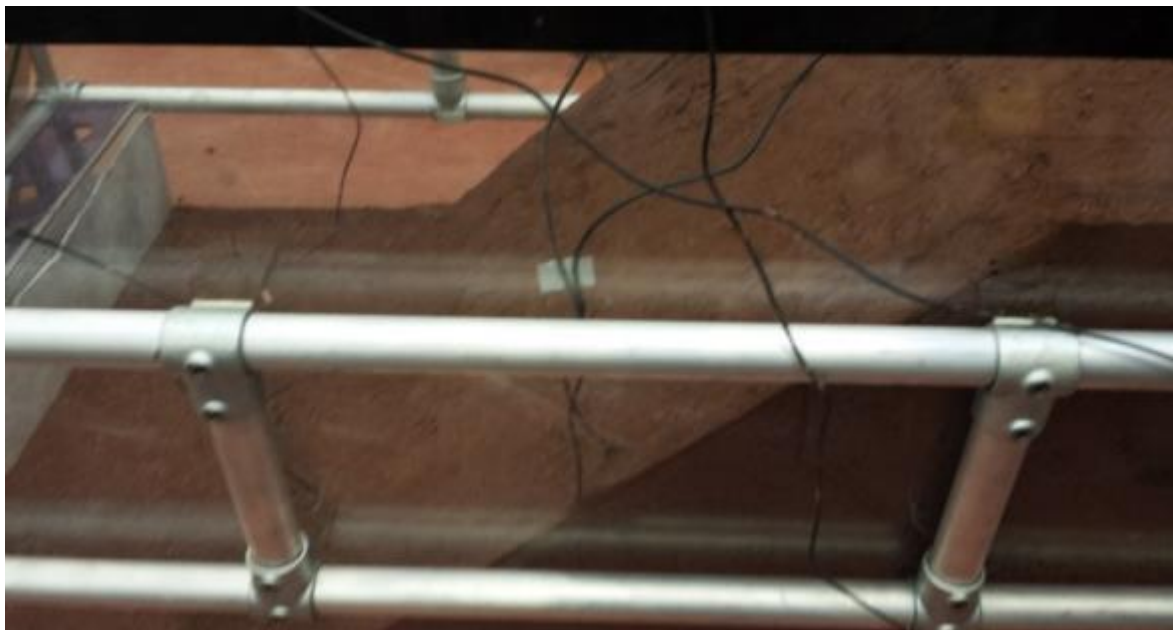


Figure 6-2: The constructed slope in a braced transparent tank

The slope model is made up of homogeneous pseudo-tropical soil. The methodology of producing the soil as well as engineering properties has been discussed in chapter 3. The basic steps of slope

construction are the same as in the previous trial test described in chapter 5. The difference is that this test was conducted in a large transparent tank. Additionally, the slope size differs slightly from the previous one. The shape and dimension of the slope are in accordance with the design as discussed in chapter 4.

6.2.3 Instrumentation

The slope was instrumented with 5TE and MPS6 sensors to monitor volumetric water content and soil suction respectively. Additionally, electrical resistivity method was used to study hydrogeological property changes during the experiment. The instruments have been calibrated prior to installation as discussed in chapter 5. The 5TE, MPS-6 and time-lapse camera used in this experiment have been described in that chapter. Therefore, only electrical resistivity apparatus will be discussed in this section.

6.2.3.1 Resistivity Apparatus

The electrical resistivity array was constructed by sourcing and coupling different components. It consists of a non-corrosive 1.5 mm diameter and 4cm long stainless-steel electrodes tied to a copper wire using double 24 ways connectors and wired up to the automatic resistivity system as shown in Fig 6.3. A stainless steel electrode was considered suitable for use because it has been found to be less affected by polarization (Herman, 2001). The resistivity data acquisition system used is called TIGRE resistivity meter and is shown in Figure 6-4.

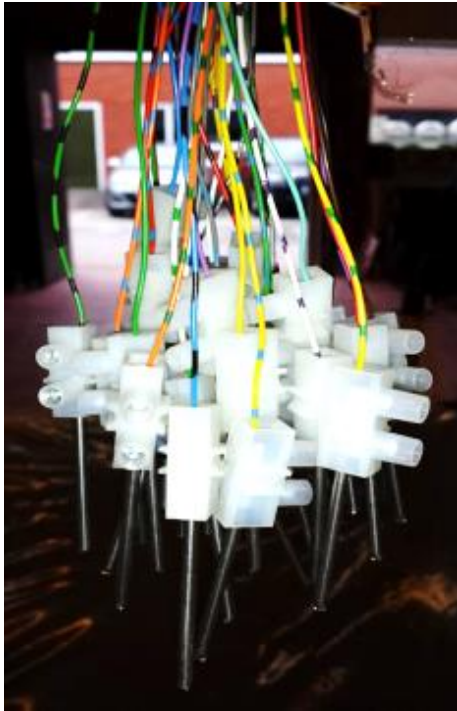


Figure 6-3: The electrodes

6.2.3.2 Resistivity data acquisition meter



Figure 6-4: Resistivity data acquisition meter (3d view). (Retrieved from <http://www.allied-associates.co.uk> on 2002/18)

It is a high-quality meter developed by Allied Associates Geophysical Ltd, to measure earth electrical resistance. The TIGRE consists of relays, which allow computer-controlled sounding and imaging. It has a maximum power output of 36 watts, manual selection of current in steps up to 200mA, a choice of sample time/signal length averaged and three frequency settings.

The TIGRE is connected to a computer system to conduct resistivity survey. By means of a control, installed on a computer, the correct electrode is automatically switched for each measurement with the help of a bank of relays enclosed in the meter. All data are logged automatically and are made available for interpretation immediately. TIGIG is Basic DOS software that was used to control the transfer of the collected data from the TIGRE.

Figure 6-5 shows the front panel of data acquisition meter, below where various units of the meter are placed. On the left-hand side of the panel, there are display and transmitter/receiver controls, while cable sockets occupy the right-hand side of the panel. The selected current is displayed on the screen of the device. Additionally, the number of cycles (repetitions), and the resistivity connection are also displayed with the current.

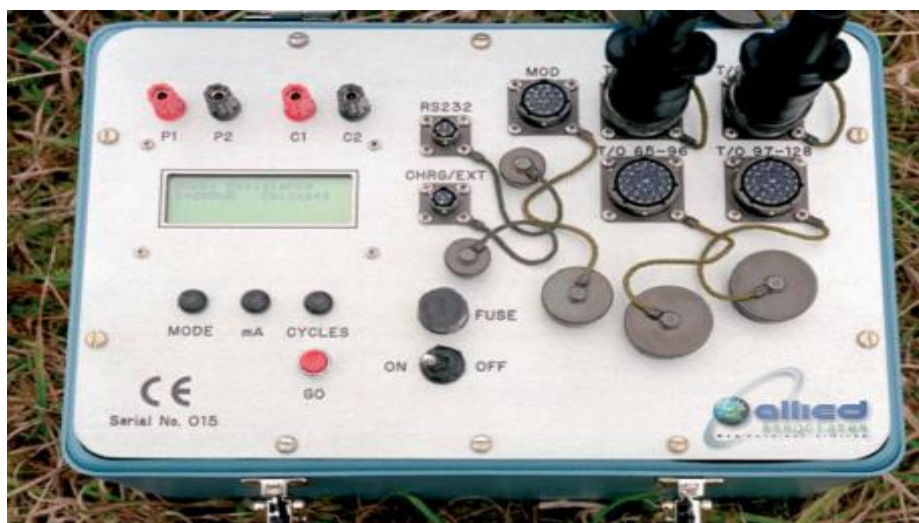


Figure 6-5: Resistivity data acquisition meter (plan view). (Retrieved from <http://www.allied-associates.co.uk> on 20/02/18)

Depending on the purpose of measurement, a basic resistivity meter or a multi-electrode system can be constructed. A multi electrode system of up to 128 electrodes is allowed by the meter, though 32 electrodes are commonly used. The whole meter is housed in a high impact and water resistant steel case with a lid as shown in Figure 6-4. More details about the TIGRE can be found in (Allied-Associates, 2006)

6.2.3.3 Complete data acquisition systems

The complete data collection system includes the sensors, data collection and storage meters, and their controlling software installed on a computer.

5TE and MPS6 were connected to decagon automatic data logger while the resistivity arrays were connected to automatic resistivity data acquisition system called TIGRE shown in Figure 6-5. The TIGRE resistivity metre and sensor data logger were connected to separate laptop computers for data collection. While the decagon sensor data logger was powered by small dry cell batteries, the Tigre resistivity was powered by two large batteries alternatively, with one used while the second was being charged. The use of two alternate batteries was to ensure the selected voltage is kept constant as allowing it to drop will affect the output of the equipment. The set-up of the two data acquisition systems is shown in Figure 6-6.



Figure 6-6: Data acquisition connected systems

6.3 Resistivity array design

Resistivity testing involves passing a current of known density through a material and record the voltage potential across a known flow path distance. The multi-electrode system is commonly used to collect large data sets required for electrical resistivity tomography (ERT) imaging. In this study, 32 number of electrodes were installed on the model at the beginning of the experiment and the sort of in-built switching system was used to activate four of the electrodes at a time automatically using a multiplexer (Herman, 2001).

Some of the factors that influence the measured potential are the type of array configuration, current used and the sensitivity of the measuring equipment. The popular types of array configurations and their characteristics (*) have been explained in 2.4.3.2.1 and are given in Table 6.1.

Table 6-1: Analysis of array configurations

CHARACTERISTICS	Wenner	Wenner– Schlumberger	Dipole– dipole	Pole– pole	Pole– dipole
Sensitivity of the array horizontal structures	++++	++	+	++	++
Sensitivity of the array vertical structures	+	++	++++	++	+
Depth of investigation	+	++	+++	++++	+++
Horizontal data coverage	+	++	+++	++++	+++
Signal Strength	++++	+++	+	++++	++

* Poor = +, Good = ++, Very good = +++, Excellent = ++++

After due consideration of many factors listed in Table 6-1, a Wenner configuration was considered suitable for use in this experiment due to its high sensitivity to horizontal structure and signal strength. Each array has thirty-two non-corrosive stainless-steel electrodes wired up and connected to the automatic data acquisition system as described previously. The spacing of the two electrodes determines the ‘effective depth’ to which the current will penetrate depending on the homogeneity of the layers. (Hack, 2000). It has been recommended by (Rücker and Günther, 2011) that the depth of penetration be at least 20% of the electrode spacing. For this reason, the electrodes spacing, and depth of penetration used are 5cm and 1cm respectively.

6.4 Experimental Programme

For control purposes, the water content, the density and initial matric suction values were recorded at the end of slope construction. The soil suction sensors (MPS-6) were installed during model construction while the volumetric water content sensors (5TE) and resistivity array were installed at the completion of slope construction. When the slope model was completed, the box was covered with polythene sheets to reduce moisture loss from the soil due to evaporation. The model slope was allowed for more than 24 hours to reach moisture equilibrium.

Before the final experiment, the trial test conducted previously in a large fibreglass box as presented in chapter 5 was repeated. But in the repeat test, the electrical resistivity method which was not used in the previous test was included. The procedure described above applies to both the trial and the final tests. In this section, the procedure for the two experiments are described and the result obtained in each experiment is reported.

6.4.1 Procedure for the Trial Experiment

After construction of slope and installation of 5TE and MPS-6 sensors, the sample was left for 21 days to allow for equilibrium to be established. During this period, the sample lost large amount of moisture. This caused a continuous drying of sample leading to the formation of minor tension cracks as shown in Figure 6.7. To avoid downward propagation of the cracks, and to make it easy to install resistivity array, a light mist was applied, and the sample was properly covered to avoid further moisture loss. Before running the test, a contact resistance of the installed resistivity array was checked but the result obtained was not good in most of the electrodes positions due to the improper contact between the slope and electrodes. To improve the contact resistance a paste of the same soil type was used to form strips along the line of array positions. The paste was prepared by adding 5% more of water and mixing manually. The arrays were then re-installed along these lines of strips as shown in Figure 6.7. The contact resistance was checked again and was found to be alright.



Figure 6-7: The installed electrical resistivity array

Two arrays were used to cover the entire length of the slope from crest through the slope to the toe. One of the two arrays was installed in the middle while the other one was installed at one side, to measure the conditions at the middle and sides respectively. The third array was installed perpendicular to the two arrays, at the middle of the sloping section, to monitor changes taking place along that section. Details of the array arrangement and the locations of other instrumentation are shown in Figure 6-8.

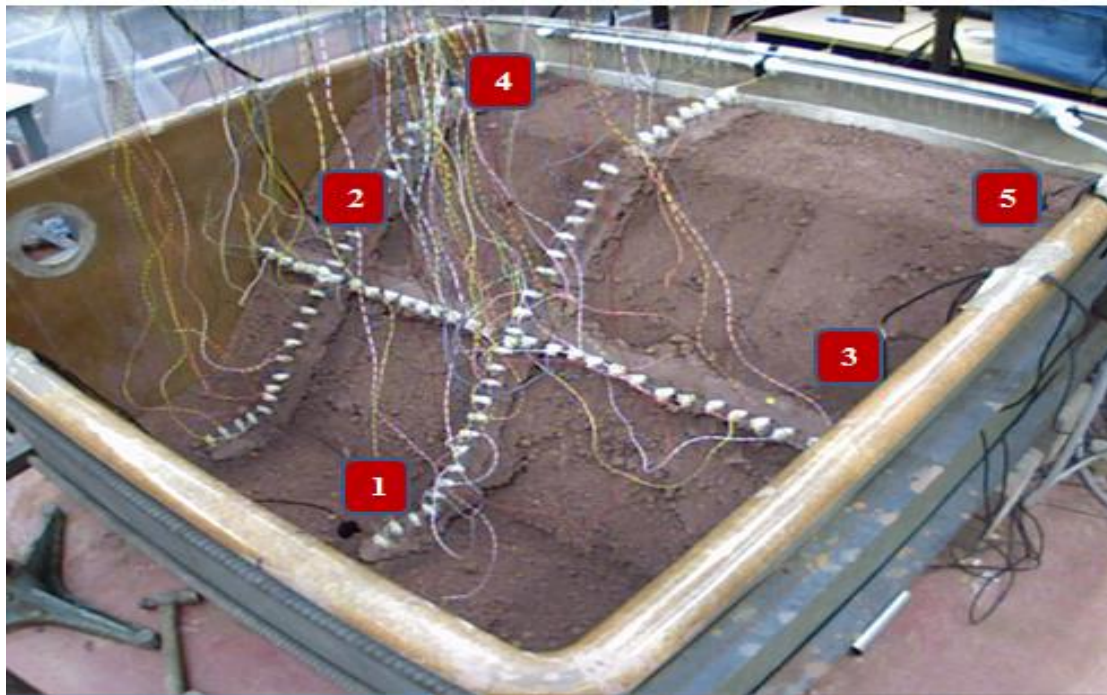


Figure 6-8: The installed electrical resistivity array (3D view)

Here, the test started by supplying water into the slope model through the supply chamber at the side of the upper end of the slope. To simulate the gradual wetting of slope with water from any natural source, the water was supplied in steps. The flow rate meter shown in Figure 6.10 was used to regulate the water flow. The geotechnical changes and geophysical processes taking place were monitored using sensors (5TE, MPS6 and ER) while the physical response was observed using the camera. The experimental set-up is shown in Figures 6-9.



Figure 6-9: Flow meter



Figure 6-10: Experimental set-up

6.4.2 Procedure for the Final Experiment

In the main experiment, a transparent experimental tank has been used. The location of the instrumentation are shown in Figure 6.11 and the detailed dimension is shown in Appendix B. The procedure for setting up the experiment is the same as the trial experiment in section 6.2.

Like the previous experiment, in this experiment, there was a considerable length of time between the construction of the slope and the commencement of the test. For this reason, a considerable amount of moisture has been lost.

During compaction, a finer particle soil was placed at the surface layer. This measure was taken to avoid having a problem with contact resistance again and to eliminate the use of soil paste strips that was thought to have inhibited slope movement. This strategy worked well as no problem was encountered during this experiment. The instrumentation in this experiment was the same as in the previous trial experiment. A light mist was applied at the surface to facilitate array installation. Details of the array arrangement and locations of other instrumentation are shown in 6-12.



Figure 6-11: The installed electrical resistivity array

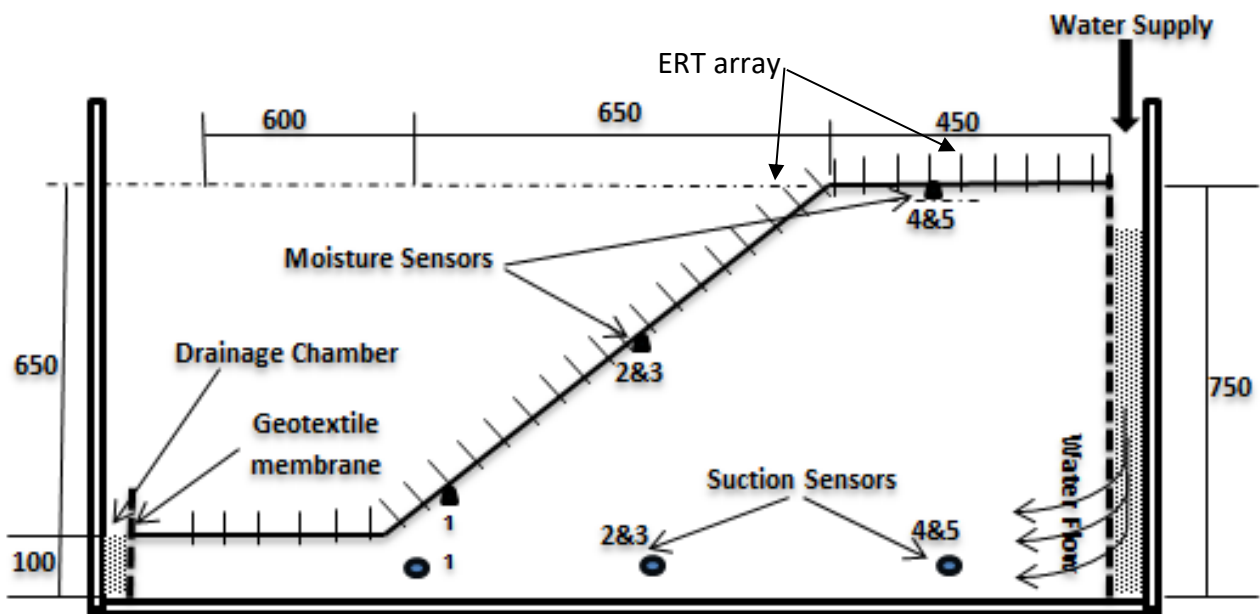


Figure 6-12: Schematic sketch of slope dimension and instrumentation

As usual, the test started by supplying water into the slope model through the supply chamber at the side of the upper end of the slope. The geotechnical changes and geophysical processes taking place were monitored using sensors (5TE, MPS6 and ER) while the physical response was observed using the camera.

6.5 Data collection

With electromagnetic sensors i.e. 5TE and MPS-6, data was collected using automatic data logging produced by Decagon Ltd. The data logger was controlled by a software installed on a laptop computer. The data collection began after the completion of slope construction and continued without break till after the experiment. For each sensor, the condition before, during and after the experiment was recorded in a single measurement.

With resistivity method, the data collection was done in a similar manner to the one with EM sensor, except that the measurements were not done continuously. There were short breaks to switch from one array to another. The resistivity data acquisition system can measure only one array at a time. After complete measurements with an array, the acquisition system is disconnected from the array and moved to another array. As mentioned earlier, three arrays were used for the resistivity survey in each of the two experiments but only the result of the final experiment is reported. The sequence of data collection with these arrays are given in table 6.2

Table 6-2: Laboratory measurements and observations

Period of Measurement	Location of measurement	Start time	Finish time	Visual Observation
Before the water flow	Side	11.34	11.56	Stable. No any sign of failure observed
	Centre	12	12.21	Stable. No any sign of failure observed
	Horizontal	12.24	12.4	Stable. No any sign of failure observed
During the water flow	Centre (1st measure.)	13.55	14.15	
	Horizontal	14.18	14.37	
	Side	14.43	15.05	Significant cracking and surface slumping in the first 500mm; Side array measurements abandoned due to slumping at side of slope
	Centre (2nd measure.)	15.06	15.28	Significant cracking and surface slumping in the first 500mm
After the water flow	Horizontal	15.3	15.42	Horizontal survey lines stopped due to slumping of slope in last 6 electrodes
	Centre	16.21	16.43	Post experiment conditions

6.6 Data processing

Data acquired at the end of the experiment includes the MPS-6 readings, 5TE readings, ERT data and photographs. The MPS-6 and 5TE reading were processed in the usual way whereas the resistivity data was inverted using Res2Div inversion software.

During the inversion, a 2D virtual model of the true resistivity was first created. Then the apparent resistivity pseudo-section was calculated, assuming a survey is conducted across the model. Lastly, the inversion was done by iteratively changing the model until it produces a calculated apparent resistivity pseudo-section that is the best fit to the actual measured apparent resistivity pseudo-section. The final inversion images were finally produced and the best representative sections were obtained. Details of the procedure of data processing and inversion can be found in Loke and Barker (1994) & Loke and Barker (1996).

6.7 Results

The results of the initial and final experiments processed data collected during the experiments are reported in this section. In the initial trial, the results consist of graphs from the sensor recorded readings and camera captured photographs while in the final experimental results, the processed resistivity data is reported in addition to the graphs and photographs.

6.7.1 Results of the trial experiment

The results shown in Figure 6-13 represents the condition before, during and after the water supply. The results of the initial condition before the water supply includes period of excessive moisture loss, followed by the period of little moisture increase before reaching a state of equilibrium. The rise of water content shown in the figure, represents the condition when the water was being supplied. These stages and more, will be explained in this section.

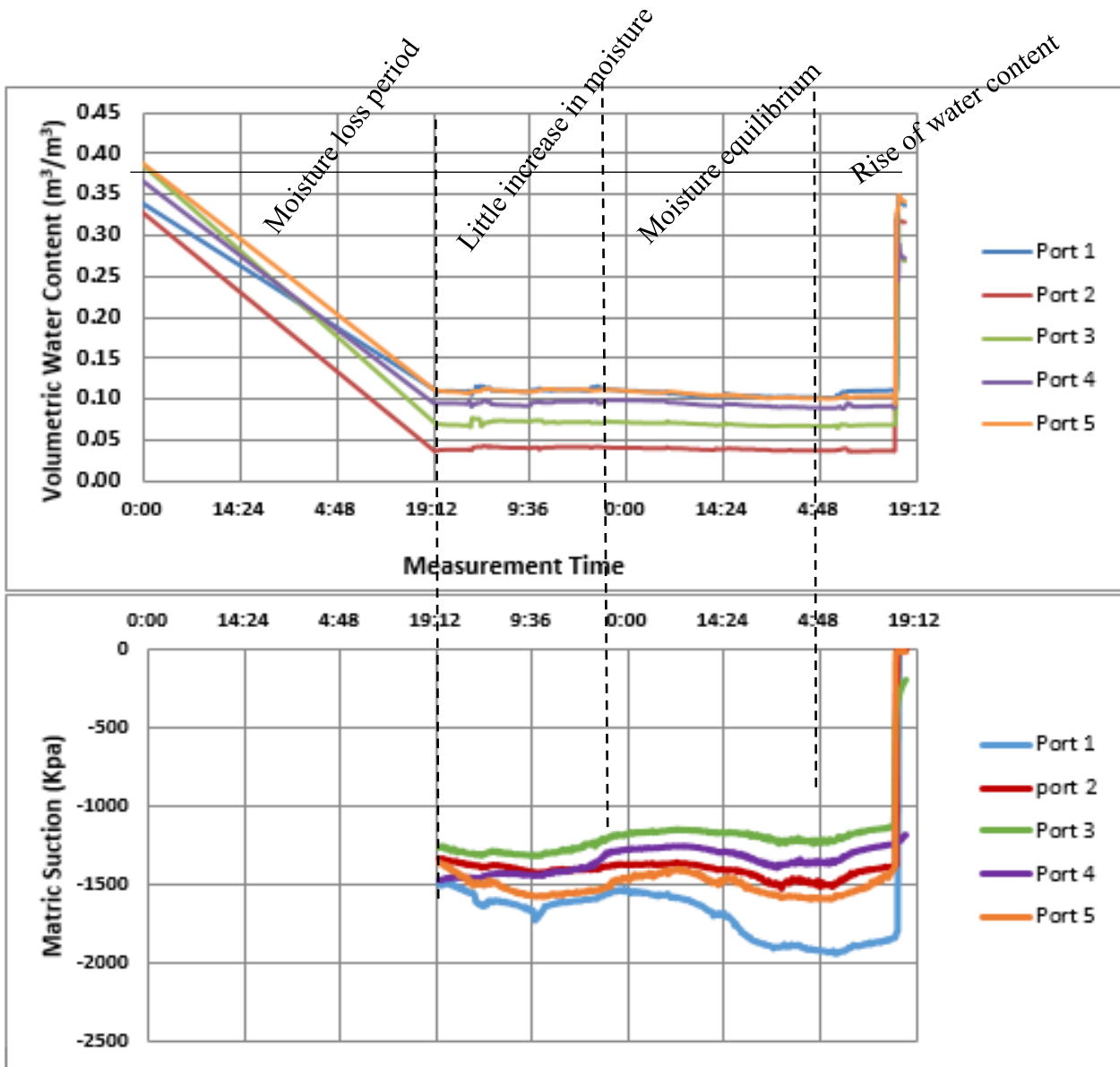


Figure 6-13: 5TE and MPS-6 measurements

6.7.1.1 Initial condition before the water supply

Figure 6-13 shows how volumetric water content dropped from a high value to about $0.06\text{m}^3/\text{m}^3$ before beginning to attain equilibrium. A high average value of about -1600Kpa has been recorded by matric suction sensors. The dropping down of the VWC to a very low value and the high value MS are indicative of the loss of moisture experienced at the initial stage. The next stage as shown on the graph, includes a simultaneous little increase in VWC and MS which was followed by a period of equilibrium shown by a relatively flat section on both graphs. The minor changes before reaching equilibrium is due to the mist applied as explained in the procedure. The observed variability among the sensors is

due to the inability to maintain moisture uniformity within the soil caused by non-uniform moisture loss. The last stage shown as rise of water content will be explained in the following section.

6.7.1.2 Condition during the water supply

The water supply into the soil caused changes to its pore-fluid properties. The increase in water content is shown by the right end of the flat section of volumetric water content graph of Figure 6-13. The reduction of matric suction was also observed within this range. For clear understanding, the section is enlarged as Figure 6-14.

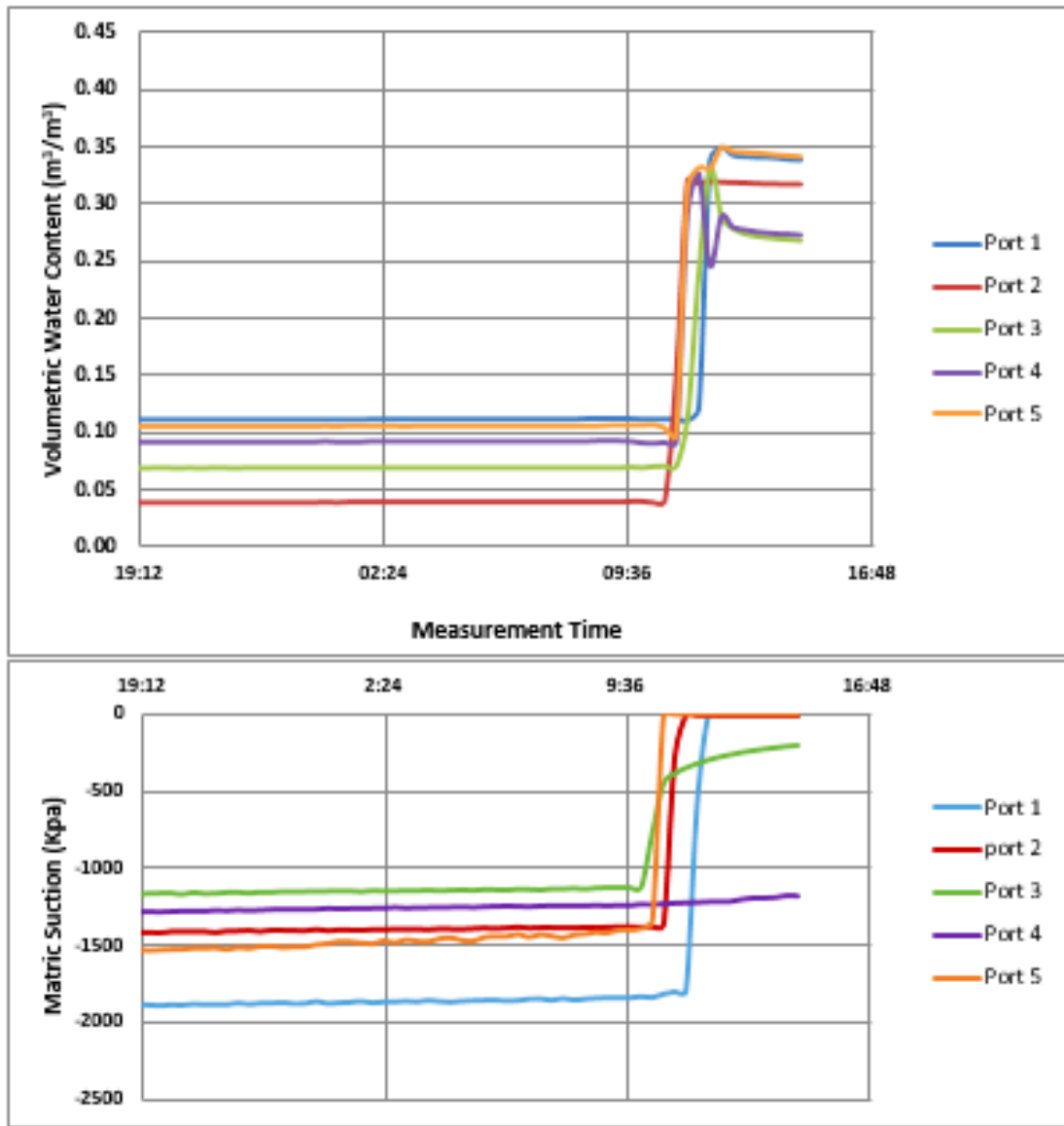


Figure 6-14: Sensor measurements during and after water supply

The increase in water supply into slope caused rapid changes in pore fluids properties at all locations and was detected by all the sensors as shown in Figure 6-14. The upper graph shows a rapid increase in water content while the lower graph shows a rapid decrease in matrix suction. In the upper graph Port 2, 4 and 5 of volumetric water content sensors were the first to increase before port 3, with port 1 being the last to record the changes. Matrix suction graph shows a similar pattern except that, the anomaly is observed with ports 3. It shows a gradual decrease in matrix suction after an initial rapid increase while port 4 showed a very slow response to the end of the experiment.

At this stage, while these hydrogeological changes were taking place within the soil, the physical response was being observed on the slope surface. This includes the initial minor settlement which later increased excessively. Similarly, some minor surface cracks were initially observed near the middle, across the width of the slope. Before the end of the experiment, multiple cracks of various sizes were formed and spread all over the slope as shown in Figure 6-15. No global movement was observed, rather, a partial movement of the soil body occurred. The water flowing in the slope was first seen on the surface at the toe around 12.00pm, while the failure was progressing. On the surface of the toe, the water appears first below port 2 before the other side of the toe.



Figure 6-15: Slope physical deformation

6.7.1.3 After the water supply

After stopping the water supply at 1.41pm, port 1 of the volumetric water content sensor, increased continuously while the sensors at the rest of the locations dropped down. Matrix suction sensors show a similar trend but anomaly was observed with ports 3 and 4. Port 3 shows a gradual increase after an initial rapid increase while port 4 shows a slow increase up to the end of the experiment.

During this time, the gradual movement of slope still continued, and the final destination was reached around 2 pm. At the end of the experiment, only collapse settlement occurs but no forward sliding was observed. This was thought to have been caused by the paste strips placed at the position of arrays, which tends to reinforce the slope and inhibit movement.

6.7.2 Results of the final experiment

The results of the final experiment presented in this section comprise of those collected by electromagnetic sensors (i.e using GPR method), electrical resistivity method, and photographic observations.

6.7.2.1 Electromagnetic sensor results

Just like the previous experiment, the results of the final experiment are presented in this section in three stages. That is, the initial and experimental condition as presented in Figure 6.16. Each is explained in the subsequent sub-sections.

6.7.2.1.1 Initial condition before the water supply

A considerable amount of moisture was lost before the water was supplied into the slope at 1.30pm. After the initial moisture loss, an average value of about $0.12\text{m}^3/\text{m}^3$ was maintained constant over a long period before the water supply. This is shown by the flat section of the upper graph in Figure

6.16. Similarly, high matric suction caused by the moisture loss, remained relatively constant over this period as shown by the relatively flat section of the lower graph in the same figure. During this period, an average value of about -750Kpa was recorded.

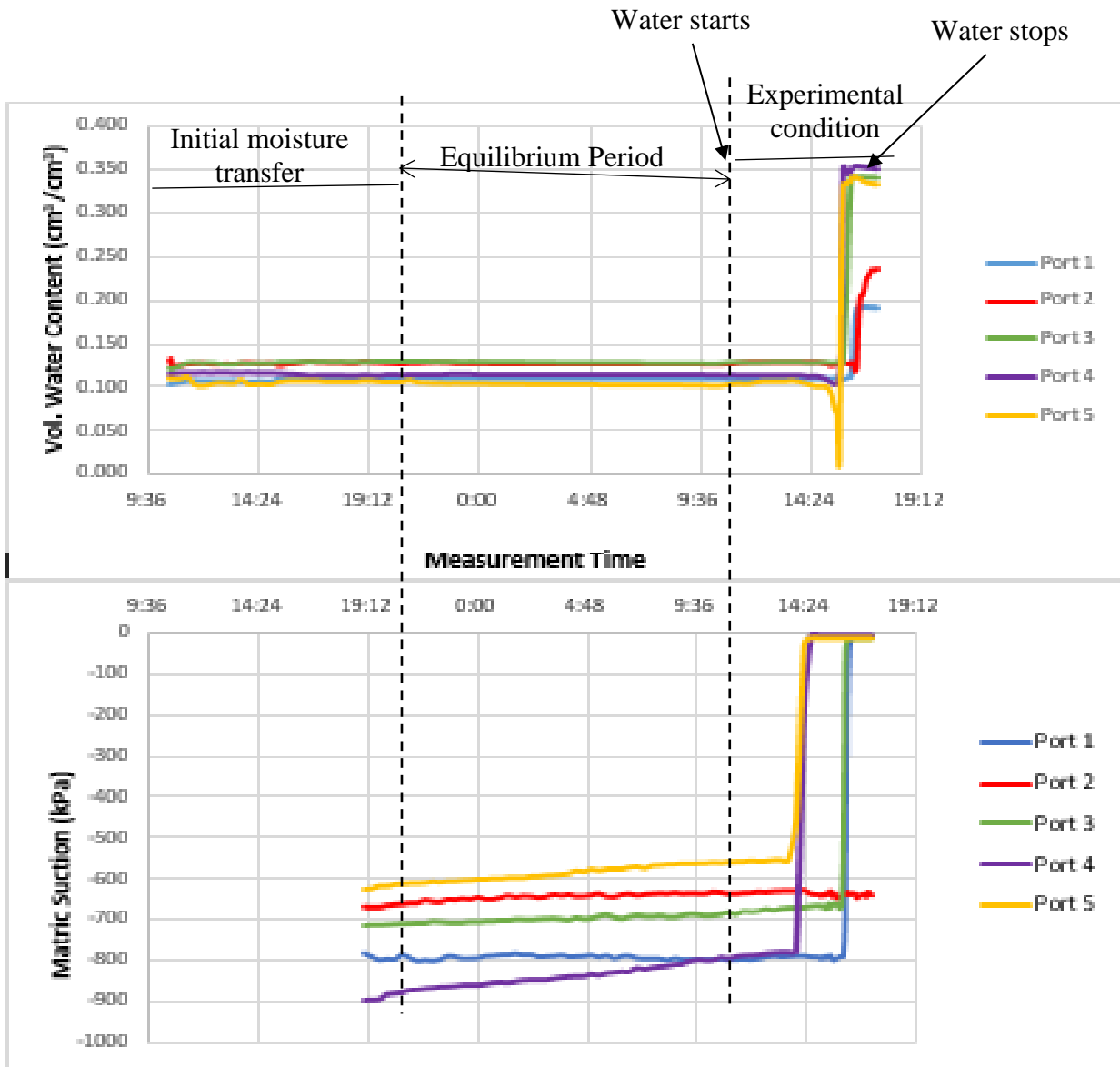


Figure 6-16: Sensor measurements

6.7.2.1.2 Experimental condition during water supply

The water supply into the soil caused a gradual and later rapid change in soil water and suction respectively. Increase in water content was recorded by volumetric water content sensors as shown by

the right end of a flat section of volumetric water content graph of Figure 6-17. The reduction of matrix suction was also observed at this point of the matrix suction graph of the same figure. To clearly understand what happened at this point and beyond, it is carved out of the Figure 6-15 and enlarged as Figure 6-17.

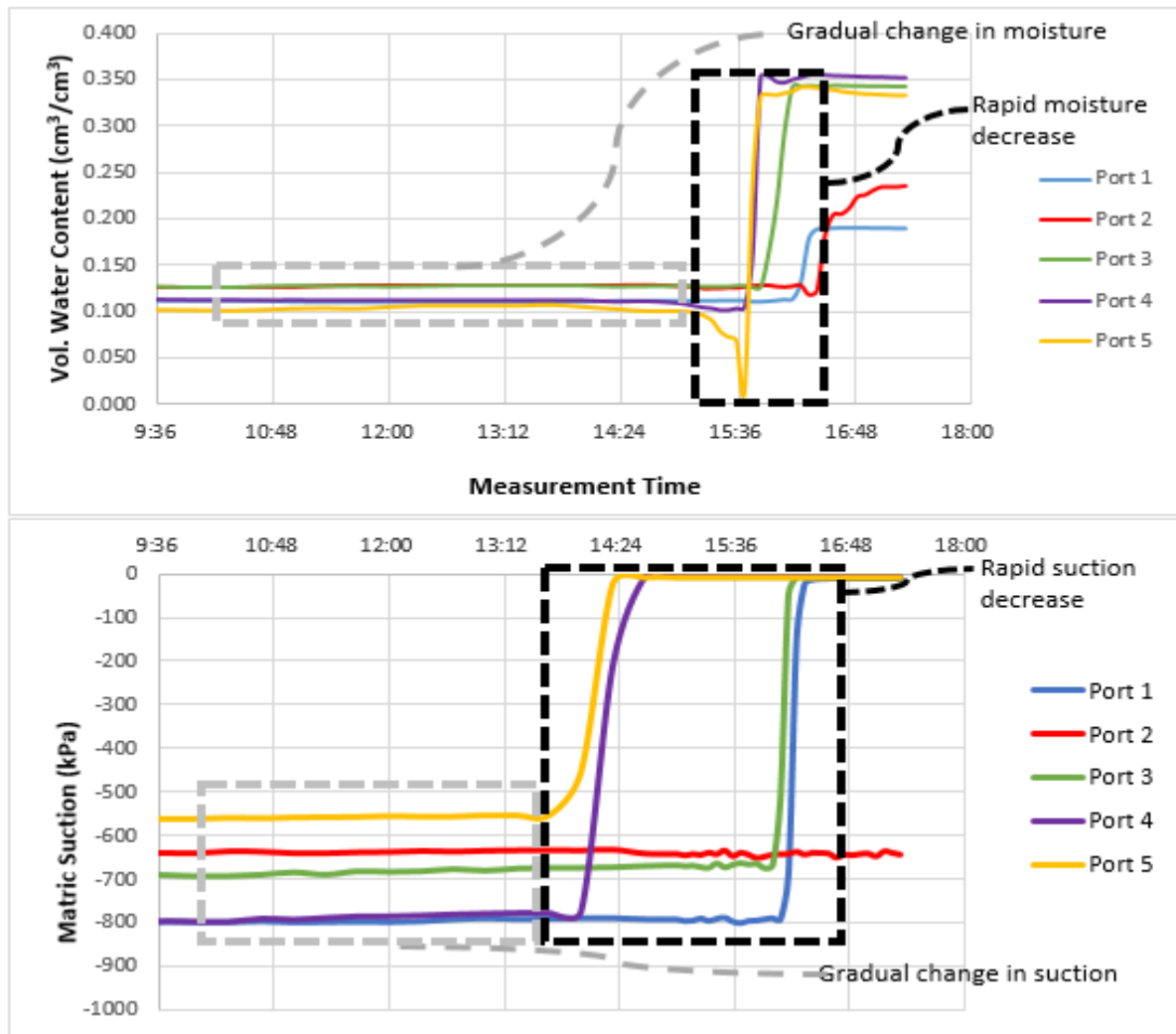


Figure 6-17: Sensor measurement during and after water supply

6.7.2.1.3 After the water supply

When the water supply was stopped, ports 3, 4 and 5 dropped down a little and maintained constant as shown in figure 6.17. Port 1 was the last to respond to the changes. Matrix suction sensors show a similar trend but anomaly was observed with ports 2. It shows little or no response to the water flow as shown in the figure.

6.7.2.2 Visual observations using camera

Just like the sensor recorded readings, the results of the final experiment are presented in this section in three stages. That is the condition before, during, and after the water supply.

6.7.2.2.1 Initial condition before the water supply

Between the time of the completion of slope construction and the commencement of the experiment with water supply, no physical change was visually observed slope. It remained stable as built.

6.7.2.2.2 Experimental condition during the water supply

The water supply at 1.30pm into the soil, a gradual rise in water level was observed around 1.55pm as shown in 6-18 – 6.19 and induced changes to pore-fluid properties of the soil body. The rise in water level can be seen when the successive photographs are compared from A to C in Figure 6.18 The observed physical responses due to these hydrogeological changes include an initial minor settlement and surface cracks as shown in Figure 6-20. Figure 6-19 shows the observed series of physical changes with time.



Figure 6-18. Rise in ground water level

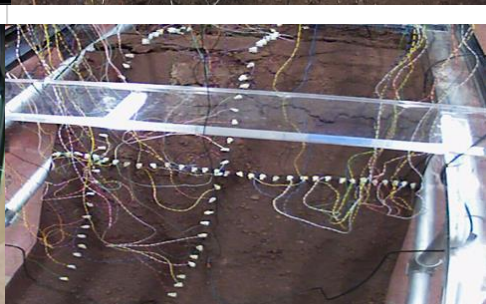
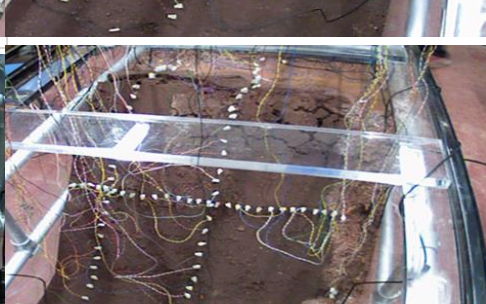
Start Time	Finish Time	Side View Observations	Plan View Observations	Descriptions
13:30	13:55			Water flow into the slope begins. The slope remains stable as no any sign of failure was observed.
13:58	14:36			Signs of instability began to manifest in form of minor settlement and minor surface cracks.
14:39	15:45			Significant cracking and excessive (collapse) settlement was observed. The first 7 electrodes of the side array, located at the crest (0 500mm) were displaced due to the slumping. Therefore, measurements with the array was
15:45	16:15			Continued as above.
15:49	16:57			The water flow at the left handside reached the surface and washed away 6 electrodes of the horizontal array. Thefore, survey with the horizontal array was stopped.

Figure 6-19: Visual observations with time

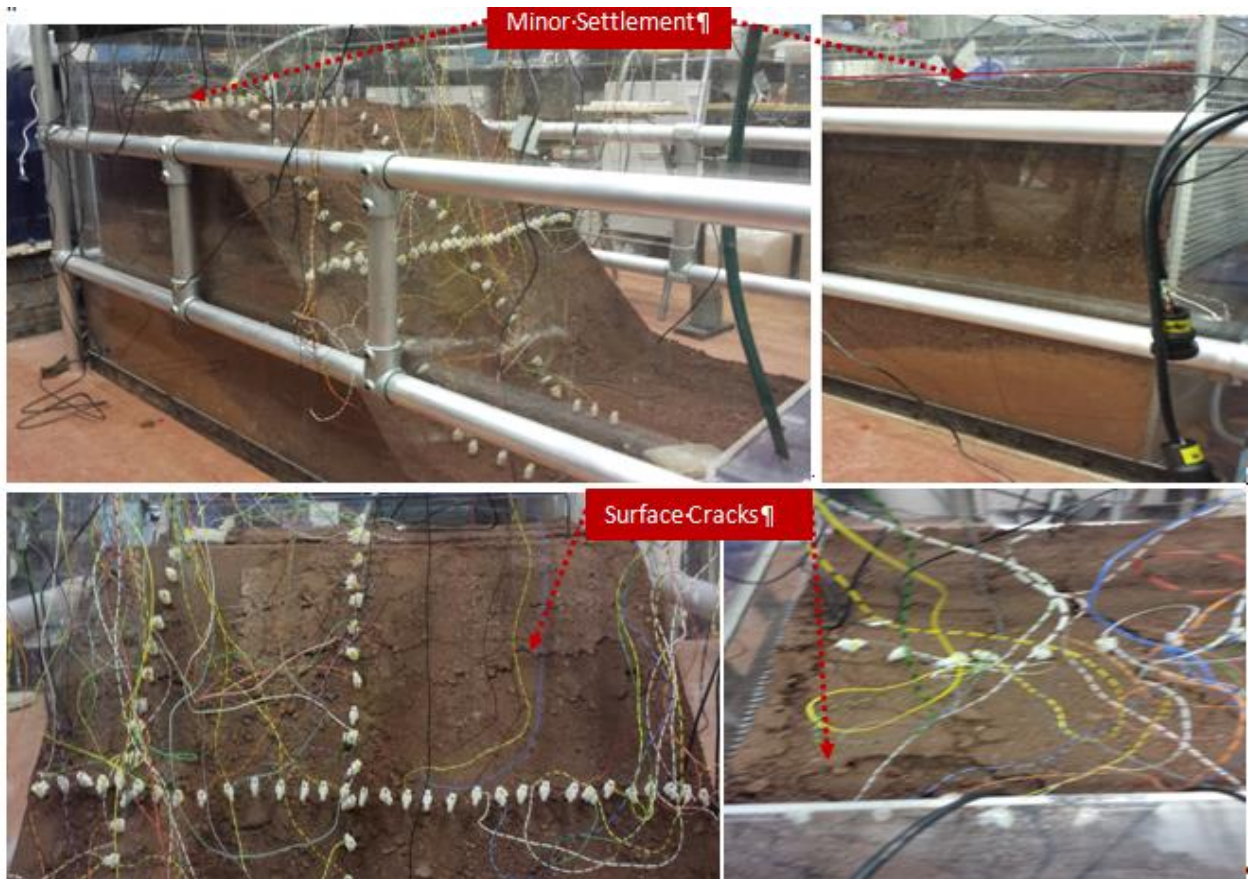


Figure 6-20: The initial physical response of the slope

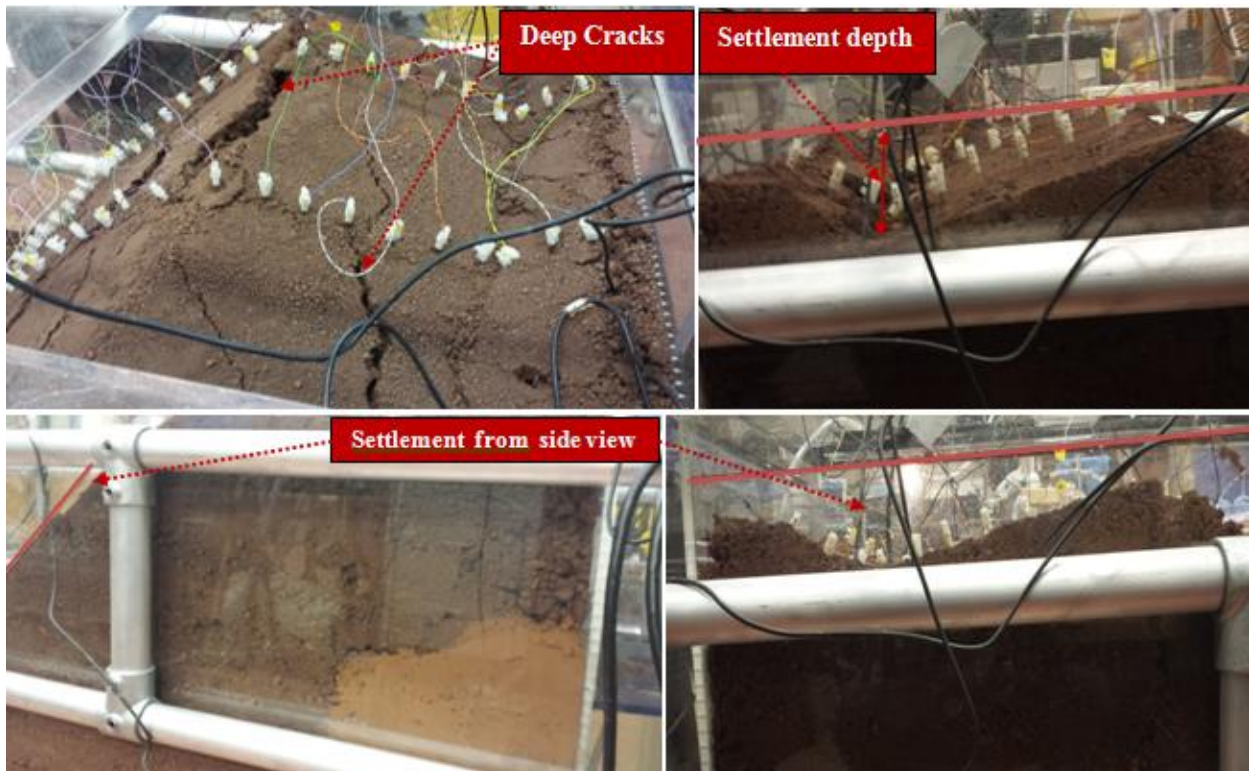


Figure 6-21: The final physical response of the slope

Before the end of the experiment, these minor failures have progressed to bigger ones. Multiple cracks of various sizes were formed and were spread all over the slope. The surface cracks propagated downwards to form deeper ones while the settlement transformed into a collapsed failure with the deepest deflection at the middle of the crest. These failures are shown in Figure 6-21.

6.7.2.2.3 Post-experimental condition - After the water supply

By the end of the experiment, the groundwater level rise to the surface and was retained at the deep deflection of the crest, after discharging the excess water at this position. The deep deflection at the crest indicates collapse settlement. The little forward movement was observed to have occurred, but the movement was only at the two sides of the slope leaving the mid-portion with no motion, though with obvious signs of weakness. These described failures are all shown in Figure 6.22. The failures are more obvious when viewed by the side as shown in Figure 6.23. With this, a comparison can be made between the original shape drawn against the transparent tank and the current shape after failure.

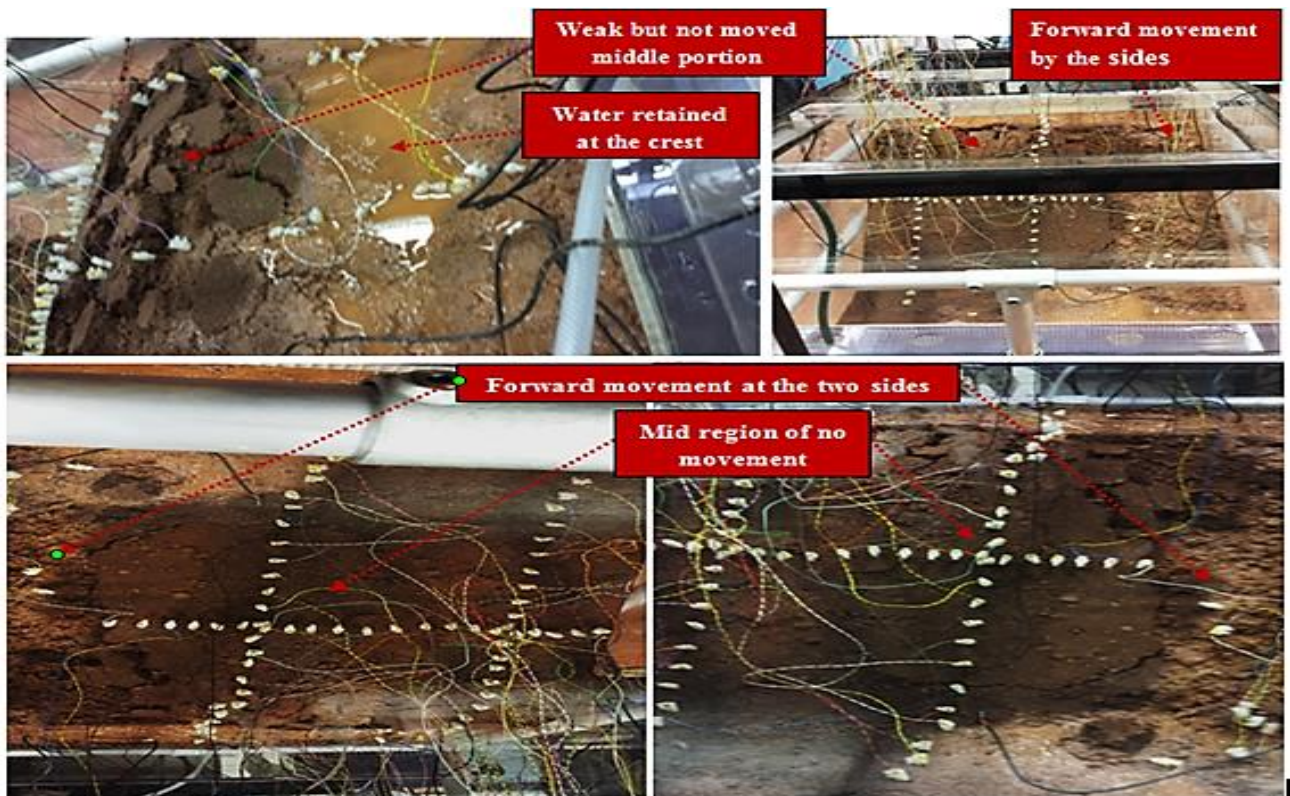


Figure 6-22: Photographic picture of post-failure condition



Figure 6-23: Side view of post-failure condition

6.7.2.3 Resistivity Survey results

The resistivity results include the measured apparent resistivity pseudo-sections (the recorded data), best fit calculated apparent resistivity pseudo-sections and the inverse models (true resistivity). These set of results were obtained for each of the measurements described in section 6.5. For illustrative purpose, one full set is presented in this section while the remaining can be found in appendix E. Subsequently, only the inverse models are presented for each array measurement. For the position of horizontal, central and side survey lines, please refer to Figure 6.24. Like the previous results, the resistivity results are also presented in this chapter. The interpretation and discussion of the results will be done in chapter 7.

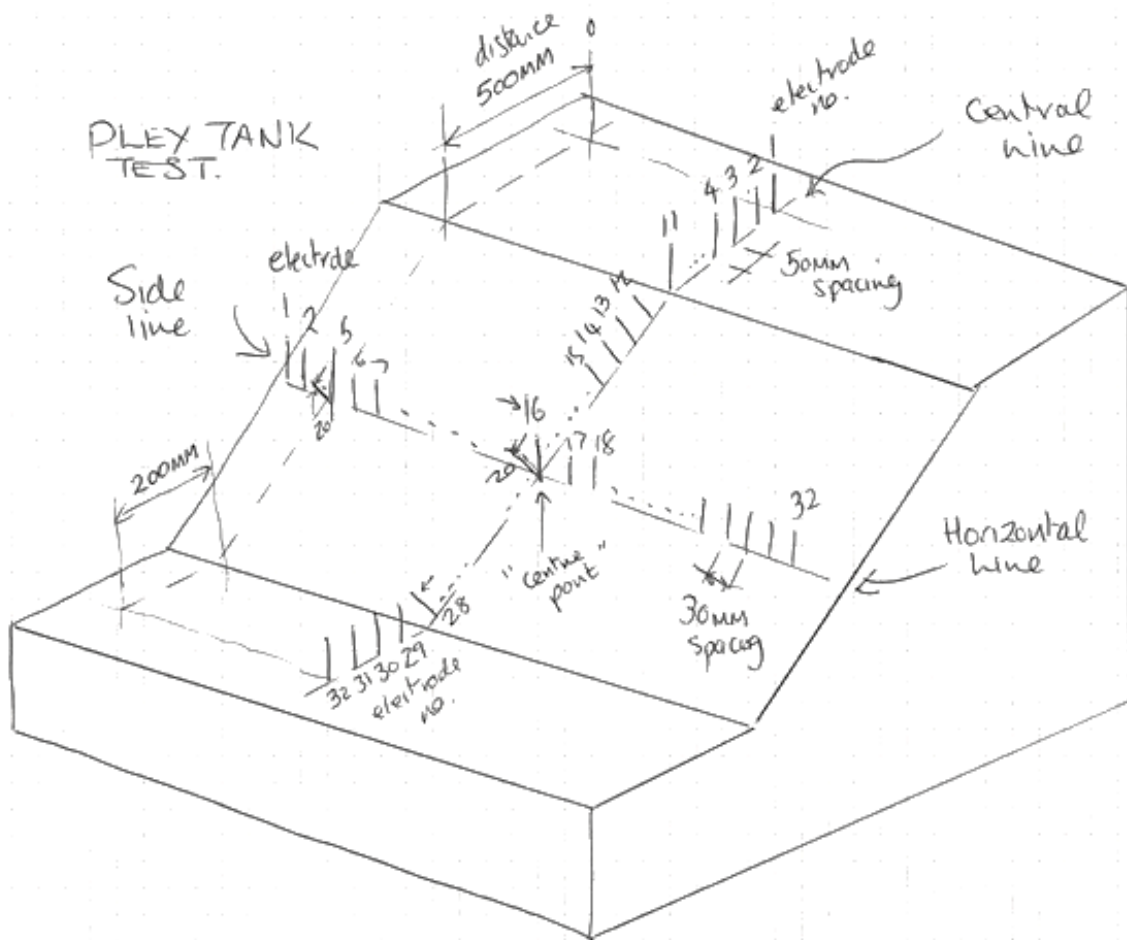
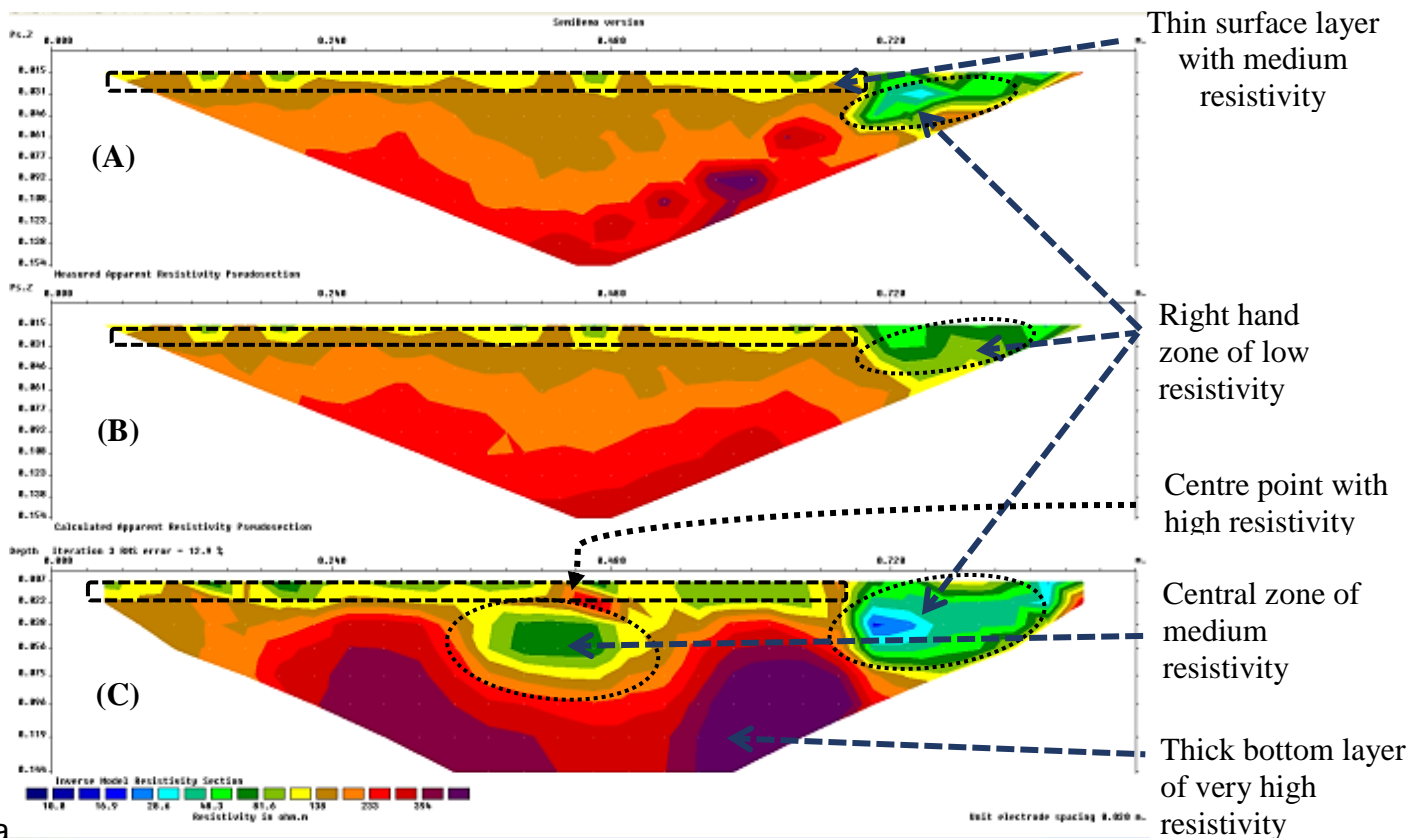


Figure 6-24: Sketch of slope with resistivity array arrangement

6.7.2.3.1 Initial condition before the water supply

Figure 6.25 shows three plots of electrical resistivity tomography horizontal line. The top plot shows the measured apparent resistivity pseudo-section (the recorded data), the middle plot shows best fit calculated apparent resistivity pseudo-section, while the bottom plot represents the inverse model, the true resistivity section that gives the best fit calculated apparent resistivity pseudo-section.



a Figure 6-25: The resistivity survey results along the horizontal line before the water supply

Comparing the calculated plotted tomography, labelled A at the top with the measured one B at the middle, it can be seen the survey results show a reasonable fit of resistivity values. Both have shown a thin layer of medium resistivity values (81-138Ω.m) overlaid on a layer with higher resistivity values (>138Ω.m). The resistivity values continue to increase in (layers) with the increase in depth. Additionally, both models have shown a portion on the right end with relatively lower resistivity values. The inverted resistivity model C located at the bottom shows a similar pattern of layering but with the top layer of relatively low resistivity values extending deep into the underlying layers at the centre. Around the surface centre of the inverse model is the point of high resistivity values above 250Ω.m. The deepest layer has the highest resistivity values of about 384Ω.m. In general, there is a reasonable fit between all the plots suggesting a high-quality survey.

Figure 6-26 shows an inverse model of resistivity profile along the central line, In the results, the crest and toe locations show relatively low resistivity values with toe showing the lowest and more variable resistivity values. The low resistivity values at the crest have extended into the lower layer. High resistivity values ($>250 \Omega.m$) in the centre of the section are consistent with the results of horizontal section shown in Figure 6.25.

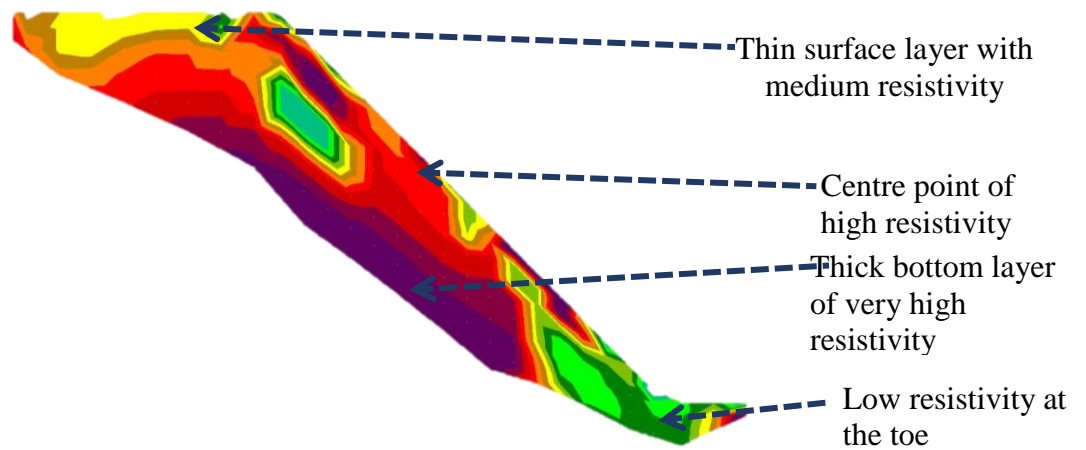


Figure 6-26: The resistivity survey results along the central line before the water supply

Figure 6-27 shows results of resistivity values along the side survey line. The inverse resistivity model is like the one obtained at the central position, but the thick bottom layer occupies a larger portion.

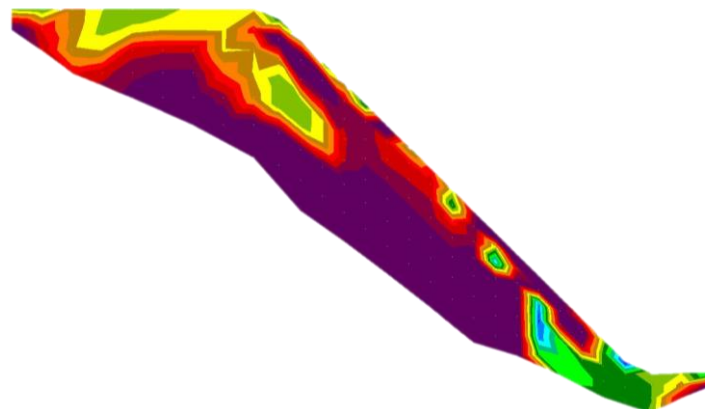


Figure 6-27: The resistivity survey results along the side array line before the water supply

6.7.2.3.2 Experimental condition during the water supply

To show the changes during the water supply, a comparison is made between the initial condition and the subsequent three scans. From the comparison made in Figure 6-28, bottom layer with very high resistivity values is continuously displaced by the low resistivity portion that was initially at the crest

location. The low resistivity portion continues to increase in values as it moves down the slope as shown between 1 and 3. At model 4 however, a sharp decrease in earlier increasing displacing resistivity values can be seen. At the toe, however, the initial low resistivity values continue to decrease from scan 1 to 4.

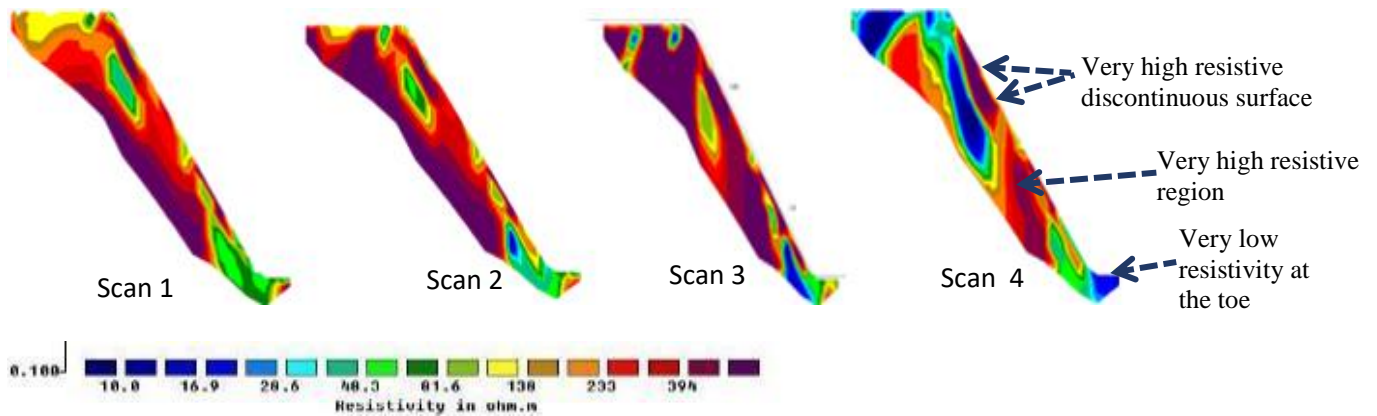


Figure 6-28: The change of resistivity during experiment along central line

Figure 6-29 shows the results of the two measurements by the side array. It compares the initial measurements and the measurement made during the water supply.

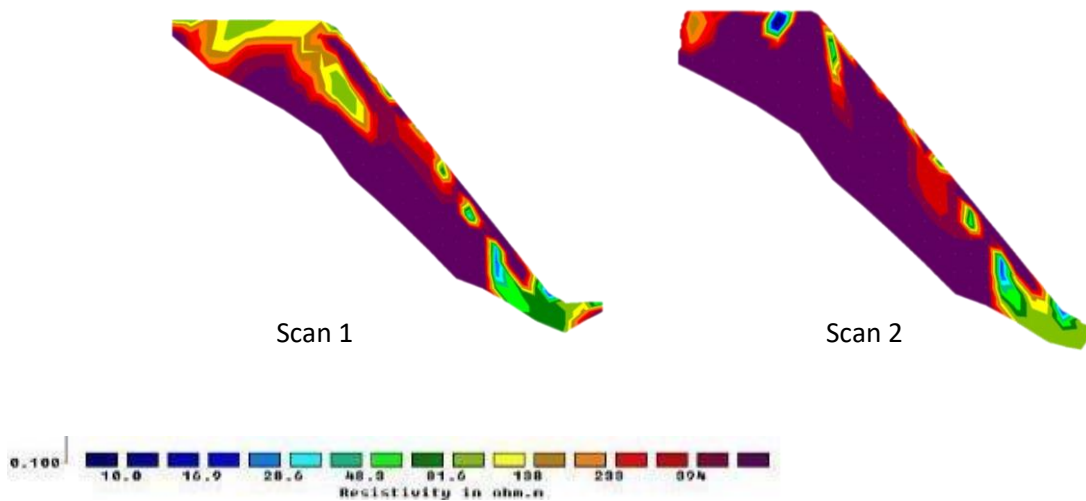


Figure 6-29: The results showing the change of resistivity during the experiment along the side line

The top two models are when the topography is applied whereas the bottom ones are without topography. From the comparison, bottom layer located in the middle with high resistivity values is partially displaced by the low resistivity portion that was initially at the crest location. At the toe, there

isn't much change between the initial and later condition. The change is consistent with the one observed at the central survey line shown in Figure 6.29.

From Figure 6-30, it can be observed that high resistive bottom has been continuously displaced by the low resistivity portion that was initially at the top central location. The low resistivity portion continues to increase in value as it moves down as shown between 1 and 3. At the far-right end, a low resistivity portion can be observed. Increase in blue portions at scan 2 indicates decrease in resistivity values at this position when compared with scan 1. But the values later increased at scan 3. At the left-hand side, the initially low resistivity layer located at the top continued to extend deep into the high resistivity bottom layer.

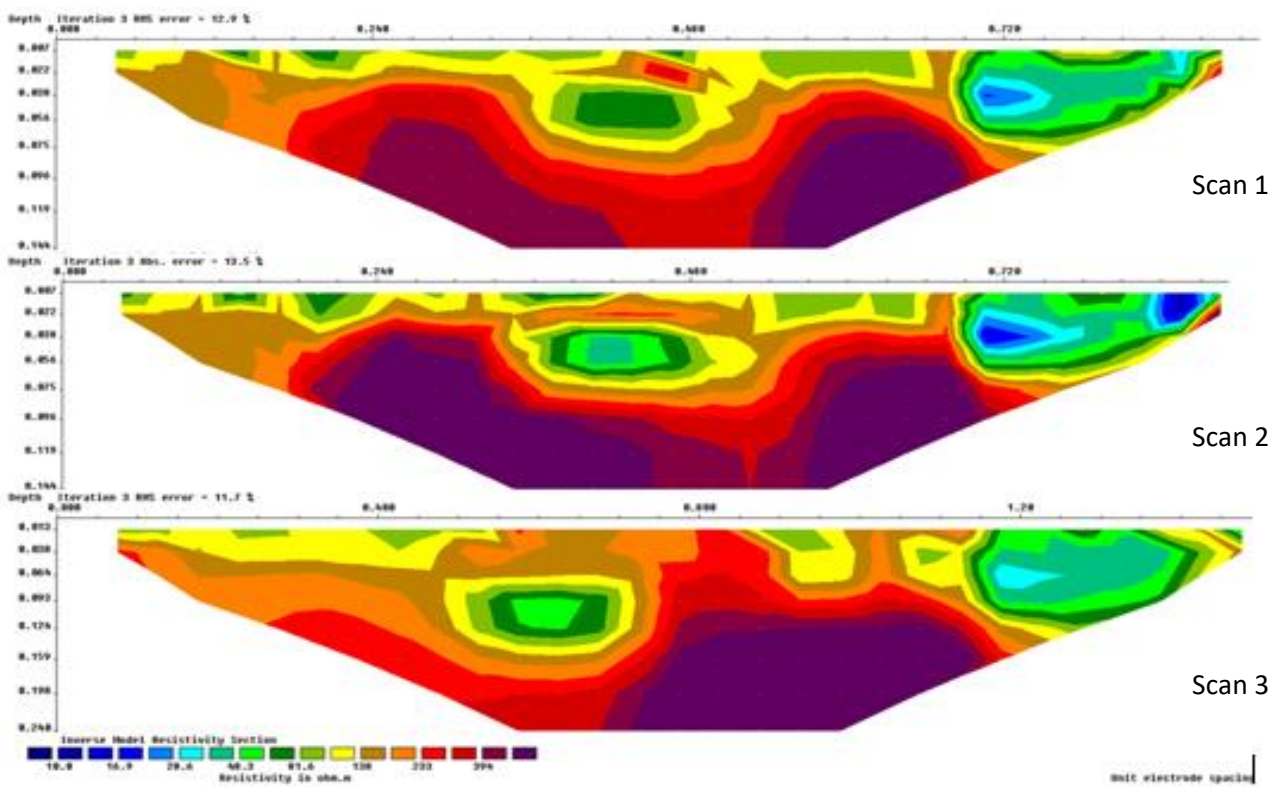


Figure 6-30: The change of resistivity result during the experiment along the horizontal survey line

In general, the changes observed are consistent with the results shown in the three figures presented in this section. All of them have shown continuous displacement of the very high resistive bottom layer with the low resistivity portion that was initially located at the top crest location. The central array has

recorded a continuous increase in resistivity values at the toe location but decreased at the end. In the horizontal survey results, there was a decrease in the initially low resistivity values at most of the locations. The change later reversed to the increase in values. Beyond the initial change, the result of the side array cannot be relied upon due to the movement of electrodes along this line during the resistivity survey, which allowed only the initial and one more measurement to be obtained. However, the results of the horizontal and central survey lines are enough to give information about the changes in condition during the experiment.

6.7.2.3.3 Post-experimental condition - After stopping the water supply

The last models i.e. number 3 and 4 in horizontal and central survey lines respectively describe the condition after the water supply has been suspended. Both have shown that greater percentage of the high resistivity valued deep bottom layer has been displaced by the low resistivity valued top portions and layer. A little portion of the deep layer remains non-displaced. From the horizontal survey result, the remaining non-displaced portion is located at the bottom right end of the slope while from the central survey line, it can be seen that part of the displaced portion has moved to the surface.

6.8 Summary

In this chapter, final experiment on a physical model to study failure mechanism of residual tropical soil slope has been presented. The experiment was conducted in a similar manner to the initial trials with a large fibreglass tank presented in chapter 5. The difference is that the electrical resistivity method was added to the number of instrumentations used previously. Additionally, a transparent acrylic tank was used in the final experiment in place of a fibreglass tank used previously. Since the electrical method has not been tried in the previous test, at the final stage, the test was first tried in the fibreglass tank before conducting the final experiment in the transparent acrylic tank. The two experiments are reported in this chapter. In each of the two, the experimental set-up and the procedure

employed in conducting the experiment was described. It is noteworthy that the initially established homogeneity of the slope model could not be maintained due to the further compaction caused by the post-construction activities during slope preparation and instrumentation. The observed density non-uniformity occurred despite the effort to prevent it. Nevertheless, it provided an opportunity to study a condition of an embankment like the real-life case. The results obtained at the end of these experiments were presented.

The actual initial condition varies from one experiment to another. However, the observed general pattern includes the initial irregular sensor readings before obtaining steady values. These initial geophysical changes recorded by the sensors did not cause any instability to the slope as no any physical changes were observed on the surface. However, the results of the initial resistivity survey show a varied degree of heterogeneity both with depth and distance.

The changes observed during the water supply includes the initial gradual increase in water content with the corresponding decrease in soil suction. Rapid changes were later observed as shown in Figure 6-14 and 6-17. The hydrological changes caused the initial surface cracks and minor settlement which later progressed into a large network of cracks, excessive (collapse) settlement and forward slope movement. These physical changes as observed by the camera are shown in Figure 6.18 to 6.21. The changes observed by electrical resistivity method are shown in Figure 6-28-6-30. Comparing the changes observed by the camera and electrical resistivity tomography, respectively, as shown in Figure 6-31 - 6-33, good agreement was observed between the two methods.

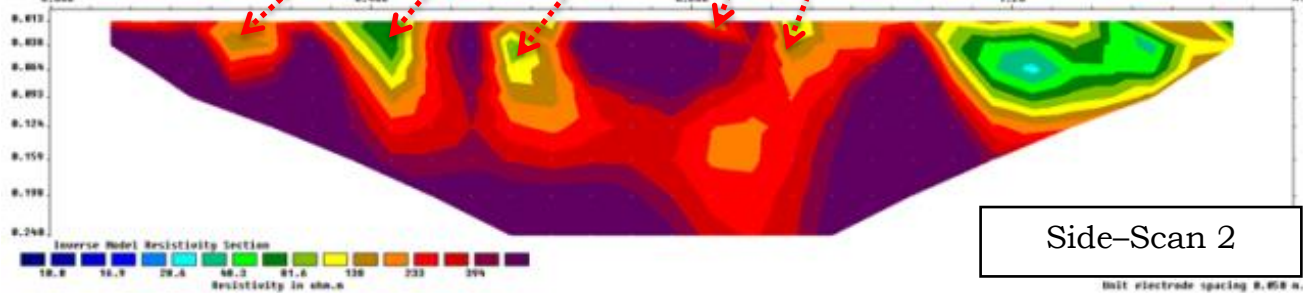
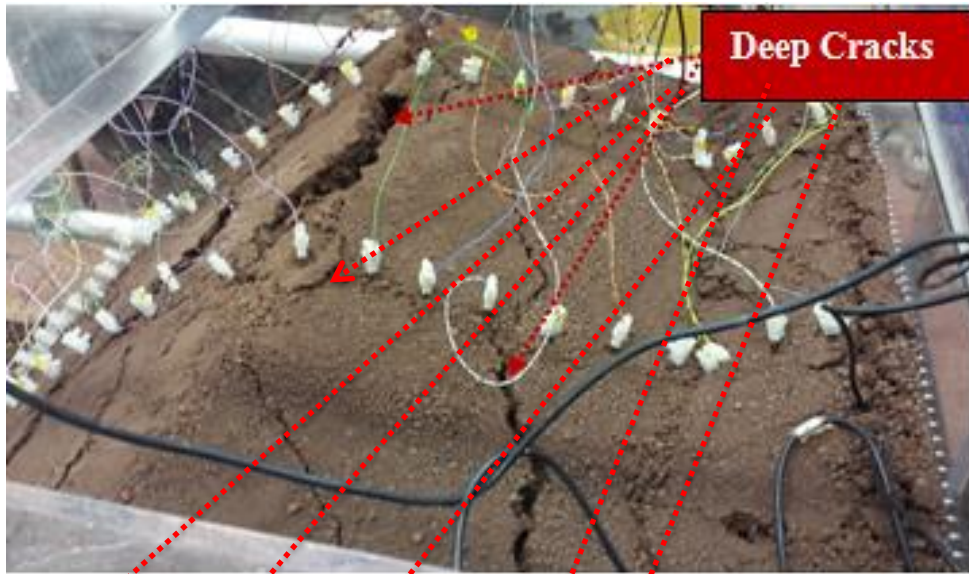
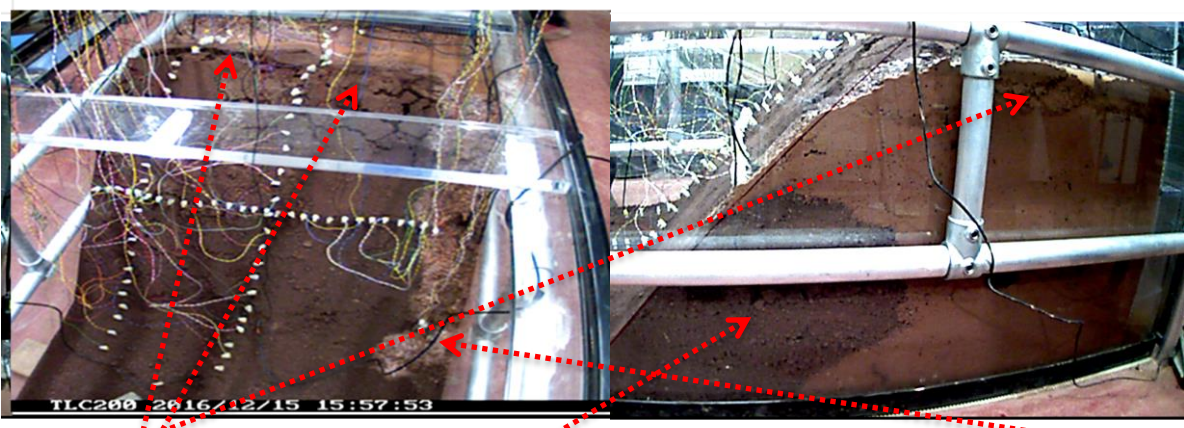


Figure 6-31: Comparing the resistivity scan 2 along the side array line with camera captured photograph



Cracks Very high resistive region Water on the toe

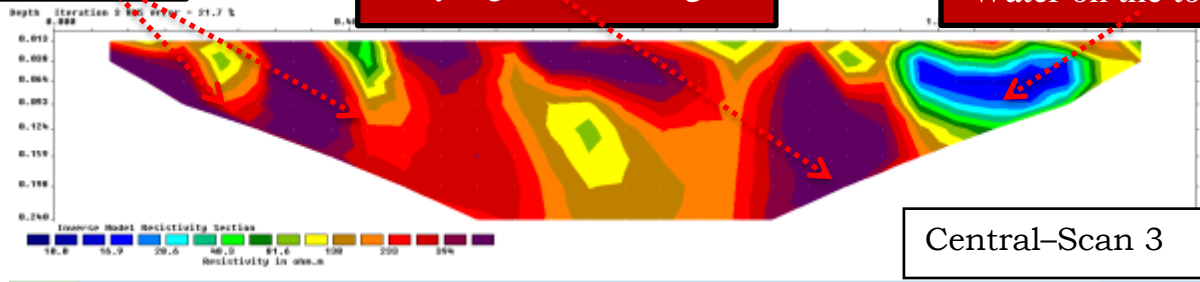


Figure 6-32: Comparing the resistivity image of scan 3 along the central line with camera captured photograph

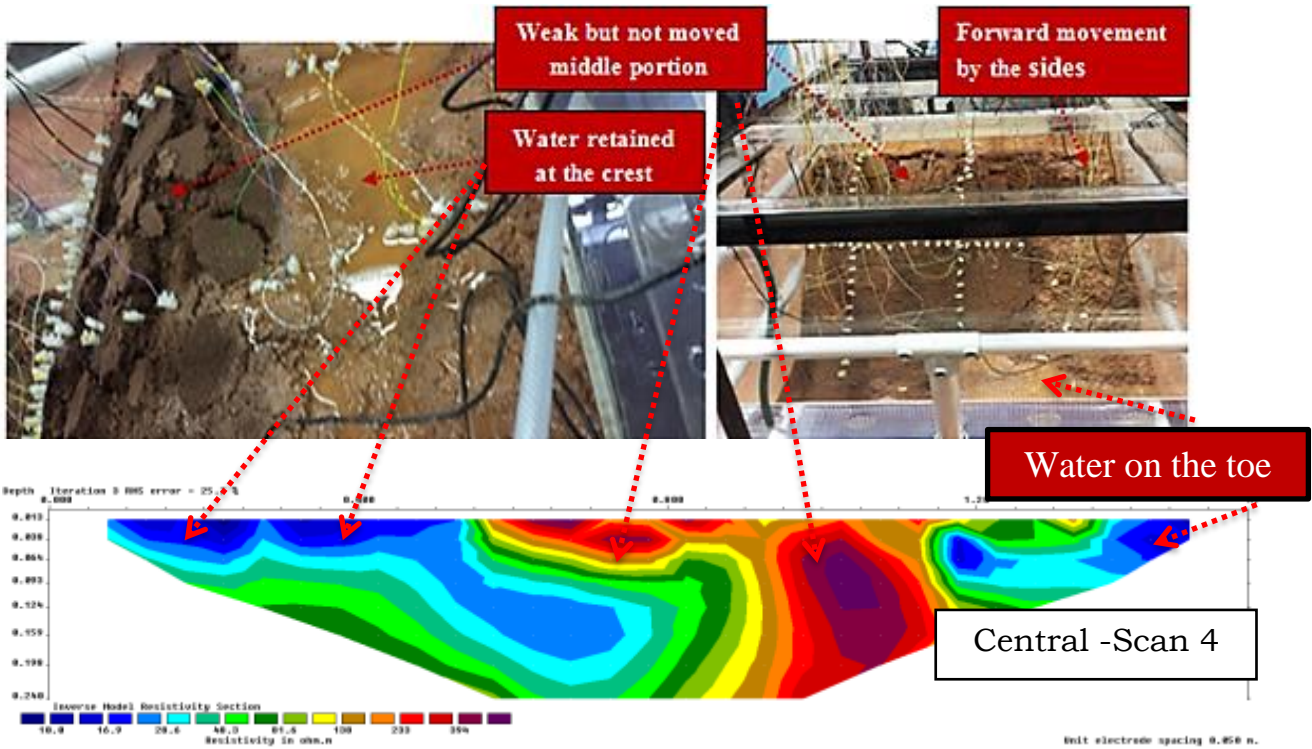


Figure 6-33: Comparing the resistivity image of scan 4 along the central line with camera captured photograph

Having studied and recorded the slope failure process to the end, the water supply was stopped. At this stage, the sensor readings remain constant after reaching their peak values. The resistivity survey results and camera photographs at this stage are also presented. A joint discussion of the results presented in this chapter can be found in chapter 7.

CHAPTER 7

DISCUSSION

7.1 Introduction

The numerical, geotechnical, geophysical and photographic results obtained in this study and presented in the previous chapters are discussed in this chapter. The results obtained by different methods used in each experiment were jointly discussed to get a better understanding of failure mechanism. The complementary role played in observing the failure processes has been highlighted and analyzed. The measured parameters are related to the changes in water content, matric suction, and slope movement. In all cases, the measurement began immediately after the completion of slope construction before the commencement of the experiment. The discussed results are, therefore, for the condition before, during and after the water supply. The potential of time-dependent sensor measurements for monitoring geophysical change in the embankment has also been discussed.

7.2 Tropical residual soil

The tropical residual soil has unique characteristics and good engineering properties which qualifies it to be a dominant material for the construction of infrastructural slopes in tropical countries. The reason for using a pseudo-tropical soil in this research has been clearly stated in chapter 1 and 3. The material used in this study is a synthetic material produced through novel methodology developed as presented in chapter 3. Although it is difficult to produce the exact replica of natural soil, previous attempts have confirmed that it is possible to reach a certain extent in replicating a natural tropical soil (Styles et al., 2001). The similarities in the index and geotechnical properties between the synthetic and the natural material as shown in Table 3.6 are enough to justify the use of the produced material in place of the natural material in this research. Moreover, the geophysical properties such as high matric suction on

exposure to the atmosphere associated with tropical soils (Rahardjo et al., 2005) exhibited by the soil as presented in chapter 6 have further increased confidence in the synthetic material.

7.3 Numerically modelling

The use of the material properties as input parameters in the numerical modelling allowed the behaviour of tropical soil slope to be simulated and studied numerically. The combination of hydrological and mechanical models during numerical modelling helped to provide a good understanding of the performance of the test slope. The ability of the modelling program to simulate deformation and volume change has provided a perfect opportunity to establish properties such as settlement and collapsibility associated with some tropical residual soils (Fredlund 1993, Brink 2000). Figure 4.11 gave an insight of these properties. Although the progressive failure is difficult to observe through parametric studies using limit equilibrium method (Gilbert 1996), the coupled analysis approach that combines finite element and limits equilibrium methods has gone a long way in providing a fair idea about the failure mechanism of the test slope.

Numerically, the failure process was described by seepage, stress/deformation analysis and obtaining stability factor of safety using finite element and limit equilibrium method respectively. It is a usual way, to express failure in terms of a factor of safety during numerical analysis (Fredlund et al., 2012). The decrease in the factor of safety connotes decrease in strength that leads to failure.

In Figure 4.16, the initial gradual decrease of factor of safety which later changed to rapid decrease represents the failure mechanism in a numerical sense. The physical meaning can be found in the discussion of experimental results in section 7.4.2. Meanwhile, a fair idea about the failure process as discussed in this section as well as obtaining a numerical model that led to the successful setting up of a laboratory experiment, justify the use of numerical modelling in this study.

7.4 Physical modelling

The extensive physical modelling exercise reported in chapter 5 was successful in establishing the possibility of translating the designed model during numerical modelling into real laboratory physical model. The feasibility study results presented in section 5.4, confirmed the suitability of material and methodology proposed to be used in the laboratory experiment. As one of the geophysical instrumentation, EM sensors which were not included in the earlier numerical study, was tried, and found suitable for use in the main experiment. The experimental evidence presented in sections 5.4.4-5.4.7 support this assertion. The use of the sensors to monitor geophysical changes in the small and large-scale trials confirmed their suitability for monitoring slope failure development in tropical residual soils. The consistent results of the repeated trials of small and large-scale trials have confirmed the repeatability and eliminated doubt about the failure pattern of test slope.

The success recorded during the physical modelling in chapter 5 allowed the main experiment to be set-up and conducted, the results of which was presented in chapter 6. The introduction of electrical resistivity tomography (ERT) in the main experiment necessitated a repeat of the large-scale trial conducted earlier as reported in chapter 5, with the added resistivity method as the only difference between the original and the repeat test. The results of the main experiment were consistent with the initial trials, although with minor differences due to some obvious reasons that will be discussed later in this section. A joint interpretation of geophysical data with the camera captured physical deformation gives an overall picture of the failure mechanism observed during both the trial and final experiments. In some cases, the numerical modelling experience is included in the joint interpretation. The interpretation and discussion are made in three phases covering the pre-, during and post-experimental conditions.

7.4.1 Initial (Pre-experimental) Condition

The irregular readings recorded by the EM sensors at the beginning of each experiment are due to the moisture movement between the particles of the soil before soil reached a state of equilibrium. The state of equilibrium is represented by the steady values following the initial irregular values.

In the trial experiment results presented in Figure 6.13, it was clear that the moisture lost was initially excessive but later reduced to a negligible rate. The moisture loss was due to the removal of polythene sheet to install instrumentation before running an experiment. A high temperature of 24°C recorded during the experiment which is a bit higher than usual, might have contributed to the excessive moisture. High temperature plays a significant role in drying the surface of soil slope thereby increasing the suction values. That is why in arid or tropical region where the temperature is excessively high, the ground surfaces are mostly dry with high suction values (Rahardjo et al., 2005). For instance, in the Nigerian northern city of Zaria, the location where the material considered in this study was sourced, the temperature can rise as high as 45°C.

The length of exposure during instrumentation varies from one experiment to another. For example, in the large-scale trial reported in chapter 5, only electromagnetic sensors were used which took less than an hour to install, while in the last two experiment involving the use of electrical resistivity array, each took more than six hours to complete the instrumentation. This difference in the period of instrumentation makes the initial values of VWC and MS to differ.

Another factor responsible for the variation of the initial values among the various trials, is the variation of initial water content during soil preparation. Although 10% water content was targeted to be mixed with dried soil, a little more or less than the targeted amount might have ended up being used, due to some unavoidable causes of errors such as room temperature variations. This can cause difference in

moisture loss during soil mixing and compaction (Sellers et al., 2010). This is, however, mitigated by keeping the room temperature as constant as possible.

Due to the above enumerated factors, the initial values shown in Figure 6.14 and 6.17 for the trial and final experiment respectively vary. The average VWC value in the trial experiment was little less than $0.1\text{cm}^3/\text{cm}^3$ with the corresponding MS of approximately -1500Kpa. While in the final experiment, the average value of VWC was a bit greater than $0.1\text{cm}^3/\text{cm}^3$ with the corresponding MS values of -700Kpa. A small difference in moisture content can produce a large difference in soil suction because this is the characteristic behavior of unsaturated soils (Fredlund et al., 2012).

The variation of VWC and MS with depths of the slope could not be measured with EM sensors. However, the resistivity survey has confirmed that there was a moisture variation with depth. The resistivity results presented in Figure 6.24 to 6.26 indicate decrease in resistivity from low values (about $81\Omega\cdot\text{m}$) on the surface to the highest resistivity values of about $384\Omega\cdot\text{m}$ at the deepest layer; suggesting a density and moisture content decrease with the increase in depths. The addition of a fine-grained soil layer to improve contact resistance, is responsible for the relatively low values at the surface.

Similarly, a considerable degree of heterogeneity was observed along the horizontal axis, in all the results of resistivity survey. Sellers et al. (2010), listed soil type, pore water chemistry, temperature, moisture content and degree of compaction as the factors affecting the resistivity of a compacted soil. The non-uniformity of density revealed by the resistivity survey results is caused by the increased activities during the extended period of instrumentation which caused additional but non-uniform compaction.

For easy interpretation, the resistivity values in the results reported in chapter 6 can be classified in to very low (less than $28.6\Omega\text{m}$), low ($28.6\text{-}81.6\ \Omega\text{m}$), medium ($81.6\text{-}233\Omega\text{m}$), high ($233\text{-}394\Omega\text{m}$) and very high (above $394\Omega\text{m}$) values. A high resistivity is shown at the surface midpoint of each resistivity model is indicative of high density. For the horizontal survey result shown in Figure 6.24 the surface high resistivity values recorded at the centre and left end of the model, a significant drop of resistivity (from high to low) values are observed at the right end. The thin surface layer with medium resistivity values represents a fine-grained layer placed at the surface during instrumentation to increase the contact resistance of the array electrodes. The light mist applied on the surface layer is what makes it have a medium resistivity value. The central zone of medium resistivity values gives the isometric view of crest location that is made up of the same fine-grained material and is a bit wetter at the lower region of that zone. The side view of this zone can be seen in Figure 6.25 and 6.26 produced from the central and side resistivity surveys without applying topography. The bottom layer shows a very high resistivity values as shown in all the results indicative of a high degree of compaction due to the additional loading imposed by the overlying layers. At each stage of compaction, the underlying layer is being further compressed by the currently compacted layer which results to the increase in the total stress to the slope and change in the pore-air and pore water pressures (Fredlund 2012).

In general, the actual initial values of water content and matric suction recorded prior to the commencement vary due to various reasons some of which have been mentioned above. However, the pattern of the initial changes was virtually the same. Not minding the initial variations, it is important to establish the initial condition at each experiment as this is crucial in the interpretation of the subsequent measured data during the experiment (Fredlund et al., 2012).

7.4.2 During the experiment

The simultaneous increase in water content and reduction of soil suction in all the trials was due to the change in pore fluid properties. The relationship between the four phases of unsaturated soil is complex

but the reduction of soil suction is likely caused by the gradual replacement of air in the voids with water (Barbour, 1998, Egeli and Pulat, 2011). The complex water content and matric suction relationship are simplified by one of the constitutive relations in unsaturated soil mechanics known as soil water characteristics curves (SWCC). This relation was used to characterize the soil during the design stage using numerical modelling. The graph shown in section 4.4 shows the relationship of the water content and matric suction based on the numerical model prediction. The curve described the soil based on the desorption (desaturation). However, the experimental results presented in chapter 5 and 6, as being discussed in this chapter are based on adsorption (saturation). In this case, an unsaturated condition is considered first at the initial stage before the water is introduced to attain a gradual saturation. The saturation and desaturation curves are not the same due to hysteresis but both or either of the two could be used to describe soil-moisture characteristic (Fredlund et al., 2012).

The initial settlement was caused by the rearrangement of soil particle due to the filling of voids with the flowing water (Rahardjo et al., 2005, Brink, 2012). The followed excessive settlement otherwise known as collapse settlement was due to the soil structure collapse induced by wetting (Jia et al., 2009). This is a characteristic feature of some tropical soil (Fredlund and Rahardjo, 1993, Fredlund and Gan, 1995, Rahardjo et al., 2005). The increase in slope weight due to the increase in volumetric water content coupled with the force of gravity naturally pulling the slope, caused the forward but downward slope movement.

The gradual and continuous decrease in soil suction with the increase in water content was consistent despite some differences in their sizes and initial conditions. The pore-water decreased from high negative values to zero and extend to positive. The pore-water pressures along the slip surface at the time of failure may be negative or positive (Fredlund et al., 2012).

Comparing successive measurements during the resistivity survey revealed the changes that occurred during the experiment. The changes are clear in the comparison made in Figure 6.27 – 6.29. For instance, in the central line shown in Figure 6.27, the high degree of moisture indicated by low

resistivity at the crest location in Scan 1, has continued to increase in value as it moves down to the toe, displacing a high resistive bottom layer as shown in the subsequent scans.

7.4.3 Post-experimental condition

At the end of the experiment, the steady values after reaching their peaks indicate that the saturation point had been reached. At this point, all the voids have been filled with water increasing the weight of the slope and aiding its downward movement. In the final experiment, the movement was mostly by the two sides of the slope as shown by post failure condition in Figure 6.22. The inability of the mid portion of the slope to move, was due to the increased density at the region caused by the increased activities during post construction period e.g. array installation process described in 7.4.1. Similar kind of slope movement was observed at the previous experiment. The water retained at the crest is a clear evidence of saturation.

The post failure condition described by the joint discussion of EM sensor readings and the camera captured photographs is similar to the one obtained by the resistivity survey. The lowest resistivity values recorded at the crest location in the last measurements each of the side and central survey lines are indications of saturation with water settling at the beginning of the model surface at that location. The low resistivity values shown in between series of discontinued high resistivity portions particularly in Figure 6.27 are indicative of the cracks at the upper part of immovable portion while the lower part of the portion that obstruct the water flow are shown with a very high resistivity values. The comparable results between the camera captured photographs and the images in resistivity survey as shown in Figure 6.29 - 6.31 validate the resistivity results and confirmed its suitability for the monitoring of tropical residual soil slopes.

7.5 Time-dependent monitoring

Time-dependent response to the changes in soil properties makes an electromagnetic sensors a powerful tool for ground studies (Cassidy, 2009). Time recorded for each value of VWC and MS allowed tracking of geophysical changes. Movement of water and eventual changes in water content and soil suction was monitored against time. The corresponding physical deformation was also possible to monitor due to the time-lapse ability of the used cameras.

The results of the trial and final experiments as presented in chapter 5 and 6 have shown that the movement of water was tracked by the sequential response of sensors as the water moves from one sensor location to another. The combination of the sensor responses recorded with time and the camera captured deformation also with time gave a complete information about the spatial and temporal changes occurring in any part of the slope at any given time. The complementary observation method can provide an efficient way of automated monitoring of slopes and embankments.

In chapter 5, the results shown that there was a time lag between the sensor-recorded initial geophysical changes and the final camera-captured, physical slope failure. The initial sensor response was recorded 4 minutes after the commencement of water supply while actual slope movement was recorded 1 hour later. This shows that the sensors can be used to serve as warning signal of impending failure. If the warning served by the sensor recorded abnormal hydrological changes is properly utilized, the catastrophe that might be caused by the subsequent slope failure could be avoided.

The results of resistivity survey compared with the camera captured photography demonstrated its ability to provide a robust slope monitoring strategy if used in integrated form with the other two observational methods used in this study. Its dual capacity to monitor water content changes as well as providing the images of the observed changes, serve as check and balance to the EM sensor monitoring and camera observations respectively. Additionally, its ability to provide a pictorial view

of the geophysical changes below the ground surface add a robustness to the integrated method of monitoring.

The study demonstrated a time-dependent monitoring capability of the integrated system of sensors and cameras.

7.6 Summary

Some of the natural soil deposits exist as unsaturated with low water contents and negative pore-water pressure such as tropical residual soil. Initially, it can have a negative pore-pressure but changes to positive with the ingress of water. These changes can cause a change in strength and volume as observed. It was observed that, the slope was initially stable (though the initial conditions vary) due to the high values of suction and low values of water content. As water content was introduced, there was slope settlement with no immediate sign of surface failure. The rearrangement of soil particles and reduction of voids caused the settlement. The movement of water caused a continuous reduction in matric suction and changed the pore fluid properties with consequent reduction of shear strength. A gradual settlement which later transformed to collapse settlement and forward movement was the manifestation of these changes.

The collapse settlement was caused by soil structure collapse induced by wetting while the forward sliding was caused by loss of shear strength which was aided by the movement of water. A collapse movement is a behaviour of many residual tropical soils and is mainly due to their low-density microstructure. In this research, this behaviour was simulated by compacting the soil at density a little drier than optimum and it was primarily designed to aid slope failure. However, the process of array installation has altered the homogeneity of the compacted slope as the areas where the arrays were located became more compacted and therefore resisted movement. Slope movement at less compacted

sides, began when the suction was completely lost, leading to the loss of strength. The increase in slope weight due to the increase in volumetric water content coupled with the force of gravity naturally pulling the slope caused the forward and downward slope movement.

The above failure mechanism was deduced from the joint interpretation of geophysical changes recorded by the EM sensors, the visual observation made with cameras and the results obtained by electrical resistivity tomography. The various methods used served as complementary in providing an overall picture of the failure mechanism. The reasonable agreement in their results shows that the geophysical methods (EM sensors and ERT) can be used for monitoring slopes of tropical residual soils.

CHAPTER 8

CONCLUSIONS AND RECOMMENDATIONS

This chapter presents the conclusions based on the findings reported in the preceding chapters. It also contains the recommendations that could be considered for further studies. These recommendations are presented based on the belief that further research will enable the key findings to be taken forward, to advance the field of study covered in this thesis.

8.1 Conclusions

From the detailed review of the literature, it could be seen that the number of slope failures is increasing in the tropical regions where the natural and man-made slopes are made up of tropical residual soil. The failures are attributed to many factors but is mainly due to the abnormal changes in ground water content. However, the slope failure process and the exact mechanisms involved in this kind of soil is not clearly understood. To date little or no effort is made to use the appropriate techniques to bridge the gap. For that reason, the research presented in this thesis centred on the use of geophysical techniques to study failure mechanism of slopes formed in residual tropical soils, taking into account that the proposed techniques have been previously tried with tropical soil with a positive indication of their suitability for this purpose (Jackson 2001).

To enable the aims of this research to be met, the work was carried out in a number of many phases and conclusions pertinent to these are presented first before overarching conclusions are detailed as follows.

- i. Development of a synthetic soil

Due to logistical limitations explained in chapter 3 of this thesis, the research had to be conducted on a synthetic soil material. A novel methodology that ensured that the material physical properties

match that of the natural residual tropical soil was developed and used to produce the synthetic material. This enabled a repeatable and controllable test soil to be used and provided a sound base from which conclusions on slope failure mechanism in tropical soils was drawn.,

ii. Modelling approaches

The use of well thought of and developed numerical and physical modelling methodologies to design and construct a model that was used for this study has significantly contributed to the attainment of the research aim and objectives. The large-scale laboratory test set up, allowed several aspects of synthetic residual tropical soil slope behaviour to be assessed. In the test, a combination of photographic, geotechnical and geophysical approaches were used to elucidate a number of features leading up to the eventual failure of the slope. Numerical modelling was particularly useful in providing an initial idea about the failure process of the test slope.

iii. Geophysical approaches

The successful use of electromagnetic sensors (5TE and MPS-6) and ERT to measure the geophysical processes has confirmed their suitability in monitoring the stability and failure development of tropical residual soil slope. It was particularly interesting to observe a time lag between the sensor recorded geophysical changes and visible physical deformation showing how a geophysical survey with electromagnetic sensors can be used to serve as early warning for imminent failure. The use of geophysics enabled a much fuller picture to be gained, covering aspects of the initial condition, subsequent pre-failure changes and ultimately the failure mechanisms involved. What was particularly useful was how variation in the initial conditions could be imaged and assessed. It was interesting to note that zones of weakness established during the initial condition geophysical survey were where the subsequent failure occurred.

iv. Failure mechanism

The slopes' physical deformation was observed, to begin with, the initial settlement and minor surface cracks and continually progress to form deep cracks, collapse failure and then a forward movement.. The initial settlement was caused by the rearrangement of soil particles caused by the flowing water that reduces the volume of the voids. The excessive settlement, known as collapse failure is a natural characteristic feature of some tropical soil and is associated with a soil structure collapse induced by wetting.

v. Real-life application

The time taken to complete the failure process is dependent on the size of the physical model. The period between the initiation of the slope failure and the occurrence of the final ultimate failure increases with the increase in the size of the physical model under study. This implies that if the right geophysical technique is used, the slope failure signs could be detected early enough to allow a timely intervention, in terms of remedial action or evacuation measures to prevent a catastrophe.

The experiment has provided an improved understanding of the failure mechanism of tropical residual soil slopes. It has also been established that the geophysical techniques that have been used to study and monitor slope stability of temperate climates, could also be used for the same purpose in tropical soils. The methods, if wisely used in monitoring slopes and embankments of the tropics, can guarantee sustainable stability and prevent the occurrence of catastrophic failures.

8.2 Recommendations

The following are the recommendations for further research.

- The use of the synthetic soil material in the study was due to the logistical limitations. Therefore, to understand both the physical and chemical properties of the soil to provide an accurate assessment of the failure behaviour of tropical residual soil, the use of natural soil is recommended for further studies.

- The controlled laboratory condition has provided an atmosphere that led to the study and understanding of the slope failure mechanism in the tropical residual soil. The successful use of geophysical techniques in this research has confirmed that they can be used for stability monitoring of tropical residual soil slopes. To determine the extent of the efficiency of the proposed monitoring strategy, as well as to confirm the output of the laboratory-based research, full-scale testing is hereby recommended.
- Two techniques i.e. EM sensors and ERT have been successfully used in this study in a complementary manner. It is recommended that other geophysical techniques such as AE and seismic methods be used in future studies. Using many methods will allow the best combination of geophysical techniques that gives the more detailed monitoring strategy, to be determined.
- Both an economic and a monitoring strategy need to be considered in developing a viable and sustainable slope monitoring system that will prevent or minimize losses, arising from embankment failures in tropical countries.

References

- BSBS 8006:1995, Code of practice for strengthened/reinforced soils and other fills.
- ABIDIN, Z., HAZREEK, M., SAAD, R., FAUZIAH, A., WIJEYSEKERA, C., BAHARUDDIN, T. & FAIZAL, M. 2012. Integral analysis of geoelectrical (resistivity) and geotechnical (SPT) data in slope stability assessment. *Academic Journal of Science*, 1, 305-316.
- ABRAMSON, L. W. 2002. *Slope stability and stabilization methods*, John Wiley & Sons Incorporated.
- ABU-HASSANEIN, Z. S., BENSON, C. H. & BLOTZ, L. R. 1996. Electrical resistivity of compacted clays. *Journal of Geotechnical Engineering*, 122, 397-406.
- AGHAMELU, O. P. & OKOGBUE, C. O. 2011. Geotechnical assessment of road failures in the Abakaliki area, southeastern Nigeria. *Intl. J. Civil & Environ. Engg*, 11, 12-24.
- ALEXANDER, L. T. & CADY, J. G. 1962. *Genesis and hardening of laterite in soils*, US Dept. of Agriculture.
- ALLIED-ASSOCIATES 2006. Tigre resistivity meter manual Rev E 0506", 2006. . *Allied Associates Geophysical Ltd*.
- ASHOUR, M. & ARDALAN, M. H. 2010. Road Embankment and Slope Stabilization.
- ASSALLAY, A., ROGERS, C. & SMALLEY, I. 1997. Formation and collapse of metastable particle packings and open structures in loess deposits. *Engineering Geology*, 48, 101-115.
- AWAISU, M. M. 1989. *The effectiveness of common stabilising agents on shika lateritic soil*. M.Sc. Thesis. Department of Civil Engineering, Ahmadu Bello University, Zaria.
- BARBOUR, S. L. 1998. Nineteenth Canadian Geotechnical Colloquium: The soil-water characteristic curve: a historical perspective. *Canadian Geotechnical Journal*, 35, 873-894.
- BARBOUR, S. L. & KRAHN, J. 2004. Numerical modelling–Prediction or process. *Geotechnical News*, 22, 44-52.
- BARDEN, L., MCGOWN, A. & COLLINS, K. 1973. The collapse mechanism in partly saturated soil. *Engineering Geology*, 7, 49-60.
- BASMA, A. A. & TUNCER, E. R. 1992. Evaluation and control of collapsible soils. *Journal of Geotechnical Engineering*, 118, 1491-1504.
- BELLO, A. 2011. Analysis of Shear Strength of Compacted Lateritic Soils. *Pacific Journal of Science and Technology*, 12, 425-433.
- BJERRUM, L. 1955. Stability of natural slopes in quick clay. *Geotechnique*, 5, 101-119.
- BJERRUM, L. 1967. Progressive failure in slopes of overconsolidated plastic clay and clay shales. *Journal of Soil Mechanics & Foundations Div*.
- BRINK, G. E. 2012. *The influence of soil suction on the collapse settlement of different soils in South Africa*. M.Sc. thesis. University of Pretoria.
- BS1377-5 1990. Methods of test for soils for civil engineering purposes. *Classification tests*. British Standards.
- CASSIDY, N. J. 2009. *Electrical and magnetic properties of rocks, soils and fluids, a chapter in Ground Penetrating Radar: Theory and Applications*, Elsevier, 2, 41-72.
- CERNICA, J. N. 1995. *Geotechnical engineering: soil mechanics*, Wiley.
- CHAMBERS, J., GUNN, D., WILKINSON, P., MELDRUM, P., HASLAM, E., HOLYOAKE, S., KIRKHAM, M., KURAS, O., MERRITT, A. & WRAGG, J. 2014. 4D electrical resistivity tomography monitoring of soil moisture dynamics in an operational railway embankment. *Near Surface Geophysics*, 12, 61-72.
- CHAMBERS, J., GUNN, D., WILKINSON, P., OGILVY, R., GHATAORA, G., BURROW, M. & SMITH, R. T. 2008. Non-invasive time-lapse imaging of moisture content changes in earth embankments using electrical resistivity tomography (ERT). Ed. Ellis, E., Yu, HS, McDowell, G., Dawson, A. & Thom, N. *Advances in Transportation Geotechnics. Proc. 1st Int. Conf. Transportation Geotechnics, Nottingham*, 475-480.
- CHAMBERS, J., WILKINSON, P., GUNN, D., OGILVY, R., PEARSON, S., KURAS, O., MELDRUM, P. & GHATAO, G. 2007. Geoelectrical monitoring of seasonal moisture content changes in an earth embankment. *13th European Meeting of Environmental and Engineering Geophysics*.
- CHANGE, N. R. C. C. O. C., TRANSPORTATION, U., EARTH, N. R. C. D. O. & STUDIES, L. 2008. *Potential Impacts of Climate Change on US Transportation*, Transportation Research Board.
- CHOI, G.-S. & KANG, C.-W. 2003. Device for detecting partial discharge in power equipment using radiated electromagnetic wave. Google Patents.

- COBOS, D. R. & CHAMBERS, C. 2010. Calibrating ECH2O soil moisture sensors. *Application Note, Decagon Devices, Pullman, WA.*
- CONTE ROBLES, O. A. 2012. *Slope stability monitoring using remote sensing techniques*, University of Arkansas.
- CORBET, S. & C, J. 2010. Revisions to BS8006 for reinforced soil – what do these mean for the industry? *Ground Engineering Slopes Conference held on 16 November 2010.*
- CRIPPS, J. & TAYLOR, R. 1981. The engineering properties of mudrocks. *Quarterly Journal of Engineering Geology and Hydrogeology*, 14, 325-346.
- DAILY, W., RAMIREZ, A., LABRECQUE, D. & NITAO, J. 1992. Electrical resistivity tomography of vadose water movement. *Water Resources Research*, 28, 1429-1442.
- DARCY, H. 1856. The public fountains of the city of Dijon. *Dalmont, Paris*, 647.
- DAVIES, O. 2011. *Numerical analysis of the effects of climate change on slope stability*. A thesis for the degree of Doctor of Philosophy (Ph.D) ANewcastle University
- DAVIES, O., ROUAINIA, M., GLENDINNING, S., CASH, M. & TRENTO, V. 2014. Investigation of a pore pressure driven slope failure using a coupled hydro-mechanical model. *Engineering Geology*, 178, 70-81.
- DE CARVALHO, J. C., DE REZENDE, L. R., CARDOSO, F. B. D. F., DE FL LUCENA, L. C., GUIMARÃES, R. C. & VALENCIA, Y. G. 2015. Tropical soils for highway construction: Peculiarities and considerations. *Transportation Geotechnics*, 5, 3-19.
- DECAGON, I. 2015. 5TE Water content, EC, and temperature sensors *Operator's manual* Decagon Devices, Pullman, WA.
- DECAGON, I. 2017. MPS-2 and MPS-6 Water Potential Sensor. *Operator's manual*. Decagon Devices, Pullman, WA.
- DIAS, R. D. A. G., M.D., . Stress-strain-strength behaviour of a Brazilian Amazon yellow latosol. . 1st International Conference on Geomechanics in Tropical Laterite and Saprolite Soils, Brasilia, , 1985. 331 – 343.
- DIBBEN, S. 1998. *The modelling of collapse in silty soils*. PhD Thesis. Nottingham Trent University, UK.
- DIJKSTRA, T. & DIXON, N. 2010. Climate change and slope stability in the UK: challenges and approaches. *Quarterly Journal of Engineering Geology and Hydrogeology*, 43, 371-385.
- DIXON, N., DIJKSTRA, T., FORSTER, A. & CONNELL, R. Climate change impact forecasting for slopes (CLIFFS) in the built environment. *Engineering Geology for Tomorrow's Cities: Proceedings, 10th International Association of Engineering Geology Congress*. Geological Society, London, 2006.
- DIXON, N., HILL, R. & KAVANAGH, J. 2003. Acoustic emission monitoring of slope instability: development of an active waveguide system.
- DIXON, N. & SPRIGGS, M. 2007. Quantification of slope displacement rates using acoustic emission monitoring. *Canadian Geotechnical Journal*, 44, 966-976.
- DIXON, N., SPRIGGS, M., MELDRUM, P., OGILVY, R., HASLAM, E. & CHAMBERS, J. 2010. Development of a low cost acoustic emission early warning system for slope instability.
- DO, J. 2003. Ground penetrating radar. *Geoenvironmental Engineering, Villanova University. Villanova.*
- DONNELLY, L., CULSHAW, M., HOBBS, P., FLINT, R. & JACKSON, P. 2005. Engineering geological and geophysical investigations of a slope failure at Edinburgh Castle, Scotland. *Bulletin of Engineering Geology and the Environment*, 64, 119-137.
- DRNEVICH, V. P. & GRAY, R. 1981. *Acoustic emissions in geotechnical engineering practice*, Philadelphia American Society For Testing & Materials.
- EGELI, I. & PULAT, H. F. 2011. Mechanism and modelling of shallow soil slope stability during high intensity and short duration rainfall. *Scientia Iranica*, 18, 1179-1187.
- EVANS, R. D., FROST, M. W., DIXON, N. & STONECLIFFE-JONES, M. Optimising the use of ground penetrating radar (GPR) for urban road investigations. *Proceedings of the 10th IAEG Congress, 6th-10th September, Nottingham, UK. 2006a.* © The Geological Society of London.

EVANS, R. D., FROST, M. W., STONECLIFFE-JONES, M. & DIXON, N. 2006b. Ground-penetrating radar investigations for urban roads. *Proceedings of ICE, Municipal Engineer*, 159 (2), pp 105-111.

EVANS, R. D., FROST, M. W., STONECLIFFE-JONES, M. & DIXON, N. 2008. A review of pavement assessment using ground penetrating radar (GPR).

12th International Conference on Ground

Penetrating Radar, June 16-19, 2008, Birmingham, UK.

FELL, R., HUNGR, O., LEROUEIL, S. & RIEMER, W. 2000. Keynote Lecture-Geotechnical Engineering Of The Stability Of Natural Slopes And Cuts And Fills In Soil. *ISRM International Symposium*. International Society for Rock Mechanics.

FOSS, I. Red soil from Kenya as a foundation material. *Proc.*, 8th ICSMFE, 1973. 73-80.

FREDLUND, D. & GAN, J. 1995. The collapse mechanism of a soil subjected to one-dimensional loading and wetting. *NATO ASI Series C Mathematical and Physical Sciences-Advanced Study Institute*, 468, 173-206.

FREDLUND, D., MORGENSTERN, N. R. & WIDGER, R. 1978. The shear strength of unsaturated soils. *Canadian geotechnical journal*, 15, 313-321.

FREDLUND, D. G. & RAHARDJO, H. 1993. *Soil mechanics for unsaturated soils*, John Wiley & Sons.

FREDLUND, D. G., RAHARDJO, H. & FREDLUND, M. D. 2012. *Unsaturated soil mechanics in engineering practice*, John Wiley & Sons.

GIDIGASU, M. 1972. Mode of formation and geotechnical characteristics of laterite materials of Ghana in relation to soil forming factors. *Engineering Geology*, 6, 79-150.

GIDIGASU, M. 1976. *Laterite Soil Engineering: Pedogenesis and Engineering Principles*. Elsevier, Amsterdam, the Netherlands.

GIDIGASU, M. Potential application of engineering pedology in shallow foundation engineering on tropical residual soils. *Proceedings of the II international conference on geomechanics in tropical soils*, Singapore, 1988. 17-24.

GILBERT, R. B., LONG, J. H. & MOSES, B. E. 1996. Analytical model of progressive slope failure in waste containment systems. *International journal for numerical and analytical methods in geomechanics*, 20, 35-56.

GLENDINNING, S., HALL, J. & MANNING, L. 2009a. Asset-management strategies for infrastructure embankments. *Proceedings of the ICE-Engineering Sustainability*, 162, 111-120.

GLENDINNING, S., LOVERIDGE, F., STARR-KEDDLE, R. E., BRANSBY, M. F. & HUGHES, P. N. 2009b. Role of vegetation in sustainability of infrastructure slopes. *Proceedings of the ICE-Engineering Sustainability*, 162, 101-110.

GOGO-ABITE, I. 2005. Slope stability of laterite soil embankments.

GRIFFITHS, D. & MARQUEZ, R. 2007. Three-dimensional slope stability analysis by elasto-plastic finite elements. *Geotechnique*, 57, 537-546.

GUNN, D., NELDER, L., CHAMBERS, J., REEVES, H., FREEBOROUGH, K., JACKSON, P., STIRLING, A. & BROUGH, M. 2005. Geophysical monitoring of the subgrade with examples from Leominster. *Proceedings of the 8th International Conference on Railway Engineering, London*.

GUNN, D., REEVES, H., CHAMBERS, J., GHATAORA, G., BURROW, M., WESTON, P., LOVELL, J., NELDER, L., WARD, D. & TILDEN SMITH, R. 2008. New geophysical and geotechnical approaches to characterise under utilised earthworks. *Advances in Transportation Geotechnics, CRC Press, Boca Raton*, 299-305.

HACK, R. 2000. Geophysics for slope stability. *Surveys in geophysics*, 21, 423-448.

HAERI, S. M., HOSSEINI, S. M., TOLL, D. G. & YASREBI, S. S. 2005. The behaviour of an artificially cemented sandy gravel. *Geotechnical & Geological Engineering*, 23, 537-560.

HARDY JR, H. 1981. Applications of acoustic emission techniques to rock and rock structures: a state-of-the-art review. *Acoustic Emission in Geotechnical Engineering Practice, ASTM STP750, American Society for Testing and Materials*, 4-92.

- HARDY JR, H. R. 2005. *Acoustic emission/microseismic activity: volume 1: principles, techniques and geotechnical applications*, CRC Press.
- HARRIS, C., DAVIES, M. C. & ETZELMÜLLER, B. 2001. The assessment of potential geotechnical hazards associated with mountain permafrost in a warming global climate. *Permafrost and Periglacial Processes*, 12, 145-156.
- HAUG, M., SAUER, E. K. & FREDLUND, D. 1977. Retrogressive slope failures at Beaver Creek, south of Saskatoon, Saskatchewan, Canada. *Canadian Geotechnical Journal*, 14, 288-301.
- HEAD, K. & EPPS, R. 1994. Manual of soil laboratory testing, permeability, shear strength and compressibility tests, Vol. 2. Pentech Press, London.
- HERMAN, R. 2001. An introduction to electrical resistivity in geophysics. *American Journal of Physics*, 69, 943-952.
- HOLDRIDGE, D. 1959. Compositional variation in Etruria marls. *Trans. British Ceramic Soc*, 58, 301-328.
- HORN, A. Swell and creep properties of an African black clay. *Engineering and Construction in Tropical and Residual Soils*, 1982. ASCE, 199-215.
- HUAT, B. B., ALI, F. H. & GUE, S. S. 2007a. Slope failures in tropical residual soils. *Tropical Residual Soils Engineering*. CRC Press.
- HUAT, B. B., GUE, S. S. & ALI, F. H. 2007b. *Tropical residual soils engineering*, CRC Press.
- HUGHES, D., KARIM, M. R., BRIGGS, K., GLENDINNING, S., TOLL, D., DIJKSTRA, T., POWRIE, W. & DIXON, N. 2015. A Comparison of numerical modelling techniques to predict the effect of climate on infrastructure slopes.
- HUGHES, P., GLENDINNING, S., MENDES, J., PARKIN, G., TOLL, D., GALLIPOLI, D. & MILLER, P. 2009. Full-scale testing to assess climate effects on embankments. *Proceedings of the ICE-Engineering Sustainability*, 162, 67-79.
- HUTCHINSON, J. N., SOMERVILLE, S. H. & PETLEY, D. J. 1973. A landslide in periglacially disturbed Etruria Marl at Bury Hill, Staffordshire. *Quarterly journal of engineering geology and hydrogeology*, 6, 377-404.
- JACKSON, D. 2013. Assessment of impacts to non-human biota associated with intrusion into waste materials environment. *Impacts to Non-Human Biota, Environment Agency, ESC Technical Memo*
- JACKSON, P., NORTHMORE, K., ENTWISLE, D., GUNN, D., MILODOWSKI, A., BOARDMAN, D., ZOURMPAKIS, A., ROGERS, C., JEFFERSON, I. & DIXON, N. 2006. Electrical resistivity monitoring of a collapsing metastable soil. *Quarterly journal of engineering geology and hydrogeology*, 39, 151-172.
- JACKSON, P., NORTHMORE, K., MELDRUM, P., GUNN, D., HALLAM, J., WAMBURA, J., WANGUSI, B. & OGUTU, G. 2002. Non-invasive moisture monitoring within an earth embankment—a precursor to failure. *Ndt & E International*, 35, 107-115.
- JEFFERSON, I. & AHMAD, M. Formation of Artificial Collapsible Loess. *Problematic Soils and Rocks and In Situ Characterization*, 2007. ASCE, 1-10.
- JIA, G., ZHAN, T. L., CHEN, Y. & FREDLUND, D. 2009. Performance of a large-scale slope model subjected to rising and lowering water levels. *Engineering Geology*, 106, 92-103.
- JIANG, M., HU, H. & LIU, F. 2012. Summary of collapsible behaviour of artificially structured loess in oedometer and triaxial wetting tests. *Canadian Geotechnical Journal*, 49, 1147-1157.
- JOHNSON, A. I. 1963. *A field method for measurement of infiltration*, US Government Printing Office.
- JURICH, D. M. & MILLER, R. J. 1987. *Acoustic monitoring of landslides*.
- KELLER, G. V. & FRISCHKNECHT, F. C. 1977. *Electrical Methods in Geophysical Prospecting*, Pergamon Press.
- KOERNER, R., MCCABE, W. & LORD, A. 1981. Acoustic emission behavior and monitoring of soils. *Acoustic Emissions in Geotechnical Engineering Practice, ASTM STP*, 750, 93-141.
- KOUSTENI, A., HILL, R., DIXON, N. & KAVANAGH, J. Acoustic emission technique for monitoring soil and rock slope instability. *Proc. Int. Symp. on Slope Stability Engineering: Geotechnical and Geoenvironmental Aspects*, 1999. 151-156.
- KRAHN, J. 2003. The 2001 RM Hardy Lecture: The limits of limit equilibrium analyses. *Canadian Geotechnical Journal*, 40, 643-660.

- KRAHN, J. 2012. Stability modeling with SLOPE/W: An engineering methodology. *GEOSLOPE/W International Ltd. Calgary, Alberta, Canada.*
- LAW, K. T. & LUMB, P. 1978. A limit equilibrium analysis of progressive failure in the stability of slopes. *Canadian Geotechnical Journal*, 15, 113-122.
- LAWTON, E. C., FRAGASZY, R. J. & HARDCASTLE, J. H. 1989. Collapse of compacted clayey sand. *Journal of Geotechnical Engineering*, 115, 1252-1267.
- LIU, C.-N., DONG, J.-J., CHEN, C.-J. & LEE, W.-F. 2012a. Typical landslides and related mechanisms in Ali Mountain highway induced by typhoon Morakot: perspectives from engineering geology. *Landslides*, 9, 239-254.
- LIU, Y. & DENG, H. Instability mechanism research on anti-orientation strata slope with alternating layers of hard and soft rock. Remote Sensing, Environment and Transportation Engineering (RSETE), 2011 International Conference on, 2011. IEEE, 3224-3227.
- LIU, Y., WANG, C. & YANG, Q. 2012b. Stability analysis of soil slope based on deformation reinforcement theory. *Finite Elements in Analysis and Design*, 58, 10-19.
- LOKE, M. & BARKER, R. Rapid least-squares inversion of apparent resistivity pseudosections. 56th EAEG Meeting, 1994.
- LOKE, M. H. & BARKER, R. 1996. Rapid least-squares inversion of apparent resistivity pseudosections by a quasi-Newton method. *Geophysical prospecting*, 44, 131-152.
- LORD JR, A. E. 2012. Acoustic emission. *Physical acoustics*, 11, 289-353.
- LOVERIDGE, F. A., SPINK, T. W., O'BRIEN, A. S., BRIGGS, K. M. & BUTCHER, D. 2010. The impact of climate and climate change on infrastructure slopes, with particular reference to southern England. *Quarterly Journal of Engineering Geology and Hydrogeology*, 43, 461-472.
- MA, R., MCBRATNEY, A., WHELAN, B., MINASNY, B. & SHORT, M. 2011. Comparing temperature correction models for soil electrical conductivity measurement. *Precision Agriculture*, 12, 55-66.
- MADU, R. 1977. An investigation into the geotechnical and engineering properties of some laterites of eastern Nigeria. *Engineering Geology*, 11, 101-125.
- MADUN, A. 2012. Laboratory Scale Seismic Surface Wave Testing for the Determination of Soil Elastic Profiles. *International Journal of Integrated Engineering*, 4.
- MALANDRAKI, V. & TOLL, D. 2000. Drained probing triaxial tests on a weakly bonded artificial soil. *Géotechnique*, 50, 141-151.
- MANTOVANI, F., SOETERS, R. & VAN WESTEN, C. 1996. Remote sensing techniques for landslide studies and hazard zonation in Europe. *Geomorphology*, 15, 213-225.
- MAYNE, P. W., JONES JR, J. S. & DUMAS, J. C. 1984. Ground response to dynamic compaction. *Journal of Geotechnical Engineering*, 110, 757-774.
- MENARD, L. & BROISE, Y. 1975. Theoretical and practical aspect of dynamic consolidation. *Geotechnique*, 25, 3-18.
- MITCHELL, J. K. & SOGA, K. 2005. *Fundamentals of soil behavior*, John Wiley & Sons New York.
- MUNTOHAR, A. S. & LIAO, H.-J. 2009. Analysis of rainfall-induced infinite slope failure during typhoon using a hydrological-geotechnical model. *Environmental geology*, 56, 1145-1159.
- NEMA-REPORT 2012. Post-Disaster Needs Assessment (PDNA), Prepared by the Nigerian National Emergency Management Agency (NEMA) with Technical Support from the World Bank and Other Partners. *Nigeria 2012 Floods.*
- NG, C. & SHI, Q. 1998. A numerical investigation of the stability of unsaturated soil slopes subjected to transient seepage. *Computers and geotechnics*, 22, 1-28.
- NI, P., WANG, S., ZHANG, S. & MEI, L. 2016. Response of heterogeneous slopes to increased surcharge load. *Computers and Geotechnics*, 78, 99-109.
- NNADI, G. 1987. Geotechnical properties of tropical residual soils. Luleå University of Technology. Research Report, Tulea. Nnadi, G., 1988. Geotechnical properties of tropi.
- NNADI, G. 1988. Geotechnical properties of tropical residual soils. Luleå University of Technology.

- OGUNSANWO, O. 1988. Basic geotechnical properties, chemistry and mineralogy of some laterite soils from SW Nigeria. *Bulletin of the International Association of Engineering Geology-Bulletin de l'Association Internationale de Géologie de l'Ingénieur*, 37, 131-135.
- OGUNSANWO, O. 1989. Some geotechnical properties of two laterite soils compacted at different energies. *Engineering Geology*, 26, 261-269.
- OH, W. T. & VANAPALLI, S. K. 2010. Influence of rain infiltration on the stability of compacted soil slopes. *Computers and Geotechnics*, 37, 649-657.
- OLA, S. 1978. Geotechnical properties and behaviour of some stabilized Nigerian lateritic soils. *Quarterly Journal of Engineering Geology and Hydrogeology*, 11, 145-160.
- OLA, S. 1980. Permeability of three compacted tropical soils. *Quarterly Journal of Engineering Geology and Hydrogeology*, 13, 87-95.
- OLHOEFT, G. R. & SELIG, E. T. Ground penetrating radar: Evaluation of railway track substructure conditions. *Proceedings, 9th International Conference on Ground Penetrating Radar*, 2002. 48-53.
- OSINUBI, K., BAFYAU, V. & EBEREMU, A. 2009. Bagasse ash stabilization of lateritic soil. *Appropriate Technologies for Environmental Protection in the Developing World*. Springer.
- OSINUBI, K. J. 1998a. Influence of compactive efforts and compaction delays on lime-treated soil. *Journal of transportation engineering*, 124, 149-155.
- OSINUBI, K. J. 1998b. Permeability of lime-treated lateritic soil. *Journal of Transportation Engineering*, 124, 465-469.
- OSINUBI, K. J. & NWAIWU, C. M. 2006. Design of compacted lateritic soil liners and covers. *Journal of geotechnical and geoenvironmental engineering*, 132, 203-213.
- OWEN, G., MORETTI, M. & ALFARO, P. 2011. Recognising triggers for soft-sediment deformation: Current understanding and future directions. *Sedimentary Geology*, 235, 133-140.
- P. ORENSE, R., SHIMOMA, S., MAEDA, K. & TOWHATA, I. 2004. Instrumented model slope failure due to water seepage. *Journal of Natural Disaster Science*, 26, 15-26.
- PAIGE-GREEN, P., PINARD, M. & NETTERBERG, F. 2015. A review of specifications for lateritic materials for low volume roads. *Transportation Geotechnics*, 5, 86-98.
- PETLEY, D. N., HIGUCHI, T., PETLEY, D. J., BULMER, M. H. & CAREY, J. 2005. Development of progressive landslide failure in cohesive materials. *Geology*, 33, 201-204.
- PITTS, J. 1983. The form and causes of slope failures in an area of West Singapore Island. *Singapore Journal of Tropical Geography*, 4, 162-168.
- PRUSZA, Z., KLEINER, D. & SUNDARAM, A. Characteristics of Guri soils. *Geological Environmental and Soil Properties*, 1983. ASCE, 183-199.
- QUINN, P., DIEDERICHS, M., HUTCHINSON, D. J. & ROWE, R. K. An exploration of the mechanics of retrogressive landslides in sensitive clay. *Proceedings of the 60th Canadian Geotechnical Conference and 8th Joint CGS/IAH-CNC Groundwater Conference*, Ottawa, Ont, 2007. 21-24.
- RAHARDJO, H., HRITZUK, K., LEONG, E. C. & REZAUR, R. 2003. Effectiveness of horizontal drains for slope stability. *Engineering Geology*, 69, 295-308.
- RAHARDJO, H., LEE, T., LEONG, E. C. & REZAUR, R. 2005. Response of a residual soil slope to rainfall. *Canadian Geotechnical Journal*, 42, 340-351.
- RAHARDJO, H., LI, X., TOLL, D. G. & LEONG, E. C. 2001. The effect of antecedent rainfall on slope stability. *Unsaturated Soil Concepts and Their Application in Geotechnical Practice*. Springer.
- RAHARDJO, H., NIO, A. S., HARNAS, F. R. & LEONG, E. C. 2014. Comprehensive instrumentation for real time monitoring of flux boundary conditions in slope. *Procedia Earth and Planetary Science*, 9, 23-43.
- RAHARDJO, H., ONG, T., REZAUR, R. & LEONG, E. C. 2007. Factors controlling instability of homogeneous soil slopes under rainfall. *Journal of Geotechnical and Geoenvironmental Engineering*, 133, 1532-1543.
- REDUCTION, D. R. 2008. A Briefing Note 01. Geneva: UN/ISDR.
- REEVES, G. M., SIMS, I. & CRIPPS, J. Clay materials used in construction. 2006. *Proceedings of the conference organised by Geological Society of London*, 2006.
- ROBERTSON, T. 1931. The origin of the Etruria Marl. *Quarterly Journal of the Geological Society*, 87, 13-29.

- ROGERS, C. 1995. Types and distribution of collapsible soils. *Genesis and properties of collapsible soils*. Springer.
- ROUAINIA, M., DAVIES, O., O'BRIEN, T. & GLENDINNING, S. Numerical modelling of climate effects on slope stability. Proceedings of the Institution of Civil Engineers-Engineering Sustainability, 2009. Thomas Telford Ltd, 81-89.
- RÜCKER, C. & GÜNTHER, T. 2011. The simulation of finite ERT electrodes using the complete electrode model. *Geophysics*, 76, F227-F238.
- SADIQ, A., JEFFERSON, M., GHATAORA, G. & CULSHAW, M. New method of producing artificial tropical residual soils from older British soils. 4th International Conference on New Developments in Soil Mechanics and Geotechnical Engineering 2-4 June 2016, Near East University, Nicosia, North Cyprus, 2016. 625-632.
- SCHUSTER, R. L. 1996. Socioeconomic significance of landslides. *Landslides: Investigation and Mitigation*. Washington (DC): National Academy Press. Transportation Research Board Special Report, 247, 12-35.
- SCHWARTZ, K. 1985. Collapsible soils. *Civil Engineering= Siviële Ingenieurswese*, 27, 379-393.
- SELLERS, R., DIXON, N., DIJKSTRA, T., GUNN, D., CHAMBERS, J., JACKSON, P. & HUGHES, P. 2010. Electrical resistivity as a tool to identify areas of progressive failure within UK infrastructure embankments. *IAEG Congress 2010, Auckland, New Zealand, 5-10 Sept 2010*. EAGE.
- SHIOTANI, T., OHTSU, M. & IKEDA, K. 2001. Detection and evaluation of AE waves due to rock deformation. *Construction and Building Materials*, 15, 235-246.
- SHRODER, J., JOHN F, CVERCKOVÁ, L. & MULHERN, K. L. 2005. Slope-failure analysis and classification: review of a century of effort. *Physical Geography*, 26, 216-247.
- SLOB, E., SATO, M. & OLHOEFT, G. 2010. Surface and borehole ground-penetrating-radar developments. *Geophysics*, 75, 75A103-75A120.
- STARR, J., PALTINEANU, I., DANE, J. & TOPP, G. 2002. Methods of soil analysis. Part 4. Physical methods. Madison, WI: Soil Science Society of America, Inc.
- STYLES, M., ENTWISLE, D., GUNN, D., HODGKINSON, E., JACKSON, P., KEMP, S., NELDER, L., NORTHMORE, K. & STEADMAN, E. 2001. A mineralogical examination of a magnetic tropical brown soil from Cambodia and a possible synthetic analogue made with soil from Devon. REPORT CR/01/096N, British Geological Survey.
- SUDHA, K., ISRAIL, M., MITTAL, S. & RAI, J. 2009. Soil characterization using electrical resistivity tomography and geotechnical investigations. *Journal of Applied Geophysics*, 67, 74-79.
- SULTAN, N., COCHONAT, P., CANALS, M., CATTANEO, A., DENNIELOU, B., HAFLIDASON, H., LABERG, J., LONG, D., MIENERT, J. & TRINCARDI, F. 2004. Triggering mechanisms of slope instability processes and sediment failures on continental margins: a geotechnical approach. *Marine Geology*, 213, 291-321.
- SURYO, E. A. 2013. *Real-time prediction of rainfall induced instability of residual soil slopes associated with deep cracks*. Queensland University of Technology.
- TABWASSAH, C. A. & OBIEFUNA, G. I. 2012. Geophysical and Geotechnical Investigation of Cham Failed Dam Project, Ne Nigeria. *Research Journal of Recent Sciences ISSN*, 2277, 2502.
- TOHARI, A., NISHIGAKI, M. & KOMATSU, M. Laboratory experiments on initiation of rainfall induced slope failure with moisture content measurements. *GeoEng2000: An International Conference on Geotechnical & Geological Engineering*, Melbourne, Australia, 2000.
- TOHARI, A., NISHIGAKI, M. & KOMATSU, M. 2007. Laboratory rainfall-induced slope failure with moisture content measurement. *Journal of Geotechnical and Geoenvironmental Engineering*, 133, 575-587.
- TOLL, D. 2001. Briefing: Rainfall-induced landslides in Singapore. *Proceedings of the institution of civil engineers-geotechnical engineering*, 149, 211-216.
- TOPP, G. C., DAVIS, J. & ANNAN, A. P. 1980. Electromagnetic determination of soil water content: Measurements in coaxial transmission lines. *Water resources research*, 16, 574-582.
- TOWNSEND, F. C. 1985. Geotechnical characteristics of residual soils. *Journal of Geotechnical Engineering*, 111, 77-94.

- TOWNSEND, F. C., MANKE, P. G. & PARCHER, J. V. 1971. The influence of sesquioxides on lateritic soil properties. *Highway Research Record*.
- TROFIMOV, V. 1990. Some experimental evidence for formation of syngenetic collapsibility of aeolian loess rocks. *Soviet Engineering Geology*, 6.
- TSAPARAS, I., RAHARDJO, H., TOLL, D. G. & LEONG, E.-C. 2003. Infiltration characteristics of two instrumented residual soil slopes. *Canadian Geotechnical Journal*, 40, 1012-1032.
- TSAPARAS, I., RAHARDJO, H., TOLL, D. G. & LEONG, E. C. 2002. Controlling parameters for rainfall-induced landslides. *Computers and geotechnics*, 29, 1-27.
- UNISDR 2008. Climate Change and Disaster Risk Reduction - A Briefing Note 01. Geneva: UN/ISDR.
- VAN GENUCHTEN, M. T. 1980. A closed-form equation for predicting the hydraulic conductivity of unsaturated soils. *Soil science society of America journal*, 44, 892-898.
- VANAPALLI, S., FREDLUND, D. & PUF AHL, D. Comparison of saturated–unsaturated shear strength and hydraulic conductivity behavior of a compacted sandy-clay till. Proceedings of the 50th Canadian Geotechnical Conference, Ottawa, 1997. 20-22.
- VAUGHAN, P. Mechanical and hydraulic properties of in situ residual soils. Proceedings of the First International Conference on Geomechanics in Tropical Soils, Brasilia, 1985. 231-63.
- VAUGHAN, P., MACCARINI, M. & MOKHTAR, S. 1988. Indexing the engineering properties of residual soil. *Quarterly Journal of Engineering Geology and Hydrogeology*, 21, 69-84.
- VILAR, O., BORTOLUCCI, A. & RODRIGUES, J. Geotechnical Characteristics of Tropical Cenozoic Sediment from São Carlos Region (Brazil). International Conference on Geomechanics in Tropical Lateritic and Saprolitic Soil. "Tropicals85, 1985. 461-470.
- WANG, B., VARDON, P. & HICKS, M. 2016. Investigation of retrogressive and progressive slope failure mechanisms using the material point method. *Computers and Geotechnics*, 78, 88-98.
- WIECZOREK, G. F. & JÄGER, S. 1996. Triggering mechanisms and depositional rates of postglacial slope-movement processes in the Yosemite Valley, California. *Geomorphology*, 15, 17-31.
- WINTER, M., DENT, J., MACGREGOR, F., DEMPSEY, P., MOTION, A. & SHACKMAN, L. 2010a. Debris flow, rainfall and climate change in Scotland. *Quarterly Journal of Engineering Geology and Hydrogeology*, 43, 429-446.
- WINTER, M., DIXON, N., WASOWSKI, J. & DIJKSTRA, T. 2010b. Introduction to land-use and climate change impacts on landslides. *Quarterly Journal of Engineering Geology and Hydrogeology*, 43, 367-370.
- WINTER, M., SHACKMAN, L. & MACGREGOR, F. 2007. Landslide management and mitigation on the Scottish road network. *Landslides and Climate Change: Challenges and Solutions*. Taylor & Francis, London, 249-258.
- WINTER, M. G., HARRISON, M., MACGREGOR, F. & SHACKMAN, L. 2013. Landslide hazard and risk assessment on the Scottish road network. *Proceedings of the Institution of Civil Engineers-Geotechnical engineering*, 166, 522-539.
- XIA, J., MILLER, R. D., PARK, C. B., HUNTER, J. A., HARRIS, J. B. & IVANOV, J. 2002. Comparing shear-wave velocity profiles inverted from multichannel surface wave with borehole measurements. *Soil dynamics and earthquake engineering*, 22, 181-190.
- ZHANG, J., JIAO, J. & YANG, J. 2000. In situ rainfall infiltration studies at a hillside in Hubei Province, China. *Engineering Geology*, 57, 31-38.
- ZHOU, Q. Y., SHIMADA, J. & SATO, A. 2001. Three-dimensional spatial and temporal monitoring of soil water content using electrical resistivity tomography. *Water Resources Research*, 37, 273-285.
- ZHU, H., ZHANG, L., ZHANG, L. & ZHOU, C. 2012. Two-dimensional probabilistic infiltration analysis with a spatially varying permeability function. *Computers and Geotechnics*. Volume 48, Pages 249-259.
- ZOURMPAKIS, A., BOARDMAN, D. & ROGERS, C. 2005. Creation of artificial loess soils. *Unsaturated Soils: Experimental Studies*. Springer.

APPENDIX D: Detailed experimental tank

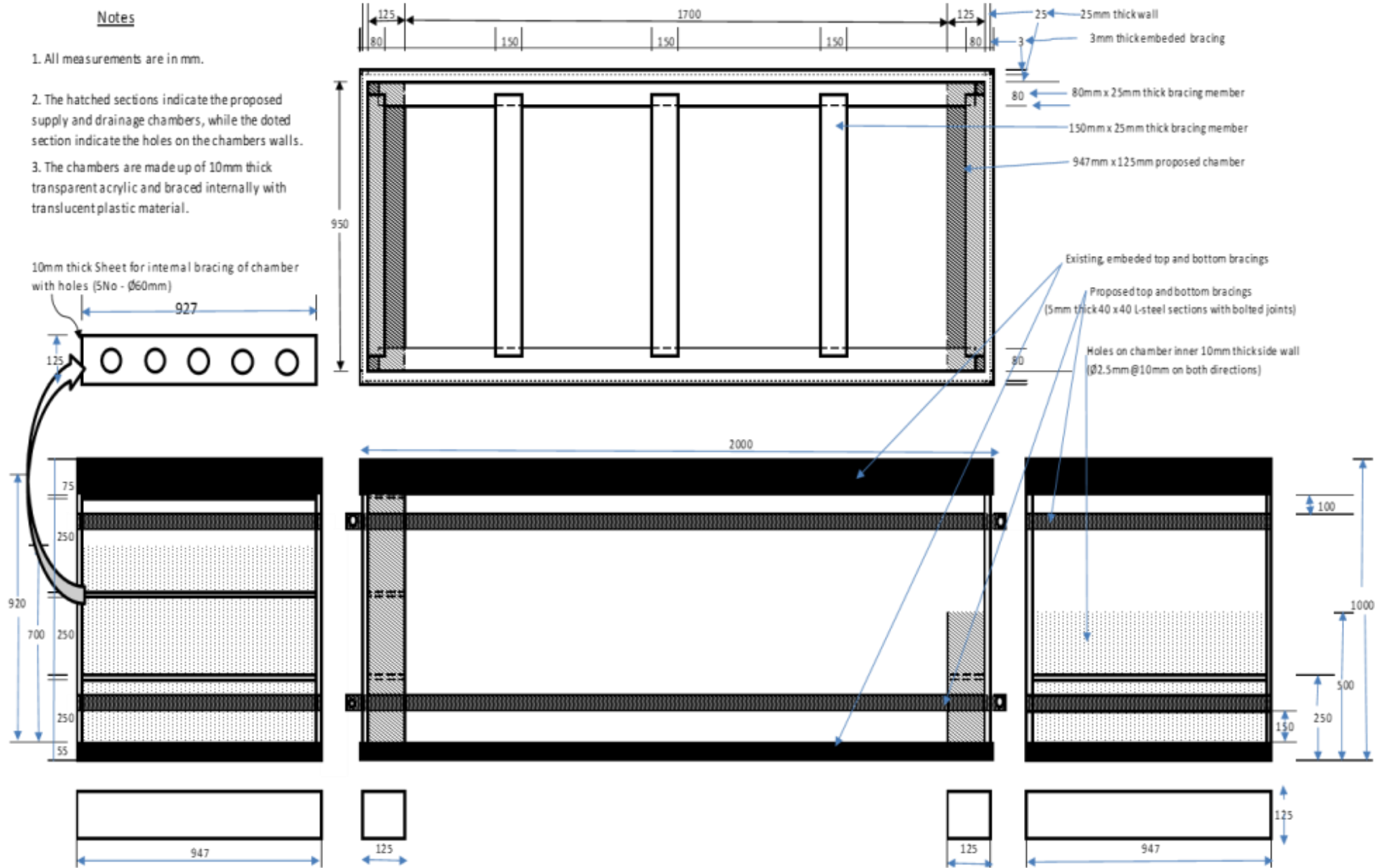
D1: Photograph of transparent tank used for final experiment



D2: Schematic diagram of transparent tank used for final experiment

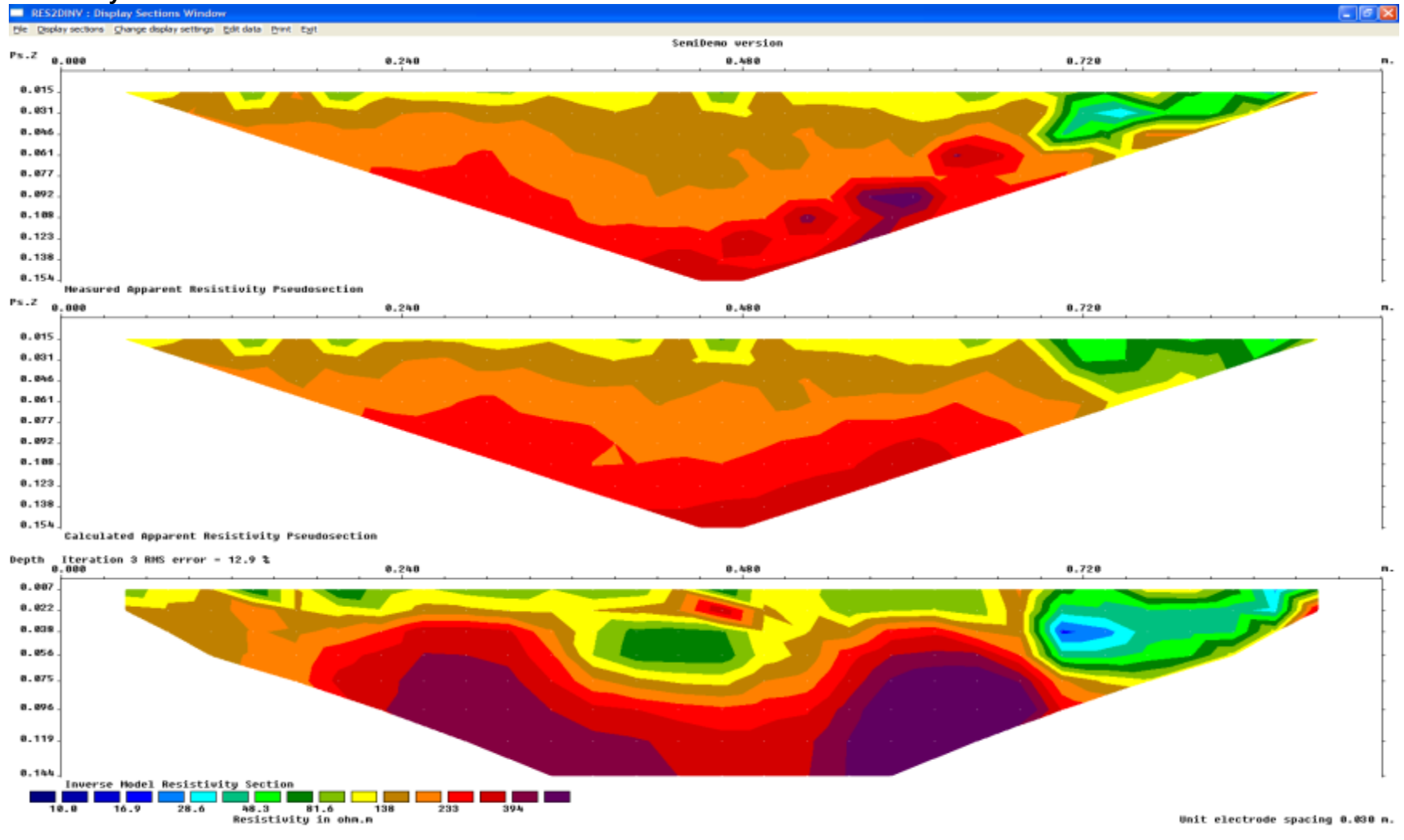
Notes

1. All measurements are in mm.
2. The hatched sections indicate the proposed supply and drainage chambers, while the dotted section indicate the holes on the chambers walls.
3. The chambers are made up of 10mm thick transparent acrylic and braced internally with translucent plastic material.

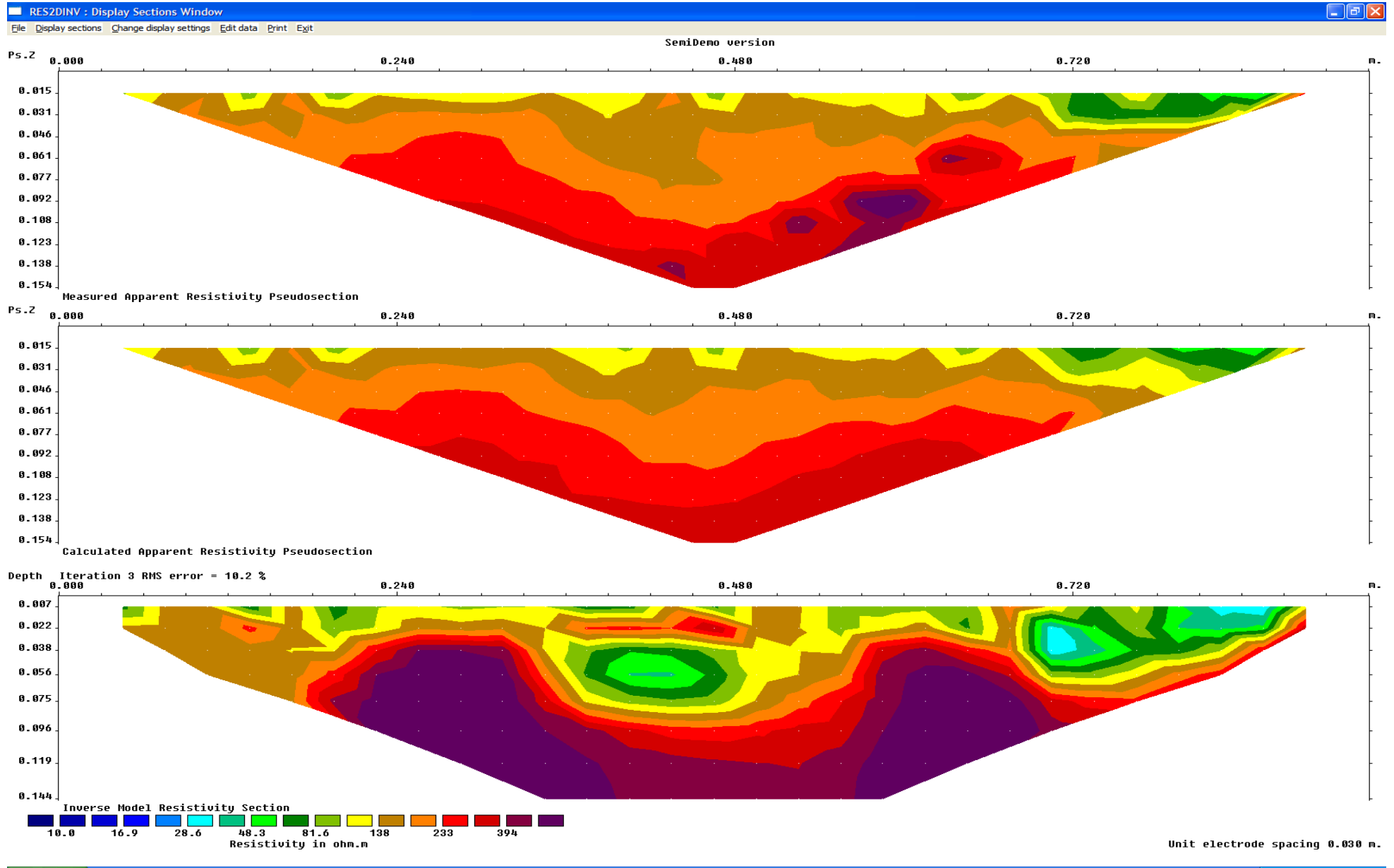


APPENDIX E: Resistivity Results

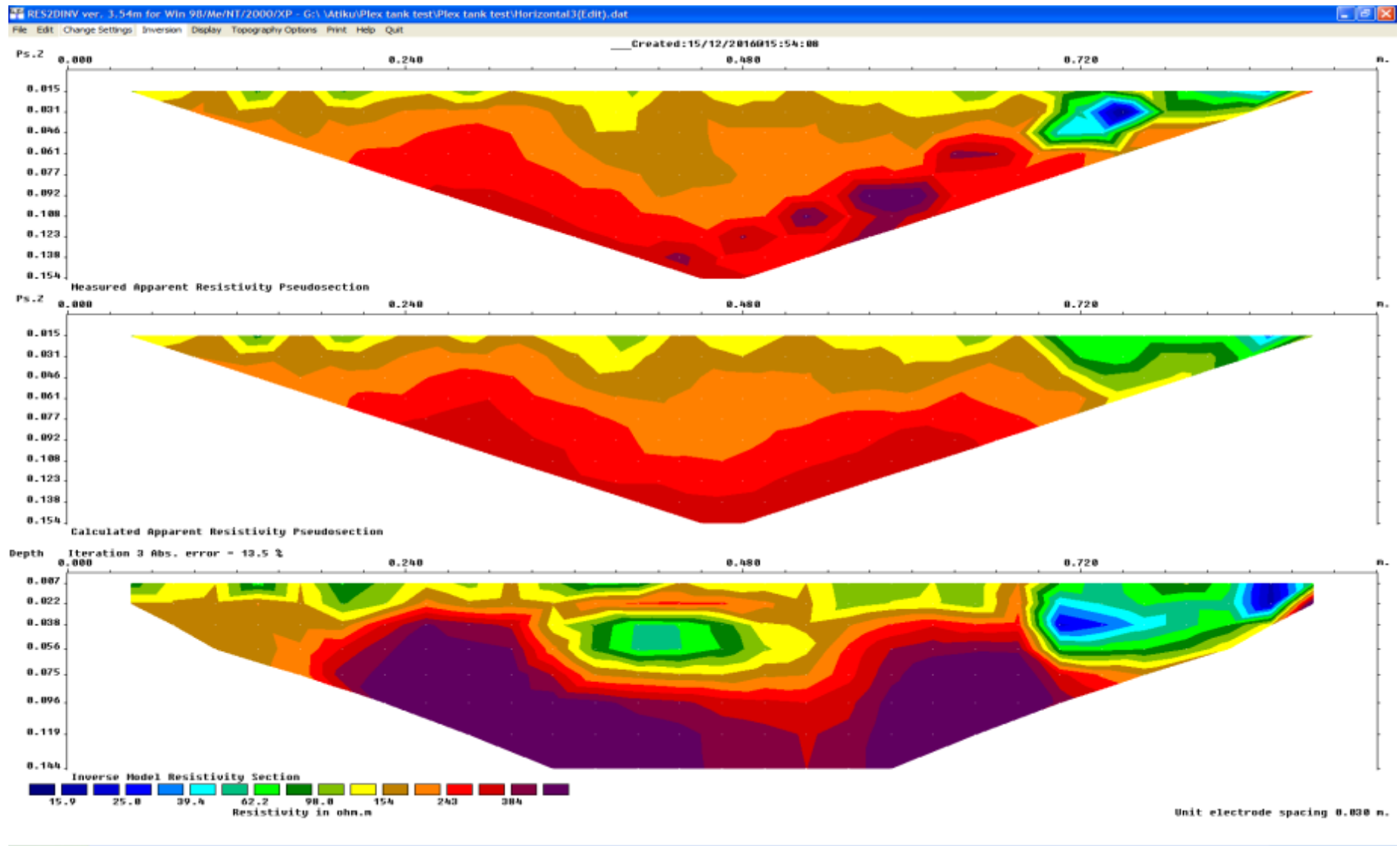
E1: Horizontal survey line - Scan 1



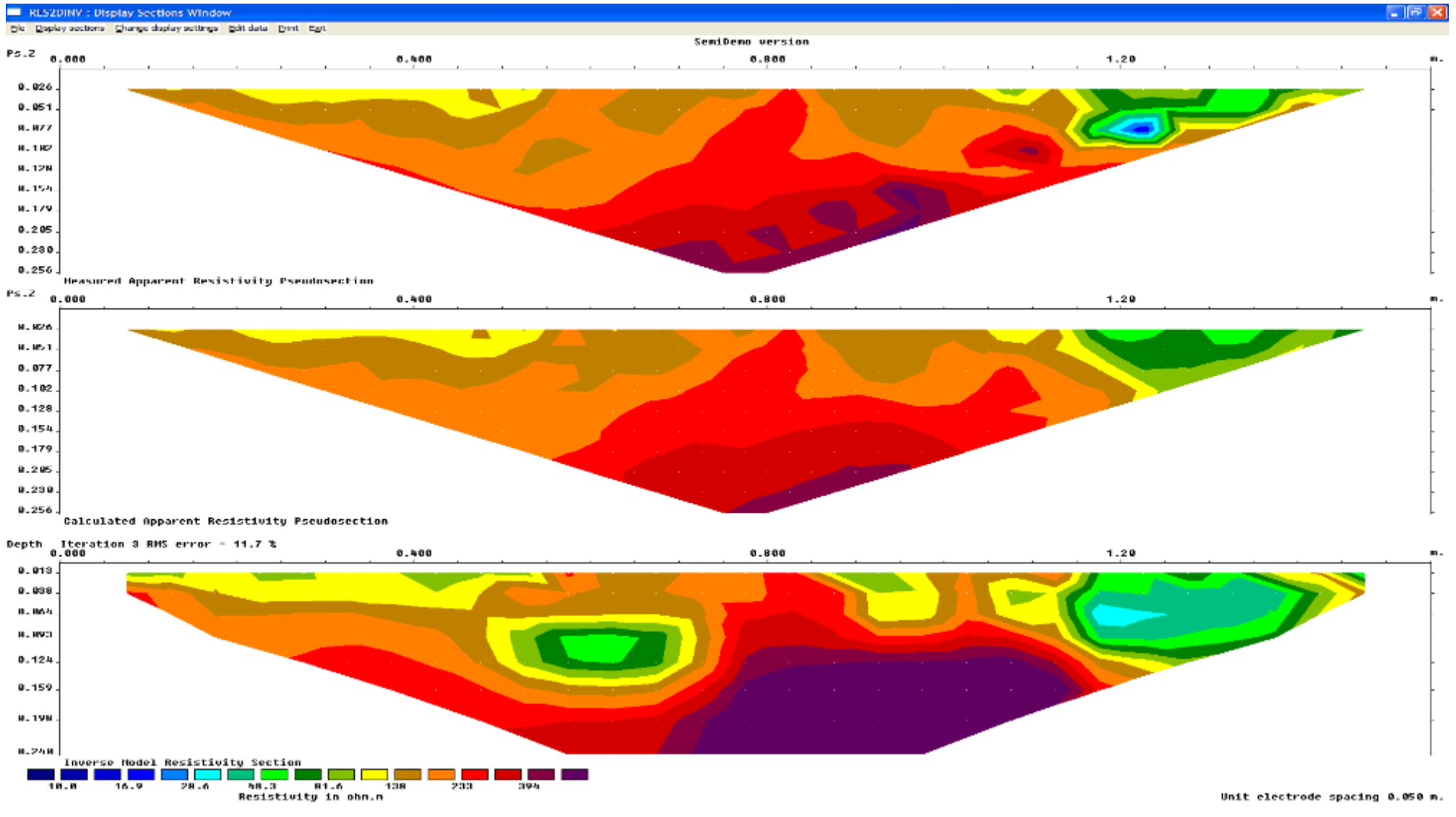
E2: Horizontal survey line Scan 2



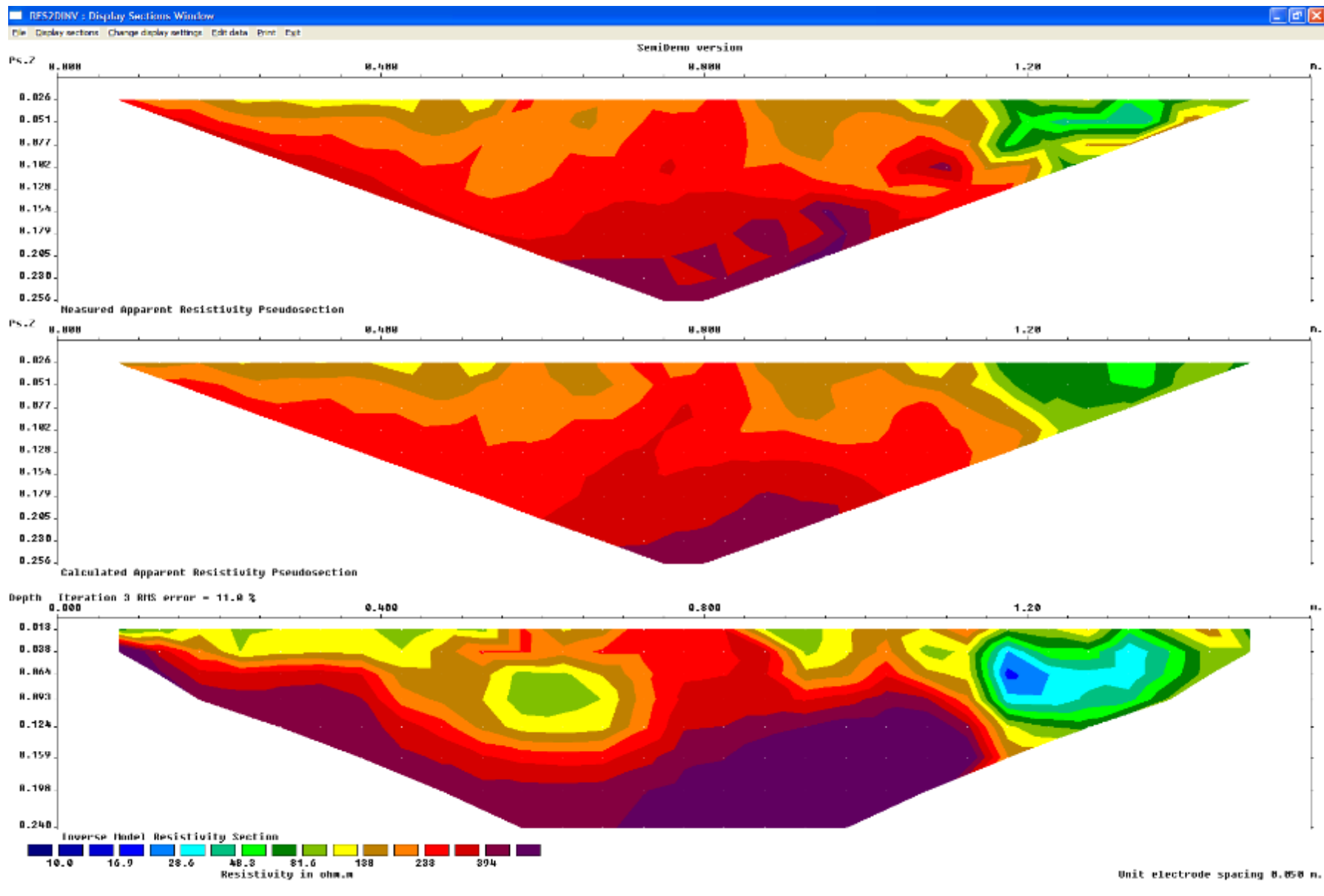
E3: Horizontal survey line -Scan 3



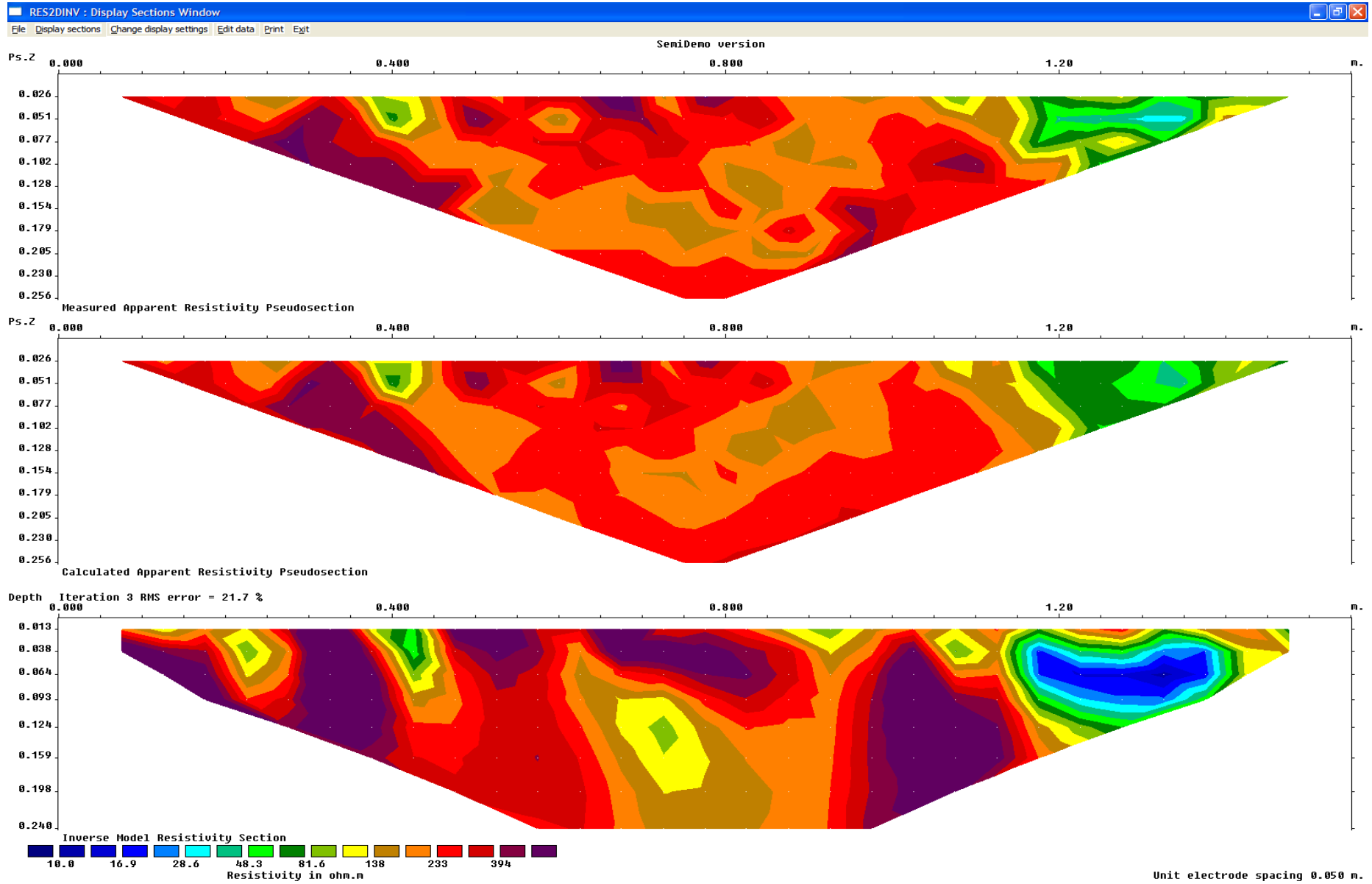
E4: Central survey line -Scan 1



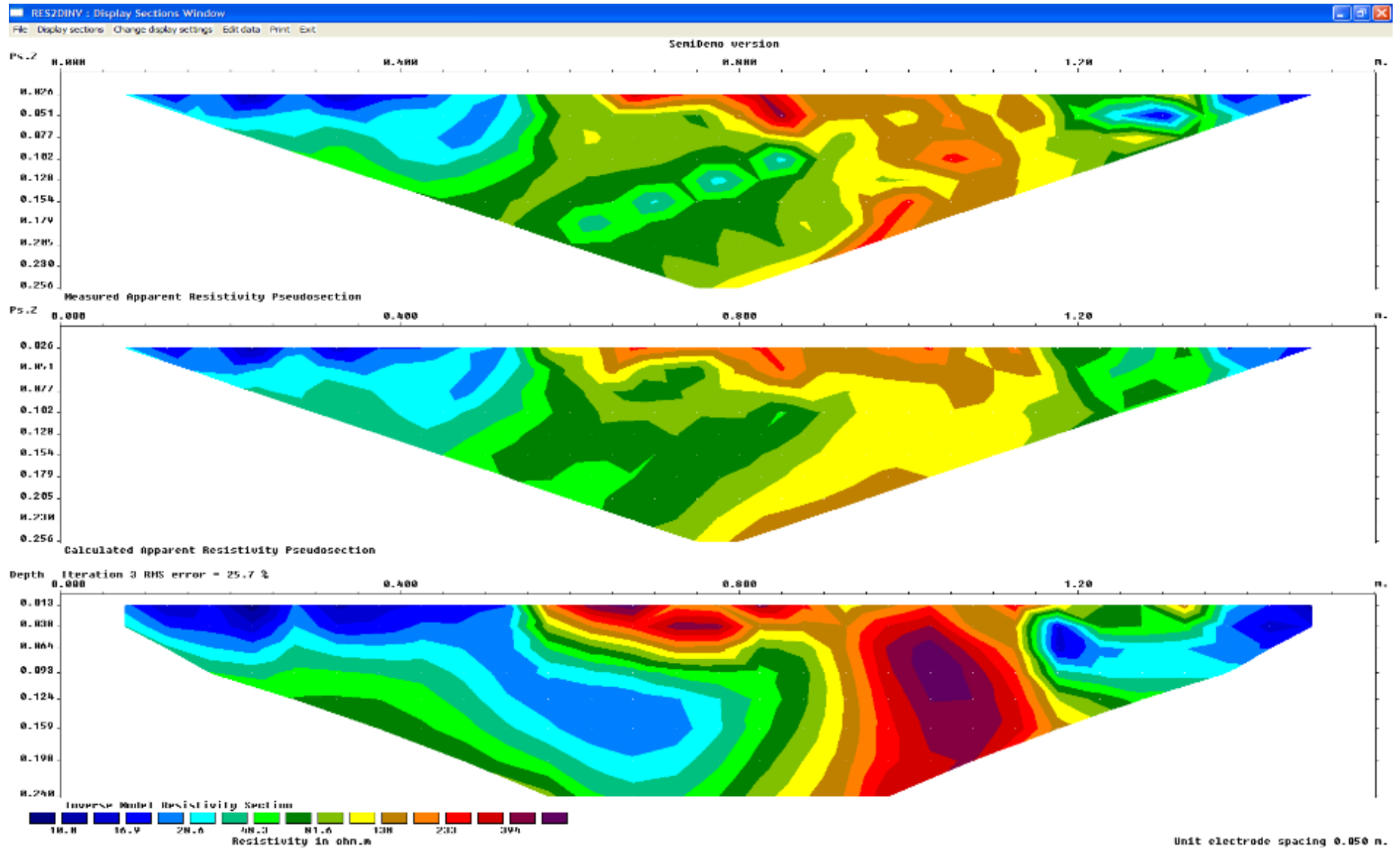
E5: Central survey line -Scan 2



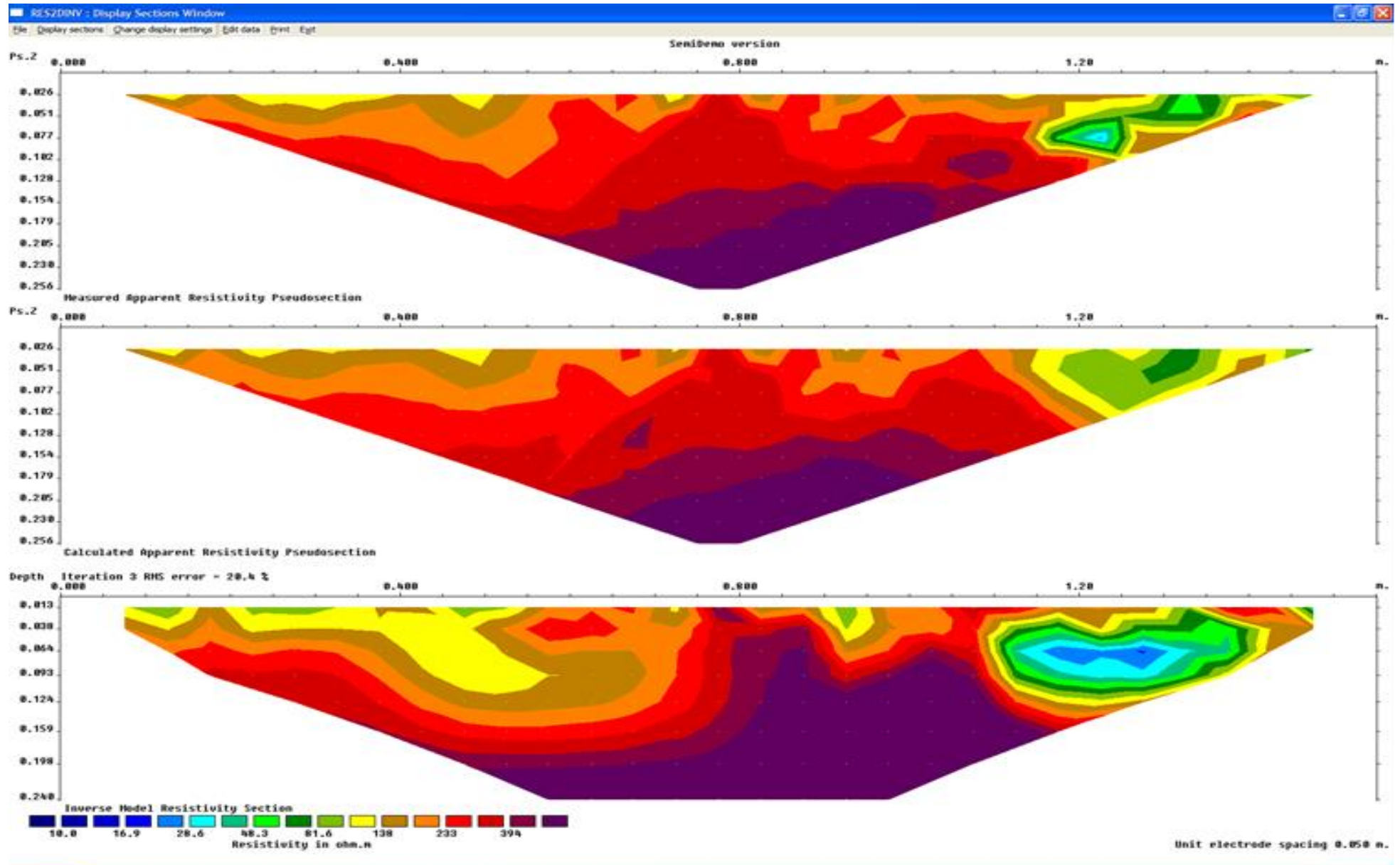
E6: Central survey line -Scan 3



E7: Central survey line -Scan 4



E8: Side survey line -Scan 1



E9: Side survey line - Scan 2

